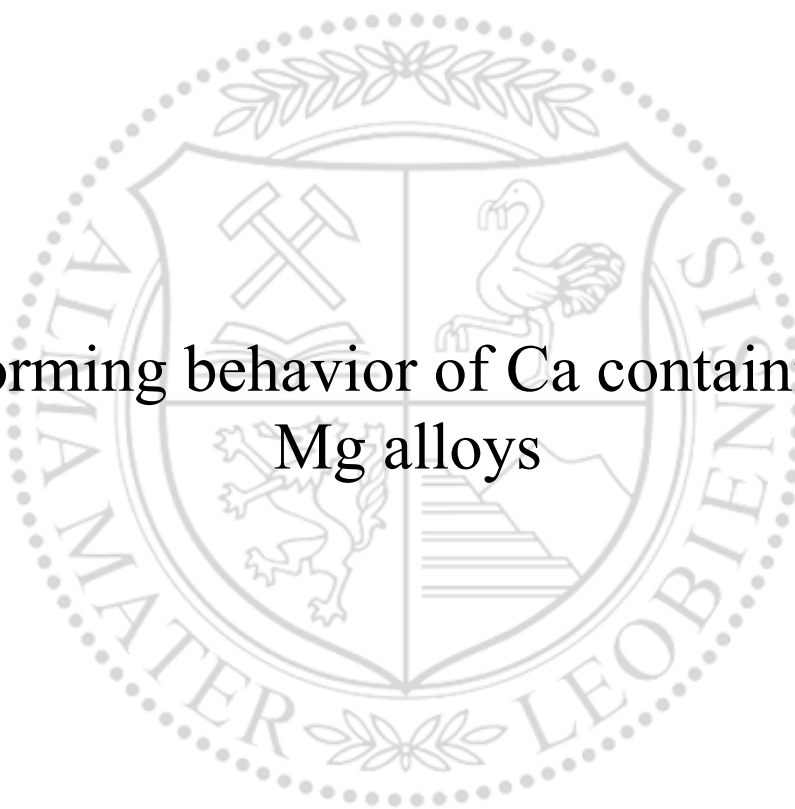




Chair of Nonferrous Metallurgy

Doctoral Thesis



Forming behavior of Ca containing
Mg alloys

Dipl.-Ing. Nikolaus Peter Papenberg

March 2023



MONTANUNIVERSITÄT LEOBEN
www.unileoben.ac.at

AFFIDAVIT

I declare on oath that I wrote this thesis independently, did not use other than the specified sources and aids, and did not otherwise use any unauthorized aids.

I declare that I have read, understood, and complied with the guidelines of the senate of the Montanuniversität Leoben for "Good Scientific Practice".

Furthermore, I declare that the electronic and printed version of the submitted thesis are identical, both, formally and with regard to content.

Date 09.03.2023

A handwritten signature in blue ink, appearing to read 'Nikolaus Peter Papenberg', written over a horizontal line.

Signature Author
Nikolaus Peter Papenberg

Acknowledgements

First and foremost I would like to thank Univ.-Prof. Dipl.-Ing. Dr. mont. Stefan Pogatscher and Univ.-Prof. Dipl.-Ing. Dr. mont. Helmut Antrekowitsch for giving me the opportunity to do this doctoral thesis as an external student at the Chair of Nonferrous Metallurgy of the Montanuniversität Leoben. My special gratitude goes to Univ.-Prof. Dipl.-Ing. Dr. mont. Peter J. Uggowitzer for the intensive support and discussions in the field of Mg alloying technology and microstructure development.

Special mention must also be made of the good cooperation with my co-authors during the writing and publishing process of the scientific publications that form the backbone of this thesis.

I would also like to thank my supervisors and colleagues at the Leichtmetallkompetenzzentrum Ranshofen for the backing received during the dissertation. The support of my colleagues was indispensable for me in the context of scientific discussions and publications, in the execution of experiments as well as subsequent material analysis and interpretation.

Last but not least my thanks goes to my family and friends for the unwavering support during the challenging time of this work.

Kurzfassung

Das Ziel dieser Arbeit ist es, das Verständnis über das Umformverhalten von mageren Mg Legierungen zu erweitern, welche durch die Zugabe von Calcium die Möglichkeit der Ausscheidungshärtung besitzen. Besonderes Augenmerk liegt dabei auf der Untersuchung des Gesenkschmiedeprozesses.

Magere Mg Legierungen besitzen nur einen geringen Gehalt an Legierungselementen, die aber bestmöglich zum Einsatz kommen sollen. Durch die begrenzte Grundfestigkeit dieser Legierungen soll der Umformprozess erleichtert werden, die dann für den Einsatz nötigen finalen Festigkeiten können durch eine nachgelagerte Wärmebehandlung (Ausscheidungshärtung) erreicht werden.

Der Großteil der wissenschaftlichen Untersuchungen von Mg Umformprozessen beschäftigt sich mit Strangpressen oder Walzen, da diese Prozesse die überwiegende Menge an ungehobenem Marktpotential darstellen. Allerdings bieten Schmiedeprozesse mit ihrer inhärent hohen Flexibilität was Prozessbedingungen und Vormaterial angeht eine gute Einstiegsmöglichkeit für die Industrie in die komplexe Thematik der Mg Umformtechnik. Auch stellt die direkte Produktion von vollständigen Mg Schmiedebauteilen Vorteile in der Analyse und Anschaulichkeit gegenüber Strangpressprofilen und Walzprodukten dar, da es sich bei diesen vorwiegend um Halbzeuge handelt.

In der vorliegenden Arbeit wurde eine aushärtbare Mg-Al-Ca-Mn-Zn Legierung (AXMZ1000) mit einem niedrigen Gesamt-Legierungsgehalt (< 2 Gewichtsprozent) auf ihre Schmiedeeignung untersucht. Dabei wurde das Umformverhalten vom Labormaßstab bis zum industriellen Umformprozess analysiert. Es wurden sowohl die Prozessparameter im Umformprozess wie auch das Vormaterial und die Wärmebehandlung variiert um Änderungen im Prozessverhalten, der Mikrostrukturentwicklung sowie den mechanischen Eigenschaften zu evaluieren. Das Umformverhalten von gegossenem Vormaterial wurde mittels Materialkarte beschrieben und ausgehend von Schmiedeversuchen im Labormaßstab bis hin zu industriellen Größenordnungen verifiziert. Tiefergehende Untersuchungen der mechanischen Eigenschaften, mittels Zug- und Ermüdungsversuchen, sowie Analysen der Mikrostrukturentwicklung wurden an isotherm geschmiedeten Bauteilen durchgeführt.

Aufgrund der durchgeführten Analysen konnte eine Abhängigkeit der Bauteilqualität vom eingesetzten Vormaterial gezeigt werden, wobei die Verwendung von stranggepresstem Material die mechanischen Eigenschaften der Schmiedebauteile deutlich verbessert. Auch wurden die Unterschiede zwischen Umformversuchen in Labor- und Industriemaßstab eingehend untersucht und Differenzen, Problemstellen sowie Limitierungen aufgezeigt.

Abstract

This work is intended to expand the understanding of lean Mg alloys forming behavior, which are precipitation hardenable due to alloying with calcium. Special attention is given to the investigation of the die forging process.

Lean Mg alloys are defined by a low overall amount of alloying elements, which are intended to be used in the most efficient way. The limited basic strength of these alloys is intended to support the forming process, while the strengths required for use can be achieved by precipitation hardening in a subsequent heat treatment.

Most scientific investigations of Mg forming processes deal with extrusion or rolling, as these processes represent most of the untapped market potential. However, forging processes, with their inherent high flexibility in terms of process conditions and feedstock material, offer a good entry point for industry into the complex subject of Mg manufacturing processes. Also, the production of finished forged Mg components presents advantages in analysis and demonstrability compared to extruded or rolled products, since the latter are mainly semi-finished products.

In the present work, a precipitation hardenable Mg-Al-Ca-Mn-Zn alloy (AXMZ1000) with a low total alloy content (< 2 weight percent) was investigated with respect to its suitability for forging processes. The forming behavior from laboratory to industrial scale forming was analyzed. The process parameters, the forging stock and the heat treatments were varied in order to evaluate changes in the process and microstructural behavior as well as the mechanical properties of the produced parts. The forming behavior of cast feedstock was described using a processing map and verified by forging trials on laboratory and industrial scale. In-depth investigations on mechanical properties, using tensile and fatigue testing, as well as microstructural development was done on isothermal forged parts.

Based on the analyses performed, it was possible to show a dependence of the forged components on the stock material used. Extruded material significantly improved the mechanical properties of the forged components. The differences between forming tests in laboratory and industrial scale were investigated in detail and differences, problem areas as well as limitations were pointed out.

Contents

1. Introduction	1
1.1. Motivation	1
1.2. Aim of this Work	2
1.3. Approach & Document Structure	3
1.3.1. Approach	3
1.3.2. Document Structure	4
1.4. State of the Art	5
1.4.1. Mg as Structural Material	5
1.4.2. Mg Wrought Alloys	6
1.4.3. Forming of Mg Alloys	6
1.4.3.1. Deformation Behavior	7
1.4.3.2. Recrystallization Behavior	8
1.4.3.3. Texture Evolution	9
1.4.4. Forging of Mg Alloys	10
1.4.5. Precipitation Hardening of Mg Alloys	10
1.4.5.1. Ca containing Mg Alloys	11
1.4.6. Lean Mg Alloys	14
1.5. Material and Methods	15
1.5.1. Alloy Design	15
1.5.2. Casting of AXMZ1000 Feedstock	15
1.5.2.1. Industrial Material Production	15
1.5.2.2. Remelting at LKR	16
1.5.3. Forming Processes	17
1.5.3.1. Stock Material Production by Extrusion	17
1.5.3.2. Forging at LKR	17
1.5.4. Heat Treatments	19
1.5.4.1. Homogenization	19
1.5.4.2. Solution Heat Treatment	19
1.5.4.3. Artificial Ageing	19
1.6. References	20
2. Magnesium for Forging Applications	25
2.1. Introduction	27
2.2. History	28
2.3. Basic Aspects of Magnesium Forging	29
2.3.1. Alloy Designations	29
2.3.2. Forming Behavior	30
2.3.3. Forging Stock	31
2.3.4. Die Design	31
2.3.5. Temperature Control	32
2.3.6. Lubrication	32
2.3.7. Trimming	33
2.3.8. Machining	33
2.3.9. Microstructure and Mechanical Properties	33
2.3.10. Heat Treatments	34
2.4. Magnesium Alloys for Forging Applications: Methodology	34

2.5. Forging of Magnesium Alloys containing Aluminum	35
2.5.1. Mg-Al-Zn-System	35
2.5.1.1. AZ31	37
2.5.1.2. AZ61	41
2.5.1.3. AZ71	42
2.5.1.4. AZ80	43
2.5.1.5. AZ91	47
2.5.2. Mg-Al-Mn-System	49
2.5.3. Mg-Al-Ca-System	50
2.6. Forging of Magnesium Alloys containing Zinc	53
2.6.1. ZK60	54
2.7. Forging of Magnesium Alloys containing Rare Earth Elements	58
2.7.1. WE43	59
2.7.2. Alloys with LPSO Structure	61
2.8. Forging of Biodegradable Magnesium Alloys	63
2.9. Forging of Various Magnesium Alloying Systems	66
2.10. Concluding Remarks	67
2.11. Appendix	69
2.11.1. CALPHAD calculations	69
2.11.2. Heat treatments and forming temperatures	70
2.11.3. Mechanical properties	72
2.12. References	79
3. Lean Wrought Magnesium Alloys	89
3.1. Introduction	91
3.2. Terms and Definitions	91
3.3. Basic Aspects of Alloy Development	93
3.4. Mg Alloys with a Low Alloying Content	96
3.4.1. Alloys containing Aluminium and Calcium	97
3.4.2. Alloys containing Zinc and Calcium	100
3.4.3. Alloys containing various alloying Elements	103
3.5. Concluding Remarks	105
3.6. Appendix	106
3.6.1. Additional Information	106
3.6.1.1. Sources for Literature Research	106
3.6.1.2. CALPHAD calculations	106
3.6.2. Alloy Overview	106
3.6.3. Mechanical Properties	109
3.7. References	116
4. Forging of AXMZ1000 Alloy on Industrial Scale	122
4.1. Introduction	124
4.2. Material and Methods	124
4.2.1. Material Design	124
4.2.2. Processing	125
4.2.3. Characterization	126
4.2.4. Processing Map	126
4.3. Results	127
4.3.1. Processing Window	127
4.3.2. Laboratory Forging Trials	128
4.3.3. Industrial Forging Trials	128
4.3.4. Microstructure	129
4.3.5. Tensile Properties	131
4.4. Discussion	132
4.4.1. Processing Window and Laboratory Forging Trials	132

4.4.2. Industrial Forging Trials	133
4.4.3. Microstructure and Mechanical Properties	135
4.5. Conclusion	136
4.6. References	136
5. Characterization of Isothermal Forged AXMZ1000 Alloy	139
5.1. Introduction	141
5.2. Design Considerations	141
5.3. Methods	143
5.4. Results	145
5.4.1. Processing Characteristics	145
5.4.2. Microstructure	146
5.4.2.1. Optical Microscopy	146
5.4.2.2. EBSD Measurements	148
5.4.2.3. AlMn Dispersoid Measurements	150
5.4.3. Tensile Properties	151
5.4.3.1. Tensile Testing	151
5.4.3.2. Fractography	151
5.4.4. Fatigue Measurements	153
5.5. Discussion	153
5.5.1. Microstructure	153
5.5.2. Tensile Properties	154
5.5.3. Fatigue Properties	156
5.6. Conclusions	157
5.7. Supplementary Materials	158
5.7.1. Extruded Stock Material	158
5.7.2. Dispersoid measurement	159
5.7.3. Fatigue Measurements	160
5.8. References	162
6. Summary & Outlook	165
A. Appendix	166
A.1. Abbreviations & Symbols	166
A.2. Unpublished Results	167

1. Introduction

1.1. Motivation

The need for a fundamental transformation of society and economy toward environmental sustainability and climate neutrality is probably the greatest challenge of our time. In particular, the energy, agriculture and transport sectors will have to change drastically in order to achieve these ambitious goals. In the transport sector increasing mobility of people and goods is causing a steady rise in energy consumption and CO₂ emissions [1]. This sector is responsible for about 30 % of the final energy consumption in Europe (2021) and thus represents the largest single energy consumer [2]. Notwithstanding new fuel and transportation concepts lightweight construction plays an increasingly important role in alleviating this development.

Modern light metals such as aluminum ($1/3$ density of steel) and magnesium ($1/5$ density of steel) represent a still largely untapped lightweight construction potential, compared to the state-of-the-art [3]. Consequently, the necessary transition in the energy and transport sectors will drastically increase the demand for specific raw materials; among other things, it is predicted that the consumption of Al in Europe will increase by 44 % till 2050, although primary production will remain unchanged [4]. An increased use of Mg as a structural material in lightweight construction could therefore provide sustainable support in this regard and increase the overall robustness of this important industrial sector. In view of the depletion of global raw material resources, which will come into focus in the coming decades, magnesium can be considered as non-critical and can thus make a long lasting and ecological sound contribution to economic development and stability [5; 6].

Magnesium has long been predicted to have great growth potential within a few years - especially in the automotive industry [7]. In reality, however, this development is still a long time coming. The reasons for this are numerous, and often the lack of know-how and insufficient development work are considered to be responsible. As early as 2001, Mordike and Ebert stated:

One of the reasons for the limited use of magnesium has been some poor properties exacerbated by a lack of development work. [7]

Since then, the situation has changed somewhat, as efforts with respect to development of magnesium wrought alloys have greatly increased, as indicated from the number of search results at the scientific database "ScienceDirect", see Figure 1.1. Although some disruptive improvements, e.g. superior corrosion resistance [8] or high strength [9], have been achieved in the scientific environment since then, the transfer to industrial applications is still limited.

Nowadays, the main reasons for the lack of industrial applications of Mg alloys are the small market size and the associated deficit of know-how. The possible advantages of Mg components have been neglected due to the suggested lack of competitiveness when compared to Al, especially with regard to the mechanical properties and processing behavior. However, most of the problems associated with the use of magnesium wrought alloys can easily be eliminated by state-of-the-art technological means and do not require any far-reaching measures to be solved.

A multitude of Mg alloys developed in recent years are characterized by above-average mechanical properties combined with good processability [10]. In particular, alloys with Ca as an alloying element have shown great potential in this regard, as they offer a wealth of advantages over conventional alloys. In addition to the good mechanical properties and age-hardening capabilities, Ca also improves the corrosion resistance, oxidation resistance and forming behavior of magnesium alloys [11]. Scientific investigations on these wrought alloys have been mostly focused on processing by extrusion or rolling, as sheet products and profiles represent the majority of the potential market [12]. Forgings,

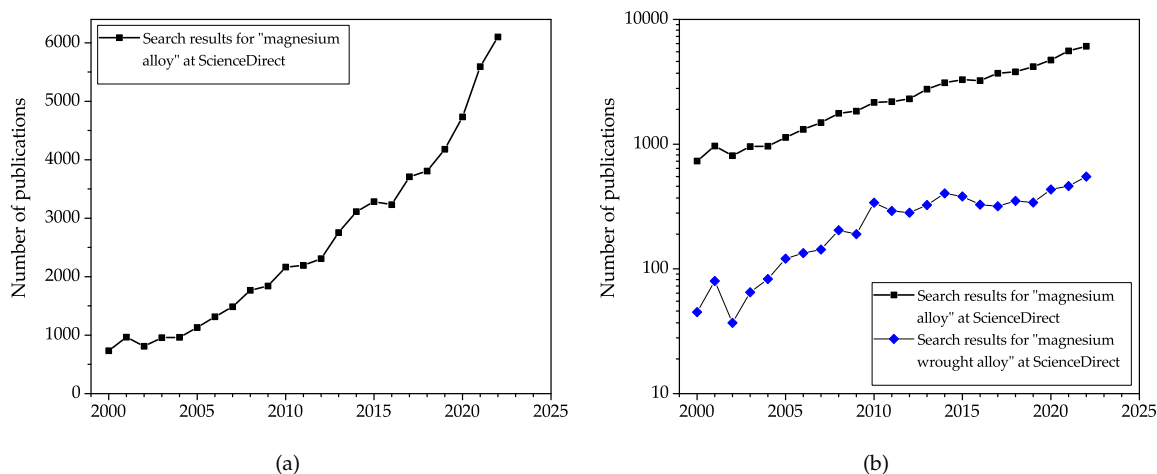


Figure 1.1.: Number of search results at the scientific database "ScienceDirect", shown annually from the year 2000 onward. Search was conducted in 03-2023.

which nevertheless play an key role in automotive applications, are mostly disregarded. Notwithstanding, the forging process shows some interesting advantages when compared to extrusion or rolling. The process layout is highly flexible, e.g. varying die and material temperatures, adjustable forming speed and die layout. The produced forgings represent nearly finished parts, allowing for a direct correlation between process and component performance, which is not possible in case of semi-finished products. Forging is therefore a very interesting forming method for new Mg wrought alloys, allowing the investigation of a broad range of process parameters and highlighting possible applications.

In this work an age-hardenable Mg-Al-Ca-Mn-Zn lean alloy is investigated in regards to forming behavior and resulting mechanical properties. The focus lies on the forging process which is analyzed on laboratory and industrial scale. This approach allows to combine scientific and industrial interests, providing manufacturers with the necessary know-how in terms of alloy composition, process parameters and resulting mechanical properties.

1.2. Aim of this Work

The use of light metals is indispensable in modern technology, which is reflected in the steadily rising consumption in recent years. Especially the transport sector is a main consumer of light metals, i.e. Al products. In the coming years it is expected that the demand will drastically increase [4], potentially causing cost and resource issues. The introduction of Mg wrought alloys in this market, fully focused on Al products, could increase the industry flexibility and robustness.

While Mg castings have already found their way into industrial applications, there is still a lack of acceptance for wrought products in the industry. This can be seen when comparing the segments of Al and Mg markets, see Figure 1.2. Wrought products only represent 3 % of the Mg market [13], which is dominated by castings. In the Al industry wrought applications are well established, the production of extrusions, rolled products and forgings encompass 66 % of the market volume (Germany 2019) [12].

Evidently the production performance is reflected in the available know-how and standardization of the used materials or, in the case of Mg wrought alloys, the lack thereof. The effort necessary to introduce a new material into an existing product portfolio is high, especially in highly regulated/standardized areas, e.g. mobility applications. The lack of adequate knowledge on Mg wrought alloys is apparent in industrial concerns regarding fundamental topics such as formability, processing, flammability,

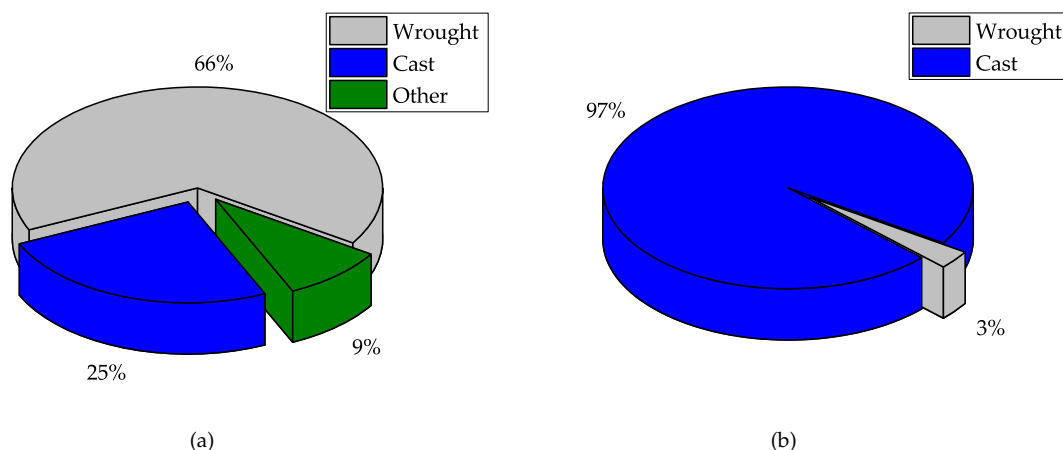


Figure 1.2.: Showing the distribution of market shares for (a) Al [12] and (b) Mg products [13], separated by half-finished (wrought) products, castings and others, e.g. powders.

corrosion behavior and mechanical properties.

This work aims to address some of the technological issues listed and to reduce reservations against the use of Mg wrought alloys on industrial level.

1.3. Approach & Document Structure

This doctoral thesis is embedded into the framework of the COMET project AMALFI (FFG No. 872641), a cooperation between industry, universities and research institutes. Most works were done and coordinated at the *Leichtmetallkompetenzzentrum Ranshofen GmbH* (LKR), industrial scale forging trials were done at *Krenhof GmbH*, while the *Montanuniversität Leoben* provided scientific support and in-depth material analysis in terms of a master thesis [14].

1.3.1. Approach

To introduce the forging industry, familiar with Al processing, into the topic of Mg wrought alloys, an age-hardenable Mg alloy was chosen as feedstock. This approach utilizes the common processing scheme consisting of homogenization, forming and age-hardening as used in 2xxx, 6xxx and 7xxx Al alloys.

The **State of the Art** (Section 1.4) gives an overview on Mg wrought alloys and their forming behavior. Detailed investigations focusing on (i) the forging process of Mg alloys in general and (ii) the alloy development and processing of Mg lean alloys can be found in Chapter 2 and 3, respectively.

The scientific literature showed only a neglectable amount of works on age-hardenable Mg forgings, even though many of the processed alloys could be artificially aged to some extent, e.g. AZ80. In contrast, lean alloys have not been analyzed regarding their forging behavior. Although some of them are specifically designed for age-hardening. Processing of these alloys mostly takes place by extrusion, coinciding well with the fact, that extruded stock is known to improve the mechanical properties of Mg forgings considerably.

The findings from scientific literature highlighted the lack of knowledge in this important field of application for Mg wrought alloys and confirmed the choice to investigate the forging behavior of age-hardenable Mg lean alloys in detail.

The selected Mg-Al-Ca-Mn-Zn alloy (AXMZ1000) can be considered a lean alloy, characterized by a low overall amount of alloying elements, which are used to the best possible effect. The alloy design

enables the formation of dispersoids for grain structure stabilization and precipitates for age-hardening capabilities. The lean characteristic on the other hand aims to enhance (i) the forming behavior by a low solute drag and (ii) the aging response by an adequate solution heat treatment window. To provide commercially available qualities the alloy was bought in industrial size batches and recast into the desired stock material sizes at the LKR.

Process investigations from forming trials to industrial scale forgings are described in Chapter 4. Material analysis and laboratory scale forgings were performed at LKR to determine the processing window and ensure adequate part properties.

Compression testing of the forging stock was used to calculate a processing map, providing information on the forming behavior based on the energy dissipation rate during the forming process.

The resulting forming window was verified in isothermal forging tests on laboratory scale. Thereby, the effect of processing parameters, forging stock and subsequent heat treatment was determined. Industrial forging trials took place at Krenhof, producing life sized automotive parts made from AXMZ1000 alloy. The chosen automotive control arm has a complex geometry and is forged in three consecutive steps. Forming experiments took place at standard production conditions, using an original forging die for Al alloys as well as the associated hydraulic forming press. Adaptions in processing, based on the laboratory trials, were investigated, aiming to produce well formed parts.

An analysis of the performance of AXMZ1000 forgings can be found in Chapter 5. To assess the overall performance of the used alloy, laboratory forged parts produced by a representative processing route were investigated in detail. The effect of stock material was analyzed and the influence on microstructure and mechanical properties evaluated. Grain size and material texture evolution provided important information on the tensile and the fatigue behavior measured as well as the damage mechanisms described.

1.3.2. Document Structure

The document structure of this doctoral thesis reflects the used approach fully. Chapter 1 provides an insight on the Motivation of this thesis and an overview of State of the Art concerning Mg wrought alloys. The chapter is concluded with an introduction of the used alloy and production methods.

An in-depth discussion on the forging of Mg alloys is provided in Chapter 2. The content of this Chapter correlates to a scientific review paper [15] published in the MDPI Journal Materials.

The topic of Mg lean alloys, materials with an overall low amount of alloying elements, is discussed in Chapter 3. The content of this Chapter correlates to a scientific review paper [16] published in the MDPI Journal Materials.

The forging process of the AXMZ1000 alloy, from laboratory trials to industrial scale forging is shown in Chapter 4. The content of this Chapter correlates to a scientific paper [17] published in the journal Springer Nature Applied Sciences.

An analysis of the isothermal forging process and AXMZ1000 alloy produced at 350 °C is shown in Chapter 5. The content of this Chapter correlates to a scientific paper [18] published in the Elsevier journal Material Science and Engineering A.

1.4. State of the Art

If the importance and technological readiness of a structural metal were to be described by their standardized alloy compositions, the differences between steel (> 5000 grades), aluminum (> 500 alloys) and magnesium (< 30 alloys) are clearly visible [13]. Nevertheless, the production of primary Mg has more than tripled since 1990 and has reached over 1000 kt per year in 2016, see Figure 1.3a. But this does not directly correlate to the use of Mg as structural material. Approximately $\frac{2}{3}$ of the produced primary Mg is used as alloying element in Al alloys and for the reduction or desulfurization in steel and titanium, shown in Figure 1.3b. The remainder is nearly solely used for cast products, i.e. high pressure die-casting, therefore wrought products currently play a negligible role on the market. This disparity between the use of cast and wrought products results from the ease of application for Mg castings when compared to wrought applications. Mg alloys show good castability, i.e. good melt flow behavior, allowing for complex part design. Additionally, low casting temperatures and reduced die-soldering phenomena increase mold-die lifespan, thereby allowing successful competition with Al products [19]. Wrought alloys on the other hand are often lacking when directly compared to their Al counterparts, which provide good forming behavior, age hardening capabilities and high strength. While this impression is mitigated when looking at the specific properties of Mg, highly relevant in case of lightweight construction, it must be acknowledged that the forming behavior of Mg alloys can be challenging.

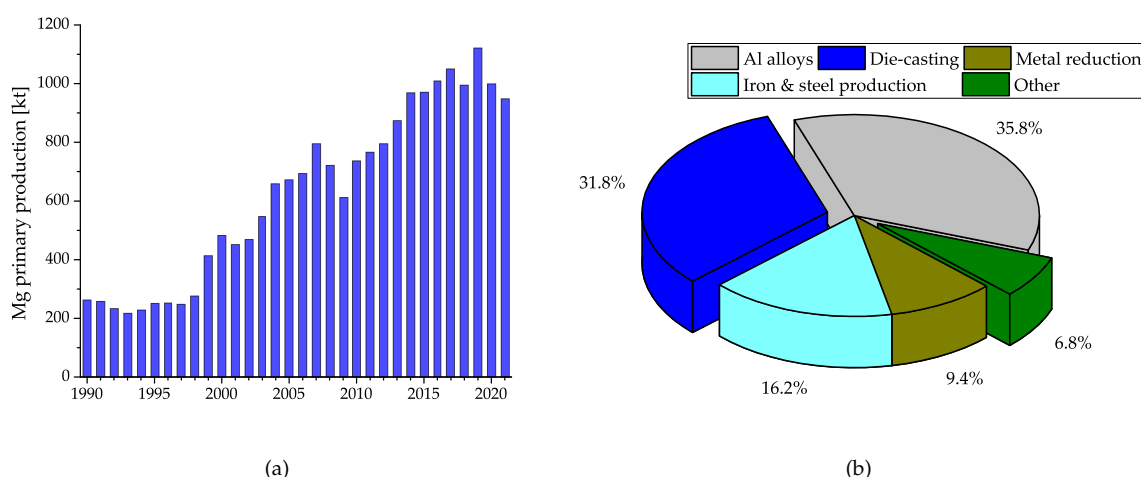


Figure 1.3.: Overview of primary production and use of Mg metal: (a) worldwide Mg primary production in 1000 tons per year [20–22]; (b) 2021 Mg metal market in % by end-user industry [23].

1.4.1. Mg as Structural Material

Mg is the lightest structural metal in use, weighing $\frac{2}{3}$ of aluminum or only $\frac{1}{5}$ of steel at 1.74 g cm^{-3} . As material density is the most important factor in lightweight construction [24], this fact alone repeatedly draws attention to Mg and its alloys, aiming for use in multiple applications, especially in the transport sector.

While the actual mechanical properties, e.g. Young's modulus (E), yield strength (YS) and ultimate tensile strength (UTS), of Mg alloys are usually lower than those of comparable steel or Al products, lightweight construction is strongly dependent on the combination of (i) specific properties, (ii) loading case and (iii) part design. As shown in Table 1.1 Mg alloys provide a good performance in terms of buckling stability of bars (\sqrt{E}/ρ) as well as bending stiffness of beams and buckling stability of plates ($\sqrt[3]{E}/\rho$), which are important qualities for part design [25].

While the material characteristics related to the Young's modulus can be easily compared, other specific features, e.g. related to tensile performance, have to be evaluated separately for each material used. These properties can vary strongly, depending on multiple factors such as alloy design and chemical composition, material processing and temper. Nevertheless, it is generally assumed that wrought products can achieve better (specific) properties than their cast counterparts, as they usually offer smaller grain sizes and a reduced amount of defects, e.g. pores and large primary phases. This explains the lasting interest in Mg wrought alloys, notwithstanding their challenging processing behavior.

Table 1.1.: Comparison of the specific and design properties of Mg with the structural materials steel and Al [25].

	density g/cm ³	Young's mod. GPa	spec. Young's mod.	buckling stability	bending stiffness
	ρ	E	E/ρ	\sqrt{E}/ρ	$\sqrt[3]{E}/\rho$
Steel	7.9	210	26.8	1.8	0.8
Aluminum	2.7	70	25.9	3.1	1.5
Magnesium	1.7	45	25.9	3.9	2.0

1.4.2. Mg Wrought Alloys

As has already been mentioned above, there is only a small number of standardized Mg alloys, mostly stemming from casting applications. Nevertheless, the definition of Mg wrought alloys shows a broad chemical spectrum, varying both in the utilized chemical elements as well as in the respective amount used. Variations range from commercially pure Mg (99.99 wt. %) to alloys with a few wt. % of alloying elements to highly alloyed materials of > 10 wt. % additions. Also the used alloying elements can be diverse, ranging from light metals, e.g. Al, to rare earth metals, e.g. Gadolinium and Yttrium, as described in ISO 3116-2019 and ISO 23694-2021.

Contrary to other structural materials Mg alloys are not strictly separated into casting and wrought alloys. The ISO 3116 lists AZ91, the single most used Mg casting alloy, as a wrought alloy as well. How this overlap of definitions emerged is unclear but it might stem from two factors: (i) as castings are the dominating industrially produced parts, easily available and already standardized alloys are adapted to be used in wrought applications; (ii) there is a tendency to combine casting and wrought processing, thereby aiming to utilize the overall good casting behavior to its fullest, e.g. liquid forging [26] and twin-roll casting [27].

As there is no strict definition of Mg wrought alloys regarding their chemical composition, it is of higher interest to concentrate on the deformation behavior of these materials in general and to provide some basic information on the challenges connected with Mg forming processes.

1.4.3. Forming of Mg Alloys

The formability of Mg alloys is strongly temperature dependent and limited at ambient temperatures. This is a clear disadvantage in case of room temperature forming operations, as well as a limiting factor for potential applications. Sheet metal components are mostly processed at room temperature (RT), e.g. by deep-drawing, thereby reducing processing cost, increasing surface quality and narrowing part size tolerances. Many structural applications require good room temperature forming behavior in use, e.g. crash structures depend on high energy absorption to increase passenger safety. In both cases, material processing and deformation in use, the low forming capabilities of Mg alloys at ambient temperatures limits their usability.

While this problem is mitigated in hot forming processes, which take place at raised temperatures anyway, additional challenges such as a strong texture development during directional forming or small processing windows have to be taken into account when using Mg alloys.

1.4.3.1. Deformation Behavior

The deformation behavior of Mg alloys is controlled by their hexagonal crystal structure. The inherent asymmetry of the unit cell, i.e. the a/c ratio, causes disparities in the applicable deformation directions, see Figure 1.4. Therefore, material deformation is possible using various slip systems and dislocation types such as (i) $\langle a \rangle$ slip on basal, prismatic and pyramidal planes and (ii) $\langle c+a \rangle$ slip on pyramidal planes. Additionally, Mg can deform by twinning in case of strain along the $[0001]$ direction of the crystal, called tensile or compressive twinning, corresponding to the loading direction.

Dislocation movement preferably takes place on close packed slip planes, i.e. planes providing a high density of atoms. Accordingly, deformation along the basal plane is strongly favored in Mg alloys. This behavior is reflected by substantial differences in the critical resolved shear stress (CRSS) needed for the activation of the various slip systems, see Table 1.2. Therefore, deformation at RT mainly takes place by dislocation movement on the basal plane or by twinning, but neither mechanism provides the necessary amount of slip systems for arbitrary deformation.

The additional activation of prismatic and pyramidal slip systems, which are needed to accommodate large strains during deformation, is only possible at raised temperatures. This is enabled by a reduction of the differences in CRSS with increasing material temperature, i.e. while the CRSS of basal $\langle a \rangle$ slip and $\{10\bar{1}2\}$ twinning is mostly constant the CRSS of the other slip systems drops with increasing temperature [28].

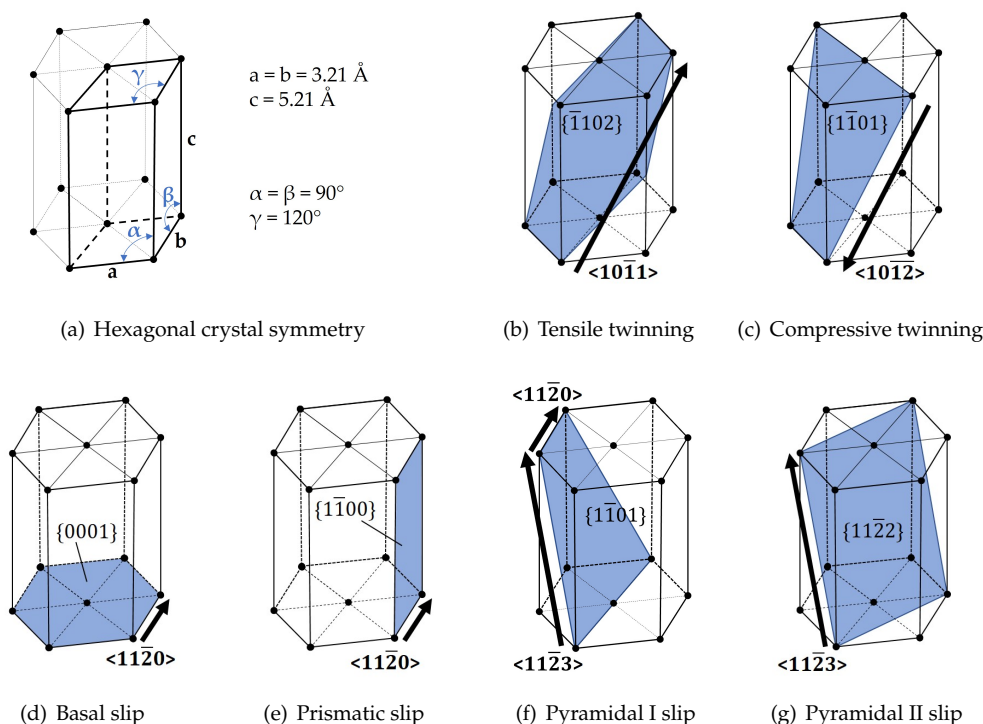


Figure 1.4.: Hexagonal crystal symmetry of Mg and available slip and twinning directions.

Table 1.2.: Overview of critical resolved shear stress (CRSS) ratio for various slip systems in Mg-Al alloys with changing Ca and Zn contents [29].

Slip System	Directions	Mg-1Al-0.05Ca [†]	Mg-1Al-0.1Ca [†]	Mg-2Zn-1Al-0.1Ca [†]
Basal <a> slip	3	1	1	1
Tensile twinning { $\bar{1}102$ }		4	4	5
Prismatic <a> slip	3	7	6	5
Pyramidal I <a> slip	3	10	12	8
Pyramidal I <c+a> slip	6	19	24	21
Pyramidal II <c+a> slip	6	52	32	26

†: CRSS ratio based on activity of basal <a> slip.

1.4.3.2. Recrystallization Behavior

It is well known, that the deformation behavior of metals is intrinsically linked to the material grain size, known as grain boundary hardening or Hall-Petch effect. The yield strength is increased and the deformation processes of grain boundary sliding and grain rotation gain importance with reducing grain size [30]. In Mg alloys also the twinning behavior is influenced, showing reduced activity in smaller grains [31; 32]. The combination of these effects as well as the reduced texture, caused by the increased spread of orientations, resulting from the increased amount of grains, have been allocated to the enhanced deformation behavior of Mg alloys with fine grained microstructures [33].

Mainly deformed materials benefit thereof, as the described behavior only starts to take effect in grain sizes < 3 μm and cast microstructures usually feature coarser grains. To reach adequate grain sizes the original microstructure, produced by casting, has to be decomposed by recrystallization (RX) processes, which can occur in multiple ways in Mg alloys.

The formation of new grains can happen during (i) (warm) forming operations, called dynamic recrystallization (DRX); (ii) meta-dynamically, meaning directly after deformation while the material temperature is still increased; or (iii) during heat treatments, referred to as static recrystallization (SRX). In all cases, sufficient deformation energy must be stored in the microstructure, represented by an increased dislocation density throughout the grains [34–36].

When producing Mg parts especially the DRX is of high importance as it can enhance material deformation behavior during the forming processes.

Not all metals feature DRX, e.g. Al alloys need particles to stabilize the grain boundaries to show this effect. In case of Mg no particles are needed, the combination of low stacking fault energy, limited slip system availability and high grain boundary diffusion rate are considered sufficient to enable DRX [37]. The low stacking fault energy of Mg alloys is responsible for increased twinning behavior and enhanced formation of partial dislocations. Thereby the recovery phenomena are reduced and stored strain energy conserved. The high grain boundary diffusion rate on the other hand, allows for an eased absorption of dislocations into subgrain boundaries, accelerating the formation of high angle boundaries and the creation of new grains.

DRX predominantly takes place at grain boundaries, twins, shear bands and near larger particles [10]. This indicates, that the accumulated strain energy is distributed non-uniformly throughout the microstructure. Therefore, the recrystallization behavior of Mg alloys is often described as discontinuous, meaning a heterogeneous nucleation of new grains, occurring in a fast and discontinuous manner.

In ref. [38] the DRX process within twinned structures is exemplarily described: existing low angle grain boundaries repeatedly absorb dislocations, created during deformation, subsequently changing into high angle boundaries. In the described example the already existing twin boundaries can be integrated into the newly recrystallized grains, see upper Section of Figure 3.2b. This type of RX process often creates bi-modal grain structures, also known as necklace structure, consisting of fine DRX grains and (deformed) remnants of the initial microstructure.

As the size of these DRX grains can easily reach below $2\ \mu\text{m}$ increased activation of grain boundary sliding and grain rotation has been reported. While the exact mechanisms are not fully understood yet, e.g. sliding of similarly orientated grain groups, it has been shown that these fine grains can ease deformation processes considerably [39].

1.4.3.3. Texture Evolution

The already described unbalanced activation of slip systems amplifies texture development, even at raised temperatures. This can lead to pronounced basal textures in wrought products, especially during directional forming processes. These strong basal textures further influence the forming behavior in subsequent processing steps, especially at ambient temperatures. Some examples for this effect of material anisotropy are the increased tensile strength in extrusion direction in case of profiles and the decreased drawing depth reported in sheet-forming.

In depth investigations show dominating basal textures in all Mg rolled products. While extruded profiles have been found to possess a larger variety of possible textures, basal fiber structure is still found in most alloys [10]. During forming processes the $[0001]$ direction of the Mg crystals is shifted to point perpendicular to the process direction, while $[10\bar{1}0]$ is orientated along the same. In typical Mg alloys, i.e. AZ series, the strong basal texture can be separated into a deformation and a recrystallization texture, which is turned around the $[0001]$ axis by $\sim 30^\circ$, aligning $[2\bar{1}10]$ to the rolling or extrusion direction, see Figure 1.5.

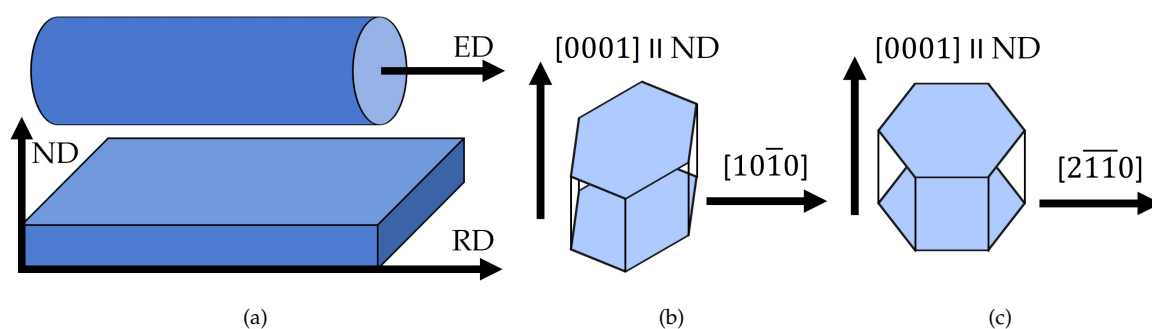


Figure 1.5.: Scheme of basal texture development, showing (a) sheet and profile axes with production direction designated as rolling (RD) or extrusion direction (ED), respectively. Orientation of Mg crystals in (b) as-formed and (c) recrystallized state according to ref. [10].

In case of REE or Ca containing alloys, the direction of $[0001]$, i.e. the normal orientation to the production direction, is fixed less sturdily and slight shifts about various axes are possible. These kind of textures, as well as the linked lower maximal intensities, are associated with improved deformation behavior. Nevertheless, it has to be kept in mind, that processing conditions can play a pivotal role in the creation of such textures as well [10].

As has been discussed, the low RT formability and pronounced material anisotropy of Mg wrought products are directly linked to the slip behavior and production process via the material texture developed therein. Therefore, it is not surprising that there are multiple attempts to influence the forming behavior and texture development of Mg wrought products. Next to process adaptations, e.g. cross rolling [40] the alloy customization by (micro-) alloying with, e.g. REE or Ca, is an accepted practice [10]. The effect of alloying additions on the CRSS of a Mg-Al alloy is exemplary shown in Table 1.2, where the combined effect of Zn and Ca is visible.

Additionally research on the influence of alloying elements on the microstructural deformation behavior, such as slip activation energies, dislocation movement and stacking fault energy, is ongoing using experimental investigations as well as theoretical approaches [41; 42].

1.4.4. Forging of Mg Alloys

Forging is a process which is able to deal well with the inherent weaknesses of Mg as a wrought metal, e.g. needing raised forming temperatures and moderate forming speed. The forging process predominately takes place at raised temperatures for all materials, accommodating the necessity of additional slip system activation in Mg alloys. Especially forging processes which apply hydrostatic stresses during forming, e.g. closed-die forging, show a high suitability for the use with Mg alloys. The moderate forming speeds (e.g. 10 mm s^{-1}) beneficial for Mg forming can be easily accommodated by the use of hydraulic presses [43]. This is industrially possible as a slightly reduced forming speed does not cause substantial losses in productivity, thereby contrasting with extrusion or rolling. The processing of Mg alloys is further simplified by the possibility to utilize different material and die temperatures, an important feature to make use of the whole forming window available.

Mg wrought products are known to produce sharp textures which can strongly influence mechanical part properties. Forgings in general show reduced texture intensities when compared to sheets and extrusions, as the process is not fully directional. Nevertheless, Mg forgings can profit from using deformed stock material, i.e. extrusions, as small grain sizes are regarded as beneficial for the forming behavior [43]. Also the mechanical strength can be improved, e.g. in extrusion direction of the stock material.

While forgings made from Al alloys are often age hardened, i.e. peak aged, this is not necessarily the case for Mg forgings. While some works report T5-temper for Mg forgings, the use of products in T6-temper seems to be uncommon [15; 43].

Further information on this topic of Mg forgings can be found in Chapter 2, which has also been published in the shape of a scientific paper [15].

1.4.5. Precipitation Hardening of Mg Alloys

The principle of precipitation strengthening is known and applicable in Mg alloys. The ageing process, which uses the formation of nano-scaled particles to impede dislocation movement is dependent on the used alloying elements and the microchemistry controlling phase formation.

While Mg alloys can be age hardened using the heat treatment sequence of (i) solution heat treatment and (ii) artificial ageing to peak hardness (T6-temper), the solutionizing step is often disregarded, producing solely artificially aged material (T5-temper). The use of the T5-temper is not motivated by an above-average precipitation effect, but rather by process limitations. In case of Mg castings, representing over 90 % of the produced parts, solution heat treatment is known to cause part warpage, due to quenching, while gas filled porosities can cause blisters on the part surface [44; 45]. Wrought alloys on the other hand are often used in the as-formed state (F-temper) as the strength of the deformed microstructure can be on the same level as achieved by peak-aged material [43; 46]. This originates from dynamic recrystallization of Mg alloys during warm forming, providing small grain sizes ($<10 \mu\text{m}$) in F-temper and thereby enabling Hall-Petch hardening. These fine grains are then coarsened during age hardening, especially by the high temperatures used during the solution heat treatment [47–49]. The application of ageing heat treatments on Mg alloys can in many cases be considered as an exchange of hardening mechanisms, from grain-boundary to precipitation strengthening [47]. Nevertheless, additional effects such as changes in texture or increased ductility by recovery processes must not be disregarded. Therefore, it is obvious that the expedience of age hardening in Mg products is directly connected to the alloy composition, the used production processes and designated part applications.

As already discussed in Section 1.4.3 Mg alloys have preferred deformation modes, i.e. basal slip, which are used for the majority of dislocation movement. Consequently, the position and shape of the precipitates formed in the Mg matrix influences the impact on dislocation movement and thereby the resulting hardening effect [50]. This effect is calculated, based on an Orowan equation, in ref. [51] for non-shearable precipitates. While rod shaped precipitates can achieve the highest number density,

the lowest inter-particle spacing can be realized by plate shaped intermetallic phases (IMP) on the pyramidal planes (Fig. 1.6a). Thereby causing the largest increase in material strength, when assuming a deformation using basal slip.

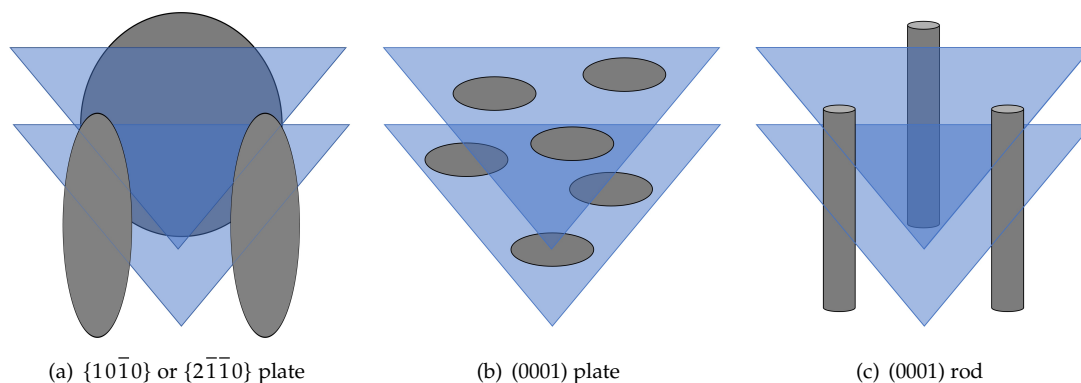


Figure 1.6.: Scheme of typical shapes and positioning of precipitates in Mg alloys, as discussed in ref. [51]. Intersecting (0001) planes (basal slip planes) are shown in blue.

As Mg also deforms readily by $\{10\bar{1}2\}$ twinning the positioning of the precipitates change accordingly. This was investigated in ref. [52] by crystal plasticity simulations. It was found that basal plates of the parent grain are especially effective against basal slip in twinned regions as well as in suppressing twin growth. Additionally, the use of precipitates in the shape of basal plates is assumed to reduce material anisotropy by hampering twinning and they show a low influence on prismatic slip. In Refs. [53; 54] the effect of dilute alloying additions on the interaction of precipitate position and number density are experimentally investigated. It was shown, that the precipitate density can be increased drastically when the phase size is reduced or IMP orientation changes, e.g. from basal plates to prismatic plates, also an increase in material hardness was reported.

Further studies on the interaction of precipitates and dislocation movement have been done for $Mg_{17}Al_{12}$ [55] and Mg-Nd phases [56]. The influence of cold deformation on the precipitation behavior is described and reviewed in [57], as well as in [58] where a hardening effect was found in pre-strained and annealed material.

The effect of precipitation hardening is thought to be most pronounced in Mg-RE alloys [51; 59], using prismatic precipitate plates for hardening. These alloys and their microstructure have been investigated by multiple authors, showing precipitation hardening over a wide range of alloy compositions [50].

But also standardized RE free alloys, i.e. the AZ series, are known to show age hardening capabilities [60]. For this purpose, the precipitation of β - $Mg_{17}Al_{12}$ phase can be used. As the Mg matrix can contain up to 12.7 wt.% of Al in a super saturated solid solution (SSSS), the hardening potential of these alloys correlates well to the Al content of the chosen alloy. This has been exemplarily shown in [60], while no age hardening was found in AZ31, alloys like AZ61 and AZ91 showed hardening response by appropriate heat treatments. However, the $Mg_{17}Al_{12}$ phase can be considered to have a lower hardening potential, when compared to the effect of other precipitates. Nevertheless, the high phase fraction achievable by the use of $Mg_{17}Al_{12}$ can be utilized to mitigate this shortcoming [61].

1.4.5.1. Ca containing Mg Alloys

In recent years Ca containing Mg alloys have increasingly come into focus, not least for the hardening possibilities available in these systems. It has been reported that the combination of REE and Ca shows

synergetic effects [62] and Ca can even be used as a substitute element in RE alloys, replacing REE in the precipitates used for hardening [63].

Ca has also been used in **Mg-Zn alloys** with good performance, these alloys are often discussed regarding medical applications, as they are known to be bioresorbable [64]. Additionally, low grain sizes can be realized in castings by grain refinement using Zr.

The focus regarding influence on hardening behavior can be set on the binary Mg-Ca and ternary Mg-Ca-Zn phases [65]. The sequence of phase formation has been investigated in detail in ref.[66]. Using a ZX20 alloy it was shown that the Mg-Ca-Zn phases evolve from Zn-Ca-rich globular clusters by forming G.P. zones and subsequently coherent $\text{Ca}_2\text{Mg}_6\text{Zn}_3$ phases; the equilibrium phase is assumed to be $\text{Ca}_2\text{Mg}_5\text{Zn}_5$. The largest increase in hardness was found to be provided by the formation of G.P. zones.

G.P. zones and solute atoms have also been found responsible for increasing material strength in pre-strained and annealed Mg-0.3Zn-0.1Ca sheets. While no hardening effect was found in solely aged sheets, the pre-strained material was strengthened by dislocation pinning [58].

Next to age hardening the precipitation of hardening phases, e.g. Mg_2Ca , has repeatedly been used to hamper grain growth during processing, thereby improving material performance [57; 67].

The **Mg-Al-Ca system** is of highest interest regarding this work and the therein used Mg-Al-Ca-Mn-Zn alloy (AXMZ1000). The phase formation in this system is regulated by the available Ca and Al in the Mg matrix. With rising Al/Ca ratio Mg_2Ca (C14, hexagonal), $(\text{Al}, \text{Mg})_2\text{Ca}$ (C36) and Al_2Ca (C15, cubic) will precipitate, while the $\text{Mg}_{17}\text{Al}_{12}$ is formed only at high Al and neglectable Ca contents. It is known, that predominately Al_2Ca (C15) phases will form if the Al/Ca ratio is > 0.8 [68–70], see Figure 1.7. This is of technical relevance, as the phases mainly used for hardening are within the precipitation sequence of the Mg_2Ca and Al_2Ca .

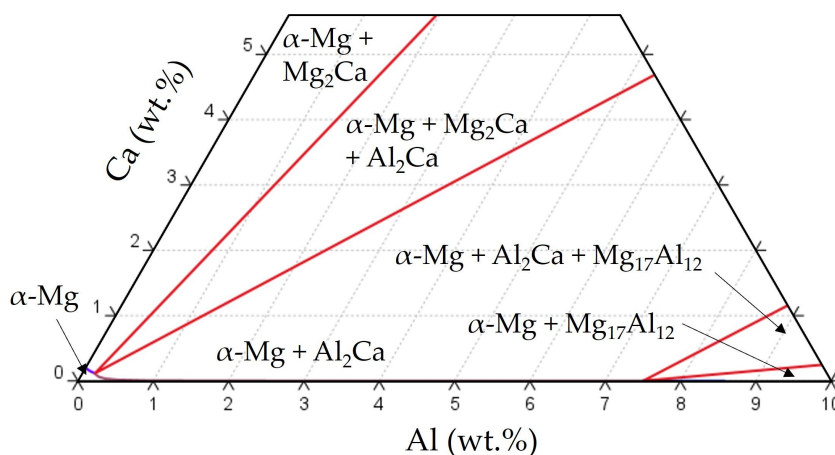


Figure 1.7.: Isothermal section of the ternary Mg-Al-Ca phase diagram at 350 °C.

The effect of Al/Ca ratio as well as the interaction with further alloying elements of Mg-Ca-Al alloys was investigated in [71]. It was found that the precipitation of Al_2Ca phase is higher efficiency in both formation and hardening effect, when compared to Mg_2Ca . This is explained by the larger lattice mismatch expected in the Mg_2Ca phases. The ageing effect of Mg_2Ca is described as limited in ref. [72] as well, due to the coarse phase appearance, caused by the low solubility of Ca in the Mg matrix. Nevertheless, the formation of Mg_2Ca can be enhanced by further element additions, e.g. Zn, causing a reduction of lattice mismatch (compare Table 1.3).

Table 1.3.: Examples for precipitation sequences of intermetallic phases in magnesium alloys.

		Precipitation sequence			Source	
Mg-Al	SSSS	→	Mg ₁₇ Al ₁₂ bcc (0001) _α plate/lath		[24]	
Mg-Zn	SSSS → G.P. zones	→	β' ₁ Mg ₄ Zn ₇ monoclinic [0001] _α rod	→	β' ₂ MgZn ₂ hcp (0001) _α plate	[24]
Mg-Zn-Al[†]	SSSS → G.P. zones	→	<i>i</i> icosahedral or diamond shape	→	Φ and/or T Φ: orthorhombic (0001) _α lath	[24]
Mg-Al-Ca	SSSS → ordered G.P. zones hcp monolayer (0001) _α disc	→	C15 Al ₂ Ca fcc (0001) _α plate		[24]	
Mg-Ca-Zn	SSSS → ordered G.P. zones hcp monolayer (0001) _α disc	→	η' MgZnCa hcp (0001) _α plate		[50]	
Mg-Sn(-Zn)	SSSS	→	β Mg ₂ Sn fcc (0001) _α plate/lath {1122} _α plate/lath [0001] _α rod/polygon		[50]	

†: sequence not well studied

SSSS: super saturated solid solution

fcc: face-centered cubic, bcc: body-centered cubic, hcp: hexagonal close-packed

The formation of **Mn containing phases** in these alloys will be discussed briefly for the sake of completeness. Mn is an often used alloying element in Mg alloys, as it is known to improve the corrosion stability by binding impurities, e.g. Fe. IMPs containing Mn are not usually considered as phases used for age hardening. They form at high temperatures, as primary particles in the melt and during subsequent heat treatment or warm forming steps. But unlike typical IMPs used for precipitation hardening Mn containing phases cannot be solutionized in Mg alloys, as their dissolution temperature is usually higher than the solidus temperature of the alloy.

Nevertheless, in case of wrought alloys, the positive effect of Mn containing dispersoids is repeatedly mentioned in scientific literature. Their use is mainly attributed to a stabilization of the microstructure, i.e. retardation of grain boundary mobility by Zener drag. This was verified by investigations on Mn dispersoids in an Mg-Al0.6-Ca0.28-Mn0.25 alloy (homogenized and extruded) [49], showing that they play a neglectable role in case of precipitation hardening, with a calculated contribution of ~ 8 MPa. The low material grain growth tendency on the other hand was largely attributed to these IMPs, demonstrating their ability to act as obstacles for grain boundary movement.

This positive effect on the homogenized and extruded microstructure of a lean AXM alloy was also described in [73], where high die exit speeds (60 m min^{-1}) were achieved only with Mn additions. While the exact reasons for this material behavior were unclear, the optimum Mn content for this alloy was found to be 0.4 wt. %.

Nevertheless, Mn containing IMPs have also been found to influence the material behavior during their formation stages. In a cast Mg-Al2.2-Ca2.0-Mn0.3 alloy enhanced creep resistance was attributed to the influence of Mn by changes in G.P.-zone formation and improved solid solution strengthening by Ca [74].

The exact phase formation is still under discussion as there are multiple possibilities for Mn containing compounds in Mg-Al alloys [75]. This has also been verified experimentally, as e.g. phases of the type Al_8Mn_5 [76; 77], Al_2Mn_3 [76] and $\beta\text{-Mn}$ [49; 77] have been reported in these materials.

It can be concluded that precipitation hardening is a viable way of strengthening Mg alloys, but the currently realized hardening potential has to be considered lower than in typical Al alloys. This is directly related to usually lower number density and aspect ratio of the hardening phases in Mg alloys [51]. Nevertheless, it has to be kept in mind that the phase formation sequences in Mg alloys are highly diverse and while a multitude of interaction between alloying elements and IMPs have been reported, research on this complex topic is ongoing.

As already mentioned before, investigations and improvements on age hardenable Mg alloys can lead to the use of low alloyed materials, as apparent in the already discussed works and further analyzed the subsequent sections.

1.4.6. Lean Mg Alloys

In recent years the scientific community strongly increased their activities in the field of Mg lean alloys, i.e. alloys with a reduced overall amount of alloying elements [10]. These alloys are specifically designed for improved performance in particular fields of application, the used alloying elements and their contents are therefore individually chosen. Especially two interesting features, for this work, can be found in the already existing portfolio of these alloys: (i) high production speeds and (ii) increased age hardening capabilities.

Also the alloys of the Mg-Al-Ca system are increasingly investigated in regards to their age hardening performance. Additionally, it has been shown, that these materials can be produced with high extrusion speeds, a combination making them especially attractive for industrial applications.

Further information on this topic of Mg lean alloys can be found in Chapter 3, which has also been published in the shape of a scientific paper [16].

1.5. Material and Methods

1.5.1. Alloy Design

The Mg alloy investigated in this work uses the alloying elements Al and Ca aiming to utilize the age-hardening capabilities available in this system. To make full use of the typical artificial ageing sequence, i.e. solutionizing and subsequent ageing heat treatment, a solution heat treatment window is needed. In the used Mg-Al-Ca-Mn-Zn alloy this is achieved by an overall low amount of alloying elements. Otherwise the Ca-containing phases could not be fully solutionized and primary phases would form directly from the melt. Next to the overall amount, the formation Ca containing intermetallic phases is influenced by the Al/Ca ratio. To achieve the highest precipitation hardening effect in the artificial ageing process, the pre-cursor phases of Al_2Ca have to be used [50]. This is achieved by a Al/Ca ratio of 1.9, used for the design of the chosen AXMZ1000 alloy.

Additionally to the age hardening capabilities already described, the use of Ca as alloying element is known to increase non-basal slip activities and reduce oxidation tendencies of Mg alloys [78]. Thereby improving the forming behavior, reducing texture intensity and increasing oxidation stability during heat treatments.

Further alloying elements used in this alloy are Mn and Zn in low concentrations (<0.5 wt. %). Mn is mostly used to improve the corrosion behavior of Mg alloys, but in this case also the formation of AlMn dispersoids is a key aspect. These particles are desired to form during homogenization heat treatment and are used to reduce grain growth throughout the processing steps at raised temperatures [49]. The addition of Zn aims for multiple effects, (i) further improvement of the non-basal slip behavior in combination with Ca [79; 80] and (ii) increased mechanical properties by a reduction of potential Ca-clusters on the grain boundaries [29].

The chemical composition of the chosen AXMZ1000 alloy is given in Table 1.4, with the content of nominal alloying elements reaching only 1.7 wt. %.

Table 1.4.: Nominal and actual chemical composition of the AXMZ1000 alloy given in wt. %. Actual chemical composition was measured by optical emission spectroscopy.

	Al	Ca	Mn	Zn	Si	Fe	Mg
nom.	0.75	0.40	0.30	0.25	–	–	Rem.
act.	0.65	0.44	0.31	0.24	0.023	0.008	Rem.

1.5.2. Casting of AXMZ1000 Feedstock

The alloy composition of AXMZ1000 has been specifically designed for wrought processing, i.e. forming and heat treatment processes, the castability has only been of minor interest in the design considerations. This is apparent in challenges in the casting process: (i) as the overall alloying content is low, even small deviations from the nominal composition are easily noticeable (valid for both alloying elements and impurities), (ii) re-productibility with exactly the same chemical composition is aggravated, (iii) the grain size of cast microstructure is coarsened, including a larger spread of the size measurements, when compared to higher alloyed materials, e.g. AZ91.

1.5.2.1. Industrial Material Production

To emulate the industrial process realistically, the alloy was produced on industrial scale (1 t batches) at *non ferrum GmbH*. The use of industrial grade material also explains the impurities found in the alloy, see Table 1.4. The main production method for primary Mg metal is the Pidgeon process, which uses ferrosilicon for the reduction of MgO. The Si and Fe impurities in the AXMZ1000 alloy are therefore residues from the production process of the primary Mg metal used.

The received ingots (see Figure 1.8a) have been remelted and cast in the desired shapes, i.e. round billets and square plates, by low pressure die casting (LPDC), providing feedstock for the extrusion and forging trials, respectively. This approach of remelting industrial produced material has the advantage of a consistent alloy composition throughout the experimental trials, i.e. if additional feedstock has to be produced.

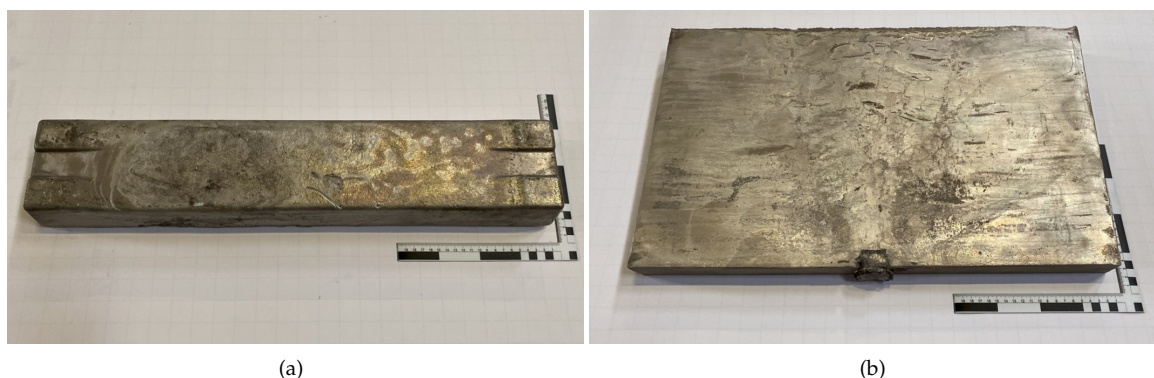


Figure 1.8.: Pictures of (a) industrial cast ingot ~8 kg, (b) plate produced by LPDC ~15 kg.

1.5.2.2. Remelting at LKR

The industrial produced material was processed by LPDC, which provides advantages in respect to process stability, melt quality and reduced atmospheric interaction when compared to gravity casting. The used casting equipment, with a setup for the production of round billets, is shown in Figure 1.9.

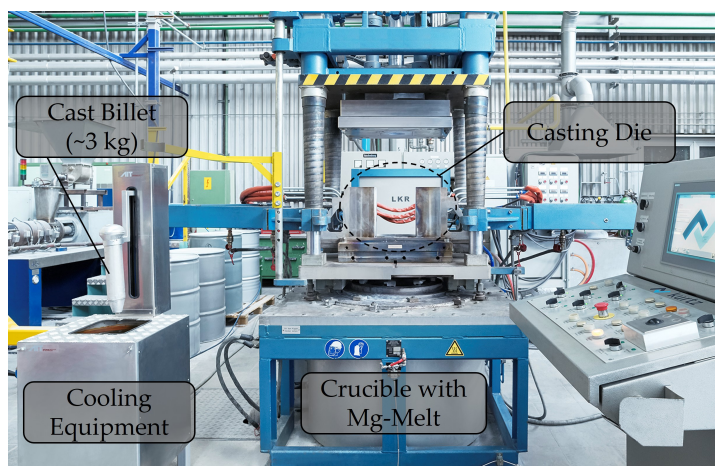


Figure 1.9.: Pictures of low pressure die casting machine (AK92, Kurtz GmbH & Co. KG) at LKR Ranshofen. Original picture ©AIT Austrian Institute of Technology/LKR Leichtmetallkompetenzzentrum Ranshofen.

The AXMZ1000 alloy was cast into two different shapes: square plates (570 × 45 × 300 mm) and round billets (∅ 75 × 275 mm). This approach was necessary to provide the stock material for the different forming processes. The material cast into plates is directly used in the forging trials, the chosen plate size allows for the machining of both, laboratory and industrial sized forging stock. Round billets on the other hand are necessary to provide stock material for the extrusion process.

The difference in geometry, plate and round billet, unit weight (~15 kg and ~3 kg), as well as resulting cooling speeds causes differing microstructures. As the extrusion process reshapes the grain structure

of the round billets fully, disparities in the original cast grain size are of minor interest in this case. On the other hand, the formation of primary particles and dispersoids precipitated in the homogenization process might have an influence on the final forged parts. The homogenized microstructures of both types of castings are shown in Figure 1.10, the possible effects on the forged parts are discussed in Chapter 5.

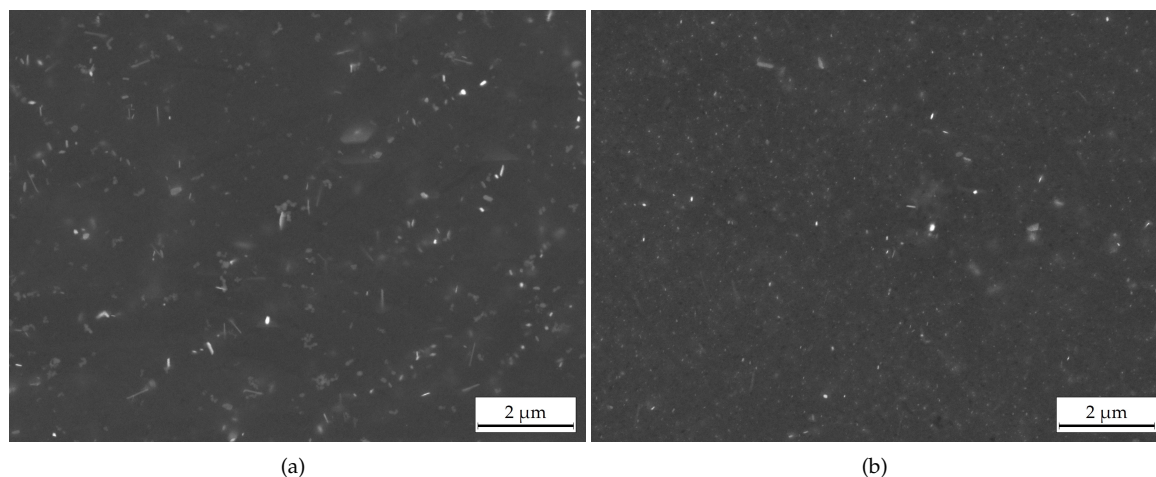


Figure 1.10.: SEM (BSE) pictures of Mn-containing phases in the homogenized microstructure of (a) plate shaped casting, (b) round cast billet.

1.5.3. Forming Processes

While the forging process is clearly the main focus of this work, the stock material can play an important role in the processing behavior as well as in the final part properties. The comparison of cast and extruded forging stock is therefore a focal point in the investigations done, see Chapter 5.

1.5.3.1. Stock Material Production by Extrusion

Extruded stock material was produced at 400 °C using a ram speed of 2 mm s⁻¹. The round feedstock (∅ 48.5 mm) was extruded to square profiles (12 × 25 mm). As the container of the extrusion press had a size of ∅ 50 mm, corresponding to the diameter of the compressed billet, an extrusion ratio of 6.5 is achieved. The used extrusion press as well as the feedstock and the produced profile is shown in Figure 1.11.

1.5.3.2. Forging at LKR

Forging took place on a hydraulic 160 t forming press with a ram speed of 10 mm s⁻¹. To allow easy material analysis a forging geometry based on the design of a piston rod was chosen. A heat-able forging die was used to produce these parts in a two step forging process, consisting of pre-forging and final forging. The hydraulic press, forging die and resulting forgings are shown in Figure 1.12a-c. The used stock material had a square cross-section (12 × 25 mm), corresponding to the size of the extruded profiles. To lubricate the forging die, thereby improving form filling and reducing sticking, a graphite slurry (BONDERITE L-FG F 599AL), diluted 1:5 with water, was applied by spray-gun.

While differences in material and die temperatures during forging operations are common practice, the laboratory forgings in this work were done at isotherm conditions only. The material and die were heated to the same temperature and the forming process took place without intermediate reheating of the material. As the chosen isotherm forming temperatures varied from 250 to 500 °C, material response changed accordingly. This was visible in the forming behavior as well as in the flow stress of



Figure 1.11.: Pictures of (a) the used 1.5 MN extrusion press (NEHP 1500.01, Müller Engineering), (b) cast feedstock and extruded square profile.

the Mg alloy, see Figure 1.13a. The output of the hydraulic press was limited to 160 t, which proved to be insufficient for forming low temperatures, as shown in preliminary trials using round forging stock ($\varnothing 22 \times 180$ mm). While the produced forgings were fully formed, the part thickness increased noticeably with lower forming temperature. To achieve a constant part thickness and allow for an accurate analysis, square forging stock (12×25 mm) with two different lengths was used in the laboratory trials, resulting in two different part designs. These measures kept part thickness of the forgings mostly constant, with maximum deviations of ~ 0.5 mm, see Figure 1.13b.

Shortened piston rods (stock material length: 95 mm) provided information over the full temperature range (Chapter 4), full length piston rods (stock material length: 180 mm) were used for in-depth investigations at a forming temperature of 350°C (Chapter 5). The different part lengths had no major influence on subsequent analysis, in case of tensile measurements the tested sample volume remained unchanged. Only the inner section of the piston rods is used for the machining of samples, the reduction in overall sample length was compensated by decreasing the areas used for clamping.

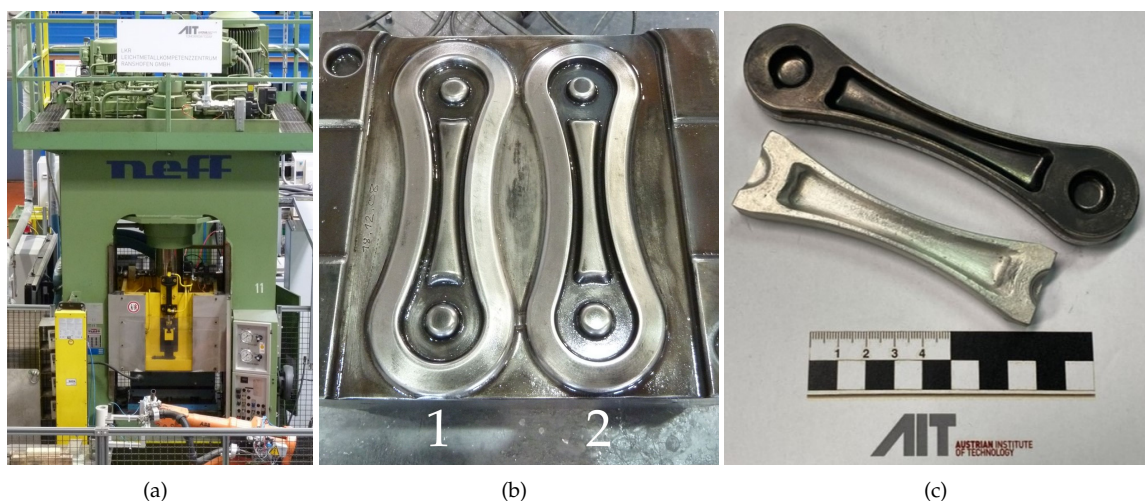


Figure 1.12.: Pictures of (a) the used hydraulic 160 t forming press (DZP 160, Walter Neff Maschinenbau GmbH), (b) forging die, with numbers indicating forming steps, (c) full length and shortened piston rods as produced in the laboratory forgings.

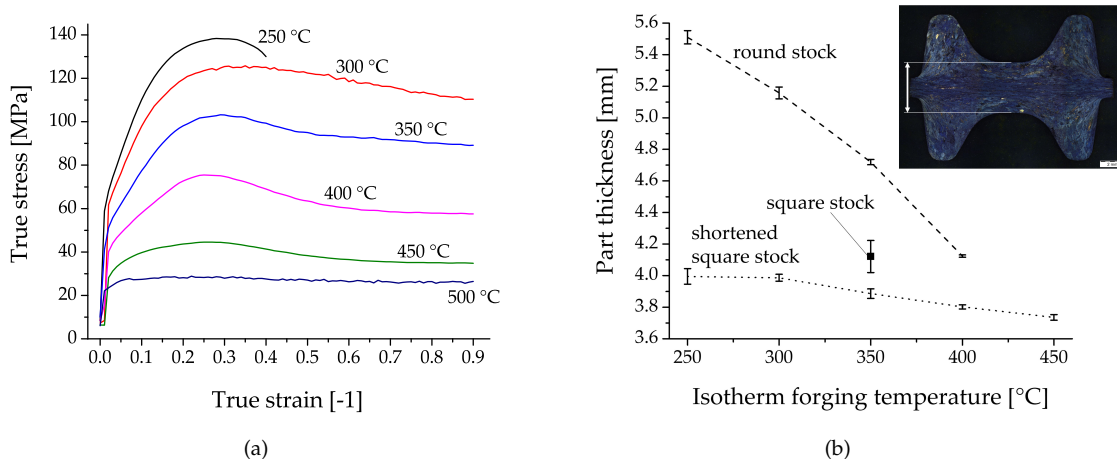


Figure 1.13.: Showing (a) stress-strain curves from compression testing at various temperatures, using a strain rate of 0.1 s^{-1} ; (b) changing part thickness of forged piston rods, made from different stock material geometries, with rising isotherm forging temperature.

1.5.4. Heat Treatments

The used AXMZ1000 alloy was designed with the classical processing scheme of age hardenable alloys in mind. Therefore the heat treatment steps of (i) homogenization, (ii) solution heat treatment and (iii) artificial ageing play an important role.

1.5.4.1. Homogenization

The homogenization heat treatment in this work was used to (i) dissolve unwanted phases formed during the casting process, (ii) improve the homogeneous distribution of alloying elements and (iii) precipitate temperature stable phases, i.e. Mn-containing dispersoids, to increase grain structure stability.

This heat treatment is usually done at high temperatures over an extended span of time, a three step heat treatment, with the following parameters: 300 °C for 3 h \rightarrow 350 °C for 2 h \rightarrow 480 °C for 4 h, was used for the AXZM100 alloy. The first and second step are solely applied to dissolve potential low melting phases, making sure to avoid oxidation events.

1.5.4.2. Solution Heat Treatment

The main purpose of the solution heat treatment is to dissolve all formed (Ca-containing) hardening phases and to create a supersaturated solid solution, for a subsequent homogeneous precipitation of the hardening phases. After heat treatment the material is quenched in water to immobilize the microstructure, thereby retaining a high amount of lattice vacancies and preventing unwanted phase formation.

To inhibit grain growth this high temperature heat treatment takes place only for a short time, here 490 °C for 0.3 h was applied. Nevertheless, the high temperatures used cause static recrystallization of the deformed microstructure, creating a fully recrystallized grain structure.

1.5.4.3. Artificial Ageing

While natural ageing is a well known phenomenon for technical materials, e.g. Al alloys, Mg alloys only show a low ageing response at ambient temperatures, see Figure 1.14a. Therefore, the final material hardness is produced in the artificial ageing heat treatment. The chosen temperatures have to correlate well with the desired hardening phases, allowing for the best possible precipitation conditions. Next

to the chosen temperature the ageing time is of high importance for the achieved material properties. The precipitation of hardening phases can take place over a multitude of different stages, as discussed in Section 1.4.5. In the used AXMZ1000 alloy the pre-cursor phases (ordered G.P. zones) of Al_2Ca (C15) [50] are used as hardening phases.

A comparison of the effect of heat treatment temperatures on material hardness is shown in Figure 1.14b. The chosen temperature and duration of this heat treatment, i.e. 200 °C for 1 h, is based on the good material performance achieved with this layout.

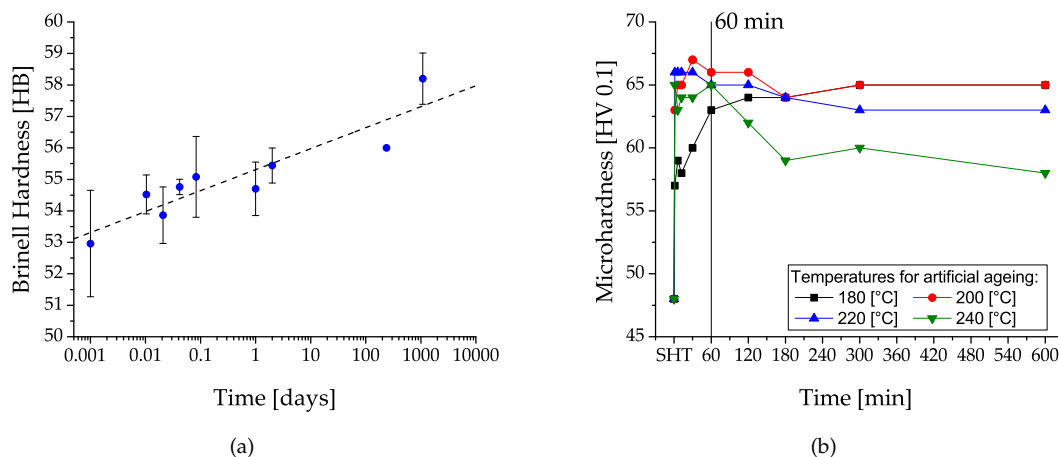


Figure 1.14.: Showing (a) natural ageing effect of the AXMZ1000 alloy, (b) artificial ageing behavior at different heat treatment temperatures.

1.6. References

- [1] Airbus Global Market Forecast 2021 – 2040, Tech. rep., Airbus (2021).
- [2] Key figures on Europe, 2021 edition, Tech. rep., European Union, ISBN 978-92-76-32158-3 (2021). doi: [10.2785/290762KS-EI-21-001-EN-N](https://doi.org/10.2785/290762KS-EI-21-001-EN-N).
- [3] F. Czerwinski, Current Trends in Automotive Lightweighting Strategies and Materials, Materials 14 (6631) (2021) 27. doi: [10.3390/ma14216631](https://doi.org/10.3390/ma14216631).
- [4] L. Gregoir, K. van Acker, Metals for Clean Energy: Pathways to solving Europe’s raw materials challenge, Tech. rep., KU Leuven, <https://eurometaux.be/media/jmxf2qm0/metals-for-clean-energy.pdf> (2022).
- [5] A. M. Diederer, Global Resource Depletion, Managed Austerity and the Elements of Hope, Eburon Academic Publishers, 2010, ISBN 978-90-5972-426-6.
- [6] U. Bardi, The Seneca Effect, Why Growth is Slow but Collapse is Rapid: Springer (2017). doi: [10.1007/978-3-319-57207-9](https://doi.org/10.1007/978-3-319-57207-9).
- [7] B. Mordike, T. Ebert, Magnesium: properties—applications—potential, Materials Science and Engineering: A 302 (1) (2001) 37–45. doi: [10.1016/S0921-5093\(00\)01351-4](https://doi.org/10.1016/S0921-5093(00)01351-4).
- [8] W. Xu, N. Birbilis, G. Sha, Y. Wang, J. E. Daniels, Y. Xiao, M. Ferry, A high-specific-strength and corrosion-resistant magnesium alloy, Nature materials 14 (12) (2015) 1229–1236. doi: [10.1038/nmat4435](https://doi.org/10.1038/nmat4435).
- [9] S. Xu, K. Oh-Ishi, S. Kamado, F. Uchida, T. Homma, K. Hono, High-strength extruded Mg–Al–Ca–Mn alloy, Scripta Materialia 65 (3) (2011) 269–272. doi: [10.1016/j.scriptamat.2011.04.026](https://doi.org/10.1016/j.scriptamat.2011.04.026).
- [10] J. Nie, K. Shin, Z. Zeng, Microstructure, Deformation, and Property of Wrought Magnesium Alloys, Metallurgical and Materials Transactions A 51 (12) (2020) 6045–6109. doi: [10.1007/s11661-020-05974-z](https://doi.org/10.1007/s11661-020-05974-z).

- [11] K. P. Rao, Y. V. R. K. Prasad, C. Dharmendra, K. Suresh, N. Hort, H. Dieringa, Review on Hot Working Behavior and Strength of Calcium-Containing Magnesium Alloys, *Advanced Engineering Materials* 20 (1701102) (2018) 1–19. doi:10.1002/adem.201701102.
- [12] Alu-Info Statistiken: Produktion und Bedarf, <http://www.aluinfo.de/produktion-und-bedarf.html>, accessed: 2022-07-03.
- [13] K. U. Kainer, 40 Years of Magnesium Research – Assessment of Contribution to the Progress in Magnesium Technology, in: 79th Annual IMA World Magnesium Conference, Budapest, IMA, 2019.
- [14] B. Trink, Mikrostrukturelle Charakterisierung einer Mg–Al–Ca–Mn–Legierung bei der Herstellung von Schmiedeteilen, Master's thesis, Montanuniversität Leoben (2020).
- [15] N. P. Papenberg, S. Gneiger, I. Weißensteiner, P. J. Uggowitzer, S. Pogatscher, Mg-Alloys for forging applications—A review, *Materials* 13(4) (985) (2020) 1–61. doi:10.3390/ma13040985.
- [16] N. P. Papenberg, S. Gneiger, P. J. Uggowitzer, S. Pogatscher, Lean Wrought Magnesium Alloys, *Materials* 14 (4282) (2021) 1–30. doi:10.3390/ma14154282.
- [17] N. Papenberg, T. Hatzenbichler, F. Grabner, P. J. Uggowitzer, S. Pogatscher, Forging of an age-hardenable Mg–Al–Ca–Mn–Zn alloy on industrial scale, *SN Applied Sciences* 5 (1) (2023) 1–11. doi:10.1007/s42452-022-05240-4.
- [18] N. P. Papenberg, A. Arnoldt, B. Trink, P. J. Uggowitzer, S. Pogatscher, Closed die forging of a Mg–Al–Ca–Mn–Zn lean alloy, *Materials Science and Engineering: A* 857 (144079) (2022) 1–13. doi:10.1016/j.msea.2022.144079.
- [19] F. D'Errico, M. Tauber, M. Just, Magnesium Alloys for Sustainable Weight-Saving Approach: A Brief Market Overview, New Trends, and Perspectives, in: S. Sunkari (Ed.), *Current Trends in Magnesium (Mg) Research*, IntechOpen, 2022. doi:10.5772/intechopen.102777.
- [20] B. Powell, P. Krajewski, A. Luo, Magnesium alloys for lightweight powertrains and automotive structures, in: *Materials, design and manufacturing for lightweight vehicles*, Elsevier, 2021, pp. 125–186. doi:10.1016/B978-0-12-818712-8.00004-5.
- [21] Primary magnesium production worldwide from 2010 to 2021, Tech. rep., Statista Inc, <https://www.statista.com/statistics/569515/primary-magnesium-production-worldwide/>, Accessed: 2022-07-26 (2022).
- [22] A Closer Look at Magnesium, Tech. rep., House Mountain Partners, <http://www.discoveryinvesting.com/blog/2015/8/10/a-closer-look-at-magnesium>, Accessed: 2022-07-26 (2022).
- [23] Metal Magnesium Market - Growth, Trends, COVID-19 Impact, and Forecasts (2022 - 2027), Tech. rep., Mordor Intelligence, <https://www.mordorintelligence.com/industry-reports/metal-magnesium-market>, Accessed: 2022-07-26 (2022).
- [24] I. Polmear, D. StJohn, J.-F. Nie, M. Qian, *Light Alloys: Metallurgy of the Light Metals*, 5th Edition, Elsevier, Butterworth-Heinemann, Oxford, UK, 2017. doi:10.1016/B978-0-08-099431-4.00009-9.
- [25] B. Klein, *Leichtbau-Konstruktion*, Springer, 2009. doi:10.1007/978-3-658-26846-6.
- [26] F. Li, W. Y. Peh, V. Nagarajan, M. K. Ho, A. Danno, B. W. Chua, M. J. Tan, Development of non-flammable high strength AZ91+ Ca alloys via liquid forging and extrusion, *Materials & Design* 99 (2016) 37–43. doi:10.1016/j.matdes.2016.03.014.
- [27] B. Jiang, W. Liu, D. Qiu, M.-X. Zhang, F. Pan, Grain refinement of Ca addition in a twin-roll-cast Mg–3Al–1Zn alloy, *Materials Chemistry and Physics* 133 (2-3) (2012) 611–616. doi:10.1016/j.matchemphys.2011.12.087.
- [28] A. Chapuis, J. H. Driver, Temperature dependency of slip and twinning in plane strain compressed magnesium single crystals, *Acta Materialia* 59 (5) (2011) 1986–1994. doi:10.1016/j.actamat.2010.11.064.
- [29] S. Nandy, S.-P. Tsai, L. Stephenson, D. Raabe, S. Zaefferer, The role of Ca, Al and Zn on room temperature ductility and grain boundary cohesion of magnesium, *Journal of Magnesium and Alloys* 9 (5) (2021) 1521–1536. doi:10.1016/j.jma.2021.03.005.
- [30] Z. Zeng, J.-F. Nie, S.-W. Xu, C. HJ Davies, N. Birbilis, Super-formable pure magnesium at room temperature, *Nature communications* 8 (972) (2017) 1–6. doi:10.1038/s41467-017-01330-9.

- [31] T. Liu, Q. Yang, N. Guo, Y. Lu, B. Song, Stability of twins in Mg alloys—a short review, *Journal of Magnesium and Alloys* 8 (1) (2020) 66–77. doi:10.1016/j.jma.2020.02.002.
- [32] B. Ravaji, S. P. Joshi, A crystal plasticity investigation of grain size-texture interaction in magnesium alloys, *Acta Materialia* 208 (116743) (2021) 1–16. doi:10.1016/j.actamat.2021.116743.
- [33] X. Wu, X. Jing, H. Xiao, S. Ouyang, A. Tang, P. Peng, B. Feng, M. Rashad, J. She, X. Chen, et al., Controlling grain size and texture in Mg–Zn–Mn alloys from the interaction of recrystallization and precipitation, *Journal of Materials Research and Technology* 21 (2022) 1395–1407. doi:10.1016/j.jmrt.2022.09.108.
- [34] O. Sitdikov, R. Kaibyshev, Dynamic recrystallization in pure magnesium, *Materials Transactions* 42 (9) (2001) 1928–1937. doi:10.2320/matertrans.42.1928.
- [35] M. Myshlyayev, H. McQueen, A. Mwembela, E. Konopleva, Twinning, dynamic recovery and recrystallization in hot worked Mg–Al–Zn alloy, *Materials Science and Engineering: A* 337 (1-2) (2002) 121–133. doi:10.1016/S0921-5093(02)00007-2.
- [36] A. D. Murphy, J. E. Allison, The recrystallization behavior of unalloyed Mg and a Mg–Al alloy, *Metallurgical and Materials Transactions A* 49 (2018) 1492–1508. doi:10.1007/s11661-018-4494-6.
- [37] J. Tan, M. Tan, Dynamic continuous recrystallization characteristics in two stage deformation of Mg–3Al–1Zn alloy sheet, *Materials Science and Engineering: A* 339 (1-2) (2003) 124–132. doi:10.1016/S0921-5093(02)00096-5.
- [38] T. Al-Samman, G. Gottstein, Dynamic recrystallization during high temperature deformation of magnesium, *Materials Science and Engineering: A* 490 (1-2) (2008) 411–420. doi:10.1016/j.msea.2008.02.004.
- [39] Q. Chen, R. Chen, J. Su, Q. He, B. Tan, C. Xu, X. Huang, Q. Dai, J. Lu, The mechanisms of grain growth of Mg alloys: A review, *Journal of Magnesium and Alloys* 10 (9) (2022) 2384–2397. doi:10.1016/j.jma.2022.09.001.
- [40] L. L. C. Catorceno, H. F. G. De Abreu, A. F. Padilha, Effects of cold and warm cross-rolling on microstructure and texture evolution of AZ31B magnesium alloy sheet, *Journal of Magnesium and Alloys* 6 (2) (2018) 121–133. doi:10.1016/j.jma.2018.04.004.
- [41] G. Zhu, L. Wang, H. Zhou, J. Wang, Y. Shen, P. Tu, H. Zhu, W. Liu, P. Jin, X. Zeng, Improving ductility of a Mg alloy via non-basal $\langle a \rangle$ slip induced by Ca addition, *International Journal of Plasticity* 120 (2019) 164–179. doi:10.1016/j.ijplas.2019.04.020.
- [42] B. Yin, Z. Wu, W. Curtin, First-principles calculations of stacking fault energies in Mg–Y, Mg–Al and Mg–Zn alloys and implications for $\langle c+a \rangle$ activity, *Acta Materialia* 136 (2017) 249–261. doi:10.1016/j.actamat.2017.06.062.
- [43] R. Nunes, I. Abbas, et al., *ASM–Handbook Volume 14: Forming and Forging*, ASM International, Materials Park, OH, USA, 1996. doi:10.31399/asm.hb.v14a.a0003998.
- [44] X. J. Wang, S.-M. Zhu, M. A. Easton, M. A. Gibson, G. Savage, Heat treatment of vacuum high pressure die cast magnesium alloy AZ91, *International Journal of Cast Metals Research* 27 (3) (2014) 161–166. doi:10.1179/1743133613Y.0000000091.
- [45] A. Kiełbus, L. Cizek, L. Pawlica, Microstructural Changes of AZ91 Magnesium Alloy After Heat Treatment, in: *Magnesium: Proceedings of the 6th International Conference Magnesium Alloys and Their Applications*, Wiley Online Library, 2003, pp. 196–201. doi:10.1002/3527603565.ch29.
- [46] S. Gneiger, N. P. Papenberg, A. R. Arnoldt, C. M. Schlögl, M. Fehlbier, Investigations of High-Strength Mg–Al–Ca–Mn Alloys with a Broad Range of Ca+Al Contents, *Materials* 14 (5439) (2021) 1–15. doi:10.3390/ma14185439.
- [47] T. Arai, G. Baker, et al., *ASM–Handbook Volume 4: Heat Treating*, ASM International, Materials Park, OH, USA, 1991. doi:10.31399/asm.hb.v04e.9781627081696.
- [48] T. Nakata, C. Xu, R. Ajima, K. Shimizu, S. Hanaki, T. Sasaki, L. Ma, K. Hono, S. Kamado, Strong and ductile age-hardening Mg–Al–Ca–Mn alloy that can be extruded as fast as aluminum alloys, *Acta Materialia* 130 (2017) 261–270. doi:10.1016/j.actamat.2017.03.046.

- [49] M. Cihova, R. Schäublin, L. B. Hauser, S. S. Gerstl, C. Simson, P. Uggowitz, J. F. Löffler, Rational design of a lean magnesium-based alloy with high age-hardening response, *Acta Materialia* 158 (2018) 214–229. doi:10.1016/j.actamat.2018.07.054.
- [50] J.-F. Nie, Precipitation and hardening in magnesium alloys, *Metallurgical and Materials Transactions A* 43 (11) (2012) 3891–3939. doi:10.1007/s11661-012-1217-2.
- [51] J. F. Nie, Effects of precipitate shape and orientation on dispersion strengthening in magnesium alloys, *Scripta Materialia* 48 (8) (2003) 1009–1015. doi:10.1016/S1359-6462(02)00497-9.
- [52] J. D. Robson, N. Stanford, M. R. Barnett, Effect of precipitate shape and habit on mechanical asymmetry in magnesium alloys, *Metallurgical and Materials Transactions A* 44 (7) (2013) 2984–2995. doi:10.1007/s11661-012-1466-0.
- [53] C. Mendis, K. Oh-Ishi, K. Hono, Enhanced age hardening in a Mg–2.4 at.% Zn alloy by trace additions of Ag and Ca, *Scripta Materialia* 57 (6) (2007) 485–488. doi:10.1016/j.scriptamat.2007.05.031.
- [54] C. Mendis, K. Oh-Ishi, T. Ohkubo, K. Hono, Precipitation of prismatic plates in Mg–0.3 Ca alloys with In additions, *Scripta Materialia* 64 (2) (2011) 137–140. doi:10.1016/j.scriptamat.2010.09.028.
- [55] G. Esteban-Manzanares, A. Ma, I. Papadimitriou, E. Martínez, J. LLorca, Basal dislocation/precipitate interactions in Mg–Al alloys: an atomistic investigation, *Modelling and Simulation in Materials Science and Engineering* 27 (075003) (2019) 1–23. doi:10.1088/1361-651X/ab2de0.
- [56] C. Wang, C. M. Cepeda-Jimenez, M. T. Pérez-Prado, Dislocation-particle interactions in magnesium alloys, *Acta Materialia* 194 (2020) 190–206. doi:10.1016/j.actamat.2020.04.055.
- [57] B. Song, J. She, N. Guo, R. Qiu, H. Pan, L. Chai, C. Yang, S. Guo, R. Xin, Regulating precipitates by simple cold deformations to strengthen Mg alloys: a review, *Materials* 12 (2507) (2019) 1–19. doi:10.3390/ma12162507.
- [58] Z. Zeng, Y. Zhu, M. Bian, S. Xu, C. Davies, N. Birbilis, J. Nie, Annealing strengthening in a dilute Mg–Zn–Ca sheet alloy, *Scripta Materialia* 107 (2015) 127–130. doi:10.1016/j.scriptamat.2015.06.002.
- [59] C. L. Mendis, K. Oh-Ishi, K. Hono, Microalloying effect on the precipitation processes of Mg–Ca alloys, *Metallurgical and Materials Transactions A* 43 (11) (2012) 3978–3987. doi:10.1007/s11661-011-1049-5.
- [60] T. Oršulová, P. Palček, Changes in hardness of magnesium alloys due to precipitation hardening, *Production Engineering Archives* 18 (2018) 46–49. doi:10.30657/pea.2018.18.08.
- [61] B. A. Esgandari, H. Mehrjoo, B. Nami, S. Miresmaeili, The effect of Ca and RE elements on the precipitation kinetics of Mg₁₇Al₁₂ phase during artificial aging of magnesium alloy AZ91, *Materials Science and Engineering: A* 528 (15) (2011) 5018–5024. doi:10.1016/j.msea.2011.03.022.
- [62] X. Gao, S.-M. Zhu, B. C. Muddle, J. F. Nie, Precipitation-hardened Mg–Ca–Zn alloys with superior creep resistance, *Scripta Materialia* 53 (12) (2005) 1321–1326. doi:10.1016/j.scriptamat.2005.08.035.
- [63] Q. Shi, A. R. Natarajan, A. Van der Ven, J. Allison, Partitioning of Ca to metastable precipitates in a Mg-rare earth alloy, *Materials Research Letters* 11 (3) (2023) 222–230. doi:10.1080/21663831.2022.2138724.
- [64] M. Cihova, E. Martinelli, P. Schmutz, A. Myrissa, R. Schäublin, A. M. Weinberg, P. Uggowitz, J. F. Löffler, The role of zinc in the biocorrosion behavior of resorbable Mg–Zn–Ca alloys, *Acta Biomaterialia* 100 (2019) 398–414. doi:10.1016/j.actbio.2019.09.021.
- [65] J. F. Nie, B. C. Muddle, Precipitation hardening of Mg–Ca (–Zn) alloys, *Scripta Materialia* 37 (10) (1997) 1475–1481. doi:10.1016/S1359-6462(97)00294-7.
- [66] R. Schaublin, M. Becker, M. Cihova, S. Gerstl, D. Deiana, C. Hebert, S. Pogatscher, P. Uggowitz, J. Löffler, Precipitation in lean Mg–Zn–Ca alloys, *Acta Materialia* 239 (118223) (2022) 1–19. doi:10.1016/j.actamat.2022.118223.
- [67] A. Shadkam, A Study of Homogenization and Precipitation Hardening Behaviour of Mg–Ca–Zn Alloys, Master's thesis, University of Waterloo (2008).
- [68] R. Ninomiya, T. Ojio, K. Kubota, Improved heat resistance of Mg–Al alloys by the Ca addition, *Acta metallurgica et materialia* 43 (2) (1995) 669–674. doi:10.1016/0956-7151(94)00269-N.

- [69] S. Liang, R. Chen, J. Blandin, M. Suery, E. Han, Thermal analysis and solidification pathways of Mg–Al–Ca system alloys, *Materials Science and Engineering: A* 480 (1-2) (2008) 365–372. doi:10.1016/j.msea.2007.07.025.
- [70] Z. Jiang, B. Jiang, H. Yang, Q. Yang, J. Dai, F. Pan, Influence of the Al₂Ca phase on microstructure and mechanical properties of Mg–Al–Ca alloys, *Journal of Alloys and Compounds* 647 (2015) 357–363. doi:10.1016/j.jallcom.2015.06.060.
- [71] J. Jayaraj, C. Mendis, T. Ohkubo, K. Oh-Ishi, K. Hono, Enhanced precipitation hardening of Mg–Ca alloy by Al addition, *Scripta Materialia* 63 (8) (2010) 831–834. doi:10.1016/j.scriptamat.2010.06.028.
- [72] K. Oh-Ishi, R. Watanabe, C. Mendis, K. Hono, Age-hardening response of Mg–0.3 at.% Ca alloys with different Zn contents, *Materials Science and Engineering: A* 526 (1-2) (2009) 177–184. doi:10.1016/j.msea.2009.07.027.
- [73] T. Nakata, C. Xu, Y. Matsumoto, K. Shimizu, T. Sasaki, K. Hono, S. Kamado, Optimization of Mn content for high strengths in high-speed extruded Mg-0.3 Al-0.3 Ca (wt%) dilute alloy, *Materials Science and Engineering: A* 673 (2016) 443–449. doi:10.1016/j.msea.2016.07.098.
- [74] T. Homma, S. Nakawaki, K. Oh-Ishi, K. Hono, S. Kamado, Unexpected influence of Mn addition on the creep properties of a cast Mg–2Al–2Ca (mass%) alloy, *Acta Materialia* 59 (20) (2011) 7662–7672. doi:10.1016/j.actamat.2011.08.049.
- [75] A. Shukla, A. D. Pelton, Thermodynamic assessment of the Al–Mn and Mg–Al–Mn systems, *Journal of phase equilibria and diffusion* 30 (1) (2009) 28–39. doi:10.1007/s11669-008-9426-5.
- [76] M. Razzaghi, H. Mirzadeh, M. Emamy, Mechanical properties of Mg–Al–Mn magnesium alloys with low Al content in the as-cast and extruded conditions, *Materials Research Express* 6 (106521) (2019) 1–7. doi:10.1088/2053-1591/ab36da.
- [77] T. Nakata, C. Xu, R. Ajima, Y. Matsumoto, K. Shimizu, T. Sasaki, K. Hono, S. Kamado, Improving mechanical properties and yield asymmetry in high-speed extrudable Mg-1.1 Al-0.24 Ca (wt%) alloy by high Mn addition, *Materials Science and Engineering: A* 712 (2018) 12–19. doi:10.1016/j.msea.2017.11.085.
- [78] F. Czerwinski, Controlling the ignition and flammability of magnesium for aerospace applications, *Corrosion Science* 86 (2014) 1–16. doi:10.1016/j.corsci.2014.04.047.
- [79] Y. Chino, T. Ueda, Y. Otomatsu, K. Sassa, X. Huang, K. Suzuki, M. Mabuchi, Effects of Ca on tensile properties and stretch formability at room temperature in Mg–Zn and Mg–Al alloys, *Materials Transactions* 52 (7) (2011) 1477–1482. doi:10.2320/matertrans.M2011048.
- [80] I. Basu, M. Chen, J. Wheeler, R. Schäublin, J. Löffler, Stacking-fault mediated plasticity and strengthening in lean, rare-earth free magnesium alloys, *Acta Materialia* 116877 (2021) 17. doi:10.1016/j.actamat.2021.116877.

2. Magnesium for Forging Applications

To provide a good overview and gain appropriate understanding of the possibilities and the works done on Mg forgings an in-depth literature study was conducted on this topic. While the investigated literature showed a broad range of used alloys and process conditions, it became apparent that there seems to be no distinctive scientific focus. As there were no comprehensive literature reviews available, the investigations done in this thesis were published in the shape of a review paper.

The following chapter gives an extensive introduction into the topic of Mg forgings. Basic information on the processing characteristics are provided as well as alloy specific investigations discussed.

Mg Alloys for Forging Applications: A Review

Published in: MDPI Journal Materials, 2020, 13, 985; [doi:10.3390/ma13040985](https://doi.org/10.3390/ma13040985)

Received: 30 December 2019; Accepted: 2 February 2020

Authors: Nikolaus Papenberg, Stefan Gneiger, Irmgard Weißensteiner, Peter J. Uggowitzer and Stefan Pogatscher

Author contribution: This review is the work of several authors, the individual contributions are subsequently listed: conceptualization, N.P., P.J.U. and S.P.; software, S.G.; investigation, N.P., S.G. and I.W.; data curation, N.P. and I.W.; writing—original draft preparation, N.P., S.G. and I.W.; writing—review and editing, N.P., S.G., I.W., P.J.U. and S.P.; visualization, N.P. and S.G.; supervision, P.J.U. and S.P.; project administration, N.P. and S.P.

Keywords: magnesium alloys; forging; literature review; overview

Abstract: Interest in magnesium alloys and their applications has risen in recent years. This trend is mainly evident in casting applications, but wrought alloys are also increasingly coming into focus. Among the most common forming processes, forging is a promising candidate for the industrial production of magnesium wrought products. This review is intended to give a general introduction into the forging of magnesium alloys and to help in the practical realization of forged products. The basics of magnesium forging practice are described and possible problems as well as material properties are discussed. Several alloy systems containing aluminum, zinc or rare earth elements as well as biodegradable alloys are evaluated. Overall, the focus of the review is on the process control and processing parameters, from stock material to finished parts. A discussion of the mechanical properties is included. These data have been comprehensively reviewed and are listed for a variety of magnesium forging alloys.

Funding: We gratefully acknowledge the financial support of this work within the scope of the AMALFI project. AMALFI is a COMET Project within the COMET–Competence Centers for Excellent Technologies Programme and funded by BMVIT, BMDW, and the federal state of Upper Austria. The COMET Programme is managed by the FFG (grant number 872641).

This work has been supported by the European Regional Development Fund (EFRE) in the framework of the EU-program "IWB Investition in Wachstum und Beschäftigung Österreich 2014-2020", and the federal state Upper Austria.

Financial support by the Christian Doppler Research Association, the Austrian Federal Ministry for Digital and Economic Affairs and the National Foundation for Research, Technology and Development is gratefully acknowledged.

Published as an open access article distributed under the terms and conditions of the Creative Commons Attribution (CC BY) license (<https://creativecommons.org/licenses/by/4.0/>). The only changes made are related to layout and internal document accessibility.

2.1. Introduction

Magnesium, the world's lightest structural metal, has attracted much attention in recent years. Possible applications of this material are closely connected to its low weight and good specific mechanical properties. Therefore, many studies focus therefore on the positive influence which Mg alloys can have on the lightweight construction of products in the transport sector such as automobile and aircraft components. In the past, intensive efforts to reduce weight are well known and have repeatedly resulted in substantial changes in the choice of materials (e.g., from steel parts to multi material mixes) and designs (e.g., introduction of space frames). Naturally, these different potential applications require materials with a multitude of properties. These have to be investigated, understood and tested before they can finally be reliably produced on an industrial scale.

Forged parts in general are typically used for structural applications with high demands on reliability, functionality and mechanical properties. These qualities are particularly important in transportation, which makes these industries a main customer of forged parts. The use of Mg provides the additional benefit of reduced mass and enables new ways of light weight design. Therefore, forged Mg parts seem to be especially well suited for applications in the transport sector.

Magnesium alloys, their properties, applications and possible developments have been described in various studies throughout the years [1–5]. The corrosion behavior, which is an integral part of many applications, has been reviewed extensively by Esmaily et al. [6] and the related topic of coatings for Mg products has been described by Gray and Luan [7]. The precipitation behavior of Mg alloys as the main source of strength in many materials is reviewed by Nie [8]. An overview of forming by extrusion processes and the resulting properties is given by Zeng et al. [9]. Although there are works on Mg alloys for forging applications [10–14], this aspect is far from being as profoundly reviewed as the above topics are.

A short introduction about the forging of Mg in Europe is given in the works of Sillekens et al. [10–12], which discuss the benefits and challenges of industrial implementation in detail. Ovsyannikov [13] briefly describes the industrial forging practice and the products made of various Mg alloys. In a publication of Dziubińska et al. [14], the application of Mg forgings in transport applications is reviewed and examples for produced components are given. General information on the forging of light metal alloys in general can be found in the works of Shan et al. [15]. Hartley and Pillinger describe the simulation of forging processes [16] and Hawryluk and Jakubik [17] present a work on forging defects.

While forged Mg products are presented in various scientific studies, industrial applications are still mostly confined to high-priced applications for sports and military use. Nevertheless, these products highlight the possible benefits and performance of forged Mg alloys. Unfortunately, however, the leap towards the use of Mg forgings in the mass market of consumer goods has not yet been successful. Examples of some forged parts made from Mg alloys are shown in Figure 2.1, which depicts forgings either commercially available or used in research and development.

In the course of the development of Mg alloys many different properties, such as flow behavior, mechanical properties and texture have been investigated and the understanding of these materials has improved steadily. Here we give an overview of the scientific literature on Mg forging. The alloys and the processing parameters used are presented and the product range is described. By presenting the efforts made in the field, the variety of available materials and the current state of the art are illustrated.

In order to provide a comprehensive overview of the most relevant aspects of Mg forging applications, we start with a brief history of the use and development (Section 2.2) as well as an introduction about the basics of Mg forging (Section 2.3). Studies using various Mg alloys for forging are discussed in Sections 2.4–2.9. Subsequently, a short conclusion is drawn in Section 2.10. Tables containing processing parameters and mechanical properties of various alloys can be found in the Appendices 2.11.2 and 2.11.3, respectively.

The main online sources used for the literature research concerning this review were: Scopus, Google Scholar, Web of Science, Espacenet and Google Patents. This review does neither include works about powder or thixo forging nor forgings for the sole purpose of grain refinement (e.g., multi axial forging).



Figure 2.1.: Various Mg forged parts, showing (u.l.) a motorbike rim produced by Brembo S.p.A. under Marchesini trademark, (u.r.) a bike suspension link made by ALLITE® Inc., (b.l.) laboratory scale piston rod forged by Light Metals Technologies Ranshofen and (b.r.) a wheel hub produced by Institut für Metallformung, University Freiberg. Reproduced with the kind permission of: Brembo S.p.A., ALLITE® Inc., Light Metals Technologies Ranshofen and TU Bergakademie Freiberg.

2.2. History

Magnesium was already known and has been scientifically investigated throughout the 19th century. However, industrial production only slowly emerged at the beginning of the 20th century, starting out in Europe, where castings and parts were already displayed 1909 in Germany. From there it crossed into the US where production picked up in the 1920s and accelerated in the 1930s [18]. The process for the production of primary Mg varied, depending on the usable local resources, ranging from electrolytic (Downs process) to carbo-thermic (Hansgirg process) and silico-thermic (Pidgeon process) [19].

The benefits of this new light weight structural material stayed not unnoticed to other assurgent industries. To cover the rising demand, the suppliers, differing by size and country, started to increase their output by producing primary Mg, Mg alloys and parts. Manufacturers from this time, still well known today, are Dow Chemical (US), Magnesium Electron (GB) and I. G. Farbenindustrie (Germany). Main customers of Mg products were aircraft and automobile industries, where engine and structural parts as well as wheels and rotors were used. As reported by Gann [18] in 1929, Mg accounted for 50 % of light metals used in German aircraft work. The Berlin Transportation Co. used Mg wheels in their motor coaches since 1926, not only to improve driving behavior but also to increase tire life.

Nevertheless, one should not forget that much of this development was pushed by the military on the eve of World War II. This is well visible in the breakdown of Mg production after 1945. Regardless, the industry searched for civil applications and production was able to grow again from the 1950s onward [2; 20]. The main Mg producers were the US until the end of the 1990s, after which China started up their own production. Today, China is by far the biggest producer of primary Mg worldwide, producing more than 80 % of the available material.

The main quantity of Mg is currently used as alloying element for Al alloys, for desulphurization in steel production and as Mg casting alloys, while wrought Mg alloys and products account only for a small fraction of the Mg in use. Nevertheless, the forming of Mg has always been a topic of interest for the scientific community and industrial applications which demand for good specific mechanical properties.

Already in 1924, the forging of Mg parts for aviation was discussed briefly by Portevin and deFleury [21].

There, the importance of heated dies is mentioned and the authors conclude that Mg alloys can be forged easily, maybe even better than high strength Al alloys. In the overview on Magnesium presented by Gann [18] in 1930/31, the importance of moderate forming-speeds is highlighted and press-forging is recommended in lieu of drop-forging. While artificial ageing was known for Mg cast products, it seems not to be applied to forgings. The degree of deformation, on the other hand, is highlighted as important for the mechanical properties.

In 1939 Haughton [22] describes the use of an isothermal forging process. Moreover, the increased formability of upset forging stock and the improved mechanical properties of forgings produced with forging steps of subsequently lowered temperatures were mentioned.

While, throughout the years, the main alloying systems for Mg are the Mg-Al, Mg-Al-Zn and Mg-Mn systems, more complex systems (e.g., containing Ce, Ag, Pb and Be) have been investigated as well [19]. In 1950, Grube et al. [23] reported on their investigations of Mg-Ce forging alloys, which were analyzed regarding their high temperature properties and creep behavior. The review on Mg-Li alloys done by Frost [24] in 1962 features forgings as well, besides the description of various forming processes and the comparison of the resulting mechanical properties.

Of special interest for the production of forgings might be the report by Shaw et al. [25] concerning the effect of lubrication on the forming behavior, and the work of Sabroff et al. [26]. The investigation on lubricants used for the forming of various materials from 1955 showed that the best results for Mg alloys were achieved by graphite-based lubricants [25]. The report of Sabroff et al. [26] from 1964, a manual on forging of all kinds of metals, describes the forging practice of Mg alloys as well. It covers the description of the most important alloys and gives information on forming behavior, lubricants, grain size control and trimming.

2.3. Basic Aspects of Magnesium Forging

In general, forgings have better mechanical properties than cast parts and show favorable microstructural flow in loading direction if produced appropriately. This originates from a reduction of casting defects, closing of pores, refinement and breaking of primary phases as well as grain refinement and material flow while forming. Forgings are thought to show the best overall mechanical properties of all Mg products [27].

The use of Mg alloys in light-weighting shows its benefits particularly in bending applications where substantial increases in stiffness, strength and reduction of instabilities are possible with equal part weight. When heavier metals are exchanged for Mg alloys, it can be beneficial to modify the geometry, but this is not always necessary. Often, the part has already been designed in a way that the originally used material can be substituted directly with Mg alloys without a critical degradation in mechanical properties [27].

2.3.1. Alloy Designations

To describe the chemical composition of an alloying system or an alloy, designation systems are widely used. While various such systems exist, the one preferentially used in scientific literature is the ASTM Standard Alloy Designation System (B951-11) and also this work uses this system.

The ASTM Standard Alloy Designation System consists of four parts, the principal alloying elements, which are defined by one letter each, are the first part. In the second part the rounded-off percentages (wt %) of the respective elements are given. The third and fourth parts are the number of standardization (starting with the letter A and omitting O and I) and the temper designation. Regrettably, the ASTM does not provide designations for all available alloying elements, therefore the designations used by the authors cited are adopted in this work. An overview of the most common alloying elements and the respective designations based on the ASTM system are given in Table 2.1 and a selection of temper designations is presented in Table 2.5 in the appendix.

Table 2.1.: Common alloying element designations based on the ASTM Standard Alloy Designation System.

Designation	Element		Designation	Element	
	Name	Abbrev.		Name	Abbrev.
A	aluminum	Al	N	nickel	Ni
B	bismuth	Bi	P	lead	Pb
Ba	barium	Ba	Q	silver	Ag
C	copper	Cu	R	chromium	Cr
D	cadmium	Cd	S	silicon	Si
E	rare earth	RE/REE	T	tin	Sn
F	iron	Fe	V	gadolinium	Gd
H	thorium	Th	W	yttrium	Y
J	strontium	Sr	X	calcium	Ca
K	zirconium	Zr	Y	antimony	Sb
L	lithium	Li	Z	zinc	Zn
M	manganese	Mn			

2.3.2. Forming Behavior

The forming behavior and suitability of Mg alloys for forging processes can be investigated with a multitude of tests, the most common are tensile and compression (upset) testing and also backwards extrusion.

Compression, upsetability or upsetting tests can be conducted with a multitude of testing parameters (e.g., temperature, strain rate,...) and sample shapes. The resulting deformation of the sample is controlled by lubrication, die design, sample shape and material behavior [28]. Most commonly, testing is done on a cylindrical billet between two flat dies: The billet is compressed till either cracks appear or to a predefined strain. Thereby, the forming behavior, possible surface defects and necessary deformation force can be measured directly. The microstructure and (depending on the sample size and analysis method) the mechanical properties of the deformed samples can be analyzed as well.

Backwards extrusion is a relatively simple testing set-up that can be implemented both experimentally and by simulation: The material is pressed into a die by a punch and the layout leaves space for the compressed material to flow into the opposite direction of the punch. Thereby a cup or a comparable form is shaped. The height of the walls of the part is dependent on the material flow behavior, lubrication and used forming load. In terms of complexity, backwards extrusion can be considered an intermediate step between compression testing and more complex die forgings. Compared to compression testing, backwards extrusion testing accomplishes higher degrees of deformation, higher hydrostatic stresses and exhibits a more complex material flow. In backwards extrusion The testing schemes and sample shapes for compression testing and backwards extrusion are depicted in Fig. 2.2.

The flow behavior of Mg alloys in compression testing is characterized by softening after reaching the peak stress. Microstructurally, this behavior is due to as dynamic recrystallization (DRX) and it is the most beneficial deformation mechanism for a successful forming of Mg parts. In case of higher forming speeds the flow stress usually increases, but this can be mitigated by an increase of the material temperature which causes a decrease in flow stress. A typical example of this behavior is given in Figure 2.3, where flow curves of cast and homogenized (425 °C for 24 h) AZ31, measured by cylindrical compression tests are shown.

When tensile testing is applied to layout a process, it is important to take into account that the necessary forging pressure might exceed the tensile strength by far [26]. Although Mg parts can be formed by hammer forging, die forging with hydraulic presses is commonly used. The main reasons for this are the reduced ductility, increased flow stress and cracking sensitivity at higher forming speeds (occurring in hammer forging). Mg alloys, like many other materials, show improved forming behavior

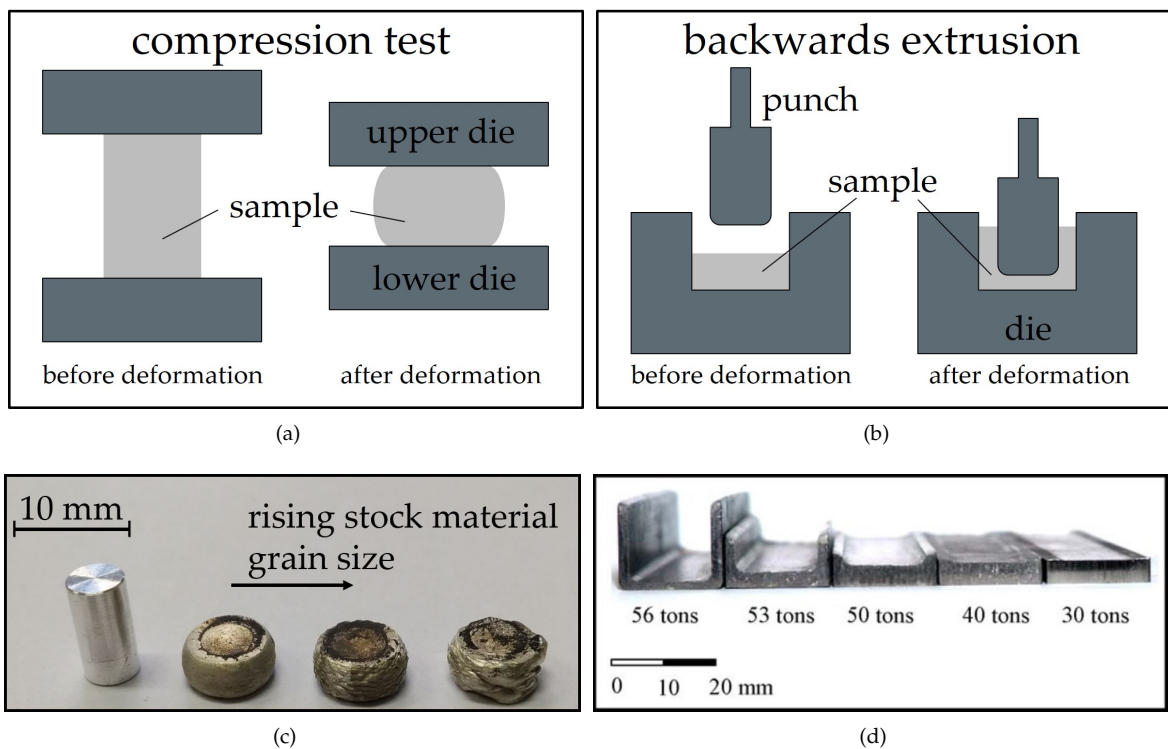


Figure 2.2.: Schemes of simplified testing set-ups for (a) compression testing and (b) backwards extrusion; (c) AXM lean alloy compression samples with varying stock material grain sizes tested at 400 °C. Picture (d) shows parts manufactured from AZ31 by backwards extrusion at 250 °C with varying forming load [29], reproduced with permission from Elsevier.

in case of increased hydrostatic stresses, because free surfaces are especially prone to cracking while forming. Therefore, a closed-die process facilitates optimal forging conditions.

2.3.3. Forging Stock

The stock material should be well homogenized to disperse eutectic phases and it should exhibit a small grain size, as grain size is a main aspect of the forming behavior in Mg alloys besides temperature and forming speed [30]. Cracking of Mg parts with coarse grains can be easily seen in the case of higher forming speeds, e.g., in the behavior of the flash. Therefore, it is not surprising that often pre-deformed stock (mainly extruded) is used for forging. It is well known that extruded Mg has a high degree of anisotropy, which strongly influences the flow behavior during forging as well as the mechanical properties in the finished part. This can be taken into account by providing increased deformation into the transverse direction, thereby improving the usually low transversal ductility [26].

2.3.4. Die Design

The die design used for Mg alloys is comparable to that applied for Al alloys. If the same dies are used, the differing processing parameters and thermal expansion coefficients might result in slightly different part sizes at room temperature (RT). Depending on the alloy it might be necessary to use additional forming steps for Mg. To achieve a good surface quality of the forged parts, the dies should have a smooth surface, which also eases metal flow while forming [30]. Magnesium can only be forged at elevated temperatures; the dies should therefore be made of materials with sufficient high-temperature strength. According to Behrens et al. [31], 1.2344 (X40CrMoV5-1), 1.2365 (32CrMoV12-28), 1.2367 (X38CrMoV5-3), 1.2714 (56NiCrMoV7) as well as other conventional low-alloy hot-work tool steels are commonly

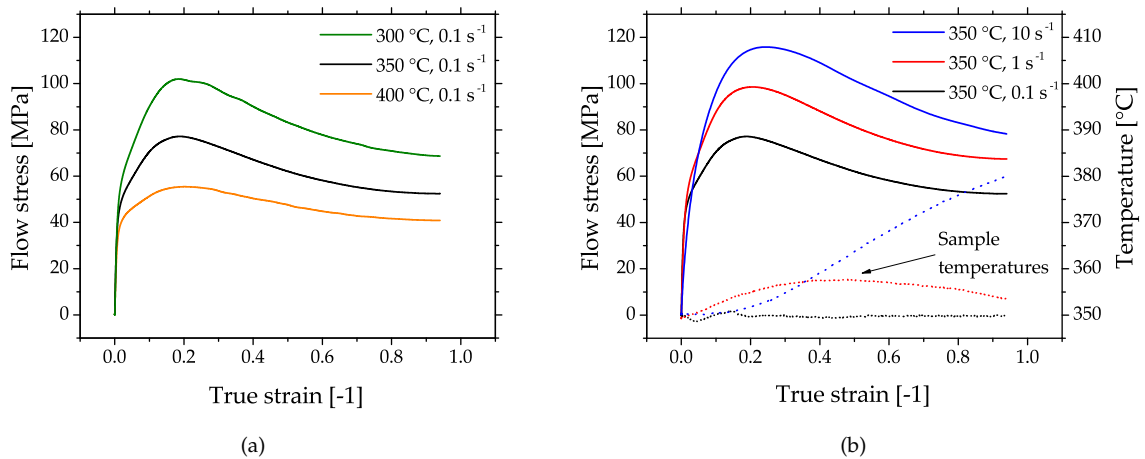


Figure 2.3.: Flow curves of cast and homogenized AZ31, obtained by cylinder compression testing. The plots show the flow stress (full lines) of samples tested with (a) varying temperatures and (b) varying strain rates. The dotted lines in (b) show the increasing sample temperatures with increasing strain rate. No temperature compensation was done for the shown flow stress values.

used [30]. For layout purposes a number of recommended radii for corner and fillet of Mg forgings are listed in ref. [27].

2.3.5. Temperature Control

Temperature control of the billet and the dies is essential in the forging process. While forging usually takes place well below the melting temperature and, therefore, fire hazard is greatly reduced, care has to be taken to avoid excessive overheating and hot spots while heating the material. The billets should be heated uniformly to achieve good forging results and avoid failures like shear or hot cracking [30]. The temperature of the forging stock depends on the material used (alloy, as-cast, homogenized or extruded) but also on the die temperatures, forming speed, billet shape and size, number of applied forging steps and degree of deformation. These factors all play a role when looking at the forming window of a product; other criteria might be mechanical or microstructural properties. The die temperatures can either promote underfilling or surface cracking if too hot or cold, respectively [26]. Controlling the forging temperature is also a way to influence the grain size of the produced part. To keep the grain size small, the forming temperature can be reduced in each forging step. Magnesium alloys are known for static recrystallization after deformation; to prevent this, the finished parts can be quenched in water. An overview of frequently used stock and die temperatures according to ref. [30] is given in Table 2.6 in the appendix.

2.3.6. Lubrication

Lubrication is an important part of every forming practice. For Mg forgings graphite-oil or graphite-water suspensions are usually used, depending on the die temperature. For higher temperatures oil-graphite suspensions are suitable. In all cases the carrier fluid evaporates from the heated dies and a thin graphite film remains on the surface [30].

According to the study on lubricants on AZ80A, conducted by Shaw et al. [25], very good results have been achieved with both, a mix of graphite also with powdered MoS₂ in water. For a further improvement of penetration into die cavities not only the dies can be lubricated but the stock material as well. This is realized by vapor blasting or etching (using acetic acid) of the billet and a subsequent dipping into the lubricant before heating it to forming temperature. According to Sabroff et al. [26] care should be taken to keep the flash regions – where friction is desired – free of lubricant.

2.3.7. Trimming

Trimming of forged Mg parts can be either done at the minimum forging temperatures or the flash can be removed by sawing at room temperature (RT). Warm trimming might pose some problems with bending or warping of the part, therefore this is only done if the flash regions are sturdy enough. Flash removal by band saw at RT is common if only small quantities of parts are produced. Mg-alloys often show brittle fracture behavior in case of trimming at room temperature using a trimming press [26; 30]. In some cases, parts might then be ruined as the brittle fracture of the flash extends into the part itself.

2.3.8. Machining

According to [27], Mg alloys can be machined easily with or without lubricants (coolants) at high speeds. Compared to other structural metals like Al, the tool wear and power required for machining is reduced and the parts obtain a smooth finished surface. Lubricants (mineral oils) are mainly used as coolants to decrease possible part distortion and chips ignition. Increased risk of fire can be the case if cutting speeds over 5 ms^{-1} are applied and feeds are smaller than 0.02 mm . Fine cuts produced by finishing might also be ignited by sparks if handled improperly.

2.3.9. Microstructure and Mechanical Properties

The microstructure and subsequently the mechanical properties of Mg forgings can vary excessively within a part. The final microstructure depends on temperature, degree of deformation and forming speed. It might be composed of twinned grains, fine recrystallized grains, necklace structures, shear bands and combinations thereof in the same part. This behavior is pronounced in as-forged parts. The example given in Fig. 2.4 stems from a laboratory-scaled piston rod [32]. The varying degrees of deformation are well visible in the microstructure of the cross-section. In the sample center a combination of deformed and fine recrystallized grains, a so-called necklace structure, is present. On the sample rim, having a lower degree of deformation, large, heavily twinned grains are prevalent. In the case of a subsequent heat treatment or slow cooling of the parts, recrystallization progress depends on available energy and nucleation points, e.g., twin and grain boundaries.

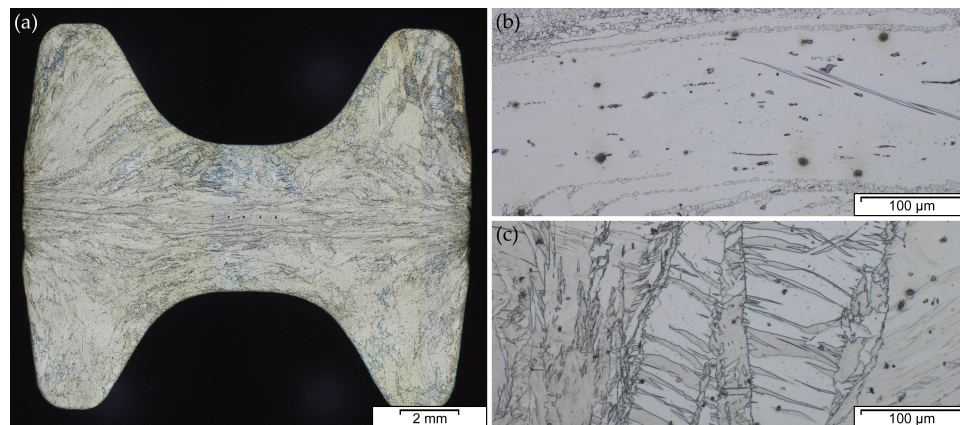


Figure 2.4.: Microstructure of an AZ31 variation (AZ31 containing 0.3 wt. %Ca and 0.2 wt. %Y) in as-forged condition, formed at 425°C stock temperature and 280°C die temperature at a ram speed of 10 mm s^{-1} , showing (a) cross-section of forged part, (b) sample center, (c) sample rim.

Corresponding to this behavior, the mechanical properties may differ considerably throughout the part. This is the case for strength properties, but especially for ductility, where the difference between twinned and recrystallized microstructure may be considerable. An overview of literature values of yield strength (YS) and ultimate tensile strength (UTS) values of various Mg alloys at RT is given in

Fig. 2.5. A more detailed summary is given in Appendix 2.11.3, where tensile properties and process information is compiled.

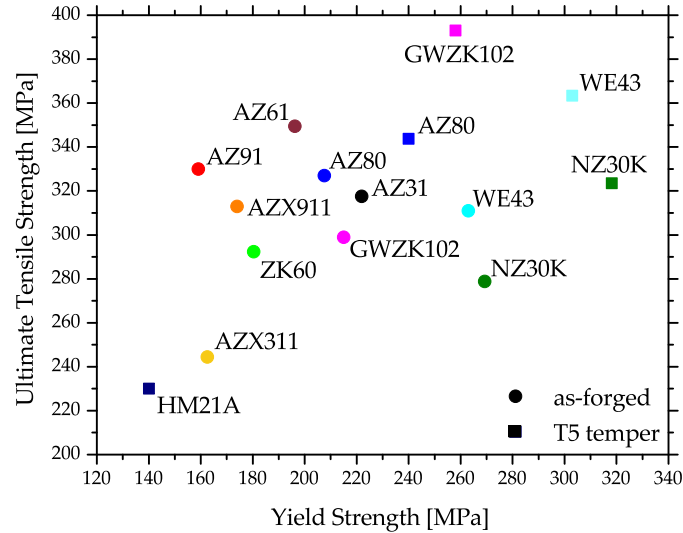


Figure 2.5.: Tensile properties of various Mg alloys, showing as-forged and artificially aged (T5) values at RT. The graphic shows mean values calculated from various scientific sources. A more detailed overview is given in Appendix 2.11.3.

2.3.10. Heat Treatments

Heat treatments for Mg alloys are similar to those known for other materials (i.e., Al). The well known steps of homogenization, solution heat treatment and artificial ageing, or a combination thereof, can be used for various alloys in the production of wrought Mg parts.

Some confusion might exist when looking at the parameters applied for heat treatments of Mg casting products, where the solution heat treatment can last for hours. This originates in the purpose of the heat treatment, which primarily aims to dissolve primary phases after casting. Adequate parameters (time and temperature) should also be used for wrought products in the homogenization heat treatment before forming. The solution heat treatment of wrought alloys, on the other hand, has a much shorter duration. This is the case because the alloying elements should already be well dispersed in the material and excessive grain growth of the usually fine grained and/or deformed microstructure should be avoided. While quenching is not necessarily done after homogenization it might very well be necessary after a solution heat treatment to prevent premature precipitation of hardening phases. Artificial ageing times and temperatures have to be adapted to the alloy used. Especially the ageing duration can vary excessively. For example, rare earth containing alloys may have ageing times of multiple days [33].

An overview of possible heat treatment temperatures and times for various alloys is given in Table 2.7.

2.4. Magnesium Alloys for Forging Applications: Methodology

In the following sections various Mg alloys used for forging applications will be discussed, concentrating on the scientific works published in the last 10 years. The literature is evaluated with regard to the alloy type under investigation and divided into sections corresponding to the alloy systems: Mg-Al (Section 2.5), Mg-Zn (Section 2.6), rare earth containing alloys (Section 2.7), biodegradable alloys

(Section 2.8) and various other alloying systems (Section 2.9). These chapters each contain a short introduction for the different alloys described, as well as phase diagrams, CALPHAD calculations and microstructural pictures, where meaningful. Subsequently scientific works investigating the respective alloys are discussed individually. Because of the diverse use of alloying elements, the investigated works are sorted in relation to the topic addressed in the corresponding literature, i.e., papers about the effects of Ca in an AZ91 alloy will be discussed in the section about aluminum calcium alloys (AX-System). This structure was chosen because even small changes of used forging stock, forming parameters and die design can result in considerable differences in forming trial results, mechanical properties and microstructural features. Readers can therefore more easily select the most interesting or beneficial study for their own work.

Additionally, a compilation of applied processing and heat treatment temperatures (App. 2.11.2) as well as mechanical properties and the respective processing parameters of the discussed scientific works (App. 2.11.3) are given in the appendices of this review.

2.5. Forging of Magnesium Alloys containing Aluminum

Aluminum was one of the first and is still the most important alloying element for Mg. More than 90% of all Mg structural applications are made from alloys within the Mg–Al system (mainly AZ91 and AM60) [34]. Al increases strength, hardness and castability of Mg alloys and allows precipitation hardening of alloys containing more than 6 wt.% [35]. Mg–Al shows eutectic behavior with a relatively high solubility limit of Al in Mg with 12.7 wt.% at the eutectic temperature and 0.5 wt.% at room temperature. The eutectic reaction $L \rightarrow \alpha \text{ (Mg)} + \beta \text{ (Mg}_{17}\text{Al}_{12})$ takes place at 437°C. As derived from the phase diagram shown in Fig. 2.6, the β -phase can be completely dissolved and exploited for precipitation hardening if the Al-content is lower than 12.7 wt.%. Nevertheless, at high Al-contents and with high amounts of eutectic due to segregations upon casting, long heat treatment times can be necessary for complete dissolution of Al into the Mg-matrix.

In the following the different sub-systems of the Mg–Al base alloys are reviewed.

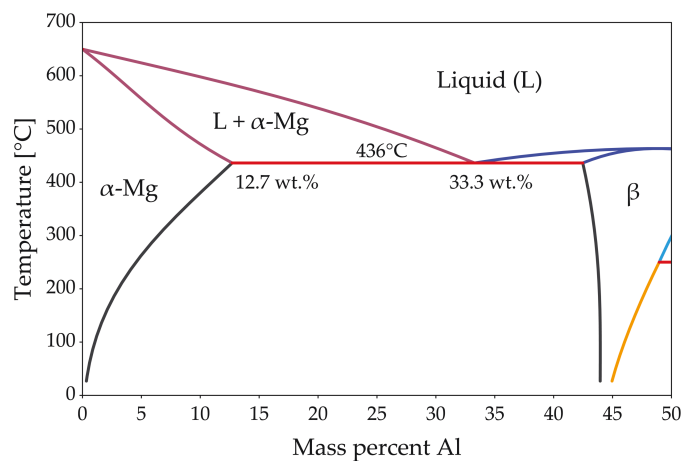


Figure 2.6.: Phase diagram of the Mg–Al binary system. For further information, see 2.11.1.

2.5.1. Mg–Al–Zn-System

For technical applications, Mg–Al alloys are often alloyed with low amounts of Zn (<1 wt.%), which further increases their strength at room temperature and their corrosion resistance [35]. Mg–Al–Zn is the most important alloying system for casting and forming applications with Al-contents ranging from 3 to 9 wt.% and Zn-contents lower than 1 wt.%. Additionally, Mn is used in minor contents likewise for

increasing the corrosion resistance [35]. Typical alloys used for forging are AZ31 (Mg – 3% Al – 1% Zn), AZ61 (Mg – 6% Al – 1% Zn), AZ80 (Mg – 8% Al, <1% Zn) and AZ91 (Mg – 9% Al – 1% Zn) where the latter is commonly used as a casting alloy but nevertheless forgeable.

The diffusion speed of Al in Mg is rather low leading to a divorced eutectic at the grain boundaries consisting of β -phase embedded in a supersaturated α -matrix. With increasing Al content, the amount of brittle β -phase at the grain boundaries increases, resulting in low ductility and limited formability. Therefore, a low Al content is usually preferred for forming operations. Nevertheless, if high strength is required, higher amounts of Al are common.

Nominal chemical compositions of commercial Mg-Al-Zn alloys are given in Table 2.2.

Table 2.2.: Nominal chemical compositions of commercial Mg-Al-Zn alloys given in wt. %.

Alloy	Al	Zn	Mn	Si	Cu	Fe	Ni	Others	Mg
AZ31 [36]	2.5 – 3.5	0.5 – 1.5	0.05 – 0.4	<0.1	<0.1	<0.03	0.005	0.1 max	Balance
AZ61 [36]	5.5 – 7.0	0.5 – 1.5	0.15 – 0.4	<0.1	<0.1	<0.03	0.005	0.1 max	Balance
AZ80 [36]	7.8 – 9.2	0.2 – 0.8	0.12 – 0.3	<0.1	<0.05	<0.005	-	0.3 max	Balance
AZ91A [37]	8.5 – 9.5	0.45 – 0.9	>0.17	<0.05	<0.025	<0.004	>0.001	0.01 max	Balance

An example for an AZ forging alloy is AZ80, which has been investigated by Sager et al. [38]. It was shown that the forming behavior of this alloy can be improved by a homogenization of the forging stock. Thereby the brittle β -Mg₁₇Al₁₂ phase is reduced and a supersaturated α -Mg solid solution is created. Precipitation of Mg₁₇Al₁₂ can occur after casting or can be used as a means of age hardening (T5 and T6 states) and it takes place continuously or discontinuously. In the discontinuous case the precipitating lamellae grow from Al rich areas (e.g., eutectic regions) into the α -Mg grains. It is usually assumed that continuous precipitation is preferable in terms of precipitation size, homogeneity and the thereby resulting in improved mechanical properties. Accordingly, the precipitation behavior of AZ91 has been investigated in detail by Braszczyńska-Malik [39]. Both types of precipitation are shown in Fig. 2.7.

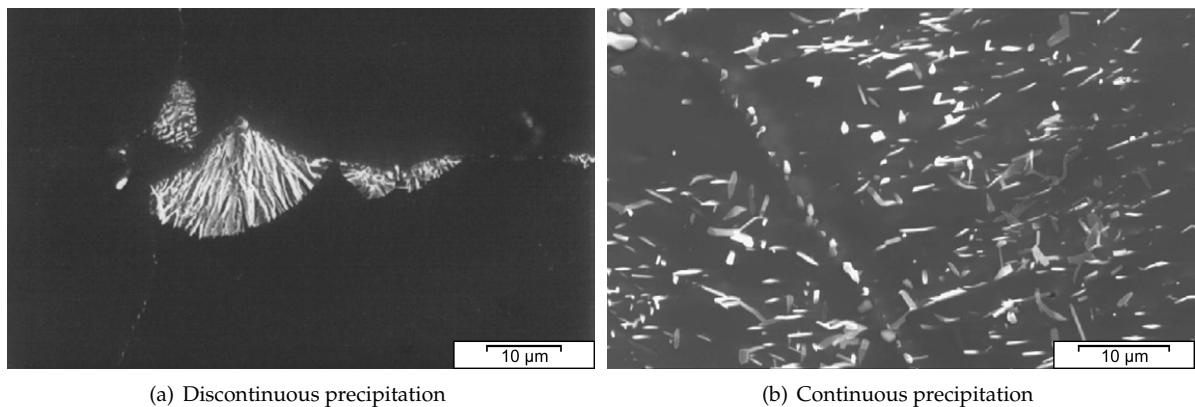


Figure 2.7.: SEM micrographs of homogenized and artificially aged AZ91, showing (a) discontinuous and (b) continuous precipitation [39]. Reproduced with permission from Elsevier.

The increasing material strength with rising Al content has also been confirmed in a comparative study of AZ31, AZ61 and AZ91 done by Madaj et al. [40]. Two different geometries, a piston rod and a plate, were forged, heat treated and analyzed by hardness measurements. The forging stock was homogenized at 380 to 420 °C for 15 h. The forming itself took place at 300 to 350 °C, depending on the alloy, with a die temperature of 150 to 170 °C. A recrystallization heat treatment (420 °C for 3 h) of the formed parts was tested on all alloys. The different alloys performed satisfactorily during forging and all parts were formed without defects. Finally, an improved hardness with increasing Al-content

was observed in all sample conditions, both for the initial and for the as-forged and the heat treated material. The highest values were reached by the as-forged AZ91 parts.

2.5.1.1. AZ31

AZ31 is well established as wrought alloy in the scientific community and has become something of a benchmark material in a multitude of applications. Therefore, many publications deal with the forming and forging of this alloy. A broad range of stock materials, from cast to highly deformed stock, as well as various processing parameters have been investigated throughout the years.

The CALPHAD calculation of AZ31 (Fig. 2.8) shows the fraction of present phases in the equilibrium state over temperatures, ranging from fully liquid to room temperature. The predominant precipitating phase is $Mg_{17}Al_{12}$, which can nevertheless be dispersed into the solid solution over a broad range of temperatures. Additionally, a minor amount of Al-Mn-phases with changing stoichiometry can start to precipitate during solidification. Zinc is present in AZ31 mainly in solid solution. Nevertheless, a ternary AlMgZn phase can be formed at low temperatures.

The microstructure of an AZ31 alloy for various processing steps is shown in Fig. 2.9. The material was cast into a steel mold and shows no distinctive features after casting. A homogenization heat treatment (415 °C for 24 h) was done to dissolve possible phases ($Mg_{17}Al_{12}$) at the grain boundaries and to ensure an even distribution of the alloying elements before forming. For the forging, the same sample geometry as depicted in Fig. 2.4 was applied. The as-forged microstructure is mostly devoid of intermetallic phases and there are differences visible depending on the degree of deformation. The sample center (Fig. 2.9 c) consists of a banded structure with fine recrystallized grains and elongated remains of the original grains. In contrast, the microstructure on the sample rim (Fig. 2.9 d) shows a high fraction of large, intensely twinned grains, showing that neither the temperature nor the degree of deformation was sufficient to start recrystallization of these grains.

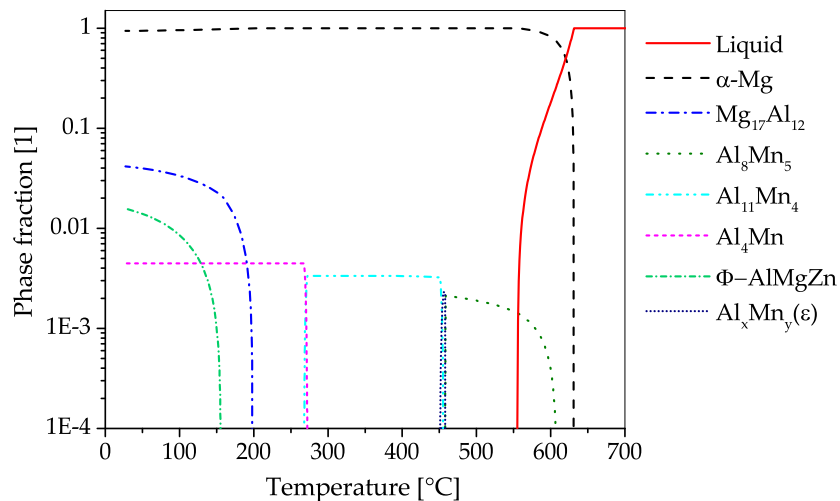


Figure 2.8.: CALPHAD calculations (for further information see 2.11.1) of AZ31 in a temperature range of 25 to 700 °C, showing phase fractions of 10^{-4} to 1.

The forgeability of AZ31 cast material was analyzed by Skubisz et al. [41]. There, the die forging trials (stock temperatures 200 to 300 °C, tool temperature 200 °C and ram speed 1 mm s^{-1}) were conducted with two different stock geometries, varying the height to diameter ratio (h/d). The best results were found in the h/d=0.8 samples formed at 300 °C. The samples produced at h/d=2.5 and other temperatures cracked while forming.

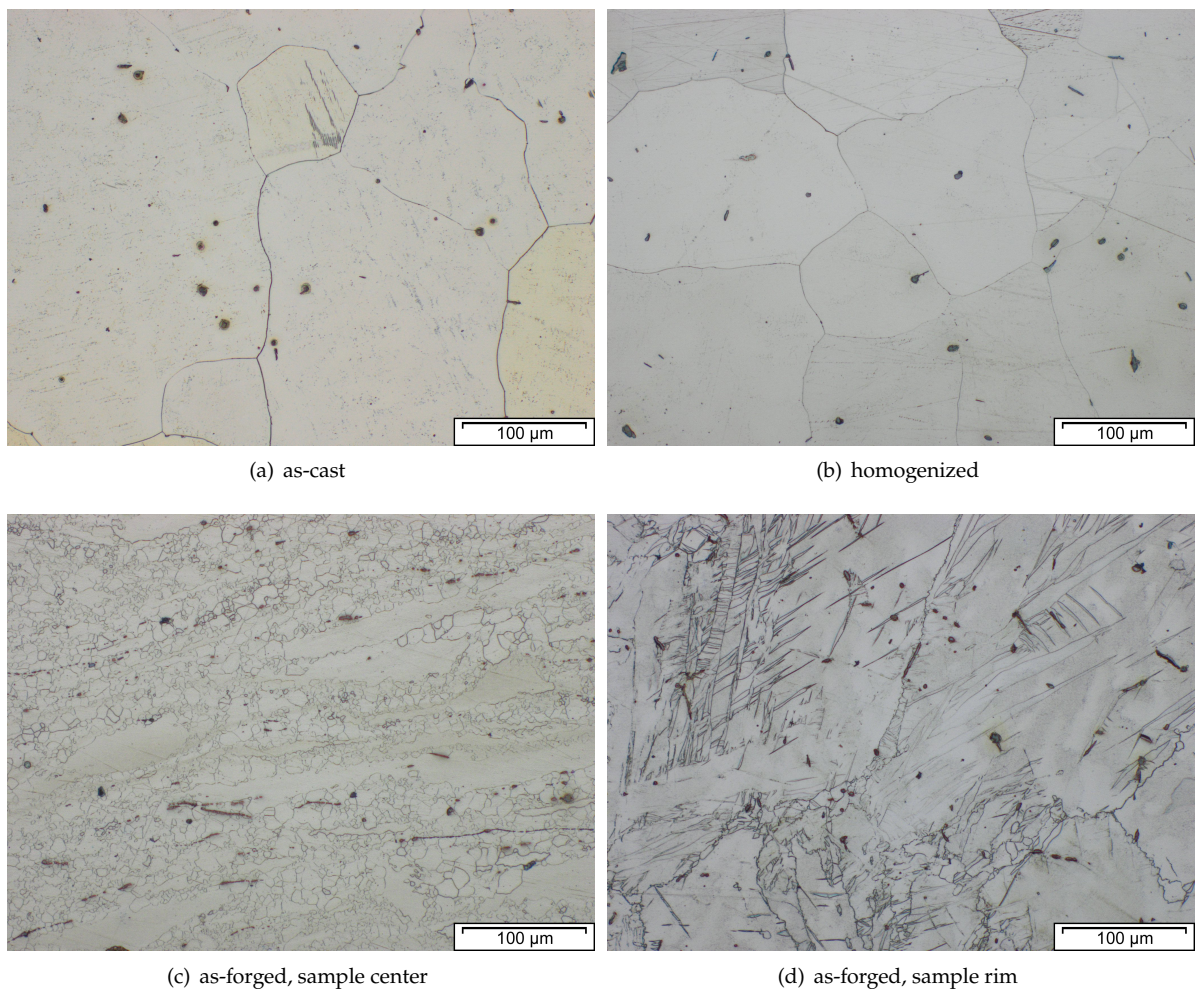


Figure 2.9.: Microstructure of AZ31 in consecutive processing steps: (a) as-cast, (b) homogenized at 415 °C for 24 h. Forging took place using a material temperature of approx. 425 °C, die temperatures of 280 °C and a ram speed of 10 mm s⁻¹. The as-forged microstructures of parts quenched in water are shown in: (c) center area having high degree of deformation and (d) flange area with a lower degree of deformation.

It is shown in multiple publications that extruded AZ31 forging stock has a superior formability at lower temperatures compared to cast AZ31. Chino et al. [42] for example conducted upsetting tests in a temperature range from 50 to 400 °C at an initial strain rate of 0.004 s⁻¹. The authors concluded that a forging temperature of at least 300 °C is advisable for samples with good surface quality. An increase of YS of the samples forged at lower temperatures was attributed to the accordingly decreasing grain size. In the work of Wong [43], testing took place between 300 to 500 °C at 0.001 to 1 s⁻¹, which yielded comparable results. Also, an increased surface roughness and a certain sensitivity to low temperatures and higher feasible forming speeds of the cast pre-material have been observed. An improvement of workability was noticed after a homogenization heat treatment (450 °C for 5 h) of the cast stock. The compression behavior of the extruded material was investigated as well, showing an anisotropy along the extrusion direction.

Such anisotropic forming behavior of extruded AZ31 was also recorded by Dai et al. [44]. In their work, samples from 3 material directions were compressed at 200, 300 and 400 °C with a strain rate ranging from 0.01 to 10 s⁻¹. They concluded that, dependent on the loading direction, the deformation processes favor either slipping or twinning.

In a comparison of extruded and continuously cast AZ31 and AZ80 presented by Viehweger et al. [45], no differences in the forging behavior were observed. While the flow curves (compression tests at 300, 350, 400 and 450 °C, with 0.1, 1 and 10 s⁻¹) and final microstructures varied in the diverse samples and alloys, the forging of simple geometries, using a punch speed of 1 to 40 mm s⁻¹ at various temperatures, was consistently successful. Skubisz et al. [46] investigated the material behavior of AZ31 at high forming speeds using a screw press. Compression testing and a FEM simulation were used for process layout and the forging took place at temperatures ranging from 170 to 350 °C. The extruded forging stock showed better formability when compared with cast material. Moreover, an improved formability was found in case of increased hydrostatic pressure while forming.

Graf et al. [47; 48] used compression testing (250 to 450 °C at 1 to 10 s⁻¹) and FEM simulation to support the die forging process of a wheel hub. To partially eliminate the brittle β -phase the cast material was homogenized at 430 °C for 6 h prior to forming. Testing of both, the cast and the extruded stock, took place at 250, 350 and 450 °C at ram speeds of 1 and 10 mm s⁻¹ and with a die temperature of 200 °C. The analysis of the forged parts showed distinct microstructural differences dependent on the forming parameters, i.e., forming speed, temperature and degree of deformation. In ref. [48] the same authors compared the forgeability of extruded AZ31 with AZ61 and AZ80. It was found that AZ31 had the worst forming behavior of the three alloys in the tested range of 250 to 450 °C at a ram speed of 10 mm s⁻¹. AZ60 could be formed well when using temperatures over 350 °C, showing a fine microstructure, attributed to the recrystallization, stimulated by Mg₁₇Al₁₂ particles. The best results were archived in AZ80, which was found to be well formable even at 250 °C.

Confirmatory results are shown in the work of Behrens and Schmidt [49], where AZ31 (as-cast as well as extruded) and extruded AZ61 were compared by forging pulley wheels. The results of either AZ31 stock was unsatisfactory in the presented forging process (300 to 400 °C at 12 to 160 mm s⁻¹ and at a die temperature of 350 °C). The extruded AZ61 stock was deformed at the same temperatures, however, the produced parts showed a better form filling behavior and higher surface quality. Subsequent tensile testing of parts forged from AZ31 and AZ61 showed an improved UTS but a reduced YS, which were claimed to be dependent on forming temperature and speed.

Cui et al. [50; 51] applied compression tests and FEM simulations to configure the forging process and die geometries of two different spur gear designs. In ref. [50] presumably extruded AZ31 was forged in two steps (at 0.5 mm s⁻¹) to a bevel gear. In the first step, the material was heated up to 300 °C while the die temperature was 275 °C, in the second step the temperature was lowered to 290 °C and 265 °C for stock and die respectively, to improve the mechanical properties of the finished parts. The part formed in ref. [51] was a straight spur gear, using extruded AZ31 as forging stock. In the supporting simulation, the resulting grain size of the formed part was calculated with help of the Zener-Hollomon parameter (ZH-parameter). Based on these results, the forging took place at 300 °C and 0.1 mm s⁻¹.

Extruded blanks of AZ31 and ZK60 were used by Poerschke [52] to forge disks with a rim and spoke design via a two-step forging process. The forgings were done at 315 to 375 °C using a screw and a hydraulic press, subsequently the microstructural behavior, showing typical banded structures, and mechanical properties of the produced parts were investigated. The parts made from ZK60 showed better tensile properties throughout the process chain when compared to the parts made of AZ31 material.

The recrystallization behavior of AZ31 and AZ61 alloy plates was analyzed by Watanabe et al. [53] to understand the grain size evolution in the forming process. The samples were deformed by upset forging in a range of 200 to 400 °C with an initial strain rate of 0.033 s⁻¹. The results were used to correlate the ZH-Parameter to the grain size of the dynamically recrystallized microstructure. It was found that the initial grain size of the material has an influence on the grain size of the recrystallized grains, and that the ZH-Parameter increases in case of decreasing grain sizes after recrystallization. AZ31 plates, as also extruded parts, usually exhibit a certain anisotropy in mechanical behavior and microstructure. This is discussed in the work of Rao et al. [54] where a rib-web-shape was forged and analyzed. A processing map and a model using the ZH-parameter was established, based on results from isothermal compression tests (300 to 550 °C, 0.0003 to 10 s⁻¹) and compared to the forming behavior of forged parts. Isothermal forging took place at temperatures ranging from 300 to 500 °C and 0.001 to 10 mm s⁻¹. Anisotropic behavior was found to be reduced in the DRX regime of the process, as the

authors concluded from the final sample shapes.

In the studies of Dziubińska et al. [55–58] AZ31 plates were used to produce various live sized brackets with ribs. For this purpose, the process was simulated and a newly designed, three slide forging press was used. The forging was done at a stock temperature of 410 °C and die temperatures ranged from 200 to 250 °C at 6 mm s⁻¹. After forming microstructures and mechanical properties varied, depending on the local strains applied in the forging process [56; 58]. This was especially apparent in the tensile properties of the brackets, an example being the YS which varied between 220 MPa and 298 MPa in the same part. The concept, challenges and possible problems of the forming process using a three slide forging press are described in [55; 57].

Lim and Yong [29] used AZ31 plate material for backwards extrusion trials. Forming took place at 200, 250 and 300 °C with 0.25 s⁻¹ in a hydraulic press. The forging process was simulated and afterwards the microstructure and the material flows within the parts were investigated. It was found that shearing damage may occur in hardly deformed areas, so called dead metal zones (Fig. 2.10).

Backwards extrusion of AZ31 with varying forming speed has been investigated by Matsumoto and Osakada [59] on cylindrical specimen. The AZ31 stock was annealed (350 °C for 1 h) before isothermal forming in the temperature range of 20 to 400 °C at an initial strain rate of 12 s⁻¹ at maximum. It was found that a decreased forming speed at the beginning of the deformation is beneficial to the forging. This is presumably caused by a more homogeneous temperature distribution within the sample.

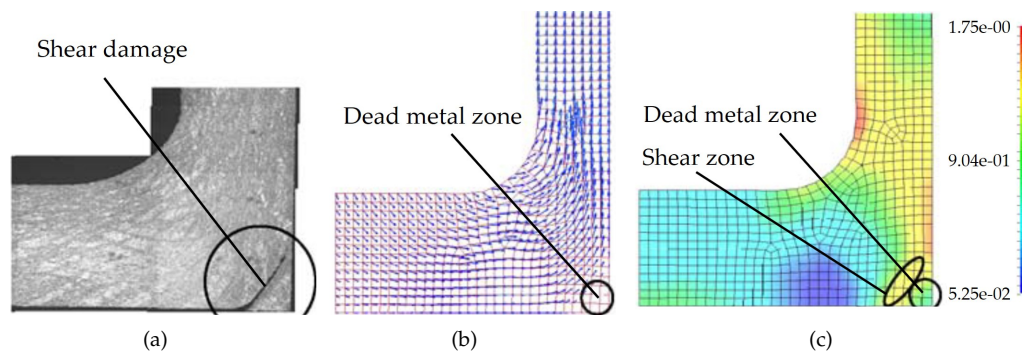


Figure 2.10.: Comparison of shear damage in an AZ31 (a) forged part, formed at 250 °C, (b) FEM simulations showing nodal vector displacement and (c) plastic strain distribution [29]. Reproduced with permission from Elsevier.

In some works, forging trials were conducted on heavily pre-deformed stock material. Takara et al. [60] used AZ31 sheets (thickness 0.8 mm) to form a part with ribs perpendicular to the surface. Parts with varying lubrication conditions were formed isothermally at 350 °C at a speed of 0.005 mm s⁻¹. In a subsequent analysis the material flow in the rib area was investigated and it could be shown that the lubrication has a profound impact on the material flow when forming parts with such small cross-sections.

Lee et al. [61] used stock material, pre-deformed by equal channel angular pressing (ECAP) with a grain size of approximately 3 μm to forge an impeller without burr. Forming took place at 300 °C, applying a strain rate of 0.001 s⁻¹, which allowed to retain the small grain size of the forging stock. The as-forged microstructure was investigated and the micro hardness measured. While forming, the grain size increased, reaching 4 to 6 μm. The resulting hardness fluctuated at 60 HV and decreased with increasing grain size.

AZ31 was used by Kápustová and Bílik [62; 63] to form a lever by closed die forging without flash. This forming process exhibits high hydrostatic stress and reduced material loss because of the missing forging flash, on the other hand it is primarily useful for the production of simple, rotary-shaped parts and requires a specifically shaped forging stock. The process and die layout was construed by FEM simulations, assuming die and material temperatures of 250 and 400 °C, respectively. The FEM calculations could be successfully verified by forming trials, where parts without defects were produced in this one step forging process.

Mróz et al. [64] used AZ31, plated with Al, to forge a bimetallic door handle. The stock material was produced by explosive welding, where an AA1050A tube was bonded to an AZ31 rod. Forming was done in three steps (bending and two forging steps) at 400 °C material temperature and die temperatures of 300 °C. A screw press capable of a tool speed of 30000 mm min⁻¹ was applied in this process. While there was no damage of the bimetallic bonding zone, the covering Al layer was unduly pressed into the forging flash. This was attributed to the low flow stress of the AA1050A cladding material at the high forming temperatures. As primary purpose of the Al coating is to protect the AZ31 center material from corrosion, the measured corrosion properties varied strongly, depending on the quality of the still existent Al surface layer. For mechanical testing AZ31 forgings without Al cladding were used. The finished forging showed improved properties (a YS of 234 MPa and 280 MPa UTS) as well as reduced grain sizes, when compared to the stock material.

The tension and compression behavior as well as fatigue properties of forged AZ31 were investigated by Toscano et al. [65; 66]. As-cast stock material was homogenized at 450 °C for 3 h and formed directly afterwards. The material was open-die forged isothermally at 450 °C at a ram speed of 6.5 mm s⁻¹, producing so called 'flatbread' or 'pancake' samples in a single step. The tensile properties of the forged and cast material are compared and while a distinct increase in strength was found in the forged samples, the elongation was reduced. The forging also showed anisotropic mechanical behavior, which was verified by texture analysis. Strain controlled fatigue testing (R= -1) was done for both materials and it could be shown that the low cycle fatigue (LCF) life of the forged samples was increased. In accompanying microstructural analyses extensive twinning could be shown. Analyses of the fracture surfaces revealed the initiation of fatigue cracking to occur at intrusions-extrusions, surface pores, extension twinning and oxide layers. In a subsequent work [67], the same material was used to form a more complex part by closed-die forging at 275 °C and 20 mm s⁻¹. The strength of the formed part was found to be increased as well as the fatigue properties (load controlled, at R= -1) when compared to the cast forging stock.

Gryguc et al. analyzed the compressive [68] as well as the tensile and fatigue behavior [69] of extruded and forged AZ31. The extruded stock was compressed isothermally up to 85 % engineering strain at 400 °C by applying strain rates of 0.002, 0.02 and 0.075 s⁻¹. From the resulting pancake-shaped parts, as well as from the extruded stock, samples for compression, tensile and fatigue testing were machined. All tested mechanical properties were found to be improved by the forging process. This was attributed to a change of texture and the change from a bimodal grain distribution to a refined and equiaxed structure. The results were supported by investigations of the fracture surfaces of the fatigue samples, which showed a dimpled fracture surface for the forged samples in comparison to a terrace-like structure in the extruded ones.

2.5.1.2. AZ61

The aluminum content of the alloy AZ61 lies in-between the two main representatives of forming and casting alloys, AZ31 and AZ91 respectively. It is considered as both, a casting as well as a wrought alloy. According to ref. [35] its Al content of 6 wt. % yields an optimum combination of ductility and strength. While this alloy can, in principle, be used in heat treated condition, this is usually not the case for forgings, which are mainly used in as-forged state [30].

The CALPHAD calculation (Fig. 2.11), shows the fraction of present phases in AZ61 over the temperature range from fully liquid to room temperature in equilibrium state. As in AZ31, the predominantly precipitating phase is Mg₁₇Al₁₂, which can nevertheless be dissolved into the solid solution over a broad range of temperatures. Additionally, a minor amount of AlMn-phases with varying stoichiometry can be found in the alloy, which already begin to precipitate during solidification. Zinc is found mainly in solid solution, however, at low temperatures an AlMgZn-ternary phase can be formed.

Skubisz et al. [41] analyzed the forming behavior of wrought AZ61 (hot deformed to 0.83 effective strain) by die forging tests. Two different stock geometries (ratio of height to diameter: 0.8 to 2.5) were used for the deformation at stock temperatures of 150, 200 and 350 °C (tool temperature 200 °C, ram speed of 1 mm s⁻¹). Only the forging at 150 °C showed cracking. Nevertheless, all samples showed adequate

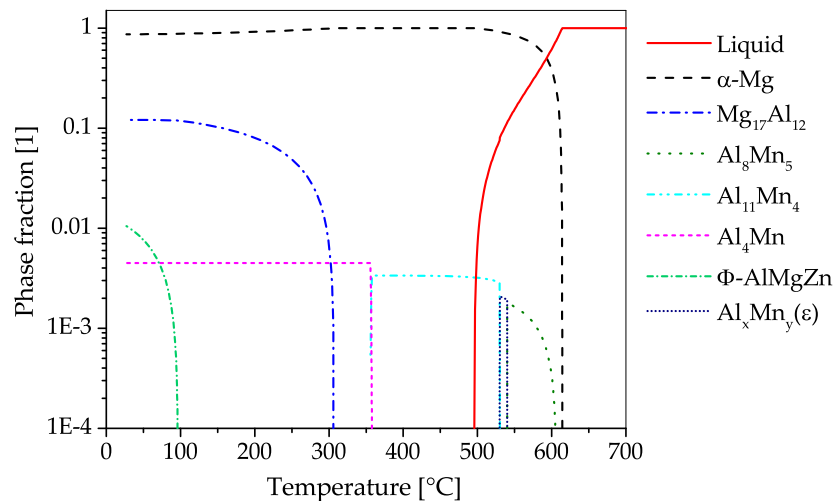


Figure 2.11.: CALPHAD calculations (for further information see 2.11.1) of AZ61 in a temperature range of 25 to 700 °C, showing phase fractions of 10^{-4} to 1.

surface quality.

Yoon et al. [70] investigated the forming behavior and process parameters of extruded AZ61 forging stock with compression testing and simulation. Forging trials were done at 350 °C with a speed of 32 mm s^{-1} . The stock material was pre-deformed by upsetting at room temperature (RT), up to an axial strain of 0.06 and 0.6 in order to compare the warm forming behavior of twinned versus recrystallized material. The produced parts were analyzed with regard to microstructure and mechanical properties. It was found that recrystallized forging stock increases the formability but reduces the achievable tensile strength in comparison to the twinned AZ61.

Various authors compared the forging behavior of AZ61 and AZ31 [48; 49; 53]. These studies are briefly described above, in Section 2.5.1.1 for AZ31. Madaj et al. [40] describes the forming behavior of AZ61 at a material temperature of 320 °C in a work comparing the formability of AZ31, AZ61 and AZ91, which is discussed in Section 2.5.1. A comparison of forging behavior and mechanical properties of AZ61, AZ80 and various TAZ alloys by Yoon and Park [71] is reviewed in Section 2.9.

2.5.1.3. AZ71

Material made from the alloy AZ71 was advocated as forging stock for large parts i.e., wheels by Fugita et al. [72]. They discussed the large grain size of Mg-Al alloy castings and the resulting problems for Mg forming products. The AZ71 alloy is reported to form a reduced grain size in casting, especially with additions of Sr and/or calcium cyanamide (CaNCN), making it a good candidate for forging without prior extrusion. Upsetting tests were conducted to investigate the forgeability in the range of 250 to 400 °C with 0.01 to 10 s^{-1} .

The CALPHAD calculation of the constituent phases in AZ71 over temperature ranging from fully liquid to room temperature in equilibrium state is given in Fig. 2.12. The predominantly precipitating phase is $\text{Mg}_{17}\text{Al}_{12}$, which can nevertheless be dispersed into the solid solution by applying heat treatment temperatures over 350 °C. Hardening of AZ71 is possible via the precipitation of the $\text{Mg}_{17}\text{Al}_{12}$ phase. Additionally, a minor amount of AlMn-phases with changing stoichiometry can be found in the alloy, starting to precipitate during solidification. The Zn present in this alloy is found solely in solid solution.

Chen et al. [73] studied the forming behavior of AZ71 with rising Nd content (0 to 2 wt.%) by rotary forging. The alloys were analyzed regarding the grain refinement properties of Nd and mechanical

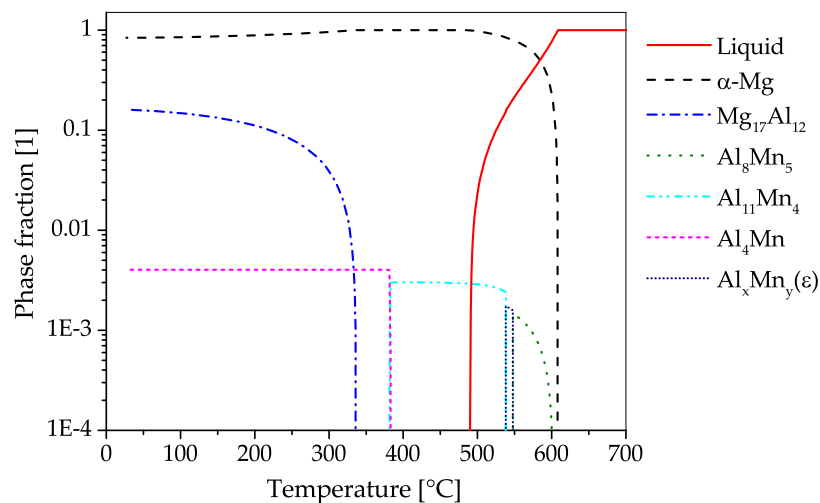


Figure 2.12.: CALPHAD calculations (for further information see 2.11.1) of AZ71 in a temperature range of 25 to 700 °C, showing phase fractions of 10^{-4} to 1.

properties throughout the process chain: casting, homogenization, forging and annealing (T5). Suitable heat treatment parameters were shown to be a homogenization at 420 °C for 6 h and annealing at 350 °C for 1 h after forming. The rotary forging itself was done at 200 °C with 3 s^{-1} up to 32 % engineering strain. The alloys containing >1 wt.%Nd could be forged without surface damage. The alloy containing 1 wt.%Nd showed sufficient grain refinement in the as-cast state and the best overall tensile properties in T5 state.

In the works of Guan et al. the forming characteristics of cast AZ70 were tested [74] and a projectile head shell was produced by die forging [75]. The semi-continuous cast material was homogenized at 410 °C for 10 to 15 h prior to forming. Flow curves, covering the range of 300 to 420 °C and 0.001 to 1 s^{-1} (showing DRX behavior in varying intensity), are presented in [74] and were subsequently used to model the flow stress based on the ZH parameter. In ref. [75] the critical processing parameters: temperature, strain rate and degree of deformation (in relationship with the grain size) are discussed and appropriate ranges selected. Based on these a projectile head shell was forged in two steps. Forming took place with a constant crosshead speed of 8 mm s^{-1} at 400 °C and 380 °C for pre-forming and punching, respectively. The finished parts were heat treated (T5 and T6) and the mechanical properties evaluated, with the T6 state showing the best overall properties.

2.5.1.4. AZ80

The alloy AZ80 was developed in the 1950 by Dow Chemical with the specific aim to be used in forged parts, e.g., die-forged wheels [13]. Even nowadays it is a commonly used alloy in the forging of Mg-products. In the as-cast state AZ80 consists of dendritic α -Mg and inter-dendritic eutectic β - $\text{Mg}_{17}\text{Al}_{12}$ phase as result of its high Al-content. To improve the forming behavior of the forging stock a homogenization heat treatment at 420 °C for 20 h was deemed suitable by Sager et al. [38]. This or a solution heat treatment makes artificially ageing (T5 or T6 states) possible for AZ80.

The CALPHAD calculation (Fig. 2.13), shows the fractions of phases present in AZ80 over the temperature range from fully liquid to room temperature in equilibrium state. The predominantly precipitating phase is $\text{Mg}_{17}\text{Al}_{12}$, which can dissolve into the α -Mg matrix at temperatures above 350 °C. The alloy can be strengthened by precipitation of $\text{Mg}_{17}\text{Al}_{12}$. Additionally, a minor amount of AlMn-phases with varying stoichiometry can be found in the alloy, which start to precipitate during solidification. Zinc is found solely in solid solution in AZ80.

The microstructure of as-cast and forged AZ80 (which is further described in ref. [76]) is depicted

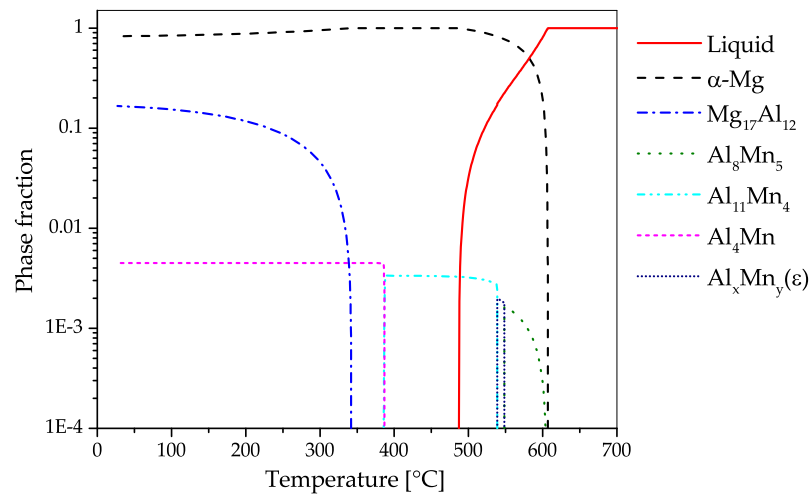


Figure 2.13.: CALPHAD calculations (for further information see 2.11.1) of AZ80 in a temperature range of 25 to 700 °C, showing phase fractions of 10^{-4} to 1.

in Fig. 2.14. The micrographs show the coarse casting microstructure (Fig. 2.14 a) as well as recrystallized grains resulting from the forming tests, which were performed at varying temperatures and deformation rates. Discontinuously precipitated β -particles ($\text{Mg}_{17}\text{Al}_{12}$) can be observed in the as-cast state while they are dispersed in the forged samples (Fig. 2.14 b-d). The grain size in the deformed microstructure increases visibly with increasing processing temperature and speed.

Multiple groups have investigated the material behavior of AZ80 by means of compression or upsetting tests to optimize their forging processes. Ju et al. [77] utilized such test results (0.001 , 0.01 and 0.1 s^{-1} , up to $420 \text{ }^\circ\text{C}$) for the FEM modelling of upsetting tests and an automotive wheel geometry. The simulation revealed distinct differences in strain rate and plastic strains throughout the work piece. In the work of Zhou et al. [78] processing maps in the range of 200 to $500 \text{ }^\circ\text{C}$ and 0.001 to 20 s^{-1} were generated, and the correlation between the yield strength and the Zener-Hollomon parameter shown. This approach was mirrored by Su et al. [79] who generated power dissipation maps (275 to $400 \text{ }^\circ\text{C}$ and 0.001 to 1 s^{-1}) to improve the forging of aerospace cover plates from extruded stock material. The power dissipation maps showed the best processing conditions to be in a temperature range of 283 to $310 \text{ }^\circ\text{C}$ at 0.001 to 0.0017 s^{-1} . This was verified by isothermal forging trials, done at 300 and $380 \text{ }^\circ\text{C}$ with a strain rate of 0.0005 s^{-1} , corresponding to a ram speed of 0.075 mm s^{-1} . The forging produced at $300 \text{ }^\circ\text{C}$ exhibits a fine grain size (average of $5 \text{ }\mu\text{m}$) and good mechanical properties of 330 MPa UTS and a YS of 260 MPa , showing the best overall properties.

Kobold, Pepelnjak et al. investigated the forming behavior of extruded forging stock in multiple loading directions with compression tests and described in several works the strongly anisotropic material response. In ref. [80] the measured material parameters are used to simulate compression tests and the forging process of a shock absorber head with different FEM programs. The differences in the sample shape resulting from compression testing at $300 \text{ }^\circ\text{C}$, $350 \text{ }^\circ\text{C}$ and $400 \text{ }^\circ\text{C}$ with deformation rates of 0.4 to 2.3 s^{-1} are discussed in ref. [81; 82]. The results of these forming trials were subsequently implemented in an anisotropic yield model to successfully simulate an industrially forged part. Similar investigations have also been conducted by Viehweger et al. [45], they studied the influence of cast versus extruded stock material on the warm forming behavior of AZ80 and AZ31. The alloys were analyzed using upsetting tests, microstructural analysis and concluding isothermal forging trials with simple testing geometries. Compression testing was done at 300 , 350 , 400 and $450 \text{ }^\circ\text{C}$ with strain rates of 0.1 , 1 and 10 s^{-1} , the resulting flow curves were used for a simulation of the forging process. Die forging was successfully done at various temperatures and punch speeds ranging from 1 to 40 mm s^{-1} .

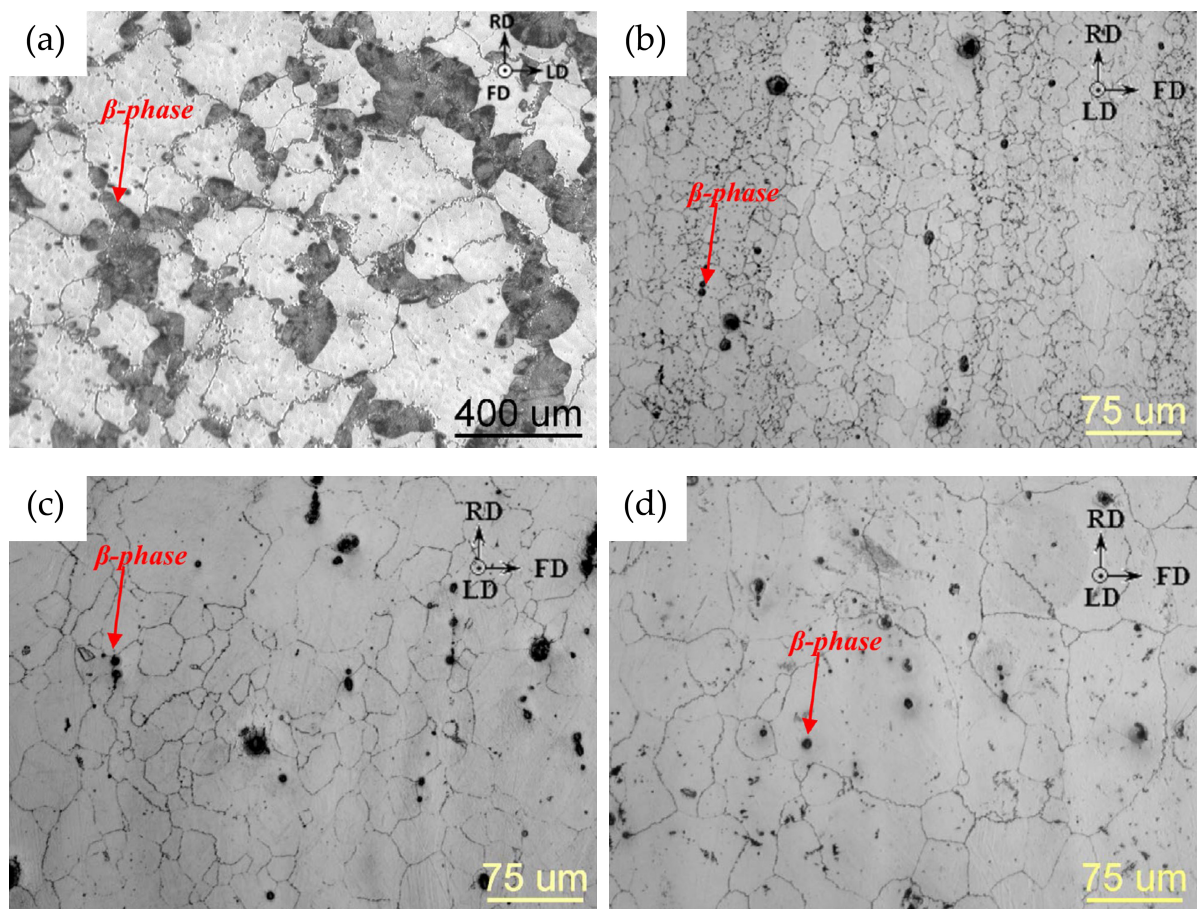


Figure 2.14.: Microstructure of AZ80 in varying conditions: (a) cast, (b) forged into 'flatbread' samples at 350 °C with 0.65 mm s^{-1} , (c) forged at 450 °C with 0.65 mm s^{-1} and (d) forged at 450 °C with 6.5 mm s^{-1} [76]. Reproduced with permission from Elsevier.

Swiostek et al. [83] compared the forging behavior of cast and extruded (350 °C, extrusion rate of 3 m min^{-1} and ratio of 8) stock material of AZ80, ZK and RE alloys by die-forging. All alloys were formed to a simple circular stepped shape in a temperature range of 200 to 450 °C, using die-temperatures of 220 °C. In case of AZ80 the alloy was additionally compared to two modified alloys containing 2.1 wt.%Ca and 1.9 wt.%RE respectively. The best forming temperature was found to be in a range of 350 to 400 °C for all alloys. The samples formed at 350 °C were further investigated by tensile, hardness and corrosion tests as well as by metallographic analysis. It was found that the modifications of AZ80 were not gainful. The microstructure of the conventional AZ80 alloy consisted of fine recrystallized grains in the range of 5 to 9 μm , while the modified alloys showed a coarser structure with grain diameters up to 20 μm . The unmodified AZ80 material showed superior results of all investigated AZ alloys regarding tensile strength, hardness and corrosion resistance. However, the best performing alloy throughout the study was found to be WE43.

Yoon et al. investigated the heat treatment, material behavior and process layout of three different automotive components: parts in the shape of a tie-rod, a control arm and a differential gear case. The tie-rod was forged isothermally at 250 °C from extruded stock material with a head speed of up to 560 mm s^{-1} [84]. The microstructural and mechanical behavior after a T5 heat treatment (177 °C up to 55 h, reaching the peak hardness at 26 h) in comparison with the extruded stock material was of

particular interest. Both, continuous and discontinuous precipitation of $Mg_{17}Al_{12}$ -phase were found to occur, showing that precipitation of the continuous type takes place mainly in the fine recrystallized grains stemming from the forging process. While the strength of the extruded material was increased by approximately 50 MPa after the T5 heat treatment, the strength of the forged and heat treated AZ80 only increased by 21 MPa, whereas its elongation to failure increased from $\sim 6\%$ to 8% . In ref. [85] a control arm was forged in a two-step process at material temperatures of $265\text{ }^{\circ}\text{C}$ and $365\text{ }^{\circ}\text{C}$ (die temperature $250\text{ }^{\circ}\text{C}$ and ram speed of 250 mm s^{-1}) from extruded stock material. While the part forged at $265\text{ }^{\circ}\text{C}$ showed the best mechanical properties, the part could not be fully formed. The mechanical properties of the part forged at $365\text{ }^{\circ}\text{C}$ were nearly at the level of the extruded stock material while exhibiting an increased elongation to failure. The differential gear case was forged isothermally from extruded AZ80 stock material at $300\text{ }^{\circ}\text{C}$ and a head speed of 150 mm s^{-1} [86]. For an improved process design, the stock material behavior was tested in advance with compressive tests at $300\text{ }^{\circ}\text{C}$ (1 s^{-1} and 10 s^{-1}), these results were subsequently used to simulate the forging process by FEM. The microstructure and the mechanical properties of the as-forged parts were compared to the extruded material, showing a slight decrease in strength but an increase of elongation to failure. This behavior was attributed to DRX, leading to a decreased dislocation density and grain refinement in the forged material.

Kevorkijan et al. [87] investigated the possible use of Mg alloys in automotive applications. For this purpose, connecting rods were forged from extruded AZ80 (and ZC71/SiC/12p) at semi-industrial scale. Closed-die forming was done at a strain rate of 0.11 s^{-1} using temperatures of $415\text{ }^{\circ}\text{C}$ (material) and $300\text{ }^{\circ}\text{C}$ (forging die). The material was heat treated (T5) at $177\text{ }^{\circ}\text{C}$ for 24 h and the mechanical properties were evaluated. The tested part reached 389 MPa UTS and a YS of 274 MPa at an elongation of 8% .

Large helicopter support beams were forged by He et al. [88]. The filling and machine load was simulated and by choosing a slow finishing speed and a semi-open-die geometry, it was possible to forge the parts at relatively low forming loads. A pre-forged billet was used for isothermal die forging at $380\text{ }^{\circ}\text{C}$ with speeds ranging from 1 to 0.005 mm s^{-1} .

In the work of Wang et al. [89] the formability of cast AZ80 is analyzed by compression tests and die forging of a wheel is shown. The stock material was homogenized at $400\text{ }^{\circ}\text{C}$ for 12 h and isothermally forged at temperatures between 360 and $400\text{ }^{\circ}\text{C}$ using a speed of 16 mm s^{-1} . In the as-forged condition UTS values of 320 to 330 MPa were reached.

Kurz et al. [90] compared the forming behavior of extruded AZ80 and modifications thereof (small additional amounts of Ce ($<1\text{ wt.}\%$) as well as Ce ($<1\text{ wt.}\%$) plus Y ($<1\text{ wt.}\%$)) to ZK60. Isothermal forgings in the shape of a stylized wheel hub were produced in a temperature range of 175 to $450\text{ }^{\circ}\text{C}$ with a ram speed of 10 mm s^{-1} . The forgings of AZ80 showed sufficient part quality from 200 to $450\text{ }^{\circ}\text{C}$, the modification with Ce and Y had the widest forming window.

Graf et al. [48] compared the forging behavior of extruded and cast AZ31, AZ61 and AZ80 – this work is discussed in Section 2.5.1.1.

A wheel-shaped part ($\text{Ø}630\text{ mm}$) was produced by Yuan et al. [91] by isothermal die forging. The forming process was simulated first and based on the simulation data, forging took place at $330\text{ }^{\circ}\text{C}$ using a speed of 1 mm s^{-1} . The produced parts were artificially aged at $150\text{ }^{\circ}\text{C}$ for 30 h, before tensile tests were done at RT and $130\text{ }^{\circ}\text{C}$. Samples from different locations within the part were tested, which resulted in differing results of up to 100 MPa at RT. The smallest grain size and best tensile values were found in the web area; 208 MPa YS and 371 MPa UTS with an elongation of 7.5% were reached at RT. The values for $130\text{ }^{\circ}\text{C}$ were 186 and 258 MPa and 42.8% for YS, UTS and elongation respectively. The worse mechanical properties of the samples from the inner wall were attributed to an absence of texture, bent flow lines and a high Schmid factor, resulting in an easy activation of the basal slip.

Chen et al. [92] used isothermal closed-die forging to produce an upper receiver from extruded AZ80 in two forging steps. The forming process was simulated based on compression tests, done at 250 to $400\text{ }^{\circ}\text{C}$ with 0.001 to 1 s^{-1} . The forging itself took place at 16 mm s^{-1} and temperatures of 320 , 350 and $380\text{ }^{\circ}\text{C}$. Out of these temperatures, $350\text{ }^{\circ}\text{C}$ turned out to be the most promising. The two-step process was chosen to avoid defects, e.g., folds or under-fillings. The as-forged parts showed a homogeneous microstructure with a grain size of 13 to $18\text{ }\mu\text{m}$ throughout. In tensile tests 294 MPa YS, 406 MPa UTS

and 15% ϵ_f were reached.

Some work in the direction of aviation applications has been done in the 'MagForming' project [93], where a doorstop and a blank for a compressor impeller were successfully forged from AZ80 (and WE43). Forging of the doorstop was done in two steps at 300 to 320 °C with a ram speed of 5 mm s⁻¹. The billet for the compressor wheel was forged in one step at 280 to 350 °C with a ram speed of 10 mm s⁻¹. A bigger forging, in the shape of Airbus window frame, was done at 320 to 330 °C using AZ80 cast plates (and AZ31 rolled plates) as stock material.

Some of the most recent work on AZ80 forged parts has been done in Canada, where parts in various sizes were produced. Forgeability of extruded and cast stock material was compared as well as the mechanical and fatigue properties investigated. The forging process itself and accompanying simulations for a control arm as well as flow curves are shown in [94].

The mechanical properties of forged AZ80 were analyzed by Gryguc et al. [76; 95]. Extruded and cast stock material was forged isothermally (375 °C and 20 mm s⁻¹ ram speed) to a part shaped like an asymmetric I-crossbeam section, and the final parts were compared. While the mechanical properties of the sample varied with texture and processing parameters, the extruded and forged material was found to be superior to the stock material in tensile tests as well as in LCF tests [95]. The same authors also investigated the mechanical behavior of as-cast and forged material (flatbread samples), which were formed isothermally in a temperature range of 350 to 450 °C at ram speeds of 0.65 mm s⁻¹ and 6.5 mm s⁻¹ [76]. It was found that the forging process significantly improved the properties of the cast material in the tested monotonic LCF and HCF (high cycle fatigue) regimes. The changes in microstructure originating from the forging process, refined grains, recrystallization and texture change, were stated to be the decisive factor in this regard.

The influence of the process and microstructure on the fatigue properties was also investigated by the work of Guo [96] where the spokes of an industrially forged AZ80 wheel were analyzed by tensile and fatigue testing. The microstructure was further studied with SEM and the phases α -Mg and β -Mg₁₇Al₁₂ were tested with nanoindentation, showing distinctive differences in stiffness. Microcracks at the boundaries between these two phases were also found to be responsible for fracture in fatigue testing.

The Mg₁₇Al₁₂ phases as well as the fracture behavior during the forging process was investigated as well by Qiang et al. [97]. In this work, AZ80 material was cast and homogenized at 400 °C for 15 h. Forging took place at 400 °C with a press speed of 12.4 mm s⁻¹. The crack initiation on the sample surface was reported to take place at the α -Mg/Mg₁₇Al₁₂ interface, in the sample interior cracks propagate mainly along the grain boundaries.

2.5.1.5. AZ91

AZ91 is the most widely used Mg alloy for casting applications and it is typically processed via high pressure die casting. As a casting alloy, AZ91 benefits from its high Al amount, leading to reduced melt temperatures and high strength due to formation of intermetallic phases. Typically, high pressure cast parts made of AZ91 are used in the as-cast state.

Nevertheless, AZ91 can also be used in the wrought form, where it achieves higher strength values (as fabricated as well as T6 state) than its contenders AZ31 and AZ61, stemming from the higher Al content [98]. Despite the rather high Al content present in the alloy, the binary phase Mg₁₇Al₁₂, typically found on the grain boundaries, can be completely dissolved by a solution heat treatment and therefore be utilized for precipitation hardening.

The precipitation behavior has been analyzed by Braszczyńska-Malik [39], using AZ91 cast material (already mentioned in Section 2.5.1). After homogenization heat treatment/solution annealing (420 °C for 24 to 26 h) the effect of artificial ageing on continuous and discontinuous precipitation was tested. It was shown that continuous precipitation is prevalent in case of dominating grain boundary diffusion while discontinuous precipitation was favored in case of volume diffusion. Solely continuous precipitation was achieved for a sample solution heat treated and artificially aged at 350 °C.

The CALPHAD calculation shown in Fig. 2.15, shows the fraction of equilibrium phases present in AZ91 over a temperature range from fully liquid to room temperature. The predominantly precipitating phase is $\text{Mg}_{17}\text{Al}_{12}$, which can also be dispersed into solid solution at annealing temperatures between 350 and 400 °C. Strengthening of AZ91 can be accomplished by precipitation of $\text{Mg}_{17}\text{Al}_{12}$. Additionally, a minor amount of AlMn-phases with varying stoichiometry can be found in the alloy, starting to precipitate during solidification. The Zn present in this alloy is found solely in solid solution.

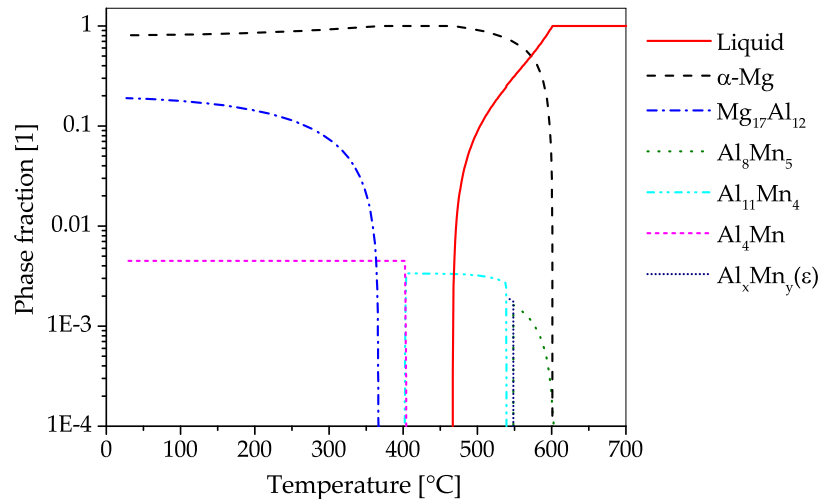


Figure 2.15.: CALPHAD calculations (for further information see 2.11.1) of AZ91 in a temperature range of 25 to 700 °C, showing phase fractions of 10⁻⁴ to 1.

The microstructure of a forged piston rod made from cast AZ91 (compare Fig. 2.1 and 2.4) is shown in Fig. 2.16. Discontinuous precipitation of the $\text{Mg}_{17}\text{Al}_{12}$ phase is visible on the grain boundaries of the as-cast material (Fig. 2.16 a). After a homogenization heat treatment at 425 °C for 24 h, these phases are mostly dissolved into the α -Mg matrix. The homogenized material was forged at approximately 300 °C, using die temperatures of 280 °C and a ram speed of 10 mm s⁻¹. The as-forged parts (air-cooled) show different microstructures, depending on the degree of deformation applied. In the sample center a bimodal microstructure is observable, consisting of very fine grains, showing the onset of recrystallization and the deformed remains of the original structure. In the less deformed flange area, the cast microstructure is still visible, however, the applied deformation led to a significant amount of twins, pervading these large grains.

Owing to the fact that AZ91 is primarily a casting alloy, published works about its forging behavior are few. Madaj et al. [40] forged AZ91 at 300 °C stock temperature for a comparison with AZ31 and AZ61, this work is reviewed in Section 2.5.1.

The works investigating AZ91 containing Ca (AZX911) are discussed in Section 2.5.3.

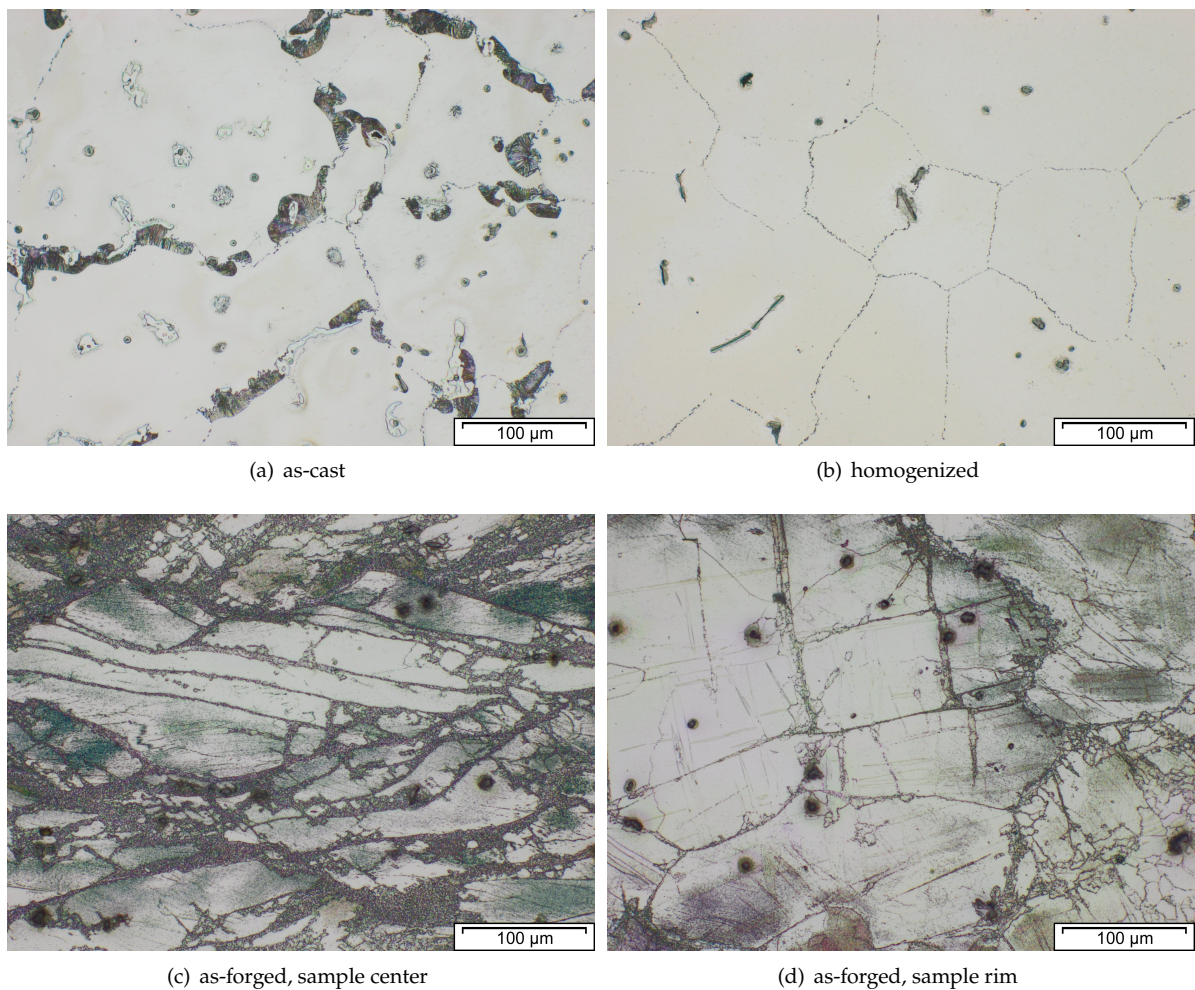


Figure 2.16.: Microstructure of AZ91 in consecutive processing steps: (a) as-cast, (b) homogenized at 425 °C for 24 h. Forging took place using a material temperature of approx. 300 °C, die temperatures of 280 °C and a ram speed of 10 mm s⁻¹. The as-forged microstructures of parts cooled at air are shown in: (c) center area having high degree of deformation and (d) flange area with a lower degree of deformation.

2.5.2. Mg-Al-Mn-System

While alloys of the AM-System are not usually used for forging, the system itself has some significance for many other Al-containing alloys. Manganese is added to Mg alloys to improve the corrosion behavior by binding unwanted Fe. It can also be utilized to create dispersoids in the casting process or in subsequent heat treatment steps.

According to Cihova et al. [99] these dispersoids (Fig. 2.17) have a negligible effect on the hardening behavior of the material, but they play an important role in the obstruction of grain boundary movement. This is of course an important feature in regard to high temperature processing and heat treatments. In their work [99] the formation and properties of these Mn-containing phases are analyzed in detail for an extruded **AXM100** alloy.

Ma et al. [100] investigated the recrystallization behavior of extruded **AM30** by compression testing followed by microstructural analyses. The isothermal testing took place at 450 °C with a strain rate of 0.001 to 0.8 s⁻¹. The developed texture was analyzed by EBSD and XRD. The twinning and DRX

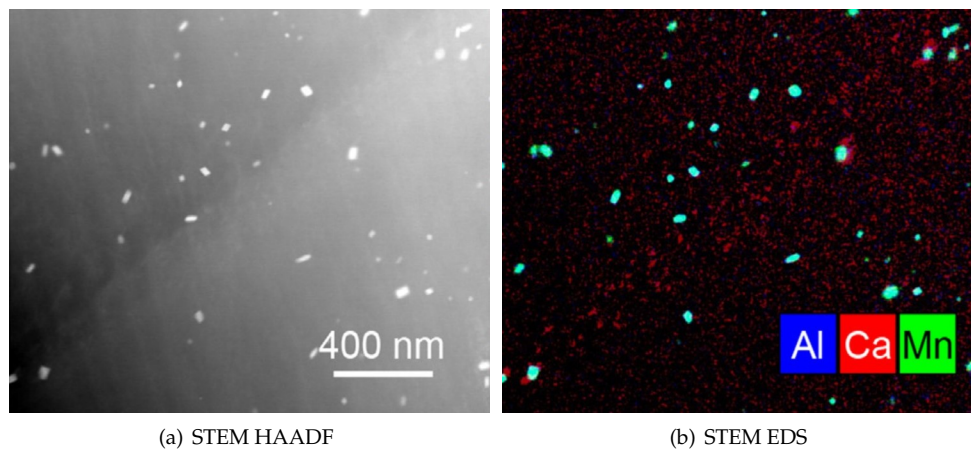


Figure 2.17.: Micrographs made by scanning transmission electron microscope (STEM) high-angle annular dark-field (HAADF) (a) and corresponding STEM energy dispersive X-ray spectroscopy (EDS) (b) of Al- and Mn-containing dispersoids (blue and green, respectively) in an extruded AXM100 alloy in T6 state. Ca-containing precipitates (shown in red) are visible as well [99]. Reproduced with permission from Elsevier.

behavior are discussed and it could be shown that the stress-strain response and the correspondent microstructure were strain rate dependent. Only at the highest strain rate (0.8 s^{-1}), a significant material softening during deformation was found. The recrystallization behavior changed with increasing strain rate. At higher speeds ripened, equiaxed grains evolved, whereas at low forming speeds an irregular grain structure was present, consisting of new fine recrystallized grains at the original grain boundaries besides grains growing from twin boundaries within the original grains.

2.5.3. Mg-Al-Ca-System

The addition of Ca to Mg-Al-alloys leads to various beneficial effects for wrought alloys, e.g., reduced anisotropy [101; 102], reduced grain size [103], increased creep resistance [104; 105] and the ability of precipitation hardening by Mg_2Ca and Al_2Ca intermetallic phases [8]. Additionally, the oxidation tendency of Mg is reduced when Ca is present in the alloy [106–108], reducing possible fire hazards during alloy preparation, melt handling and high temperature processing (e.g., heat treatment, forging,...).

The CALPHAD calculation (Fig. 2.18), shows the fraction of phases present in AZX311 over a temperature range from the melt to room temperature in equilibrium state. If Ca is added to Mg-Al alloys either Mg_2Ca or Al_2Ca can be formed, this depends on the Mg-Al ratio present. In this alloy the predominant precipitating phase is Al_2Ca , which can be used for precipitation hardening. The Al_2Ca phase is formed while casting or in subsequent heat treatment steps. In the shown case Al_2Ca once formed cannot be fully dispersed into the α -Mg matrix again. Additionally, a minor amount of AlMn-phases with changing stoichiometry can be found in the alloy, starting to precipitate during solidification. Zn is found mainly in solid solution, nevertheless, an AlMgZn-ternary phase can be formed at low temperatures.

The microstructure (cast, homogenized and as-forged) of an AZXW3110 alloy is shown in Fig. 2.19 a-d. The gravity cast material features large grains with Al_2Ca phases precipitated at the grain boundaries and the grain interior. Most of these phases were successfully dissolved in the homogenization heat treatment, which was done at $415 \text{ }^\circ\text{C}$ for 24 h. From the homogenized material a piston rod (see Fig. 2.1 and 2.4) was forged at a ram speed of 10 mm s^{-1} , using temperatures of approx. $425 \text{ }^\circ\text{C}$ and $280 \text{ }^\circ\text{C}$ for material and dies, respectively, and subsequently water-cooled. The appearance of the resulting as-forged microstructure depends on the degree of deformation applied. The heavily deformed sample center shows very small recrystallized grains together with large, deformed grains. In the microstruc-

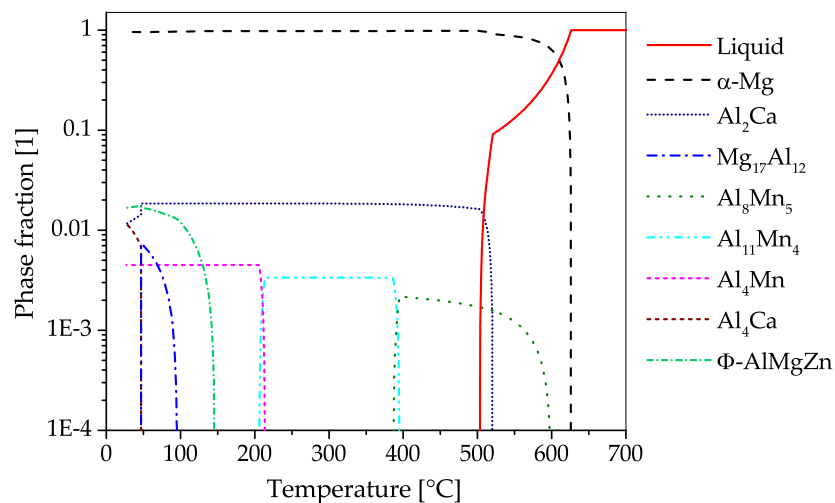


Figure 2.18.: CALPHAD calculations (for further information see 2.11.1) of AZX311 in a temperature range of 25 to 700 °C, showing phase fractions of 10^{-4} to 1.

ture from the flange, where less deformation was applied, heavily twinned grains are visible, while recrystallized areas are scarce.

In the work of Kim et al. [109] AZ31 was modified with 1 wt.% Ca resulting in a **AZX311** alloy, which was electromagnetically cast and isothermally extruded at 320 °C. This stock was forged into a pulley within two forging steps. The forming process was supported by strain-rate-change tests (in the range of 200 to 400 °C) and a simulation of the forming steps. In the first step the billet was upset in an open die at 350 °C up to 35 % engineering strain. The second step was done in a closed die at presumed temperatures of 310 °C (stock) and 320 °C (die) with a speed of 41 mm s⁻¹. Tensile properties were measured at various positions throughout the part, showing distinctive differences in YS, UTS and elongation. These results were explained by differences in the microstructure within the forged part.

The forging behavior of an as-cast **AZX312** alloy was investigated by Suresh et al. [110]. Therefore, compression tests were conducted in a temperature range from 300 to 500 °C using strain rates of 0.0003 to 10 s⁻¹. These results were used to generate a processing map and to simulate a cup shaped forging. Both, the processing map and the simulation were verified by isothermal forging trials and subsequent microstructural analyses. Forging of cup shaped parts took place at 300 to 500 °C and 0.01 to 10 s⁻¹. The recommended forging conditions, resulting in a homogeneous grain structure, are found to be 425 to 450 °C at a strain rate of 0.001 to 0.01 s⁻¹.

A comparison of AZ31 with increasing Ca content (0 to 2.5 wt.%) was done by Papenberg and Gneiger [32]. In this work, the Ca-containing alloys were additionally modified with ~0.25 wt.% Y, which is known to further improve flammability resistance. The used **AZXW** alloys were homogenized at 415 °C for 24 h after casting. Compression tests, performed at 300 to 400 °C with a strain rate of 0.1 to 5 s⁻¹ showed an increased flow stress of the 2.5 wt.% Ca containing alloy at 300 °C compared to AZ31. Closed-die forging of piston rod shaped parts was done at a stock temperature of 400 °C and a die temperature of 220 °C. The formed rods were heat treated at 350 °C for 0.5 h for recrystallization purposes. Tensile testing and microstructure analysis was done on as-forged and heat treated samples. An increasing Ca content resulted in a slightly improved YS but a decreased elongation. The heat treatment reduced the UTS and YS of the samples but improved the elongation significantly.

Hakamada et al. investigated the forming behavior of **AZX911** by means of hot compression, followed by tensile tests and microstructural analysis. In [111; 112] continuous cast AZ91 is compared to AZX911 in as-cast and homogenized (410 °C for 24 h) condition. Compression tests were conducted at 300 °C with a strain rate of 0.001 s⁻¹ and 0.1 s⁻¹ up to a true strain of 1.6. It was found that recrystallization is

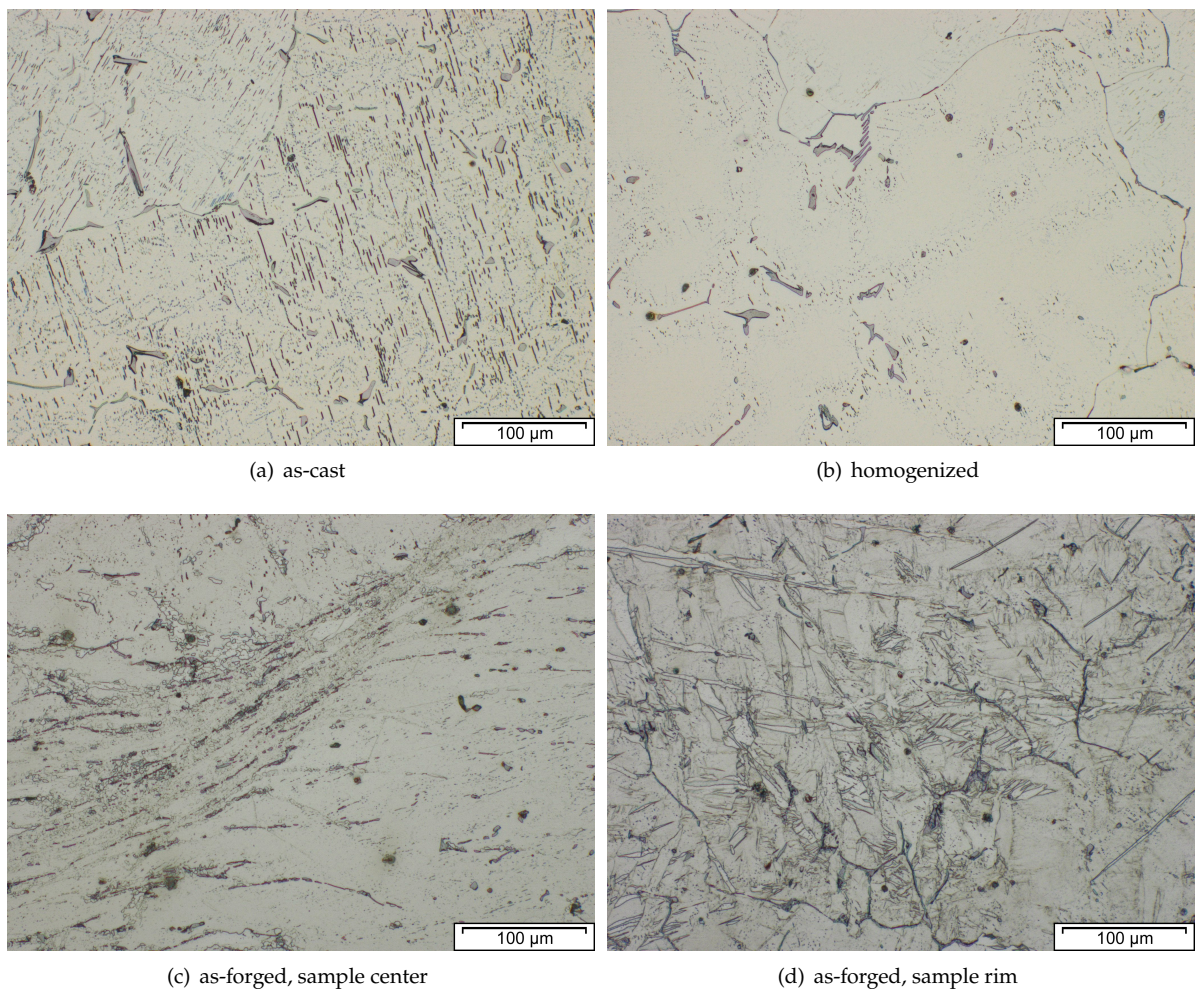


Figure 2.19.: Microstructure of AZXW3110 in consecutive processing steps: (a) as-cast, (b) homogenized at 415 °C for 24 h. Forging took place using a material temperature of approx. 425 °C, die temperatures of 280 °C and a ram speed of 10 mm s⁻¹. The as-forged microstructures of parts quenched in water are shown in: (c) center area having high degree of deformation and (d) flange area with a lower degree of deformation.

enhanced by the second phase particles in the Ca-containing alloy, especially if the particles are finely distributed. Also, a homogeneous distribution of Al is thought to improve the DRX properties by lowering the stacking fault energy. Therefore, the homogenized AZX911 alloy showed the most uniform grain size after compression testing, while the other tested samples exhibited a bimodal microstructure. Tensile tests at RT and 300 °C with 0.001, 0.01, 0.1 and 1 s⁻¹ showed an overall improvement of the tensile properties in the deformed samples when compared to as-cast material as well as large elongations to failure (284 %) of the AZX911 material at 300 °C. At RT the Ca containing alloy showed an increased YS but reduced ductility in general. The influence of different grain sizes on the forming behavior of as-cast AZX911 was investigated in ref. [113] by compression tests at 250, 300 and 330 °C using 0.01, 0.1 and 1 s⁻¹ up to a true strain of 1.6. A finer initial grain structure showed a slightly higher flow stress but considerably better free surface quality. An improved DRX behavior, which was found as well, is thought to originate at the smaller dispersed second phase particles (Al₂Ca) and grain boundaries.

A die-cast AXE622 (Mg-Al-Ca-RE) alloy was also examined by the same authors [114]. The homogenized material (410 °C for 108 h) was deformed by compression (300 °C with 0.1 s⁻¹ up to 1.6 true strain),

followed by an analysis of the evolving microstructure and the mechanical properties. An additional sample was annealed at 425 °C for 200 h after hot deformation, which resulted in an enlarged grain structure. The compressed samples showed an increase in texture strength as well as an increased tension/compression anisotropy when compared to the as-cast material. The sample in the deformed state had the highest YS as well as compressive yield strength (YSc) of all tested samples, which was attributed to the small grain size in this condition. Annealing the deformed microstructure intensified the tension/compression anisotropy and improved the elongation in tensile testing but did not increase the strength of the material.

Three different **ABaX** alloys, a system interesting because of its creep resistance, were investigated by Suresh et al. [115] and Rao et al. [116; 117], using a similar procedure as in [54; 110]: cup shaped parts were formed based on results of compression tests, simulation and generation of processing maps. The processing maps (calculated at a strain of 0.5) showed growing domains of instability with rising alloying content, nevertheless DRX regions, which are preferred zones for forming operations, were found as well. A comparison of the forming behavior of these alloys, based on processing maps, is shown in Figure 2.20. The as-cast alloys (ABaX422 [115], ABaX633 [116] and ABaX844 [117]) were formed into cup shaped parts at 300 to 500 °C with 0.01 to 10 mm s⁻¹. The forming behavior of the forged samples confirmed the processing maps as the well-shaped parts were produced in the predicted DRX regimes. For these components the forming parameters varied between 380 °C and 0.01 mm s⁻¹ up to 500 °C with a forming speed of 1 mm s⁻¹. A comparison of ABaX422 and ABaX633 material [116] showed increased compressive strength (tested at 25 to 250 °C) and creep resistance (at 200 °C) with rising alloying content. This is thought to stem from both, an enhanced solid solution strengthening and an increased amount of intermetallic phases containing Ba and Ca.

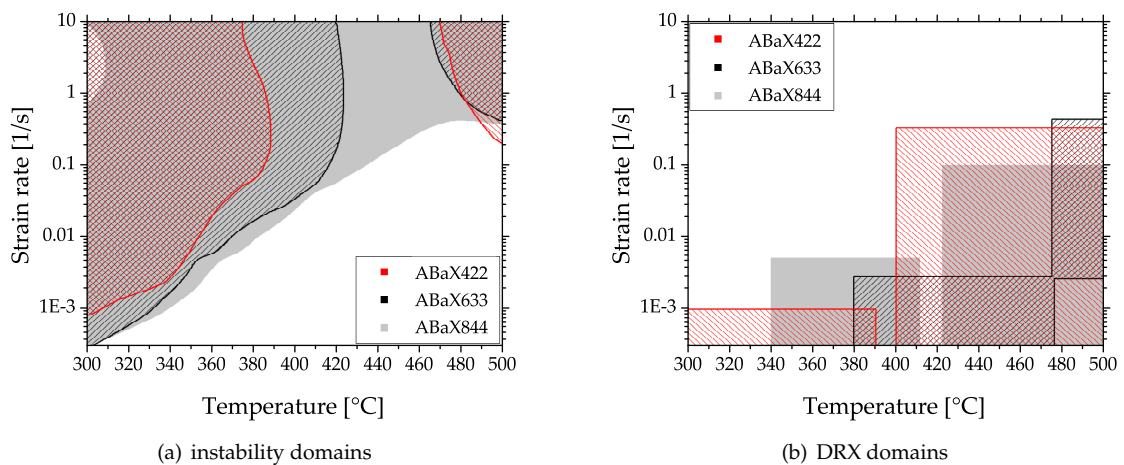


Figure 2.20.: Comparison of the forming behavior at 0.5 strain of ABaX alloys with rising alloying content. Showing (a) domains of instability and (b) DRX domains, based on the processing maps calculated in ref. [115–117].

2.6. Forging of Magnesium Alloys containing Zinc

Zinc is, besides Al, the most important alloying element for Mg, mainly due to its strengthening ability. Mg-Zn forms a eutectic phase at 340 °C which decomposes at temperatures beneath 325 °C to α -Mg and a MgZn intermetallic phase (Fig. 2.21). It is possible to precipitation harden binary Mg-Zn alloys by utilizing coherent GP-zones as well as semi-coherent intermediate precipitates [8]. Grain refinement in Mg-Zn alloys can be achieved by the addition of Zr, leading to ZK alloys with relatively good formability and strength. Examples of alloys are ZW3 (Mg – 3 %Zn – >0.5 %Zr), which was used as-forged

aircraft wheels and helicopter gearbox housings [118], and the widely used ZK60A (Mg – 6%Zn – >0.45%Zr). Because of their good biocompatibility, Mg–Zn–Ca alloys are interesting candidates for biomedical applications, which is discussed further in Section 2.8. Other wrought alloys using Zn as major alloying element include the Mg–Zn–Mn system, where ZM21 (Mg – 2%Zn – 0.5%Mn) is one well-known representative.

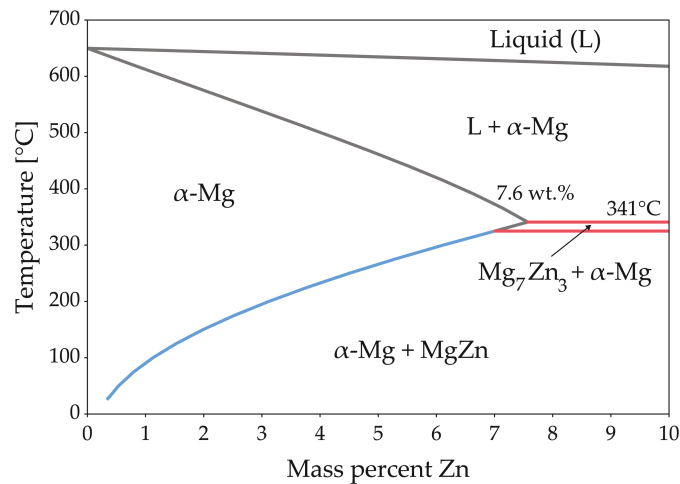


Figure 2.21.: Phase diagram of the Mg-Zn system. For further information, see 2.11.1.

A ZA21 alloy was investigated by Sanyal et al. [119] by compressive deformation. Cast stock material was cut into cuboid-shaped samples and isothermally deformed to flatbread samples between hot plates. Forming took place at 250, 350 and 450 °C, up to a reduction of approximately 75 %, subsequently the samples were quenched in water. Microstructural analysis showed a rising amount of fine DRXed grains with increasing processing temperature, nevertheless the sample deformed at 350 °C showed the least intensity of basal texture. The microstructure of all samples consisted of α-Mg and the τ -Mg₃₂(Al,Zn)₄₉-phase, which is typical for these type of alloys. Tensile testing showed decreasing strength with rising processing temperatures, the maximum being a YS of 232 MPa and 306 MPa UTS in the material processed at 250 °C, while the best elongation (10.7 %) was found in the sample compressed at 350 °C. This decrease of material strength was attributed to the rising amount of DRXed grains and the reduction of nano-sized τ -phase particles with rising forming temperature.

2.6.1. ZK60

ZK60, containing Mg – 6%Zn – >0.45%Zr, is one of the most widely known forging alloys and is applied i.e., for the production of wheels in motor sport applications [3]. Because of its commercial deployment this alloy has been investigated thoroughly by various authors. The effect of twinning and stacking faults on the forming behavior and grain size of rolled ZK60 has been investigated in [120]. The microstructural changes taking place during the homogenization of cast ZK60 were studied by Zhang et al. [121]. There, satisfying homogenization treatment parameters were found to be 470 °C for 14 h, resulting in a uniform microstructure without an assembly of intermetallic phases.

The CALPHAD calculation of ZK60 (Fig. 2.22), shows the fraction of equilibrium phases over the temperature range from fully liquid to room temperature. MgZn phases can be found in the lower temperature range, but it is possible to fully disperse these phase into the α-Mg matrix using a temperature of 300 to 400 °C. Additionally, a negligible amount of Zr containing phases can be found in the alloy, stemming from the Zr used for grain refinement.

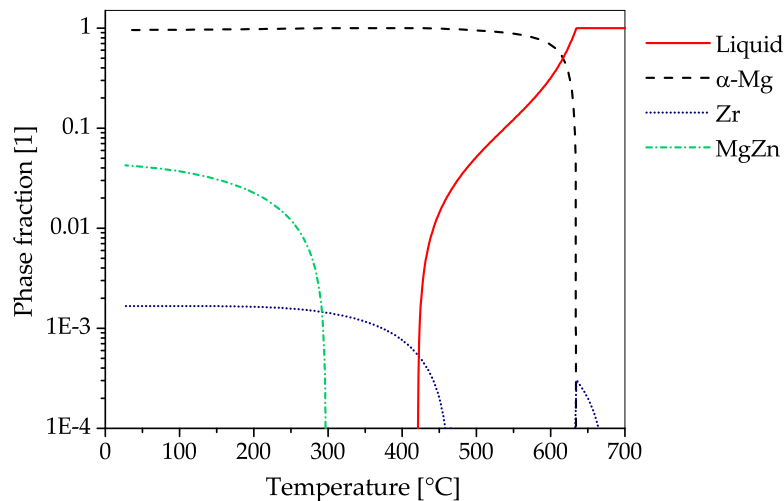


Figure 2.22.: CALPHAD calculations (for further information see 2.11.1) of ZK60 in a temperature range of 25 to 700 °C, showing phase fractions of 10^{-4} to 1.

Nevertheless, care should be taken when forging this ZK60 at high temperatures. The low-melting eutectic phases, which can be present in this alloy may cause damage of the formed part. According to [30] forming at temperatures of 315 °C might cause rupturing. An example of a ruptured part and its microstructure is shown in Fig. 2.23. The fractures along the grain boundaries of the ruptured part are easily recognizable when compared to the well-formed part shown in Fig. 2.24.

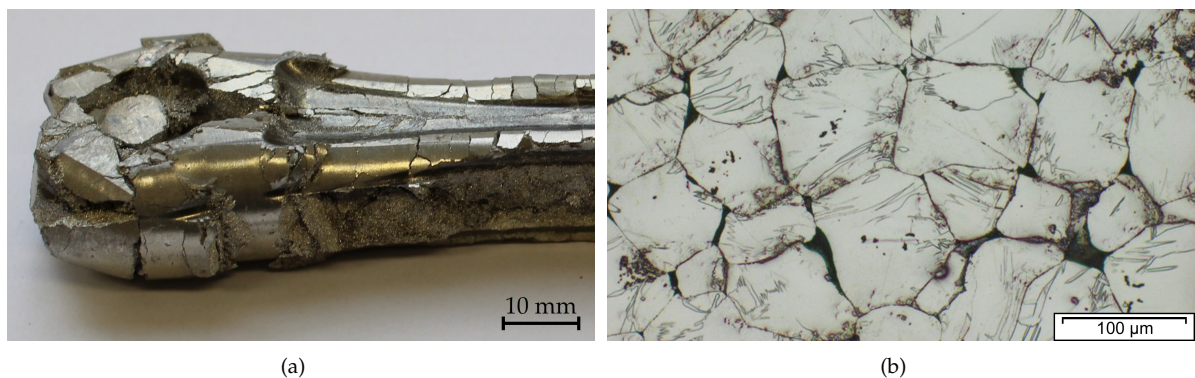


Figure 2.23.: Picture (a) shows a piston rod, made from a ZK60 variant, ruptured in the forging process. The microstructure at the sample center is depicted in (b). Fracture along the grain boundaries is easily visible. A well formed part, produced from the same alloy, is shown in Fig 2.24.

The homogenized and as-forged microstructure of a part made from a ZKXW6000 is shown in Fig. 2.24. This alloy is a ZK60 variant alloyed with trace amounts of Ca and Y to improve processing safety. The material was cast into a steel mold and subsequently homogenized at 370 °C for 8 h, this improves the processing behavior by a reduction of eutectic phases with a low melting temperature (MgZn). From the homogenized material a laboratory-scaled piston rod was forged at a ram speed of 10 mms^{-1} . Temperatures of approximately 300 °C for the material and 280 °C for the dies were used, subsequently the formed part was cooled at air. The microstructure of the as-forged sample varies, depending on the degree of deformation applied within the part. The sample center Fig. 2.24 c shows

elongated grains together with very fine grains which can be seen as the onset of dynamic recrystallization. In the lower deformed area of the flange Fig. 2.24 d, the grain structure from casting can still be recognized, also low amounts of twins and newly recrystallized grains are visible.

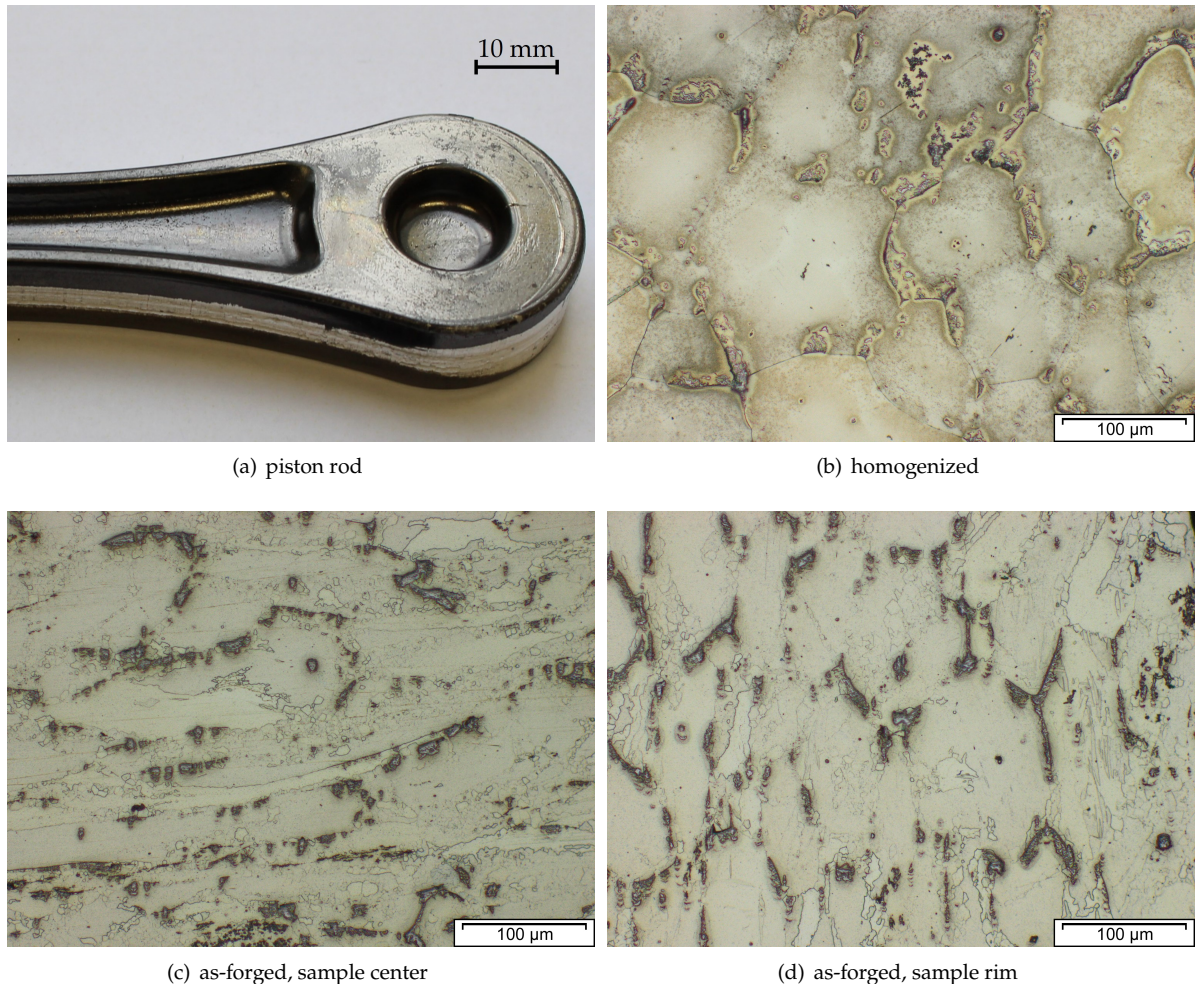


Figure 2.24.: Finished part (a) and microstructures of a ZK60 variant in consecutive processing steps: (b) homogenized at 370 °C for 8 h. Forging took place using a material temperature of approx. 300 °C, die temperatures of 280 °C and a ram speed of 10 mm s⁻¹. The as-forged microstructures of parts cooled at air are shown in: (c) center area having high degree of deformation and (d) flange area with a lower degree of deformation.

Processing maps for as-cast ZK60 stock (produced by squeeze casting) were created by Wang et al. [122]. Compression tests were carried out between 250 and 450 °C using strain rates of 0.001 to 10 s⁻¹. The best forming condition were found to be 375 °C at a strain rate of 0.001 s⁻¹. The corresponding DRX domain was shown to range between 300 and 375 °C together with strain rates of 0.001 to 0.01 s⁻¹. In the unstable domains of the processing map, the samples show twinning, flow localization and cracking. These results were also used by Li et al. [123], who compared them to their own processing maps of extruded ZK60. Li et al. analyzed their material in a temperature range of 250 to 400 °C and 0.001 to 1 s⁻¹ by compression tests. Two domains where forming should be possible without material failures were found: a DRX domain between 250 and 325 °C at strain rates of 0.001 to 0.03 s⁻¹ as well as a zone, in the range of 340 to 380 °C and 0.001 to 0.003 s⁻¹, where superplastic deformation is thought to occur. The comparison of the cast material used in [122] and the extruded stock showed a distinct improve-

ment of the forming behavior, which is attributed to the grain refinement resulting from prior extrusion.

In the work of Ogawa et al. [124] ZK60 was deformed by upsettability tests and backwards extrusion. The material was deformed with a mean strain rate of 10 s^{-1} at 100 to 400 °C applying die temperatures of RT and 100 °C for the upper and lower die respectively. Apparently, the stock material was aged at 150 °C for 24 h before testing. The compression tests were most successful in the range of 300 to 400 °C. At 250 °C unstable deformation and at lower temperatures fracture was observed, over 400 °C the samples oxidized heavily. In subsequent backwards extrusion experiments cups with varying extrusion ratios were produced. There, the stock material and the container were heated to temperatures of 100 to 300 °C, the punch on the other hand was kept at RT. Forming was mostly successful, all forged at temperatures over 250 °C were formed without flaws, even at 200 °C cups with an extrusion ratio greater than 3.7 were produced. These results are attributed to the increased hydrostatic pressure affecting the material positively in this forming process.

A similar testing design, for both compression and backwards extrusion, is described by Matsumoto and Osakada [125]. In contrast to ref. [124], the material was brought to forging temperature directly in the heated forming tools, thereby reducing material heating and transferring time. The changes in material and processing behavior in case of billet shape modifications were investigated by simulation and forging trials. A decrease of forming load was achieved by a billet shape which allows pre-straining before the die is fully filled. The heating method showed reduced oxidation of the billets, which has its merits for small sample sizes and flat products.

Hadadzadeh et al. analyzed the forming behavior of ZK60 in as-cast and homogenized, as well as in as-extruded condition by means of compression testing [126; 127]. To determine a suitable homogenization temperature, the as-cast material was tested with differential scanning calorimetry (DSC), the homogenization then took place at 400 °C for 4 h, followed by quenching in water. Isothermal compression tests were performed up to a true strain of 1 at 300 to 450 °C and 0.001 to 1 s^{-1} . The flow curves of the extruded material show a strong anisotropy with high values in extrusion direction, as it is typical for Mg alloys. Surprisingly, the cast and homogenized samples have comparable or higher values of flow stress. Simulations based on the Ludwig equation were capable to predict the flow curves accurately and to provide insight about the strain rate sensitivity and strain hardening behavior [127]. The microstructure of the cast and homogenized material, which was analyzed in [126], showed partial DRX behavior. While testing, a basal texture (perpendicular alignment of $\langle 0001 \rangle_{Mg}$ especially present after uniaxial deformation) developed in all compressed samples. With raising temperatures and forming speed the texture intensified towards the basal poles.

Jung et al. [128] compared as-cast (die cast and semi-continuous cast) and as-extruded material by tensile testing and upsetting tests. Isothermal forming was done at 280 to 400 °C at 0.01 and 0.1 s^{-1} . The extruded material showed the best performance in terms of critical height reduction, followed by the semi-continuously cast samples, which reached comparable values at high forming temperatures and 0.01 s^{-1} . A severe drop in formability was discovered in the die-cast material above 320 °C, this behavior was attributed to low-melting eutectic phases which might cause rupturing because of the formation of micro voids.

In the works of Karparvarfard et al. [129–132] cast and extruded ZK60 was used for forging trials with various geometries accompanied by investigations of microstructure and mechanical properties. In ref. [129; 130] cast stock was used to produce flatbread samples by isothermal open-die forging. Before deformation, the forging stock was held at forming temperature for 3.5 h. As the samples deformed with 350 °C and 0.65 mm s^{-1} showed cracks after forming, only samples forged at 450 °C were used for the following investigations. Tensile and compression tests as well as analyses of texture and microstructure were conducted on a part formed from cast stock material at a speed of 0.65 mm s^{-1} [129]. While the values of the forged samples for YS and UCS increased substantially (at minimum by 20 MPa), the YSc, UTS and tensile elongation did not change and the compressive fracture strain even decreased. The microstructural analysis revealed the alignment of c-axes mainly along the forging direction as well as a refined bimodal grain structure for the as-forged material. The fracture surfaces of the as-cast material showed less dimples and a more brittle appearance in general. In ref. [130] fatigue testing and fracture surface analysis were done on a sample formed at 6.5 mm s^{-1} . The forged samples showed

higher fatigue strength when compared to the as-cast material in general. A strain dependent deformation behavior could be observed in the forged ZK60; it changed from dislocation slip to twinning and detwinning with rising strain amplitude. In the HCF regime crack nucleation is caused by persistent slip bands and intermetallic precipitates, whereas in higher strain regimes twin formation seems to be responsible for damage propagation.

A small part with varying thickness was forged from extruded ZK60 stock in ref. [131]. Semi-closed die forging was done at 450 °C and a ram speed of 0.4 mms⁻¹, the produced parts were then investigated by compression testing and microstructural analysis. The forged compression samples showed a slight reduction of strength but an improvement of failure strain when compared to the as-extruded material. This behavior is mirrored on the fracture surface, where dimples - a sign for increased plastic deformation - can be found mainly on the forged samples. This behavior is attributed to the changes in microstructure: the bimodal structure from the as-extruded material changed to a pancake structure, accompanied by an increase of texture intensity with rising degree of deformation in the formed part. As-cast ZK60 was used as stock material for a larger forging in the shape of an I-beam section in [132]. Isothermal closed-die forging was done at 250 °C with a speed of 20 mm s⁻¹. The formed part showed a bimodal grain size, consisting of elongated grains surrounded by small round grains, which indicates DRX. Furthermore, a basal texture started to develop in the forged material, based on the degree of deformation. In the subsequent tensile and fatigue testing a distinct improvement of the forged samples was shown when compared to the as-cast material. The YS (depending on the sample location) was increased by up to 93 % (268 MPa) but the elongation reduced to 9 % ϵ_f . The fatigue life, tested stress controlled at 140, 160 and 180 MPa using R = -1, showed an order of magnitude improvement in the forged material, regardless of the loading stress. This is attributed to the grain refinement and texture of the forged part, resulting in a higher strength and an alteration of the deformation mechanisms. Simulations of the forged parts analyzed by Karparvarfarad et al. in ref. [132], as well as the forging process of an automotive control arm made of extruded ZK60 are described in the work of Paracha [94], which has already been mentioned in Section on AZ80.

An investigation of the forging behavior of extruded AZ31 and ZK60 by Poerschke [52] has already been discussed in the Section on AZ31.

A comparison of forgings made from extruded stock material, published by Swiostek et al. [83] was already described in Section 2.5.1.4. Amongst others, ZK60 was compared to a modified ZK60 alloy with additional 2.1 wt.% RE and to a ZK30 alloy. The samples produced by die forging at 350 °C (F-temper) showed an inhomogeneous microstructure, consisting of large deformed grains as well as fine recrystallized ones. The tensile properties of all ZK alloys were similar, with ZK60 reaching the highest UTS but the RE modified alloy showed the best YS with the lowest elongation. ZK30 was reported to exhibit the best corrosion resistance among the ZK alloys, nevertheless all other tested materials (various AZ80 alloys and WE43) had substantially lower corrosion rates than the ZK alloys.

Kurz et al. [90] analyzed the forming window of extruded ZK60 and modifications thereof (small additional amounts of Ce (<1 wt.%) as well as Ce (<1 wt.%) plus Y (<1 wt.%), in comparison to AZ80. In the forming trials (described in the section about AZ80), the modification of ZK60 with Ce improved the forming behavior at low (175 °C) and high temperatures (up to 450 °C). The unmodified ZK60 alloy on the other hand failed by hot cracking at a forming temperature of 400 °C.

2.7. Forging of Magnesium Alloys containing Rare Earth Elements

Rare earth elements (REE or RE) are a group of seventeen metals including the lanthanides, Y and Sc, which can often be found together in geological deposits. The group can further be divided into 'light' rare earth elements (lanthanides La to Eu - atomic numbers 57 to 63) and 'heavy' rare earth elements (Y, Sc and lanthanides from Gd to Lu - atomic numbers 64 to 71). Although it is postulated that most properties of REE are rather similar [133], there are significant differences when alloyed to Mg. In common, all of them form eutectics with Mg and exhibit a certain amount of solid solubility. High-temperature intermetallic compounds, that can form with Mg are often used to generate creep-resistant

Mg alloys [134] and can also be utilized for precipitation hardening [8]. Wrought Mg-alloys containing REE offer a wide variety of alloying systems ranging from industrial established Mg-Zn-RE [13; 135] and Mg-Y-RE alloys (e.g., WE43) to high strength Mg-REE alloys with LPSO (long period stacking order) structure [136; 137].

2.7.1. WE43

WE43 is considered a benchmark alloy for a good combination of mechanical properties, corrosion and oxidation behavior. It has been investigated intensively and is used in various applications. Moreover, it is a candidate of interest for e.g., the aviation industry. Since a relatively high amount of expensive Y is used, this alloy is higher priced than most other Mg alloys. On the other hand, Mg-RE alloys using Ce and La or Mischmetal (Ce/La) are comparably cheap.

The CALPHAD calculation (Fig. 2.25) shows the fraction of phases present in WE43 over the temperature range from fully liquid to room temperature in equilibrium state. High-temperature stable Mg-RE phases already start to form in the melt or may precipitate in subsequent heat treatments. In contrast, the $Mg_{24}Y_5$ phase is only stable up to approximately 320 °C. In case of ageing treatments this Y-containing phase or not yet precipitated RE phases can be used for precipitation hardening. Small amounts of predominantly Zr-containing particles may also occur in this alloy.

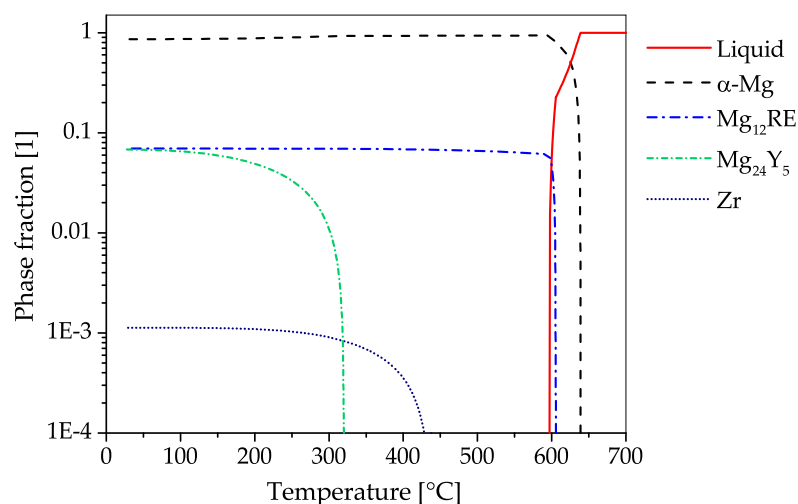


Figure 2.25.: CALPHAD calculations (for further information see 2.11.1) of WE43 in a temperature range of 25 to 700 °C, showing phase fractions of 10^{-4} to 1.

The microstructure (cast, homogenized and as-forged) of a WE43 alloy is shown in Fig. 2.26. The as-cast microstructure (Fig. 2.26 a) consists of grains with an average size $>50 \mu\text{m}$ and intermetallic phases mainly located along the grain boundaries. The cast material was then homogenized at 525 °C for 24 h (Fig. 2.26 b) in order to improve the processing behavior via a reduction of phases at the grain boundaries. The grain size increased visibly, also newly precipitated RE-phases can be seen in the grain interiors. From the homogenized material a piston rod (see Fig. 2.1 and 2.4) was forged at a ram speed of 10 mm s^{-1} , using temperatures of approximately 380 °C and 280 °C for material and dies respectively. The formed part was air-cooled. The as-forged microstructures of sample center and sample rim look similar. The grain shapes and size are reduced corresponding to the applied degree of deformation, but the structure itself did not change considerably from the homogenized material, showing phases on the grain boundaries and grain interior.

Panigrahi et al. [33] investigated the ageing behavior of upset forged WE43. The forging stock (cube

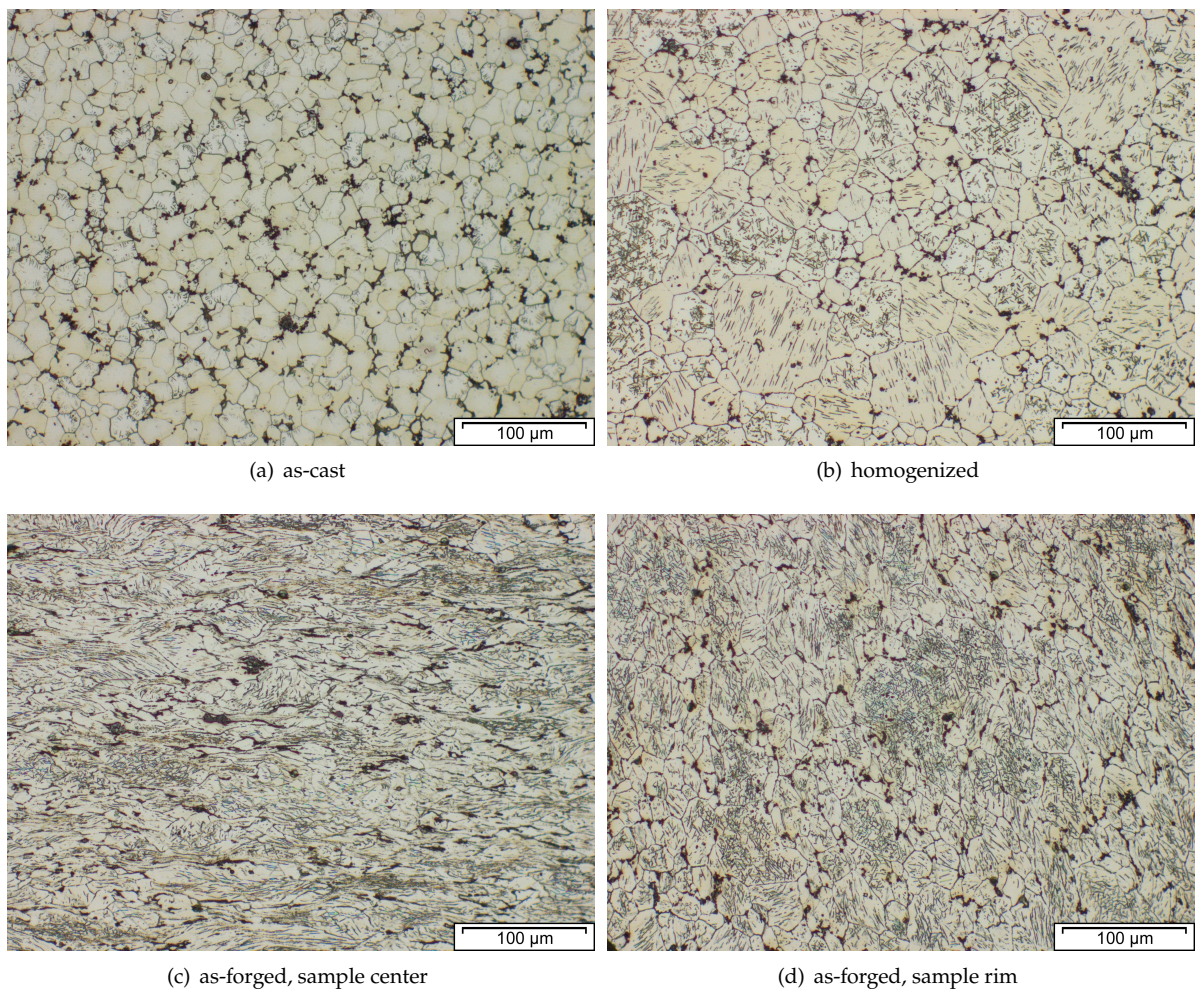


Figure 2.26.: Microstructure of WE43 in (a) as-cast state as well as (b) homogenized at 525 °C for 24 h. The material was forged at temperatures of 380 °C and 280 °C for material and die respectively using a ram speed of 10 mm s⁻¹. The as-forged, air-cooled microstructures of (c) sample center and (d) sample rim are depicted as well.

shaped samples cut from a WE43 plate in F temper) were forged at 380 °C and 1 s⁻¹ up to a deformation of 1.2 true strain. The effect of varying T5 ageing temperatures (150, 180 and 210 °C) was investigated by hardness measurements, tensile testing and metallographic analysis which included EBSD measurements and an investigation of the fracture surface. The highest tensile strength (344 ± 11 and 388 ± 12 MPa, for YS and UTS respectively) was reached by the sample heat treated at 180 °C for 60 h. These high values are thought to stem from overlapping effects of work hardening, fine grain size and precipitation strengthening.

In the comparison of forging alloys presented by Swiostek et al. [83] (already discussed in Section 2.5.1.4 and 2.6.1), as-extruded WE43 stock was forged at ranging from 450 to 300 °C, using a die temperature of 220 °C. The parts formed from WE43 developed cold cracks at forging temperatures of 300 °C and required the highest forging forces of all compared materials (various ZK and AZ80 alloys). The forming force of WE43 showed a distinctive drop between 350 °C and 400 °C, nearly dropping to the level of the other alloys. As-forged samples from all alloys deformed at 350 °C were further investigated. The microstructure of the analyzed sample from WE43 showed a fine-grained microstructure with grain diameters of 5 to 9 μm. WE43 also displayed the highest values for YS, UTS, elongation and hardness

at room temperature, as well as the best corrosion resistance in salt spray testing.

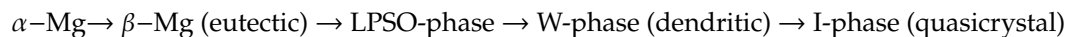
Henry et al. [138] used extruded forging stock to investigate the formability and mechanical properties of open-die forged WE43. The extruded stock material was heat treated at 525 °C for 8 h before forming. Cylindrical samples were compressed to a 'pancake' shape using temperatures of 360 to 480 °C with strain rates of 0.006 to 8 s⁻¹ to reach deformations of 35 to 85 % strain. The microstructure of the forged parts varied widely. Heavily deformed grains with coarse precipitates (360 °C) could be found as well as fully recrystallized grains without visible precipitates (480 °C), dependent on the forming speed. A T5 heat treatment (recommended at 180 to 260 °C) was used to reach a YS >225 MPa and UTS of 350 MPa.

Some work on the topic of aviation applications has been done in the 'MagForming' project, where a door stop and a blank for a compressor impeller were successfully forged from WE43 (and AZ80) [93]. Especially for the compressor wheel the good mechanical properties of WE43 at high temperatures are a topic of interest. Forging of the door stop was done in two steps at 300 to 350 °C with a ram speed of 5 mms⁻¹. The billet for the compressor wheel was forged in one step at temperatures between 300 °C and 400 °C with ram speeds of 10 to 30 mms⁻¹.

2.7.2. Alloys with LPSO Structure

This type of alloy was produced the first time by rapidly solidified powder metallurgy in the early 2000s. Soon afterwards it was shown that casting was also a viable route of production [139]. These alloys, mainly of the Mg-Zn-Y and Mg-Zn-Gd systems, combine high strength and acceptable room temperature ductility with good high temperature performance. A detailed overview of the microstructure and phases as well as the most relevant works for these alloys is given in ref. [136; 137].

Mg-Zn-Y alloys do not only form the LPSO-phase (Mg₁₂ZnY), but may as well contain varying amounts of α -Mg, MgZn, I-phase (Mg₃YZn₆), W-phase (Mg₃Y₂Zn₃) and β -Mg (Mg₂₄Y₅). The preferred phase is shown to be closely dependent on the Zn/Y ratio present in the alloy, and follows the forming trend of:



with rising Zn/Y ratio [136]. The LPSO-phase itself has several possible stacking sequences (i.e., 6H, 10H, 14H, 18R, 24R structure type) which may change during processing steps and heat treatment.

As the production of relevant quantities of this alloys by casting was made possible, forming (and forging) soon became a topic of interest. Nevertheless, the works about forgings still seem to be limited to basic characterizations with upset forging being the main forming process. For a better overview of the investigated alloys discussed in this section, the composition (wt. % and at. %) of each are listed in Table 2.3.

Asakawa and Hirukawa [140] investigated the forming behavior of the alloys **Mg-2Gd-1Zn** and **Mg-2Gd-1Zn-0.2Zr** with upset forging. The as-cast material was heat treated at 520 °C for 2 h, quenched in water with 80 °C and annealed again at 400 °C for 1 h. Forging took place at 380 °C with a press speed of 5 and 250 mms⁻¹ up to reduction ratios of 30, 50 and 80 %. The variation of cooling rate while casting and the addition of 0.2 at. % Zr reduced the grain size considerably (from 2800 to 57 μm) and positively influenced the forming behavior. This material also showed favorable tensile properties of 299 MPaUTS and an elongation of 15.4 %. The influence of forging temperature, speed and degree of deformation on forming behavior and mechanical properties of the parts was investigated as well. While higher temperatures and a low forming speed show improved quality of the formed part, the mechanical properties were enhanced with reduced temperatures and low forming speed but with increased reduction ratio.

In the works of Han, Xu and Shan [141; 142] a cast **GWZK102** alloy was forged and aged. The homogenized (510 °C for 10 h and quenched in water with 80 °C) forging stock was formed at 470 °C, subsequently the material was aged at 200, 225 and 250 °C for up to 80 h. While an effect of age hardening could be shown for all samples, the highest strength was reached after 60 h at 200 °C, reaching values of 406 MPaUTS with 5.9 % elongation. The in-depth study of the microstructure showed a grain

Table 2.3.: Overview of the chemical compositions of the investigated alloys in the works reviewed in Section 2.7.2 given in wt. % and at. %.

Alloy	Y		Gd		Zn		Zr		Mg	Source
	wt %	at %	wt %	at %	wt %	at %	wt %	at %		
Mg-2Gd-1Zn			11.5	2.00	2.40	1.00			Balance	[140]
Mg-2Gd-1Zn-0.2Zr			11.4	2.00	2.38	1.00	0.66	0.20	Balance	[140]
GWZK102	2.00	0.61	10.0	1.73	0.50	0.21	0.30	0.09	Balance	[141–143]
Mg-Zn-Y	2.15	0.60			0.53	0.20			Balance	[144]
	6.84	2.00			2.51	1.00			Balance	[144; 145]
	15.5	5.00			6.82	3.00			Balance	[144]
	20.4	7.00			8.58	4.00			Balance	[144]
	24.6	9.00			12.4	6.00			Balance	[144]
Mg-Zn-Y-Zr	1.01	0.29			5.99	2.34	0.39	0.11	Balance	[146]
	1.93	0.58			12.0	4.92	0.41	0.12	Balance	[146]

refinement of the α -Mg grains and precipitation of the LPSO phase (14H type) during forging. These LPSO phases are known to inhibit dislocation glide and grain growth. Moreover, the formation of β' -phase precipitates during the ageing process was found. The high strength of the GWZK102 alloy is therefore attributed to these precipitated LPSO and β' -phases. The overageing visible in this alloy is thought to stem from precipitate free zones, grain growth and coarsening of secondary phases.

The same alloy was forged to the shape of a bracket in a study presented by Shan et al. [143]. The forging process was simulated in advance and the die design was adapted according to the results. The material was forged isothermally at 407 °C (at presumably 1 mm s⁻¹) to two differing billet shapes. The parts were successfully produced and subsequently aged at 200 °C for up to 80 h. The peak strength was reached after 63 h, showing tensile properties of 243 MPa YS, 380 MPa UTS and an elongation of 4.07%. The increase in strength is attributed to the precipitation of β' and β'' -phases, but LPSO phases were not mentioned specifically.

A comparison of Mg-Zn-Y two-phase alloys with different LPSO phase fractions was done by Matsumoto et al. [144] using cast material with varying amounts of Zn (6, 4, 3, 1 and 0.2 at. %) and Y (9, 7, 5, 2 and 0.6 at. %). Therefore, the approximate volume fraction (ϕ) of the LPSO Phase ranged from 1 to 100%, changing the material behavior accordingly. Figure 2.27 shows the as-cast microstructures of the investigated alloys. The cast material was homogenized at 500 °C for 10 h before doing upsettability tests at material temperatures in a range of 200 to 500 °C and an initial strain rate of 0.31 s⁻¹ (8.3 mm s⁻¹). Isothermal testing was performed at 200 °C, for all other temperatures the tool was heated to 250 °C. While all alloys showed comparable behavior at 500 °C the alloys Mg₉₂Zn₃Y₅ and Mg₈₉Zn₄Y₇ showed high strength even at higher temperatures. Values of up to 400 MPa were reached at 200 and 300 °C. This performance is thought to be related to the interaction of the α -Mg and LPSO phase boundaries. Isothermal forging experiments (setup comparable to [59]), were done on the Mg₉₇Zn₁Y₂ alloy at 300 °C with an average speed of 80 mm s⁻¹. A simulation of the forging process and the forces required, based on the rule of mixture (α -Mg and LPSO phase), was implemented and showed improved results when compared to conventional methods.

Matsumoto et al. compared cast with extruded Mg₉₇Zn₁Y₂ by compression experiments in an earlier publication [145]. Testing was done as already described before, and while the extruded samples showed a high strength at 200 and 300 °C, the ductility was not improved when compared to the cast material. This behavior changed at higher temperatures for the material extruded at 350 °C which showed good formability at 400 °C testing temperature. While the α -Mg phase accommodated deformation by twinning, the LPSO structures showed kink deformation. Both results are to be expected in these types of alloys.

Two Mg-Zn-Y-Zr alloys containing the eutectic I-phase were investigated by Garcés et al. [146]. The alloys, containing Zn_{2.34}Y_{0.29}Zr_{0.11} and Zn_{4.92}Y_{0.58}Zr_{0.12} (in at. %), were compressed to a reduction of

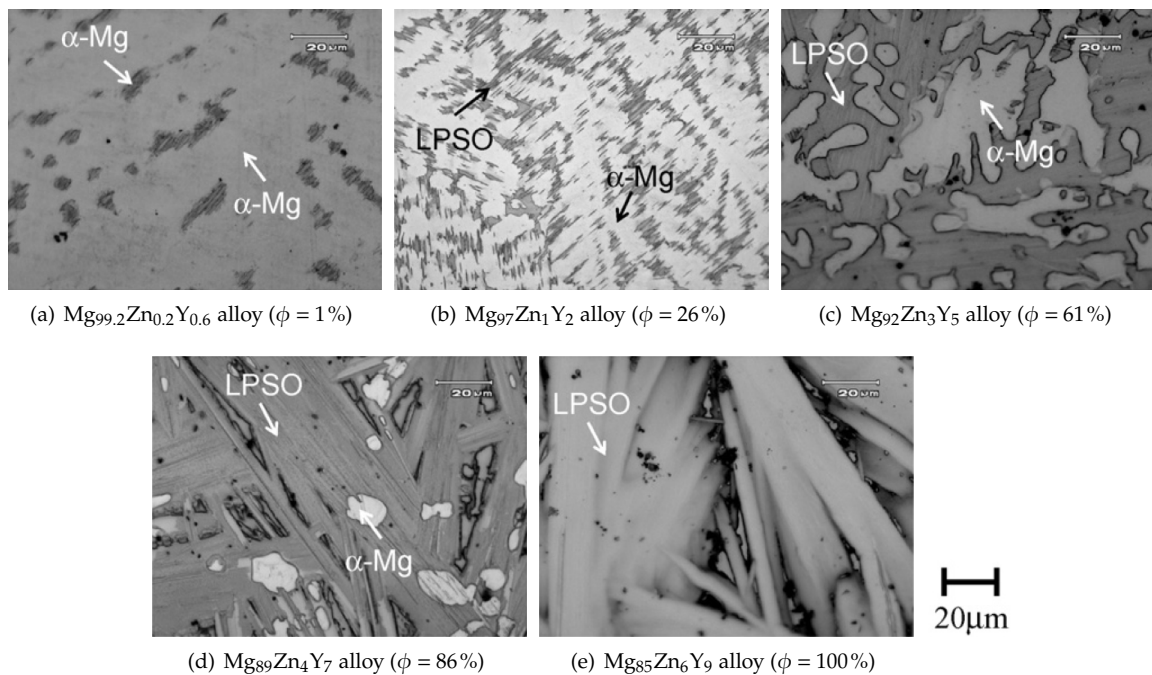


Figure 2.27.: Microstructure of as-cast Mg-Zn-Y alloys with varying LPSO volume fraction (ϕ) [144]. The scale bar applies to all figures (a) to (e). Reproduced with permission from Elsevier.

92%. Three passes were applied, in which the material was reheated to the starting temperature of 400 °C and held at this temperature for 20 min after each pass. In the subsequent tensile and compression tests at RT, values of ~ 350 MPa UTS and UCS > 450 MPa were reached by the higher alloyed material. After forming, fracturing of the I-phase (contributes to grain refinement) and the precipitation of Mg-Zn binary phases (known for strength improvement) are shown by TEM analyses.

2.8. Forging of Biodegradable Magnesium Alloys

While biodegradable products made from Mg alloys are commercially available nowadays, forging is not a common production process. The possible alloying elements in biodegradable alloys are greatly restricted and product dimensions and pricing make uncommon production methods i.e., ECAP viable. Nevertheless, a short introduction to biodegradable Mg alloys is subsequently given and works using forged material discussed.

Mg is a trace element, naturally present in the human body and also reported to be beneficial for bone healing [147]. Therefore, Mg alloys are in the focus as fully biodegradable implant materials for screws, plates, pins and stents. A full consumption of tissue-supporting implants during and after rebuilding of the damaged bone or tissues eliminates the necessity of a second surgical operation for implant removal. Major requirements are excellent biocompatibility of all alloying elements and a very low risk of allergic reactions. Accordingly, Mg-Zn-Ca (ZX) alloys are attractive candidates for biodegradable implants. A sufficiently low in-vivo degradation rate is required to ensure the stabilization during the healing process (up to 12 weeks). Further, the formation of gaseous H_2 , which usually goes along with implant degradation, has to be controlled to amounts tolerable by the surrounding tissue. The degradation rate is influenced by the difference in the chemical potential of matrix and precipitates [148] and also by the volume fraction of intermetallic precipitates, as well as grain size [149] and matrix composition [150; 151]. Moreover, it is recommended to keep the content of the common impurities of Mg as Be, Fe, Ni and Cu as low as possible, because they tend to precipitate and form corrosion cells in Mg-alloys [152].

The CALPHAD calculation (Fig. 2.28), shows the fraction of present phases in ZX10 over the temperature range from fully liquid to room temperature in equilibrium state. During casting only the α -Mg is forming. Because of the low content of alloying elements the volume content of precipitating phases is very low. Nevertheless, Mg_2Ca may form between 200 °C and 400 °C. A ternary phase, $\text{Ca}_2\text{Mg}_6\text{Zn}_3$, can precipitate between RT and 300 °C.

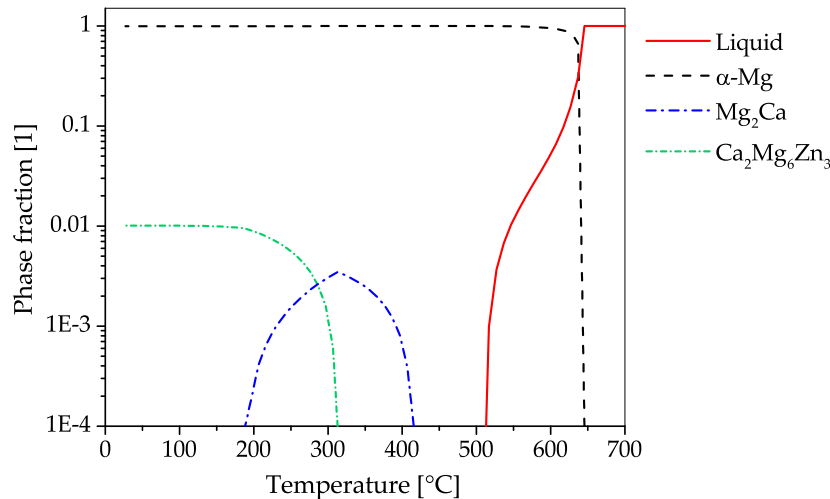


Figure 2.28.: CALPHAD calculations (for further information see 2.11.1) of ZX10 in a temperature range of 25 to 700 °C, showing phase fractions of 10⁻⁴ to 1.

With respect to biocompatibility, the applicable alloying elements are strictly limited. There exist numerous studies concerning the strength-enhancing effects of rare earths, Zr, Y, Zn and Ca, but in particular Zn and Ca eliminate the risks concerning insufficient biocompatibility. As intermetallic particles or rare earths might accumulate in the human body, lean Mg-Zn-Ca alloys are of great interest. Calcium is a major constituent of hydroxyapatite $\text{Ca}_5(\text{PO}_4)_3(\text{OH})$, the crystalline phase of bone. It is reported to improve the osseointegration rate and to be beneficial for bone healing, however, for biocompatibility, the alloy should contain max. 1 wt. % of Ca [153]. Intermetallic phases in Ca-containing Mg alloys are reported to distribute uniformly and to be advantageous for processing and final microstructures, as they facilitate particle stimulated nucleation and DRX [154]. During degradation of Mg-Ca alloys, Ca is consumed by the surrounding bone. If Ca is in solid solution, the corrosion rate is slightly reduced [155], whereas the influence of intermetallic Ca-containing precipitates on the corrosion behavior strongly depends on the respective chemical potential of matrix and precipitates [156]. Alloying Mg with Zn leads to a strength increase by solid-solution (systematically analyzed in ref. [157] and calculated to amount about 20 MPa per wt. %). The other possible strengthening mechanism is the formation of intermetallic precipitates, e.g., $\text{Ca}_3\text{Mg}_6\text{Zn}_3$ in combination with Ca or - if the Zn content is reduced - $(\text{Mg,Zn})_2\text{Ca}$, which is less noble than the Mg-matrix [158] and diminishes therefore selective corrosion attack. Zinc is also reported to enhance DRX during hot-working [159].

Besides the requirement for excellent biocompatibility, also adequacy of mechanical properties for the application in biodegradable implants has to be ensured. The elastic modulus of Mg alloys of 41 to 45 GPa is closer to that of bone (3 to 20 GPa) than the elastic modulus of Ti-, Fe- or Zn-based alloys, which reduces the risk of bone-matter decomposition, strength loss and stress-shielding [148]. The initially low yield strength (YS) of < 30 MPa and ductility of as-cast Mg can be enhanced significantly by grain refinement, solid solution strengthening and age hardening. Intermetallic particles, which are present during hot working are reported to enable particle stimulated nucleation and, subsequently, DRX. This is shown by Zhang et al. for Mg-Zn-Ca alloys [154] or by

Robson et al. for Mg-Mn alloys [160]. Their grain boundary pinning effect promotes a fine-grained microstructure after hot-working and/or annealing [150; 161]. Grain refinement is a very effective method of strengthening in Mg-alloys, as the strengthening coefficient is more than four times higher than in Al-alloys [162]. Besides grain-boundary strengthening, a further positive effect of a fine-grained microstructure, resulting from DRX, is the weakening of a strong basal texture. This results in a reduction of the directional strength-anisotropy of the final implant and the risk of failure of the implant.

At present, the main application for hot and cold working of Mg-alloys is not to produce the final shape of an implant, but to take advantage of a wide range of possibilities for microstructure adjustment and design. The standard production process for biodegradable Mg-alloys usually comprises a homogenization treatment, followed by extrusion, forging or hot rolling and an optional annealing and/or a further deformation process as hot- or cold-working or severe plastic deformation (SPD). As the development of biodegradable Mg-alloy tends to a limitation of alloying elements to nutritional elements and a reduction in the content of alloying elements, the following description of several studies comprising hot and cold working follows this trend in a similar order.

The relationships of processing and properties of the alloy system ZX, representing Mg-Zn-Ca alloys, were investigated in several works. Kang et al. present in [163] a study of the influence of the point of the homogenization annealing within a two-step deformation process of a Mg – 4% Zn – 0.5% Ca (ZX41) alloy. The initially conducted homogenization heat treatment comprises a first annealing step at 380 °C for 20 h and a second holding step at 510 °C for 3 h. The forging was performed at 300 °C and a speed of 0.1 s⁻¹ to a height reduction of 50 % and extrusion was performed at 280 °C with an extrusion ratio of 16:1 and a ram speed of 0.01 mm s⁻¹. Conducting the homogenization heat treatment after the forging process lead to dissolution of the intermetallic MgZn₂ particles at the grain boundaries. The authors concluded that this hindered DRX during the following extrusion process and, therefore, resulted in increased YS and ultimate tensile strengths (UTS) of 320.7 MPa and 385.2 MPa, respectively, together with an elongation of 12.8 %. The reduced fraction of DRX is further reported to maintain a pronounced basal texture, which additionally contributed to the increase in strength. If the homogenization heat treatment was conducted before the forging step, a high amount of stored energy led to a higher recrystallized fraction during and after subsequent extrusion. The lower YS and UTS of 271 MPa and 370.9 MPa as well as the higher elongation of 21.7 % are explained by the almost fully DRXed microstructure.

The influence of processing parameters on microstructure and mechanical properties of a Mg – 1% Zn – 0.3% Ca (ZX10) and Mg – 0.5% Zn – 0.15% Ca (ZX00) alloy and, moreover, the influence of intermetallic particles present during deformation were studied by Hofstetter et al. [164]. The cast material was initially homogenized and solution annealed at 350 °C for 12 h and 450 °C for 8 h. Prior to hot forming, different heat treatments were conducted at 250 °C, in order to homogeneously distribute the intermetallic particles in the ZX10 and to dissolve them in the ZX00 material. The hot forming behavior of the material was analyzed by compression tests in a deformation dilatometer at 325 to 450 °C and finally by direct and indirect extrusion tests. In both extrusion tests an extrusion rate of 25:1 and a ram speed of 0.5 mm s⁻¹, corresponding to a strain rate of 0.74 s⁻¹, were applied. The authors show that a high volume fraction of Laves phase particles during hot-deformation leads to a fine grained microstructure, but the amount of particles has only a slight effect on the recrystallized volume fraction. A comparison between direct and indirect extrusion shows higher volume fractions of recrystallized grains (97 % compared to 78 %) at an extrusion temperature of 325 °C. Fully recrystallized microstructures could be obtained by a final heat treatment, which might lead to severe grain growth in the particle-free ZX00 alloy. The best-balanced mechanical properties (238 MPa YS, 265 MPa UTS, 31 % ϵ_f) were achieved after indirect extrusion at 300 °C. The ZX10 material, produced from Mg in ultra-high purity and processed with the same extrusion parameters (except a reduced ram speed of 0.15 s⁻¹) shows an excellent *in-vivo* degradation performance, which was assigned to the very low content of impurities and intermetallic particles [150]. Grün et al. already tested ZX00 material (aged and indirectly extruded at 300 °C) in small and large animals, showing low degradation rates, adequate H₂ evolution and undisturbed bone formation and in-growth [165].

How forging speed and temperature of an open-die forming process influence the microstructure, mechanical properties and finally the corrosion resistance of a **binary Mg – 1% Ca alloy** is presented by Harandi et al. in ref. [156]. A variation of the preheating temperature from 250 °C to 350 °C and 450 °C showed that increasing forging temperatures lead to refined grains in the final material, resulting in higher ductility, whereas the maximum hardness was achieved at a forging temperature of 350 °C. In contrast, the variation of the forging speed of 40, 50, 60 and 65 stocks per minute did not result in significant changes. Mg₂Ca particles were found inside the α -Mg grains as well as at the grain boundaries, but the overall phase fraction decreased with increasing forging temperature, which is a possible explanation for the reduction of hardness in the material forged at 450 °C. The corrosion resistance of the forged material could not be improved compared to the as-cast material.

As some studies show that the degradation rate is partially influenced by the grain size, processing Mg-alloys by SPD can be a promising way for refining and homogenizing the microstructure [166]. The most practicable SPD processes are equal channel angular pressing and high-pressure torsion as they allow to process sufficiently large amount of material for mechanical testing as well as implant manufacturing.

2.9. Forging of Various Magnesium Alloying Systems

In the work of Zheng et al. [167] the flange of an automotive clutch was forged of as-cast **NZ30K** (Mg–Nd–Zn–Zr), an alloy which is known for good creep resistance. The forming conditions were determined in tensile (200 to 400 °C, at 0.01 s⁻¹) and compression tests (250 to 400 °C, at 0.001 to 10 s⁻¹) primarily showing the temperature dependence of the forging process. The best results were expected between 350 to 400 °C with a strain rate of 0.001 to 1 s⁻¹. Therefore, forming took place at 400 °C stock temperature and 250 °C die temperature, followed by artificial ageing (T5). The mechanical properties were investigated by tensile testing, the T5 state showing YS and UTS values of 318 MPa and 324 MPa respectively. Creep testing was done at 200 and 250 °C with an applied stress of 100 MPa for up to 150 h. The measured steady-state creep rate of NZ30K at 200 °C is an order of magnitude lower than the creep rate of AZ91, confirming the good high temperature behavior of NZ30K.

An investigation of multiple **TAZ** (Mg–Sn–Al–Zn) alloys regarding their forging behavior, grain size evolution and mechanical properties was done by Yoon and Park [71]. They compared the performance of extruded forging stock made from TAZ541, TAZ711 and TAZ811 to AZ61 and AZ80. The TAZ alloys were homogenized at 460, 480 and 500 °C for 12 h, the AZ stock was homogenized at 440 °C for 15 h. The parts were forged in a temperature range of 250 to 450 °C with the strain rates of 2 to 10 s⁻¹. A T-shaped part was used to analyze the forging behavior of the alloys, while a part in the approximate shape of a control arm was used for further testing. In the forming process the TAZ alloys showed better performance when compared to the AZ samples. The analysis of the parts forged at 450 °C showed a bimodal microstructure in the TAZ711 alloy, while the grain size of the AZ61 part was quite homogeneous. The tensile properties of the as-forged samples depend on the processing temperature, the forgings at 250 °C reached the highest strengths in this study. The alloys TAZ711 and TAZ811 show a higher YS but a reduced elongation when compared to the AZ samples. Tested TAZ alloys reached YS of 360 MPa and UTS of 380 MPa.

Semi-closed die forging of a **TX31** alloy was done by Rao et al. [168], using as-cast stock material. TX31 shows a good creep resistance due to ternary Mg–Sn–Ca phases in the Mg matrix. In their work Rao et al. analyze the forming behavior of TX31 by means of a processing map (at a strain of 0.5), that shows two domains of interest for forming. The experimental trials, where cylindrical stock was forged into cup shaped parts, were done at 350 to 500 °C using a forming speed of 0.01 to 10 mm s⁻¹. The forging experiments were accompanied by simulations, which allowed to describe the forces necessary for forming accordingly. The microstructure of the forged parts varied in terms of grain size as well as shape and size of the secondary particles. The samples forged in the domain ranging from 350 to 500 °C at strain rates of 1 to 10 s⁻¹ showed preferable properties. The microstructure consists of DRX grains

and a reduced amount of Mg-Sn-Ca particles, the forming parameters are therefore recommended by the authors for the use in forging operations.

2.10. Concluding Remarks

Before concluding this work, it might be beneficial to look at the conclusions drawn and prospects given at the dawn of Mg production, therefore three quotes from a review authored by Houghton in 1939 are discussed briefly in the following:

The reactive nature of magnesium has seriously interfered with its much wider adoption; to those who still associate the metal mainly with the ribbon which is burned to give a flashlight for photography, it seems incredible that magnesium can be used for structural purposes. [22]

While not many people still know that Mg once was used for photography flashlights, this statement is in principle still valid today. A big issue to this day is the fire hazard conceived by industry and consumers, showing itself in the ban of Mg products in aircraft interiors till 2015 [169] by the Federal Aviation Administration (FAA) or the brochure on 'Safe Magnesium' issued by the International Magnesium Association (IMA) [170]. This ultimately lead to the development of 'non flammable' Mg alloys either containing high amounts of RE elements (e.g., WE43) or Ca (and Y) which reduce the oxidation tendency and partially even exhibit self-extinguishing behavior.

Another topic linked to the reactive nature of Mg and its alloys is the corrosion behavior, an important aspect for producers and users of Mg products. This directly correlates to the next quote:

Nothing has been found or appears likely to be found, which will produce a "stainless magnesium". [22]

The corrosion behavior of Mg has been an issue since the beginning of its use in structural applications. While various methods for corrosion protection exist [7] and have been known since the first half of the 20th century [22], so called 'stainless' Mg alloys have only been reported in 2015 by Xu et al. [171]. In their work a Mg-Li alloy was shown to form a stable Li_2CO_3 film with complete coverage on the surface, protecting the Mg-Li matrix beneath from corrosion.

The final quote from 1939 highlights another main nuisance for the production and use of Mg alloys (i.e., wrought alloys), the poor ductility at RT, that has already been a hot topic to that time:

Much more progress has been made on alloys for use at room temperature. ... Work is now being carried out at the laboratory on the properties of alloys which have been rolled at 200 °C. This work is not yet complete, but interesting results have already been obtained. [22]

The ductility shown by Mg alloys is of course dominated by their hexagonal crystal structure, which does only provide 3 of the necessary 5 independent slip systems for arbitrary deformation at RT. The activation of additional slip systems above 200 °C is therefore important for any major forming operation.

The urge to improve the deformation behavior of Mg alloys at low temperatures is prevalent in many activities, showing itself notably in the development works on sheets, where the use of RE and Ca containing alloys has shown to improve the ductility by texture modification. Also, the utilization of fine grain sizes, leading to a better distribution of deformation throughout the microstructure, is a topic in this regard.

The recently published (2018, 2019) works of Wu et al. [172] and Ahmad et al. [173], in which a modulation of the hexagonal crystal structure by alloying is discussed, gives rise to new expectations in terms of low temperature ductility of Mg alloys in the near future.

While a lot of issues hindering industrial application have been solved and the development as well as understanding of these alloys has increased over the years, there is still potential to improve processability and performance in use.

Some topics of interest for Mg forgings have been discussed by Suh et al. [174] in their review on Mg sheet alloys, i.e., texture development and age hardenability.

The anisotropy generated by forming is an issue for all Mg forming processes. Especially sheet and extruded products show distinctive textures [175] which can have profound influences on the mechanical material properties. The use of extruded stock material for forged products influences therefore the forging process itself as well as the properties of the final product [82]. The texture solely created by forging on the other hand is markedly reduced, when compared to extrusion and rolling, and might therefore not be such an intensely discussed topic.

The development of age hardenable alloys on the other hand is an important future topic for forged products as well. The absence of studies discussing such parts is easily visible throughout this review. While some authors conduct T5 treatments [33; 91; 138] and others have shown the increase of material ductility after recrystallization treatment [32; 75], there are nearly no forged parts in T6 state mentioned in the investigated literature [75; 99]. This might be the case because only few Mg alloys exist which show age hardening to a strength beyond that gained by work hardening in the forging process.

A comparatively new type of alloying design for Mg alloys aims to change this. These materials called 'micro alloyed' [176] or 'lean alloy' [99] try to achieve a high final strength by fine grain sizes and precipitation hardening, utilizing heat treatments after the forming processes. In the forming process itself these alloys show low strength, permitting forming operations with reduced forces. A further benefit is the reduction of material costs by using low amounts of alloying elements.

Alloys which aim for application in higher temperature regimes are still heavily dependent on the use of RE alloying elements. The development of the materials showing LPSO phases is an intriguing development in this regard and it will be interesting to see the progress made with these alloys in the future.

The recycling of Mg products is not a topic in this work, nevertheless a few words should be said, as it plays an important role in the overall structure of the Mg market. The raw materials for primary production of magnesium are available in unlimited abundance but its extraction is very energy intensive. Recycling of already existing alloys is much more energy-efficient and therefore of vested industrial interest. While some products are recycled in grade and can therefore be used repeatedly for Mg products, several specific problems like rapid melt oxidation and complex removal of impurities hinders efficient recycling in general. Additionally, a vast amount of magnesium is dissipated in use (i.e., for iron desulphurization, Grignard reagents and pyrotechnics) or used as an alloying element for aluminum alloys and therefore lost for recovering metallic magnesium. An overview on the topic of magnesium recycling can be found in the work of Ditze and Scharf [177], additional in-depth information on the recycling of Mg in the EU (2017) is given in ref. [178].

While the increasing knowledge and development as well as the possible future research topics of Mg forgings have been described in this section, one main issue – the low rate of industrial application – has not yet been discussed. According to the review authored by Sillekens et al. [11], the main reason for this is the sub-critical market size for wrought Mg products, which can be described as a feedback loop: the lack of available stock material [83] promotes a scarceness of know-how, which accordingly decreases the possible applications and increases the prices of realized products, which in turn dampens the industrial interest.

Mg forgings are predominantly made from deformed feedstock (i.e., extruded or rolled), in order to take advantage of the already refined grain size for the forging operations. Thereby, the improved material flow behavior aids the die filling and is beneficial for the surface quality of the produced part. This stock material is needed in a wide range of shapes and sizes for various forgings. While it is possible to buy extruded material and plates, the market is small and the variety of available alloys is even smaller. The use of cast forging stock gives more freedom of choice in case of alloy selection and reduces the price by skipping one forming step but has disadvantages as well. Depending on the applied casting process and part size, the grain size and number of defects may increase, also machining/scalping steps will most likely be necessary.

The know-how necessary for industrial-sized forging applications is diversified. Production parameters like die design, process layout, heat treatments and machining behavior have to be known, but also additional technologies as for example surface treatments need to be available. After production the

resulting part properties have to be verified. This commonly includes corrosion tests and mechanical testing to obtain e.g., tensile properties and for some parts fatigue or creep testing as well as fracture mechanical investigations might be required. For many of these listed points even basic information is hardly available and the appropriate development effort can be intense.

The above listed problems but also the already mentioned conceived fire hazard and susceptibility of Mg alloys to corrosion are inhibiting factors for a broad range of industrial applications. The parts available at present are mainly found in the high-priced fields like defense and sportive products. In these cases the whole process chain can be trimmed to optimal performance of one product, but this mostly entails protected process design and small product quantities, which does little to increase the overall industrial acceptance. Nevertheless, the ever-increasing range of Mg alloys, better mechanical properties and improved understanding of production routes rise hope for an increased amount of Mg wrought products in the coming years.

In particular, we expect an increase of industrial forged parts made from Mg alloys in the near future, as supported by market trends, such as lightweighting. The wide range of possible processing parameters for forgings, when compared to other Mg forming processes, eases the entry into the production of Mg forgings for manufacturers. Further progress might be achieved by the use of alloys designed for specific forming operations, thereby improving the processing behavior, increasing work safety and enhancing the properties of the finished part.

The authors hope that this work, which aims to give an overview of the processing parameters and possible resulting properties of Mg forgings, can provide useful aid in the future production of such components.

2.11. Appendix

2.11.1. CALPHAD calculations

The figures showing binary phase diagrams and CALPHAD calculations were done with the software Thermo-Calc Version 2019a. For this purpose the databases Thermo-Calc TCBIN v 1.1 and ThermoTech TTMG5 were used, respectively. The specific alloy compositions used are shown in Table 2.4.

Table 2.4.: Alloy compositions in wt. % used for CALPHAD calculations in this work.

Alloy	Al	Zn	Mn	Ca	Zr	Y	Ce	La	Mg
AZ31	3.0	1.0	0.2						Balance
AZ61	6.3	1.0	0.2						Balance
AZ71	7.69	0.54	0.18						Balance
AZ80	8.0	0.5	0.2						Balance
AZ91	9.0	0.625	0.2						Balance
AZX311	3.0	1.0	0.2	1.0					Balance
WE43					0.4	4.0	1.74	1.16	Balance
ZK60		6.0			0.6				Balance
ZX10		1.0		0.3					Balance

2.11.2. Heat treatments and forming temperatures

A short overview of common temper designations used in Mg alloys is given in Table 2.5; Table 2.6 summarizes recommendations for forging and die temperatures for various Mg alloys. Additionally, a selection of commonly used temperatures and times for Mg heat treatments is given in Table 2.7.

Table 2.5.: Common temper designations based on [179].

Designation	Explanation
F	as-fabricated
O	annealed, recrystallized
W	solution heat treated
T4	solution heat treated and naturally aged
T5	artificially aged only
T6	solution heat treated and artificially aged
H1	strain hardened only
H2	strain hardened and partially annealed
H3	strain hardened and stabilized

Table 2.6.: Recommended forging temperatures for various Mg alloys in °C by [30].

Alloy	Workpiece	Forging die
AZ31B	290–345	260–315
AZ61A	315–370	290–345
AZ80A	290–400	205–290
EK31A	370–480	345–400
HM21A	400–525	370–425
QE22A	345–385	315–370
ZE42A	290–370	300–345
ZE62	300–345	300–345
ZK21A	300–370	260–315
ZK60A	290–385	205–290

Table 2.7.: Heat treatment parameters of various Mg alloys, based on recommendations from literature.

Alloy	Parameter	Source
Homogenization		
AZ31	450 °C for 3 h	[66]
AZ70	410 °C for 10 to 15 h	[75]
AZ71	420 °C for 6 h	[73]
AZ80	420 °C for 20 h	[38]
	400 °C for 12 h	[89]
AZ91	413 °C, 16 to 24 h	[35]
	413 °C, 6 h + 352 °C, 2 h + 413 °C, 10 h	[35]
ZK60	470 °C, 14 h	[121]
ZK61	499 °C, 2 h	[35]
	482 °C, 10 h	[35]
WE43	525 °C, 4 to 8 h	[35]
Anneal/ stress relieving		
AZ31 O	345 °C, 2 h	[35]
AZ31 F	260 °C, 15 min	[35]
AZ31 H24	150 °C, 1 h	[35]
AZ61 F	260 °C, 15 min	[35]
AZ80 F	260 °C, 15 min	[35]
AZ80 T5	200 °C, 1 h	[35]
ZK60 F	260 °C, 15 min	[35]
ZK60 T5	150 °C, 1 h	[35]
T5 - artificial ageing		
AZ71	350 °C, 1 h	[73]
AZ80	177 °C, 16 to 24 h	[35]
AZ91	216 °C, 4 h	[35]
	168 °C, 16 h	[35]
ZK60	150 °C, 24 h	[35]
ZK61	149 °C, 48 h	[35]
WE43	180 °C, 60 h	[33]
T6 - solution heat treatment[†] + artificial ageing		
AZ91	413 °C +168 °C, 16 h	[35]
	413 °C +216 °C, 5 to 6 h	[35]
ZK61	499 °C + 180 °C, 16 h	[35]
WE43	525 °C, quenching in water at 65 °C + 250 °C, 16 h	[35]
Maximum Temperatures		
AZ91	418 °C	[35]
ZK61	502 °C	[35]
WE43	535 °C	[35]

†: Times for solution heat treatment are usually process and part dependent and can therefore not be given here.

Table 2.8.: Mechanical properties of various forged Mg alloys tested at room temperature.

Alloy	Temper	YS [MPa]	UTS [MPa]	ϵ_f [%]	ϵ_{other} [%]	YSc [MPa]	UCS [MPa]	Source	Process Parameters
AZ31		170	260		15 (in 50 mm)			[27]	
	F	290	360		15 (A5)			[58]	rolled + forged at 410 °C, temperature ranging of 250 °C at 0.6 mm s ⁻¹ , sample from rib position
	F	221	312		12 (A5)			[58]	rolled + forged at 410 °C, temperature ranging of 250 °C at 0.6 mm s ⁻¹ , sample from base position
	F	220-298	310-365		11-16 (A5)			[56]	rolled and annealed plate, forged at a stock temperature of 410 °C and a die temperature of 200 °C at 0.6 mm s ⁻¹ , one-rib bracket
	F	216-250	303-350		12-15.5 (A5)			[56]	rolled and annealed plate, forged at a stock temperature of 410 °C and a die temperature of 200 °C at 0.6 mm s ⁻¹ , two-rib bracket
	F	136	278	12.4		78-116	278-316	[66]	cast, homogenized at 450 °C for 3 h, isothermal forged at 450 °C and 6.5 mm s ⁻¹
	F	180-189	347-369					[49]	extruded + formed at 300 to 400 °C, 12 to 160 mm s ⁻¹ using a die temperature of 350 °C
	F	234	280		14.4 (A5)			[64]	forged at 400 °C material and die temperatures of 300 °C in three steps, using a screw press
AZX311	F	121-204	203-286		21-41			[109]	cast-extruded 320 °C + two step forged, the billet was upset in an open die at 350 °C up to 35 % engineering strain; second step in a closed die at presumed temperatures of 310 °C (stock) and 320 °C (die) with 41 mm s ⁻¹
AZ61	F	180	295					[27]	
	F	194-231	398-410	18-21	12 (in 50 mm)	125		[49]	extruded + formed at 300 to 400 °C, 12 to 160 mm s ⁻¹ using a die temperature of 350 °C
AZ70	F		295.2	8.88				[75]	cast + homogenized at 410 °C for 10 to 15 h, two step forged with 8 mm s ⁻¹ at 400 °C and 380 °C respectively
	O		291.5	11.52				[75]	cast + homogenized at 410 °C for 10 to 15 h, two step forged with 8 mm s ⁻¹ at 400 °C and 380 °C respectively
	T5		300.2	9.12				[75]	cast + homogenized at 410 °C for 10 to 15 h, two step forged with 8 mm s ⁻¹ at 400 °C and 380 °C respectively
	T6		310.7	13.28				[75]	cast + homogenized at 410 °C for 10 to 15 h, two step forged with 8 mm s ⁻¹ at 400 °C and 380 °C respectively

Table 2.8 continued from previous page

Alloy	Temper	YS [MPa]	UTS [MPa]	ϵ_f [%]	ϵ_{other} [%]	YSc [MPa]	UCS [MPa]	Source	Process Parameters
AZ71	T5		253		10.7			[73]	AZ71 + 1 wt.%Nd, cast + homogenized at 420 °C for 6 h, rotary forged at 200 °C with 3 s ⁻¹ to an eng. strain of 32 %, annealed to T5 at 350 °C for 1 h
AZ80	F	230	330		11 (in 50 mm)	170		[27]	cast + isothermal forged at 350 °C, 0.65 mm s ⁻¹
	T5	250	345		6 (in 50 mm)	195		[27]	cast + isothermal forged at 450 °C, 0.65 mm s ⁻¹
	F	173.8	311.9	14.1		124.5	373	[76]	cast + isothermal forged at 450 °C, 6.5 mm s ⁻¹
	F	176.9	310.6	15.8		111.2	366.7	[76]	cast + isothermal forged at 450 °C, 6.5 mm s ⁻¹
	F	181.7	306.1	14.2		69.2	325.9	[76]	cast + isothermal forged at 375 °C, 20 mm s ⁻¹
	F	110.7	239.8	7.2				[95]	cast + isothermal forged at 375 °C, 20 mm s ⁻¹
	F	175	312.1	14.1				[95]	extruded + isothermal forged at 375 °C, 20 mm s ⁻¹
	F	226.8	351.1	17.5				[95]	extruded + isothermal forged at 375 °C, 20 mm s ⁻¹
	F	219.2	341.3	20.5				[95]	extruded + isothermal forged at 375 °C, 20 mm s ⁻¹
	F	196	315	16		159	402	[86]	extruded + isothermal forged at 380 °C, 0.075 mm s ⁻¹
	F	206	318					[79]	extruded + isothermal forged at 300 °C, 0.075 mm s ⁻¹
	F	260	330					[79]	extruded + forged at 265 °C, die temperature 250 °C, 20 mm s ⁻¹
F	248	361	15		190		[85]	extruded + forged at 365 °C, die temperature 250 °C, 20 mm s ⁻¹	
F	207	349	16		175		[85]	extruded + forged at 400 °C, die temperature 300 °C, 0.11 s ⁻¹ ,	
T5		274	389		1			[87]	heat treated (T5) at 177 °C for 24 h
F		320-330						[89]	cast + homogenized at 400 °C for 12 h and isothermal forged at 360 to 400 °C and 16 mm s ⁻¹
T5		280.2	370.6		7.5			[91]	forged at 330 °C with 1 mm s ⁻¹ , artificially aged at 150 °C for 30 h, sample in web position
T5		155.5	270.3		5.3			[91]	forged at 330 °C with 1 mm s ⁻¹ , artificially aged at 150 °C for 30 h, sample in flange
F		294	406	15				[92]	extruded + forged with 16 mm s ⁻¹ at 350 °C
AZ91	F	159	330	16.1				[111]	cast + homogenized (410 °C for 24 h), compressed at 300 °C with 0.1 s ⁻¹ up to 1.6 true strain
AZX911	F	174	313	10.7				[111]	cast + homogenized (410 °C for 24 h), compressed at 300 °C with 0.1 s ⁻¹ up to 1.6 true strain

Table 2.8 continued from previous page

Alloy	Temper	YS [MPa]	UTS [MPa]	ϵ_f [%]	ϵ_{other} [%]	YSc [MPa]	UCS [MPa]	Source	Process Parameters
GWZK102	F	210	308		4.2			[141]	cast + homogenized at 510 °C for 10 h and quenched in water with 80 °C, forged at 470 °C
	T5	273	406		5.9			[141]	cast + homogenized at 510 °C for 10 h, quenched in water with 80 °C, forged at 470 °C, ageing at 200 °C for 60 h
	F	220	290		5.94			[143]	isothermal forged at 407 °C at presumably 1 mm s ⁻¹
	T5	243	380		3.84			[143]	isothermal forged at 407 °C at presumably 1 mm s ⁻¹ , T5 ageing at 200 °C for 63 h
HM21A	T5	140	230		15 (in 50 mm)	115		[27]	
M1A		160	250		7 (in 50 mm)			[27]	
NZ30K	F	269.3	278.8		12.2			[167]	cast + forged at 400 °C stock temperature and 250 °C die temperature, with a strain rate of 0.001 to 1 s ⁻¹
	T5	318.2	323.5		11.2			[167]	cast + forged at 400 °C stock temperature and 250 °C die temperature, with a strain rate of 0.001 to 1 s ⁻¹
WE43	T5	> 225	350					[138]	extruded + heat treated (525 °C for 8 h), forged (360 to 480 °C) with strain rates of 0.006 to 8 s ⁻¹ to an amount of 35 to 85 % strain, aged at 180 to 260 °C
	F	263 ± 7	311 ± 11		23 ± 3			[33]	F temper plate, forged at 380 °C and 1 s ⁻¹ up to a deformation of 1.2 truestrain
ZA21	T5	286 ± 10	341 ± 4		28 ± 1			[33]	F temper plate, forged at 380 °C and 1 s ⁻¹ up to a deformation of 1.2 truestrain, ageing at 150 °C for 104 h
	T5	344 ± 11	388 ± 12		23 ± 1			[33]	F temper plate, forged at 380 °C and 1 s ⁻¹ up to a deformation of 1.2 truestrain, ageing at 180 °C for 60 h
	T5	318 ± 9	368 ± 10		17 ± 1			[33]	F temper plate, forged at 380 °C and 1 s ⁻¹ up to a deformation of 1.2 truestrain, ageing at 210 °C for 32 h
	F	232 ± 4	306 ± 11		7.8 ± 0.4			[119]	cast + isothermally forged at 250 °C, quenched in water
ZK60	F	168 ± 2	250 ± 2		10.7 ± 1.2			[119]	cast + isothermally forged at 350 °C, quenched in water
	F	151 ± 7	236 ± 7		7.1 ± 1.1			[119]	cast + isothermally forged at 450 °C, quenched in water
	F	215	305		16	160		[27]	
	F	163 ± 10	286 ± 4	26 ± 3		111 ± 1	390 ± 6	[129]	cast + forged at 450 °C, 0.65 mm s ⁻¹

Table 2.9.: Mechanical properties of Mg alloys tested at elevated temperatures.

Alloy	Temper	Temperature [°C]	Testing Speed [s ⁻¹]	UTS [MPa]	YS [MPa]	ϵ_p [%]	ϵ_f [%]	ϵ_{other} [%]	YSc [MPa]	Source	Process Parameters
AZ31	as-cast	300	1						139	[48]	
	as-cast	300	5						140	[48]	
	as-cast	300	10						148	[48]	
	as-cast	350	1						113	[48]	
	as-cast	350	5						117	[48]	
	as-cast	350	10						122	[48]	
	as-cast	400	1						88	[48]	
	as-cast	400	5						95	[48]	
	as-cast	400	10						104	[48]	
	extruded	300	1						166	[48]	
	extruded	300	5						189	[48]	
	extruded	300	10						230	[48]	
	extruded	350	1						120	[48]	
	extruded	350	5						150	[48]	
	extruded	350	10						171	[48]	
	extruded	400	1						74	[48]	
extruded	400	5						100	[48]		
extruded	400	10						113	[48]		
AZ61	as-cast	300	1						134	[48]	
	as-cast	300	5						145	[48]	
	as-cast	300	10						150	[48]	
	as-cast	350	1						105	[48]	
	as-cast	350	5						122	[48]	
	as-cast	350	10						127	[48]	
	as-cast	400	1						90	[48]	
	as-cast	400	5						101	[48]	
	as-cast	400	10						108	[48]	
	extruded	300	1						160	[48]	
	extruded	300	5						200	[48]	
	extruded	300	10						210	[48]	
	extruded	350	1						125	[48]	
	extruded	350	5						150	[48]	
	extruded	350	10						170	[48]	
	extruded	400	1						75	[48]	
extruded	400	5						100	[48]		

Table 2.9 continued from previous page

Alloy	Temper	Temperature [°C]	Testing Speed [s ⁻¹]	UTS [MPa]	YS [MPa]	ϵ_p [%]	ϵ_f [%]	ϵ_{other} [%]	YSc [MPa]	Source	Process Parameters
	extruded	400	10						120	[48]	
AZ80	as-cast	325	1.5×10^{-4}	42.3	38.6	1.5	6.2			[38]	cast
	cast + hom	325	1.5×10^{-4}	45.5	42.5	1	13			[38]	cast + hom. at 420 °C, 5 h
	cast + hom	325	1.5×10^{-4}	46.7	43.5	2.5	10.1			[38]	cast + hom. at 420 °C, 20 h
	as-cast	375	1.5×10^{-4}	24.6	24.4	0.5	14			[38]	cast
	cast + hom	375	1.5×10^{-4}	28.4	27.8	0.75	10.8			[38]	cast + hom. at 420 °C, 5 h
	cast + hom	375	1.5×10^{-4}	26.4	24.4	0.6	17.3			[38]	cast + hom. at 420 °C, 20 h
	as-cast	420	1.5×10^{-4}	14.6	14.3	0.65	2.1			[38]	cast
	cast + hom	420	1.5×10^{-4}	15.7	15.1	0.75	17.1			[38]	cast + hom. at 420 °C, 5 h
	as-cast	300	1						148	[48]	
	as-cast	300	5						160	[48]	
	as-cast	300	10						171	[48]	
	as-cast	350	1						113	[48]	
	as-cast	350	5						128	[48]	
	as-cast	350	10						139	[48]	
	as-cast	400	1						92	[48]	
	as-cast	400	5						108	[48]	
	as-cast	400	10						114	[48]	
extruded		300	1					149	[48]		
extruded		300	5					214	[48]		
extruded		300	10					223	[48]		
extruded		350	1					130	[48]		
extruded		350	5					163	[48]		
extruded		350	10					176	[48]		
extruded		400	1					87	[48]		
extruded		400	5					116	[48]		
extruded		400	10					126	[48]		
T5		130	1×10^{-3}	258.4	186.1			42.8		[91]	forged at 330 °C with 1 mm s^{-1} , artificially aged at 150 °C for 30 h, sample in web position
T5		130	1×10^{-3}	226.8	124.5			30.3		[91]	forged at 330 °C with 1 mm s^{-1} , artificially aged at 150 °C for 30 h, sample in flange

Table 2.9 continued from previous page

Alloy	Temper	Temperature [°C]	Testing Speed [s ⁻¹]	UTS [MPa]	YS [MPa]	ϵ_p [%]	ϵ_f [%]	ϵ_{other} [%]	YSc [MPa]	Source	Process Parameters
HM21A	T5	200		110	90			49 (in 25mm)		[27]	
	T5	315		90	76			37 (in 25mm)		[27]	
	T5	370		76	55			43 (in 25mm)		[27]	
M1A		93		165	121			25		[27]	
		120		145	107			26		[27]	
		150		131	93			31		[27]	
		200		114	69			34		[27]	
		260		83	45			67		[27]	
		315		41	28			140		[27]	

2.12. References

- [1] I. Polmear, Recent Developments in Light Alloys, *Materials transactions* 37 (1) (1996) 12–31. doi:10.2320/matertrans1989.37.12.
- [2] B. Mordike, T. Ebert, Magnesium: properties—applications—potential, *Materials Science and Engineering: A* 302 (1) (2001) 37–45. doi:10.1016/S0921-5093(00)01351-4.
- [3] S. R. Agnew, Wrought magnesium: a 21st century outlook, *JOM* 56 (5) (2004) 20–21. doi:10.1007/s11837-004-0120-8.
- [4] C. Bettles, M. Gibson, Current wrought magnesium alloys: Strengths and weaknesses, *JOM* 57 (5) (2005) 46–49. doi:10.1007/s11837-005-0095-0.
- [5] Z. Yang, J. Li, J. Zhang, G. Lorimer, J. Robson, Review On Research And Development Of Magnesium Alloys, *Acta Metallurgica Sinica (English letters)* 21 (5) (2008) 313–328. doi:10.1016/S1006-7191(08)60054-X.
- [6] M. Esmaily, J. Svensson, S. Fajardo, N. Birbilis, G. Frankel, S. Virtanen, R. Arrabal, S. Thomas, L. Johansson, Fundamentals and advances in magnesium alloy corrosion, *Progress in Materials Science* 89 (2017) 92–193. doi:10.1016/j.pmatsci.2017.04.011.
- [7] J. Gray, B. Luan, Protective coatings on magnesium and its alloys—a critical review, *Journal of alloys and compounds* 336 (1-2) (2002) 88–113. doi:10.1016/S0925-8388(01)01899-0.
- [8] J.-F. Nie, Precipitation and hardening in magnesium alloys, *Metallurgical and Materials Transactions A* 43 (11) (2012) 3891–3939. doi:10.1007/s11661-012-1217-2.
- [9] Z. Zeng, N. Stanford, C. H. J. Davies, J.-F. Nie, N. Birbilis, Magnesium extrusion alloys: a review of developments and prospects, *International Materials Reviews* (2018). doi:10.1080/09506608.2017.1421439.
- [10] W. Sillekens, D. Letzig, The MagForge project: European Community research on forging of magnesium alloys, in: K. U. Kainer (Ed.), *Magnesium: Proceedings of the 7th International Conference on Magnesium Alloys and their Applications*, Wiley-VCH, Weinheim, GER, 2007.
- [11] W. Sillekens, G. Kurz, R. Werkhoven, Magnesium forging technology: state-of-the-art and development perspectives, in: L. Katgerman, F. Soetens (Eds.), *New Frontiers in Light Metals: Proceedings of the 11th International Aluminium Conference – 'INALCO'2010*, IOS Press, Amsterdam, NL, 2010, pp. 329–337. doi:10.3233/978-1-60750-586-0-329.
- [12] W. Sillekens, F. Chevalleyre, G. Gantar, European Community research on forging of magnesium alloys (MagForge): state of affairs, in: K. U. Kainer (Ed.), *Magnesium: Proceedings of the 8th International Conference on Magnesium Alloys and their Applications*, Wiley-VCH, Weinheim, GER, 2010, pp. 1392–1397.
- [13] B. Ovsyannikov, Die-Forged Disks for Automobile Wheels in Magnesium Alloys, in: K. U. Kainer (Ed.), *Magnesium: Proceedings of the 7th International Conference Magnesium Alloys and their Application*, Wiley-VCH, Weinheim, GER, 2007, pp. 352–356.
- [14] A. Dziubińska, A. Gontarz, M. Dziubiński, M. Barszcz, The forming of magnesium alloy forgings for aircraft and automotive applications, *Advances in Science and Technology Research Journal* 10 (31) (2016) 158–168. doi:10.12913/22998624/64003.
- [15] D. Shan, W. Xu, Y. Lu, Study on precision forging technology for a complex-shaped light alloy forging, *Journal of Materials Processing Technology* 151 (1-3) (2004) 289–293. doi:10.1016/j.jmatprotec.2004.04.075.
- [16] P. Hartley, I. Pillinger, Numerical simulation of the forging process, *Computer methods in applied mechanics and engineering* 195 (48-49) (2006) 6676–6690. doi:10.1016/j.cma.2005.03.013.
- [17] M. Hawryluk, J. Jakubik, Analysis of forging defects for selected industrial die forging processes, *Engineering Failure Analysis* 59 (2016) 396–409. doi:10.1016/j.engfailanal.2015.11.008.
- [18] J. A. Gann, Magnesium Industry's Lightest Structural Metal, *SAE Transactions* 25/26 (1930/1931) 620–641.
- [19] W. K. Zinszer, Magnesium, Its Manufacture and Alloys, *Transactions of the Kansas Academy of Science* (1903-) 46 (1943) 161–163. doi:10.2307/3624945.

- [20] I. Polmear, D. StJohn, J.-F. Nie, M. Qian, *Light Alloys: Metallurgy of the Light Metals*, 5th Edition, Elsevier, Butterworth-Heinemann, Oxford, UK, 2017. doi:10.1016/B978-0-08-099431-4.00009-9.
- [21] A. Portevin, R. Defleury, *Ultra-light alloys and their utilization on aircraft*, Tech. rep. (1924).
- [22] J. Haughton, *Magnesium and Its Alloys Recent Developments in Great Britain*, *Industrial & Engineering Chemistry* 31 (8) (1939) 969–971. doi:10.1021/ie50356a011.
- [23] K. Grube, J. Davis, L. Eastwood, C. Lorig, H. Cross, *Improvement of High-Temperature Properties of Magnesium-Cerium Forging Alloys*, Tech. rep. (1950).
- [24] P. Frost, *Magnesium-Lithium Alloys A Review of Current Developments*, Tech. rep. (1962).
- [25] H. Shaw, F. Boulger, C. Lorig, *Development of Die Lubricants for Forging and Extruding Ferrous and Nonferrous Materials*, Tech. rep. (1955).
- [26] A. Sabroff, F. Boulger, H. Henning, J. Spretnak, *A Manual on Fundamentals of Forging Practice*, Tech. rep. (1964).
- [27] R. Nunes, J. Adams, et al., *ASM-Handbook Volume 2: Nonferrous Alloys and Special-Purpose Materials*, ASM International, Materials Park, OH, USA, 1992. doi:10.31399/asm.hb.v02.a0001075.
- [28] G. E. Dieter, H. A. Kuhn, S. L. Semiatin, *Handbook of Workability and Process Design*, ASM International, Materials Park, OH, USA, 2003.
- [29] S. Lim, M. Yong, *Plane-strain forging of wrought magnesium alloy AZ31*, *Journal of materials processing technology* 171 (3) (2006) 393–398. doi:10.1016/j.jmatprotec.2005.07.011.
- [30] R. Nunes, I. Abbas, et al., *ASM-Handbook Volume 14: Forming and Forging*, ASM International, Materials Park, OH, USA, 1996. doi:10.31399/asm.hb.v14a.a0003998.
- [31] C. Bettles, M. Barnett, *Advances in wrought magnesium alloys: fundamentals of processing, properties and applications*, Elsevier, Woodhead Publishing, Cambridge, UK, 2012. doi:10.1016/B978-1-84569-968-0.50017-X.
- [32] N. Papenberg, S. Gneiger, *Closed Die Forging of Mg-Al-Zn-Ca-Y Alloys*, in: R. Kawalla, U. Prah, M. Moses, H. Wemme, J. Luft, M. Kirschner (Eds.), *Resource Efficient Material and Forming Technologies*, Vol. 918 of *Materials Science Forum*, Trans Tech Publications Ltd, Pfaffikon, CH, 2018, pp. 28–33. doi:10.4028/www.scientific.net/MSF.918.28.
- [33] S. Panigrahi, W. Yuan, R. Mishra, R. DeLorme, B. Davis, R. Howell, K. Cho, *A study on the combined effect of forging and aging in Mg-Y-RE alloy*, *Materials Science and Engineering: A* 530 (2011) 28–35. doi:10.1016/j.msea.2011.08.065.
- [34] C. Moosbrugger, *Engineering Properties of Magnesium Alloys*, ASM International, Materials Park, OH, USA, 2017.
- [35] M. M. Avedesian, H. Baker, et al., *ASM specialty handbook: magnesium and magnesium alloys*, ASM International, Materials Park, OH, USA, 1999, ISBN 978-0-87170-657-7.
- [36] DIN 1729-1, *Magnesiumlegierungen; Knetlegierungen*, Standard, Deutsches Institut für Normung (Aug. 1982). doi:10.31030/1086326.
- [37] DIN EN 1753:1997, *Magnesium und Magnesiumlegierungen - Blockmetalle und Gußstücke aus Magnesiumlegierungen*, Standard, Deutsches Institut für Normung (Aug. 1997). doi:10.31030/7375448.
- [38] C. Sager, I. Yakubtsov, W. MacDonald, S. Shook, B. Diak, M. Niewczas, *Physical metallurgy of Mg AZ80 alloys for forging applications*, in: E. A. Nyberg, S. R. Agnew, N. R. Neelameggham, M. O. Pekguleryuz (Eds.), *Magnesium Technology 2009*, TMS, Warrendale, PA, USA, 2009, pp. 405–410.
- [39] K. Braszczyńska-Malik, *Discontinuous and continuous precipitation in magnesium-aluminium type alloys*, *Journal of Alloys and Compounds* 477 (1-2) (2009) 870–876. doi:10.1016/j.jallcom.2008.11.008.
- [40] M. Madaj, M. Greger, V. Karas, *Magnesium-alloy die forgings for automotive applications*, *Materials and Technology* 49 (2) (2015) 267–273. doi:10.17222/mit.2013.174.

- [41] P. Skubisz, J. Sińczak, S. Bednarek, Forgeability of Mg–Al–Zn magnesium alloys in hot and warm closed die forging, *Journal of Materials Processing Technology* 177 (1-3) (2006) 210–213. doi:10.1016/j.jmatprotec.2006.04.091.
- [42] Y. Chino, M. Mabuchi, K. Shimojima, Y. Yamada, C. Wen, K. Miwa, M. Nakamura, T. Asahina, K. Higashi, T. Aizawa, Forging characteristics of AZ31 Mg alloy, *Materials Transactions* 42 (3) (2001) 414–417. doi:10.2320/matertrans.42.414.
- [43] T. W. R. Wong, High Temperature Forging of AZ31B Magnesium Alloy, Master's thesis, University of Waterloo (2016).
- [44] Q. Dai, D. Zhang, X. Chen, On the anisotropic deformation of AZ31 Mg alloy under compression, *Materials & Design* 32 (10) (2011) 5004–5009. doi:10.1016/j.matdes.2011.06.017.
- [45] B. Viehweger, A. Karabet, M. Düring, L. Schaeffer, Forging of Mg-Alloys AZ31 and AZ80, *Materialwissenschaft und Werkstofftechnik* 36 (5) (2005) 211–217. doi:10.1002/mawe.200400856.
- [46] P. Skubisz, J. Sińczak, Precision forging of thin-walled parts of AZ31 magnesium alloy, *Archives of Metallurgy and Materials* 52 (2) (2007) 329–336.
- [47] M. Graf, M. Ullmann, R. Kawalla, Property-oriented production of forged magnesium components, *Materials Today: Proceedings* 2 (2015) 76–84. doi:10.1016/j.matpr.2015.05.022.
- [48] M. Graf, M. Ullmann, R. Kawalla, Influence of initial state on forgeability and microstructure development of magnesium alloys, *Procedia Engineering* 81 (2014) 546–551. doi:10.1016/j.proeng.2014.10.037.
- [49] B.-A. Behrens, I. Schmidt, Improving the properties of forged magnesium parts by optimized process parameters, *Journal of Materials Processing Technology* 187–188 (2007) 761–765. doi:10.1016/j.jmatprotec.2006.11.057.
- [50] J. Liu, Z. Cui, Hot forging process design and parameters determination of magnesium alloy AZ31B spur bevel gear, *Journal of Materials Processing Technology* 209 (18-19) (2009) 5871–5880. doi:10.1016/j.jmatprotec.2009.06.015.
- [51] Z.-y. Jin, N.-n. Li, Q. Zhang, Y. Kai, Z.-s. Cui, Effects of forging parameters on uniformity in deformation and microstructure of AZ31B straight spur gear, *Transactions of Nonferrous Metals Society of China* 27 (10) (2017) 2172–2180. doi:10.1016/S1003-6326(17)60243-7.
- [52] D. Poerschke, The Effects of forging on the microstructure and tensile properties of magnesium alloys AZ31 and ZK60, Case Western Reserve University, Cleveland, OH, USA (2009).
- [53] H. Watanabe, H. Tsutsui, T. Mukai, K. Ishikawa, Y. Okanda, M. Kohzu, K. Higashi, Grain size control of commercial wrought Mg-Al-Zn alloys utilizing dynamic recrystallization, *Materials transactions* 42 (7) (2001) 1200–1205. doi:10.2320/matertrans.42.1200.
- [54] K. Rao, Y. Prasad, K. Suresh, Materials modeling and simulation of isothermal forging of rolled AZ31B magnesium alloy: anisotropy of flow, *Materials & Design* 32 (5) (2011) 2545–2553. doi:10.1016/j.matdes.2011.01.050.
- [55] A. Gontarz, A. Dziubińska, Forming of flat parts with ribs from magnesium alloy, *Aircraft Engineering and Aerospace Technology: An International Journal* 86 (4) (2014) 356–360. doi:10.1108/AEAT-10-2012-0188.
- [56] A. Dziubińska, A. Gontarz, K. Horzelska, P. Pieśko, The microstructure and mechanical properties of AZ31 magnesium alloy aircraft brackets produced by a new forging technology, *Procedia Manufacturing* 2 (2015) 337–341. doi:10.1016/j.promfg.2015.07.059.
- [57] A. Dziubińska, A. Gontarz, A new method for producing magnesium alloy twin-rib aircraft brackets, *Aircraft Engineering and Aerospace Technology: An International Journal* 87 (2) (2015) 180–188. doi:10.1108/AEAT-10-2013-0184.
- [58] A. Dziubińska, A. Gontarz, K. Dziedzic, Qualitative research of AZ31 magnesium alloy aircraft brackets produced by a new forging method, *Archives of Metallurgy and Materials* 61 (2) (2016) 1003–1008. doi:10.1515/amm-2016-0171.

- [59] R. Matsumoto, K. Osakada, Ductility of a magnesium alloy in warm forging with controlled forming speed using a CNC servo press, *Journal of Materials Processing Technology* 210 (14) (2010) 2029–2035. doi:10.1016/j.jmatprotec.2010.07.024.
- [60] A. Takara, L.-F. Chian, S. W. Chung, H. Somekawa, H. Watanabe, Y. Takigawa, K. Higashi, Suppression of macroscopic defects through the control of friction between workpiece and dies in a forged magnesium alloy part with ribs, *Materials transactions* 49 (5) (2008) 898–902. doi:10.2320/matertrans.ERM200904.
- [61] J. Lee, S. Kang, D. Yang, Novel forging technology of a magnesium alloy impeller with twisted blades of micro-thickness, *CIRP annals – Manufacturing Technology* 57 (1) (2008) 261–264. doi:10.1016/j.cirp.2008.03.064.
- [62] M. Kapustová, J. Bílik, The Description of Precision Forging Technology in Closed Die of Mg Alloy AZ31 Using Computer Simulation, in: K. Wongseedakaew (Ed.), *Applied Mechanics and Materials*, Vol. 686, Trans Tech Publ, 2014, pp. 78–81. doi:10.4028/www.scientific.net/AMM.686.78.
- [63] M. Kápustová, J. Bílik, The rationalization of production of magnesium alloy drop forgings using FEM simulation regarding forging process, *Tehnicki Vjesnik-Technical Gazette* 24 (5) (2017) 1323–1329. doi:10.17559/TV-20151126173017.
- [64] S. Mróz, A. Gontarz, K. Drozdowski, H. Bala, P. Szota, Forging of Mg/Al bimetallic handle using explosive welded feedstock, *Archives of Civil and Mechanical Engineering* 18 (2) (2018) 401–412. doi:10.1016/j.acme.2017.09.005.
- [65] D. Toscano, S. Shaha, B. Behraves, H. Jahed, B. Williams, Effect of forging on microstructure, texture, and uniaxial properties of cast AZ31B alloy, *Journal of Materials Engineering and Performance* 26 (7) (2017) 3090–3103. doi:10.1007/s11665-017-2743-2.
- [66] D. Toscano, S. K. Shaha, B. Behraves, H. Jahed, B. Williams, Effect of forging on the low cycle fatigue behavior of cast AZ31B alloy, *Materials Science and Engineering: A* 706 (2017) 342–356. doi:10.1016/j.msea.2017.08.086.
- [67] D. Toscano, S. Shaha, B. Behraves, H. Jahed, B. Williams, X. Su, Influence of low temperature forging on microstructure and low cycle fatigue behavior of cast AZ31B Mg alloy, in: D. Orlov, V. Joshi, S. K.N., N. N. R. (Eds.), *Magnesium Technology 2018*, Springer, Cham, CH, 2018, pp. 267–273. doi:10.1007/978-3-319-72332-7_41.
- [68] A. Gryguc, H. Jahed, B. Williams, J. McKinley, Magforge–mechanical behaviour of forged AZ31B extruded magnesium in monotonic compression, in: H. Chikwanda, S. Chikosha (Eds.), *Light Metals Technology 2015*, Vol. 828 of *Materials Science Forum*, Trans Tech Publications Ltd, Pfaffikon, CH, 2015, pp. 291–297. doi:10.4028/www.scientific.net/MSF.828-829.291.
- [69] A. Gryguc, S. Shaha, H. Jahed, M. Wells, B. Williams, J. McKinley, Tensile and fatigue behaviour of as-forged AZ31B extrusion, *Frattura ed Integrità Strutturale* 10 (38) (2016) 251–258. doi:10.3221/IGF-ESIS.38.34.
- [70] J. Yoon, J. Lee, Effect of initial microstructure on Mg scroll forging under warm forming condition, *Materials Transactions* 55 (2) (2014) 238–244. doi:10.2320/matertrans.M2013274.
- [71] J. Yoon, S. Park, Forgeability test of extruded Mg–Sn–Al–Zn alloys under warm forming conditions, *Materials & Design* 55 (2014) 300–308. doi:10.1016/j.matdes.2013.10.008.
- [72] M. Fujita, N. Sakate, S. Hirabara, Y. Yamamoto, Magnesium alloy cast material for plastic processing, magnesium alloy member using the same, and manufacturing method thereof, US Patent 6,143,097 (Nov. 7 2000).
- [73] J.-K. Chen, Y.-C. Chen, H.-T. Li, K.-S. Chan, C.-J. Chang, Effects of Nd and rotary forging on mechanical properties of AZ71 Mg alloys, *Transactions of Nonferrous Metals Society of China* 25 (10) (2015) 3223–3231. doi:10.1016/S1003-6326(15)63955-3.
- [74] S.-K. Guan, L.-H. Wu, L.-G. Wang, Flow stress and microstructure evolution of semi-continuous casting AZ70 Mg-alloy during hot compression deformation, *Transactions of Nonferrous Metals Society of China* 18 (2) (2008) 315–320. doi:10.1016/S1003-6326(08)60055-2.
- [75] S. Guan, L. Wu, P. Wang, Hot forgeability and die-forging forming of semi-continuously cast AZ70 magnesium alloy, *Materials Science and Engineering: A* 499 (1-2) (2009) 187–191. doi:10.1016/j.msea.2007.11.136.

- [76] A. Gryguc, S. K. Shaha, S. B. Behraves, H. Jahed, M. Wells, B. Williams, X. Su, Monotonic and cyclic behaviour of cast and cast-forged AZ80 Mg, *International Journal of Fatigue* 104 (2017) 136–149. doi:10.1016/j.ijfatigue.2017.06.038.
- [77] F. Ju, Z. Xia, B. Diak, O. Ojo, W. MacDonald, M. Niewczas, Modeling and Simulation of Mg AZ80 Alloy Forging Behaviour, Tech. rep., SAE Technical Paper (2008). doi:10.4271/2008-01-0214.
- [78] H. Zhou, Q. Li, Z. Zhao, Z. Liu, S. Wen, Q. Wang, Hot workability characteristics of magnesium alloy AZ80—A study using processing map, *Materials Science and Engineering: A* 527 (7-8) (2010) 2022–2026. doi:10.1016/j.msea.2009.12.009.
- [79] Z. Su, L. Wan, C. Sun, Y. Cai, D. Yang, Hot deformation behavior of AZ80 magnesium alloy towards optimization of its hot workability, *Materials Characterization* 122 (2016) 90–97. doi:10.1016/j.matchar.2016.10.026.
- [80] T. Pepelnjak, R. Werkhoven, D. Kobold, K. Kuzman, Analysis of Warm Magnesium Forging in Digital Environment, *Journal for Technology of Plasticity* 35 (1-2) (2010) 13–24.
- [81] D. Kobold, G. Gantar, T. Pepelnjak, Finite element analysis of magnesium AZ80 wrought alloy anisotropic behaviour during warm forging, *Mechanika* 18 (3) (2012) 251–258. doi:10.5755/j01.mech.18.3.1876.
- [82] D. Kobold, T. Pepelnjak, G. Gantar, K. Kuzman, Analysis of deformation characteristics of magnesium AZ80 wrought alloy under hot conditions, *Journal of Mechanical Engineering* 12 (56) (2010) 823–832, UDC 621.73:669.721.5.
- [83] J. Swiostek, J. Bober, C. Blawert, D. Letzig, W. Hintze, K. Kainer, Die forging of commercial and modified magnesium alloys, in: K. U. Kainer (Ed.), *Magnesium: Proceedings of the 7th International Conference on Magnesium Alloys and their Applications*, Wiley-VCH, Weinheim, GER, 2007, pp. 344–351.
- [84] J. Yoon, J. Lee, J. Lee, Enhancement of the microstructure and mechanical properties in as-forged Mg–8Al–0.5 Zn alloy using T5 heat treatment, *Materials Science and Engineering: A* 586 (2013) 306–312. doi:10.1016/j.msea.2013.08.031.
- [85] J. Yoon, S.-i. Lee, Warm forging of magnesium AZ80 alloy for the control arm in an automobile, *Proceedings of the Institution of Mechanical Engineers, Part D: Journal of Automobile Engineering* 229 (13) (2015) 1732–1738. doi:10.1177/0954407014567909.
- [86] J. Yoon, J. Lee, Process design of Warm-Forging with extruded Mg-8Al-0.5 Zn alloy for differential case in automobile transmission, *International Journal of Precision Engineering and Manufacturing* 16 (4) (2015) 841–846. doi:10.1007/s12541-015-0110-5.
- [87] V. Kevorkijan, T. Smolar, V. Dragojevič, D. Lenarčič, AZ80 and ZC71/SiC/12p closed die forgings for automotive applications: technical and economic assessment of possible mass production, *Materials science and technology* 19 (10) (2003) 1386–1390. doi:10.1179/026708303225007988.
- [88] H. He, S. Huang, Y. Yi, W. Guo, Simulation and experimental research on isothermal forging with semi-closed die and multi-stage-change speed of large AZ80 magnesium alloy support beam, *Journal of Materials Processing Technology* 246 (2017) 198–204. doi:10.1016/j.jmatprotec.2017.03.015.
- [89] W. Qiang, Z.-M. Zhang, X. Zhang, J.-M. Yu, Precision forging technologies for magnesium alloy bracket and wheel, *Transactions of Nonferrous Metals Society of China* 18 (2008) 205–208. doi:10.1016/S1003-6326(10)60203-8.
- [90] G. Kurz, W. H. Sillekens, R. J. Werkhoven, D. Letzig, Forgeability of modified AZ and ZK wrought magnesium alloys, in: K. U. Kainer (Ed.), *Magnesium: Proceedings of the 8th International Conference on Magnesium Alloys and their Applications*, Wiley-VCH, Weinheim, GER, 2010, pp. 463–468.
- [91] L. Yuan, Z. Zhao, W. Shi, F. Xu, D. Shan, Isothermal forming of the large-size AZ80A magnesium alloy forging with high mechanical properties, *The International Journal of Advanced Manufacturing Technology* 78 (9-12) (2015) 2037–2047. doi:10.1007/s00170-014-6780-9.
- [92] Q. Chen, X. Zhang, J. Lin, H. Zhan, Z. Zhao, Z. Xie, B. Yuan, Isothermal closed-die forming process of magnesium alloy upper receiver: numerical simulation and experiments, *The International Journal of Advanced Manufacturing Technology* 102 (1) (2019) 685–694. doi:10.1007/s00170-018-03209-5.

- [93] E. Hombergsmeier, A. Fein, MagForming-Development of new magnesium forming technologies for the aeronautic industry, Sixth European Aeronautics Days–Aerodays, Madrid (2011).
- [94] Paracha, Talal, Modelling of the Forging Process for a Magnesium Alloy Automotive Control Arm, Master’s thesis, University of Waterloo (2018).
- [95] A. Gryguc, S. Behraves, S. Shaha, H. Jahed, M. Wells, B. Williams, X. Su, Low-Cycle Fatigue Characterization and Texture Induced Ratcheting Behaviour of Forged AZ80 Mg Alloys, *International Journal of Fatigue* 116 (2018) 429–438. doi:10.1016/j.ijfatigue.2018.06.028.
- [96] F. Guo, Understanding the microstructure and fatigue behavior of magnesium alloys, Master’s thesis, University of Leicester (2010).
- [97] G. Qiang, H.-G. Yan, Z.-H. Chen, H. Zhang, Fracture behaviors of AZ80 magnesium alloy during multiple forging processes, *Transactions of Nonferrous Metals Society of China* 16 (4) (2006) 922–926. doi:10.1016/S1003-6326(06)60352-X.
- [98] S. Gneiger, N. Papenberg, S. Frank, R. Grading, Investigations on microstructure and mechanical properties of non-flammable Mg–Al–Zn–Ca–Y Alloys, in: D. Orlov, V. Joshi, S. K.N., N. N. R. (Eds.), *Magnesium Technology 2018*, Springer, Cham, CH, 2018, pp. 105–113. doi:10.1007/978-3-319-72332-7_17.
- [99] M. Cihova, R. Schäublin, L. B. Hauser, S. S. Gerstl, C. Simson, P. Uggowitz, J. F. Löffler, Rational design of a lean magnesium-based alloy with high age-hardening response, *Acta Materialia* 158 (2018) 214–229. doi:10.1016/j.actamat.2018.07.054.
- [100] Q. Ma, B. Li, A. Oppedal, W. Whittington, S. Horstemeyer, E. Marin, H. E. Kadiri, P. Wang, M. Horstemeyer, Effect of Strain Rate on Dynamic Recrystallization in a Magnesium Alloy under Compression at High Temperature, in: S. N. Mathaudhu, W. H. Sillekens, N. R. Neelameggham, H. N. (Eds.), *Magnesium Technology 2012*, Springer, Cham, CH, 2012, pp. 307–310. doi:10.1007/978-3-319-48203-3_56.
- [101] T. Ebeling, C. Hartig, R. Bormann, J. Bohlen, D. Letzig, Effects of Calcium on Texture Evolution and Plastic Anisotropy of the Magnesium Alloy AZ31, in: K. U. Kainer (Ed.), *Magnesium: Proceedings of the 7th International Conference on Magnesium Alloys and their Applications.*, Wiley VCH, Weinheim, GER, 2007, pp. 158–164.
- [102] M. U. Chaudry, H. T. Kim, D. S. Park, S. Y. Kim, K. Hamad, J.-G. Kim, On the high formability of AZ31-0.5 Ca magnesium alloy, *Materials* 11 (11) (2018) 2201. doi:10.3390/ma11112201.
- [103] P. Li, B. Tang, E. Kandalova, Microstructure and properties of AZ91D alloy with Ca additions, *Materials Letters* 59 (6) (2005) 671–675. doi:10.1016/j.matlet.2004.11.006.
- [104] A. A. Luo, B. R. Powell, M. P. Balogh, Creep and microstructure of magnesium-aluminum-calcium based alloys, *Metallurgical and Materials Transactions A* 33 (3) (2002) 567–574. doi:10.1007/s11661-002-0118-1.
- [105] M. O. Pekguleryuz, A. A. Kaya, Creep resistant magnesium alloys for powertrain applications, *Advanced engineering materials* 5 (12) (2003) 866–878. doi:10.1002/adem.200300403.
- [106] B.-H. Choi, B.-S. You, W.-W. Park, Y.-B. Huang, I.-M. Park, Effect of Ca addition on the oxidation resistance of AZ91 magnesium alloys at elevated temperatures, *Metals and Materials International* 9 (4) (2003) 395–398. doi:10.1007/BF03027194.
- [107] L. Jin-Kyu, J. Hyung-Ho, K. K. Shae, Effect of CaO addition on ignition behavior in molten AZ31 and AZ91D Magnesium alloys, *Rare Metals* 25 (6) (2006) 155–159. doi:10.1016/S1001-0521(08)60072-8.
- [108] S. K. Kim, J.-K. Lee, Y.-O. Yoon, H.-H. Jo, Development of AZ31 Mg alloy wrought process route without protective gas, *Journal of Materials Processing Technology* 187 (2007) 757–760. doi:10.1016/S1001-0521(08)60072-8.
- [109] W. Kim, H. Lee, J. Park, M. Kim, U. Yoon, Forging of Mg–3Al–1Zn–1Ca alloy prepared by high-frequency electromagnetic casting, *Materials & Design* 30 (10) (2009) 4120–4125. doi:10.1016/j.matdes.2009.05.003.
- [110] K. Suresh, K. Rao, Y. Prasad, N. Hort, K. Kainer, Study of hot forging behavior of as-cast Mg–3Al–1Zn–2Ca alloy towards optimization of its hot workability, *Materials & Design* 57 (2014) 697–704. doi:10.1016/j.matdes.2014.01.032.

- [111] M. Hakamada, A. Watazu, N. Saito, H. Iwasaki, Tensile Properties of Forged Mg-Al-Zn-Ca Alloy, *Materials transactions* 49 (3) (2008) 554–558. doi:10.2320/matertrans.MRA2007261.
- [112] M. Hakamada, A. Watazu, N. Saito, H. Iwasaki, Grain Refinement and Superplasticity Induced by Hot Compression of Continuously-Casted Mg-9Al-1Zn-1Ca and Mg-9Al-1Zn Alloys, *Materials transactions* 50 (4) (2009) 711–718. doi:10.2320/matertrans.MBW200819.
- [113] M. Hakamada, K. Shimizu, T. Yamashita, A. Watazu, N. Saito, H. Iwasaki, Effect of initial microstructures on hot forging of Ca-containing cast Mg alloys, *Journal of materials science* 45 (3) (2010) 719–724. doi:10.1007/s10853-009-3990-x.
- [114] M. Hakamada, A. Watazu, N. Saito, H. Iwasaki, Tension/compression anisotropy in hot forged Mg-Al-Ca-RE alloy, *Materials transactions* 50 (7) (2009) 1898–1901. doi:10.2320/matertrans.M2009083.
- [115] K. Suresh, K. Rao, Y. Prasad, N. Hort, H. Dieringa, Hot forging of Mg-4Al-2Ba-2Ca (ABaX422) alloy and validation of processing map, *Transactions of Nonferrous Metals Society of China* 28 (8) (2018) 1495–1503. doi:10.1016/S1003-6326(18)64790-9.
- [116] K. Rao, C. Dharmendra, Y. Prasad, N. Hort, H. Dieringa, Optimization of thermo-mechanical processing for forging of newly developed creep-resistant magnesium alloy ABaX633, *Metals* 7 (513) (2017). doi:10.3390/met7110513.
- [117] K. Rao, C. Dharmendra, Y. Prasad, H. Dieringa, N. Hort, Hot Forging Behavior of Mg- 8Al- 4Ba- 4Ca (ABaX844) Alloy and Validation of Processing Map, in: D. Orlov, V. Joshi, S. K.N., N. N. R. (Eds.), *Magnesium Technology 2018*, Springer, Cham, CH, 2018, pp. 289–296. doi:10.1007/978-3-319-72332-7_45.
- [118] A. P. Mouritz, *Introduction to aerospace materials*, Woodhead Publishing, Cambridge, UK, 2012. doi:10.1533/9780857095152.1.
- [119] S. Sanyal, S. Kanodia, R. Saha, T. Bandyopadhyay, S. Mandal, Influence of hard plate hot forging temperature on the microstructure, texture and mechanical properties in a lean Mg-Zn-Al alloy, *Journal of Alloys and Compounds* 800 (2019) 343–354. doi:10.1016/j.jallcom.2019.06.026.
- [120] S. Zhu, S. P. Ringer, On the role of twinning and stacking faults on the crystal plasticity and grain refinement in magnesium alloys, *Acta Materialia* 144 (2018) 365–375. doi:10.1016/j.actamat.2017.11.004.
- [121] D. Zhang, J. Peng, B. Jiang, C. Yang, P. Ding, Research on the Homogenization of ZK60 Magnesium Alloy Ingot, *Materials Science Forum* (2005) 341–344. doi:10.4028/www.scientific.net/MSF.488-489.341.
- [122] C. Wang, X. Wang, H. Chang, K. Wu, M. Zheng, Processing maps for hot working of ZK60 magnesium alloy, *Materials Science and Engineering: A* 464 (1) (2007) 52–58. doi:10.1016/j.msea.2007.03.003.
- [123] J. Li, J. Liu, Z. Cui, Characterization of hot deformation behavior of extruded ZK60 magnesium alloy using 3D processing maps, *Materials & Design* 56 (2014) 889–897. doi:10.1016/j.matdes.2013.11.037.
- [124] N. Ogawa, M. Shiomi, K. Osakada, Forming limit of magnesium alloy at elevated temperatures for precision forging, *International Journal of Machine Tools and Manufacture* 42 (5) (2002) 607–614. doi:10.1016/S0890-6955(01)00149-3.
- [125] R. Matsumoto, K. Osakada, Development of warm forging method for magnesium alloy, *Materials Transactions* 45 (9) (2004) 2838–2844. doi:10.2320/matertrans.45.2838.
- [126] A. Hadadzadeh, S. K. Shaha, M. A. Wells, H. Jahed, B. W. Williams, Microstructure and Texture Evolution During Hot Deformation of Cast-Homogenized ZK60 Magnesium Alloy, in: K. N. Solanki, D. Orlov, A. Singh, N. R. Neelameggham (Eds.), *Magnesium Technology 2017*, Springer, Cham, CH, 2017, pp. 513–519. doi:10.1007/978-3-319-52392-7_70.
- [127] A. Hadadzadeh, M. A. Wells, Analysis of the hot deformation of ZK60 magnesium alloy, *Journal of magnesium and alloys* 5 (4) (2017) 369–387. doi:10.1016/j.jma.2017.09.002.
- [128] K. Jung, S. Lee, Y. Kim, B. Ahn, E. Kim, G. Lee, Assessment of ZK60A magnesium billets for forging depending on casting methods by upsetting and tomography, *Journal of Mechanical Science and Technology* 27 (10) (2013) 3149–3153. doi:10.1007/s12206-013-0835-y.

- [129] S. Karparvarfard, S. K. Shaha, S. B. Behraves, H. Jahed, B. W. Williams, Microstructure, texture and mechanical behavior characterization of hot forged cast ZK60 magnesium alloy, *Journal of Materials Science & Technology* 33 (9) (2017) 907–918. doi:10.1016/j.jmst.2017.04.004.
- [130] S. Karparvarfard, S. K. Shaha, S. B. Behraves, H. Jahed, B. W. Williams, Fatigue characteristics and modeling of cast and cast-forged ZK60 magnesium alloy, *International Journal of Fatigue* 118 (2019) 282–297. doi:10.1016/j.ijfatigue.2018.03.019.
- [131] S. Karparvarfard, S. Shaha, A. Hadadzadeh, S. Behraves, H. Jahed, M. Wells, B. Williams, Characterization of Semi-Closed Die-Forged ZK60 Mg Alloy Extrusion, in: K. N. Solanki, D. Orlov, A. Singh, N. R. Neelameggham (Eds.), *Magnesium Technology 2017*, Springer, Cham, CH, 2017, pp. 329–334. doi:10.1007/978-3-319-52392-7_47.
- [132] S. Karparvarfard, S. Shaha, S. Behraves, H. Jahed, B. Williams, Fatigue life improvement of cast ZK60 Mg alloy through low temperature closed-die forging for automotive applications, in: G. Henaff (Ed.), *MATEC Web of Conferences*, Vol. 165, EDP Sciences, Les Ulis,FR, 2018. doi:10.1051/mateconf/201816506009.
- [133] J. Voncken, Physical and Chemical Properties of the Rare Earths, in: *The Rare Earth Elements*, Springer, 2016, pp. 53–72. doi:10.1007/978-3-319-26809-5_3.
- [134] B. Mordike, Creep-resistant magnesium alloys, *Materials Science and Engineering: A* 324 (1-2) (2002) 103–112. doi:10.1016/S0921-5093(01)01290-4.
- [135] L. L. Rokhlin, *Magnesium alloys containing rare earth metals: structure and properties*, CRC Press, London, UK, 2003. doi:10.1201/9781482265163.
- [136] F. Lu, A. Ma, J. Jiang, D. Yang, Q. Zhou, Review on long-period stacking-ordered structures in Mg-Zn-RE alloys, *Rare Metals* 31 (3) (2012) 303–310. doi:10.1007/s12598-012-0510-y.
- [137] N. Tahreen, D. L. Chen, A Critical Review of Mg–Zn–Y Series Alloys Containing I, W, and LPSO Phases, *Advanced Engineering Materials* 18 (12) (2016) 1983–2002. doi:10.1002/adem.201600393.
- [138] D. Henry, M. Turski, P. Lyon, T. Wilks, An Introduction to the Forging of Elektron 43 – A High Performance Wrought Magnesium Alloy, in: M. Alderman, M. V. Manuel, N. Norbert Hort, N. R. Neelameggham (Eds.), *Magnesium Technology 2014*, Springer, Cham, CH, 2014, pp. 281–284. doi:10.1007/978-3-319-48231-6_53.
- [139] T. Itoi, T. Seimiya, Y. Kawamura, M. Hirohashi, Long period stacking structures observed in Mg₉₇Zn₁Y₂ alloy, *Scripta Materialia* 51 (2) (2004) 107–111. doi:10.1016/j.scriptamat.2004.04.003.
- [140] R. Asakawa, K. Hirukawa, Technology for manufacturing magnesium alloy components with excellent heat resistance, *Kobelco technology review* 31 (2013) 76–81.
- [141] X. Han, W. Xu, D. Shan, Effect of precipitates on microstructures and properties of forged Mg–10Gd–2Y–0.5 Zn–0.3 Zr alloy during ageing process, *Journal of Alloys and Compounds* 509 (35) (2011) 8625–8631. doi:10.1016/j.jallcom.2011.06.086.
- [142] W. Xu, X. Han, D. Shan, Precipitates formed in the as-forged Mg–Zn–RE alloy during ageing process at 250 C, *Materials Characterization* 75 (2013) 176–183. doi:10.1016/j.matchar.2012.09.009.
- [143] D. Shan, W. Xu, X. Han, X. Huang, Study on isothermal precision forging process of rare earth intensifying magnesium alloy, *Materials Science and Engineering: B* 177 (19) (2012) 1698–1702. doi:10.1016/j.mseb.2011.10.006.
- [144] R. Matsumoto, M. Otsu, M. Yamasaki, T. Mayama, H. Utsunomiya, Y. Kawamura, Application of mixture rule to finite element analysis for forging of cast Mg–Zn–Y alloys with long period stacking ordered structure, *Materials Science and Engineering: A* 548 (2012) 75–82. doi:10.1016/j.msea.2012.03.088.
- [145] R. Matsumoto, M. Yamasaki, M. Otsu, Y. Kawamura, Forgeability and flow stress of Mg–Zn–Y alloys with long period stacking ordered structure at elevated temperatures, *Materials transactions* 50 (4) (2009) 841–846. doi:10.2320/matertrans.MRA2008255.
- [146] G. Garcés, A. Müller, E. Oñorbe, P. Pérez, P. Adeva, Effect of hot forging on the microstructure and mechanical properties of Mg–Zn–Y alloy, *Journal of materials processing technology* 206 (1-3) (2008) 99–105. doi:10.1016/j.jmatprot.2007.12.014.

- [147] A. Chaya, S. Yoshizawa, K. Verdelis, N. Myers, B. J. Costello, D. T. Chou, S. Pal, S. Maiti, P. N. Kumta, C. Sfeir, In vivo study of magnesium plate and screw degradation and bone fracture healing, *Acta Biomaterialia* 18 (2015) 262–269. doi:10.1016/j.actbio.2015.02.010.
- [148] N. Sezer, Z. Evis, S. M. Kayhan, A. Tahmasebifar, M. Koç, Review of magnesium-based biomaterials and their applications, *Journal of Magnesium and Alloys* 6 (1) (2018) 23–43. doi:10.1016/j.jma.2018.02.003.
- [149] Y. Liu, D. Liu, C. You, M. Chen, Effects of grain size on the corrosion resistance of pure magnesium by cooling rate-controlled solidification, *Frontiers of Materials Science* 9 (3) (2015) 247–253. doi:10.1007/s11706-015-0299-3.
- [150] J. Hofstetter, M. Becker, E. Martinelli, A. M. Weinberg, B. Mingler, H. Kilian, S. Pogatscher, P. J. Uggowitzer, J. F. Löffler, High-strength low-alloy (HSLA) Mg-Zn-Ca alloys with excellent biodegradation performance, *JOM* 66 (4) (2014) 566–572. doi:10.1007/s11837-014-0875-5.
- [151] J. Hofstetter, E. Martinelli, S. Pogatscher, P. Schmutz, E. Povoden-Karadeniz, A. M. Weinberg, P. J. Uggowitzer, J. F. Löffler, Influence of trace impurities on the in vitro and in vivo degradation of biodegradable Mg-5Zn-0.3Ca alloys, *Acta Biomaterialia* 23 (2015) 347–353. doi:10.1016/j.actbio.2015.05.004.
- [152] D. Persaud-Sharma, A. McGoron, Biodegradable Magnesium Alloys: A Review of Material Development and Applications, *Journal of Biomimetics, Biomaterials and Tissue Engineering* 12 (2011) (2012) 25–39. doi:10.4028/www.scientific.net/JBBTE.12.25.
- [153] R. Radha, D. Sreekanth, Insight of magnesium alloys and composites for orthopedic implant applications – a review, *Journal of Magnesium and Alloys* 5 (3) (2017) 286–312. doi:10.1016/j.jma.2017.08.003.
- [154] B. Zhang, Y. Wang, L. Geng, C. Lu, Effects of calcium on texture and mechanical properties of hot-extruded Mg-Zn-Ca alloys, *Materials Science and Engineering: A* 539 (2012) 56–60. doi:10.1016/j.msea.2012.01.030.
- [155] N. T. Kirkland, N. Birbilis, M. P. Staiger, Assessing the corrosion of biodegradable magnesium implants: a critical review of current methodologies and their limitations., *Acta biomaterialia* 8 (3) (2012) 925–36. doi:10.1016/j.actbio.2011.11.014.
- [156] S. E. Harandi, M. Hasbullah Idris, H. Jafari, Effect of forging process on microstructure, mechanical and corrosion properties of biodegradable Mg-1Ca alloy, *Materials & Design* 32 (5) (2011) 2596–2603. doi:10.1016/j.matdes.2011.01.042.
- [157] A. C. Hänzi, A. S. Sologubenko, P. Gunde, M. Schinhammer, P. J. Uggowitzer, Design considerations for achieving simultaneously high-strength and highly ductile magnesium alloys, *Philosophical Magazine Letters* 92 (9) (2012) 417–427. doi:10.1080/09500839.2012.657701.
- [158] A. D. Südholz, N. T. Kirkland, R. G. Buchheit, N. Birbilis, Electrochemical Properties of Intermetallic Phases and Common Impurity Elements in Magnesium Alloys, *Electrochemical and Solid-State Letters* 14 (2) (2010) C5. doi:10.1149/1.3523229.
- [159] K. Rao, K. Suresh, Y. Prasad, C. Dharmendra, N. Hort, H. Dieringa, High Temperature Strength and Hot Working Technology for As-Cast Mg–1Zn–1Ca (ZX11) Alloy, *Metals* 7 (10) (2017) 405. doi:10.3390/met7100405.
- [160] J. D. Robson, D. T. Henry, B. Davis, Particle effects on recrystallization in magnesium-manganese alloys: Particle-stimulated nucleation, *Acta Materialia* 57 (9) (2009) 2739–2747. doi:10.1016/j.actamat.2009.02.032.
- [161] J. D. Robson, D. T. Henry, B. Davis, Particle effects on recrystallization in magnesium-manganese alloys: Particle pinning, *Materials Science and Engineering: A* 528 (12) (2011) 4239–4247. doi:10.1016/j.msea.2011.02.030.
- [162] Y. Chen, Z. Xu, C. Smith, J. Sankar, Recent advances on the development of magnesium alloys for biodegradable implants, *Acta Biomaterialia* 10 (11) (2014) 4561–4573. doi:10.1016/j.actbio.2014.07.005.
- [163] J.-W. Kang, C.-J. Wang, K.-K. Deng, K.-B. Nie, Y. Bai, W.-J. Li, Microstructure and mechanical properties of alloy fabricated by the combination of forging, homogenization and extrusion process, *Journal of Alloys and Compounds* 720 (2017) 196–206. doi:10.1016/j.jallcom.2017.05.232.

- [164] J. Hofstetter, S. Rüedi, I. Baumgartner, H. Kilian, B. Mingler, E. Povoden-Karadeniz, S. Pogatscher, P. J. Uggowitzer, J. F. Löffler, Processing and microstructure-property relations of high-strength low-alloy (HSLA) Mg-Zn-Ca alloys, *Acta Materialia* 98 (2015) 423–432. doi:10.1016/j.actamat.2015.07.021.
- [165] N. G. Grün, P. Holweg, S. Tangl, J. Eichler, L. Berger, J. J. van den Beucken, J. F. Löffler, T. Klestil, A. M. Weinberg, Comparison of a resorbable magnesium implant in small and large growing-animal models, *Acta Biomaterialia* 78 (2018) 378–386. doi:10.1016/j.actbio.2018.07.044.
- [166] Y. Estrin, A. Vinogradov, Extreme grain refinement by severe plastic deformation: A wealth of challenging science, *Acta Materialia* 61 (3) (2013) 782–817. doi:10.1016/j.actamat.2012.10.038.
- [167] X. Zheng, J. Dong, D. Yin, W. Liu, F. Wang, L. Jin, W. Ding, Forgeability and die-forging forming of direct chill casting Mg-Nd-Zn-Zr magnesium alloy, *Materials Science and Engineering: A* 527 (16-17) (2010) 3690–3694. doi:10.1016/j.msea.2010.03.002.
- [168] K. Rao, K. Suresh, Y. Prasad, N. Hort, K. U. Kainer, Hot forging of cast magnesium alloy TX31 using semi-closed die and its finite element simulation, in: B. Mishra, M. Ionescu, T. Chandra (Eds.), *THERMEC 2013*, Vol. 783 of *Materials Science Forum*, Trans Tech Publications Ltd, Pfaffikon, CH, 2014, pp. 449–454. doi:10.4028/www.scientific.net/MSF.783-786.449.
- [169] AS8049C:2015-08, Performance Standard for Seats in Civil Rotorcraft, Transport Aircraft, and General Aviation Aircraft, Standard, SAE International (Aug. 2015). doi:10.4271/AS8049C.
- [170] Safe Magnesium, International Magnesium Association, <https://cdn.ymaws.com/www.intlmag.org/resource/resmgr/safety/lr-ima-safe-magnesium-flyer-.pdf> (2018).
- [171] W. Xu, N. Birbilis, G. Sha, Y. Wang, J. E. Daniels, Y. Xiao, M. Ferry, A high-specific-strength and corrosion-resistant magnesium alloy, *Nature materials* 14 (12) (2015) 1229–1236. doi:10.1038/nmat4435.
- [172] Z. Wu, R. Ahmad, B. Yin, S. Sandlöbes, W. Curtin, Mechanistic origin and prediction of enhanced ductility in magnesium alloys, *Science* 359 (6374) (2018) 447–452. doi:10.1126/science.aap8716.
- [173] R. Ahmad, B. Yin, Z. Wu, W. Curtin, Designing high ductility in magnesium alloys, *Acta Materialia* 172 (2019) 161–184. doi:10.1016/j.actamat.2019.04.019.
- [174] B.-C. Suh, M.-S. Shim, K. Shin, N. J. Kim, Current issues in magnesium sheet alloys: where do we go from here?, *Scripta Materialia* 84 (2014) 1–6. doi:10.1016/j.scriptamat.2014.04.017.
- [175] S. Kleiner, P. J. Uggowitzer, Mechanical anisotropy of extruded Mg–6% Al–1% Zn alloy, *Materials Science and Engineering: A* 379 (1-2) (2004) 258–263. doi:10.1016/j.msea.2004.02.020.
- [176] K. Hono, C. Mendis, T. Sasaki, K. Oh-Ishi, Towards the development of heat-treatable high-strength wrought Mg alloys, *Scripta Materialia* 63 (7) (2010) 710–715. doi:10.1016/j.scriptamat.2010.01.038.
- [177] A. Ditze, C. Scharf, *Recycling of Magnesium*, Ditze & Scharf, Clausthal-Zellerfeld, Germany, 2008.
- [178] N. Bell, R. Waugh, D. Parker, *Magnesium Recycling in the EU*, Tech. rep. (2017).
- [179] T. Arai, G. Baker, et al., *ASM-Handbook Volume 4: Heat Treating*, ASM International, Materials Park, OH, USA, 1991. doi:10.31399/asm.hb.v04e.9781627081696.

3. Lean Wrought Magnesium Alloys

The literature study on the development of age-hardenable Mg wrought alloys showed interesting results regarding the interaction of alloy design and overall content of alloying elements used. It could be shown, that a trend towards alloys with a low amount of alloying elements exists in the scientific community when regarding age-hardenable Mg wrought alloys. Also the increased use of Ca in these materials was noted. To relay these interesting findings on a broad scale the investigations done on this topic were published in the shape of a literature review.

The following chapter gives an overview of lean wrought Mg alloys available in scientific literature. The alloying systems, processing conditions as well as the resulting mechanical properties are discussed in detail.

Lean Wrought Magnesium Alloys

Published in: MDPI Journal Materials, 2021, 14, 4282; [doi:10.3390/ma14154282](https://doi.org/10.3390/ma14154282)

Received: 9 June 2021; Accepted: 26 July 2021

Authors: Nikolaus P. Papenberg, Stefan Gneiger, Peter J. Uggowitzner and Stefan Pogatscher

Author contribution: This review is the work of several authors, the individual contributions are subsequently listed: conceptualization, N.P., P.U. and S.P.; software, S.G.; investigation, N.P. and P.U.; data curation, N.P. and P.U.; writing—original draft preparation, N.P. and P.U.; writing—review and editing, N.P., S.G., P.U. and S.P.; visualization, N.P. and S.G.; supervision, P.U. and S.P.; project administration, N.P. and S.P.

Keywords: magnesium alloys; dilute alloys; lean alloys; literature review; overview

Abstract: Lean magnesium alloys are considered attractive candidates for easy and economical hot forming. Such wrought alloys, defined here as materials with a maximum alloying content of one atomic or two weight percent, are known to achieve attractive mechanical properties despite the low alloy content. The good mechanical properties and the considerable hardening potential, combined with the ease of processing, make them attractive for manufacturers and users alike. This results in potential uses in a wide range of applications, from rolled or extruded components to temporary biomedical implants. The characteristic behavior of these alloys and the optimal use of suitable alloying elements will be discussed and illustrated exemplarily.

Funding: We gratefully acknowledge the financial support of this work within the scope of the AMALFI project. AMALFI is a COMET Project within the COMET–Competence Centers for Excellent Technologies Programme and funded by BMK, BMDW, and the federal state of Upper Austria. The COMET Programme is managed by the FFG (grant number 872641).

This work has been supported by the European Regional Development Fund (EFRE) in the framework of the EU-program "IWB Investition in Wachstum und Beschäftigung Österreich 2014-2020", and the federal state Upper Austria.

Published as an open access article distributed under the terms and conditions of the Creative Commons Attribution (CC BY) license (<https://creativecommons.org/licenses/by/4.0/>). The only changes made are related to layout and document internal accessibility.

3.1. Introduction

Magnesium is widely acknowledged as the lightest structural metal and therefore known as being a good candidate for applications where product weight plays an important role [1]. Many of such potential applications are structural parts, which are usually produced by forming processes and are characterized by improved homogeneity, reduced defect size and enhanced mechanical properties compared to castings.

Nevertheless, more than 90 % of Mg parts in use are produced by casting [2], showing that the use of Mg in structural applications and the utilization of wrought products in general is still lacking.

While it has been demonstrated repeatedly, that Mg wrought alloys can show a wide spectrum of mechanical, chemical and physical properties [3–5], multiple reasons for their limited use can be found. Particularly noteworthy is the small number of industrially available alloying compositions, lack of stock material, the use of high-priced alloying elements and last but not least a lack of practical knowledge regarding material processing and utilization [6–8]. Especially the experience deficit highlights the mismatch of cast and wrought products. This difference is deeply rooted and has been amplified by the challenging forming behavior of Mg alloys, discouraging manufacturers and preventing widespread application.

Numerous attempts have been done to improve the forming behavior and performance of Mg wrought alloys by adaptation of processing and alloying, but with mixed results. Nevertheless, steady progress has been made and nowadays Mg products can be produced at high speeds [9] and can exhibit remarkable mechanical properties [10; 11]. In recent years alloying concepts using only low amounts of alloying elements have shown impressive results in a broad range of topics [4; 12; 13]. This design approach attempts to make full use of the alloying elements and tries to combine processing and material response in the best possible way. Since this principle can be applied to various systems within the Mg alloy range, the possible applications are diverse and the topics of investigations are correspondingly wide ranged.

In the case of materials for structural applications at industrial scale, e.g., extruded profiles, the main drivers are low material and production costs. This can be realized with cheap alloying elements but more importantly with high production speeds [14]. The deformation behavior in multiple subsequent forming operations is also a crucial issue, i.e., in sheet forming. In other areas, such as bio-medical applications, corrosion behavior is the focus of interest.

This review aims to give a short overview of the topic ‘lean wrought magnesium alloys’, by summarizing and discussing multiple relevant scientific publications in this field. For this study the authors limited the selection of investigated works to publications using ternary and more complex Mg wrought alloys, with a combined alloying content lower than ~ 1 atomic percent (at.%) and ~ 2 weight percent (wt.%). As the focus of this review lies on the conventional processing of these alloys, works concerning production by severe plastic deformation (SPD) or powder metallurgy are not covered.

For the ease of understanding we first consider often used terms and definitions in Section 3.2 and basic aspects of alloy developments in Section 3.3. Various alloys and their applications are discussed in Section 3.4, a brief conclusion is given in Section 3.5. For further clarification a summary of the discussed alloys is provided in the Appendices 3.6.2 and 3.6.3, listing the chemical compositions and the mechanical properties, including the corresponding processing parameters.

3.2. Terms and Definitions

When searching for scientific literature on the topic of ‘low alloyed Mg alloys’ it becomes apparent that this is a diffuse subject. There are no clear definitions of the alloy specifications and the terms describing them are constantly changing. For a better understanding we briefly discuss the commonly used terms in the following paragraphs.

When adding small amounts of alloying elements to already existing materials the term **micro-alloying** is often used. Typically, the added elements are kept below 1 wt.% to be called micro alloying [15]. This practice is well known and used for an abundance of materials, to improve specific

material properties and processing behavior. Typical applications for Mg alloys are reductions of the texture by addition of rare earth elements (RE/REE) [16], the use of Ca and Y to enhance the oxidation stability [17; 18] and Mn additions to improve the corrosion behavior [3]. As a micro alloyed material is not necessarily an alloy with low alloying content, this review will only deal with micro-alloyed materials that meet our definition of lean alloys.

The abbreviation **HSLA**, meaning 'High Strength Low Alloyed' is used in ref [19]. The described Mg alloys replicate the approach of increased material strength by grain refinement, as known from the steel industry. This is achieved by the use of a small amount of alloying elements influencing the recrystallization and grain growth behavior during hot forming processes.

The terms **low alloyed**, **dilute** and **lean** all aim to describe Mg alloys using only a small overall amount of added elements. The maximum amount of used alloying elements can nevertheless vary considerably, ranging from 0.16 wt. % [20] up to 3.82 wt. % [21]. The reason for this is the difficulty to define a strict range of the total amount of used additions for the term low alloyed. The term can be subjectively interpreted, as most wrought alloys are low-alloyed when compared to casting alloys.

Despite these challenges an attempt to define the term 'lean alloy' has been done in refs. [22; 23], where the authors constrict themselves to alloys using alloying elements up to a sum of 1 at. %. As these works concentrate on alloys using mainly light elements, e.g., Al and Ca, this seems reasonable. On the other hand, this definition proves insufficient when applied to alloys with heavy elements, e.g., REE. Other possible weighting or limiting definitions only seem to increase the complexity of this problem and can therefore not be the preferred approach. While at. % is often used in studies on alloy development, phase descriptions and element solubility, we will use wt. % as a reference system, as it is the most common way to describe Mg alloys and improves the ease of comparability significantly. Nevertheless, tables containing the chemical compositions of the discussed alloys in wt. % and at. % can be found in Appendix 3.6.2.

In this review we will limit ourselves on conventionally processed wrought alloys with a maximum alloying content of ~ 1 at. % or ~ 2 wt. %. Additionally, the selected alloys are required to have at least two alloying elements. This has been done to narrow the range of the discussed alloys down to reasonable level, while still maintaining a broad range of possible alloys and processing schemes. In this way, a more focused approach on this interesting and diverse topic is made possible. For better understanding an overview of the amount of alloying elements in wt % and at % is shown in Fig. 3.1. There, the alloys discussed in this work as well as binary alloys and the chosen limitations are depicted. Some alloys outside the limitations have been included as they are used for comparison within the investigated works.

As the discussed materials are within a narrow range, regarding their chemical composition, the nomenclature will consist of the alloying elements and their corresponding amount in wt. %, e.g., Mg-1.0Zn-0.5Ca or Mg-0.3Al-0.2Ca-0.5Mn. While a little laborious to read, this description allows for an easy comparison of the alloys and directly shows the relevant chemical composition.

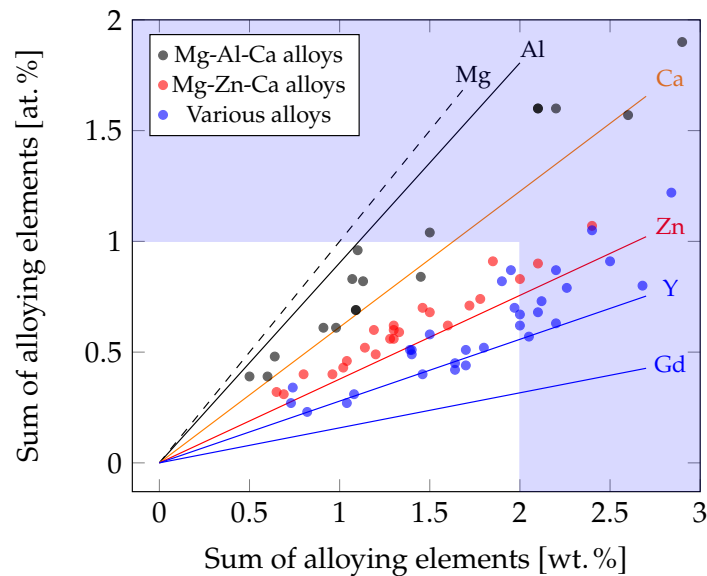


Figure 3.1.: Effect of alloying elements and content on the alloys discussed in this work (limits of ~ 1 at. % and ~ 2 wt. %). Dots mark individual alloys, while lines show the trend of binary Mg alloys with the indicated element.

3.3. Basic Aspects of Alloy Development

The development and improvement of Mg alloys is a very complex subject, that combines information from a wide range of multiple metal physic phenomena [24]. It is important to realize that the interaction of microstructural features is an intrinsic feature. Slight changes of alloying content can influence solidus temperature, precipitation behavior, possible activation of slip systems or oxidation behavior. Therefore, only a fragmentary introduction, which is furthermore trimmed to the use of lean alloys, can be given here. It is further essential to keep in mind, that the microstructural properties and effects during the production process (i.e., raised temperatures) and behavior in use, can differ greatly.

As the main aim of Mg wrought alloys development is their production by forming operations such as extrusion or rolling, it is imperative to be aware of their challenging deformation behavior. Mg alloys, including the lean variants, can show a broad variety of microstructural features during processing, dependent on alloy and forming parameters, as shown exemplarily in Fig. 3.2. The original microstructure resulting from the casting process is deformed and the grains may exhibit twinning and/or areas of dislocation slip. When the temperature is sufficiently high, recrystallization becomes a common feature. It usually starts during the forming process and can occur dynamical (during forming), meta-dynamical (during cooling processes) and statical (during heat treatments). The nucleation points for new grains are manifold, e.g., twins, grain boundaries and particles. Dynamic recrystallization behavior during forming often results in a broad grain size distribution. The combination of newly formed small grains and original deformed microstructure is typically called necklace structure [25; 26].

The material's forming ability is controlled by the hexagonal crystal structure and the ensuing large differences in critical resolved shear stress (CRSS) of the available slip and twinning systems. Deformation is mostly accommodated by dislocation movement on the basal plane or by twinning, but neither mechanism provides the necessary amount of slip systems for arbitrary deformation, therefore deformation at room temperature (RT) is impeded considerably. Consequently, most forming operations in which the material is forced to accommodate large strains, take place at elevated temperatures. Here, the activation of the prismatic and pyramidal slip systems is advantageous, which is made possible by the converging CRSS values.

The differences in CRSS between the deformation mechanisms [4] also amplifies the texture development during directional forming processes (and subsequent heat treatments), leading to pronounced

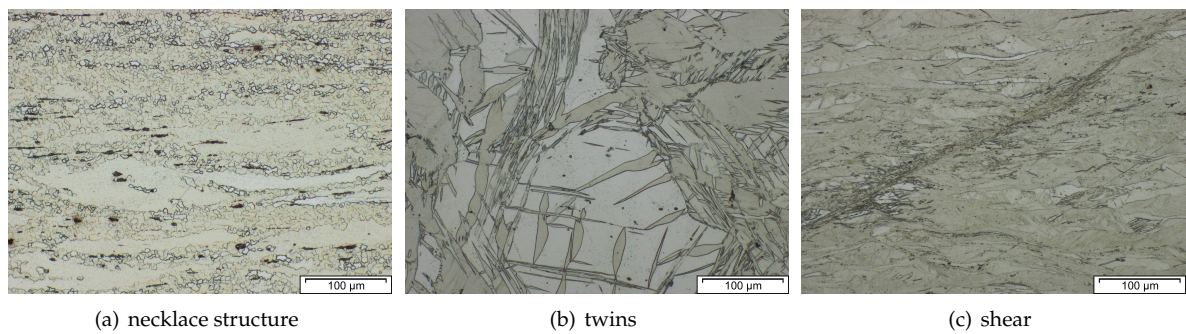


Figure 3.2.: Examples of microstructural features common in deformed Mg alloys. Pictures show a Mg-Al-Ca lean alloy produced at LKR Light Metals Technologies Ranshofen in as-forged state.

basal textures in various investigated Mg sheets and profiles [13; 27]. Such a strong structural anisotropy is reflected in the mechanical properties, e.g., the ratio of tensile yield strength (YS) and compressive yield strength (YSc) [28], as well as in the forming behavior of these products.

As the deformation behavior and the texture development are intrinsically linked, it is not surprising that extensive studies are being conducted regarding this aspect. Next to process adaptations [13], e.g., cross rolling, the alloy customization by (micro-) alloying with, i.e., REE or Ca, is an accepted practice for texture reduction and enhanced forming behavior [16; 29–32]. Especially the combination of Zn and Ca is known to improve the forming behavior of various Mg alloys. While effects on texture weakening and increased non-basal slip by these elements are well known, Basu et al. [33] have recently investigated this effect in detail, using micro-pillar indentation at RT. It was found, that even dilute additions of Zn and Ca lower the stacking fault energy drastically, thereby promoting pyramidal $\langle c+a \rangle$ dislocations and reducing mobility of basal slip, enabling a more homogeneous material deformation.

In the case of lean alloys further improvement in the deformation behavior is achieved by a reduction of solute drag, as these materials evidently feature a reduced amount of soluble alloying elements. However, as this effect is dependent on the solubility potential of the alloying elements used, no general description can be given here [34; 35].

As material strength is the feature dominating the potential fields of application for structural materials, the possible means and design principles of increasing mechanical strength are briefly discussed below. In case of dilute alloys only grain refinement and precipitation hardening are relevant, as solid solution strengthening is not a viable option.

Grain refinement is well known for its positive influence on strength and deformation behavior of practically all metallic materials, in particular for Mg. This property is important for an improved performance during forming operations [36] and is often regarded as the main strengthening mechanism in dilute Mg alloys [4]. The effect of grain refinement is typically described via the Hall Petch relationship, which predicts a significant rise of YS for fine grained structures. This formulation is based on the assumption of an isotropic poly-crystalline material, therefore the application on wrought Mg alloys with their tendency for texture formation might give diffuse values, as the Hall Petch relationship shows a dependence on texture and strain [37–40]. Additionally, a decline in the ascend of the Hall Petch slope (k_y) is reported for Mg alloys with a grain diameter (d) smaller than 2 to 3 μm [39]. As many Mg parts are investigated in F-temper further uncertainty is added for the evaluation of the Hall Petch relationship by the interaction of deformed and recrystallized microstructures. For comparison an extract of the Hall Petch behavior for some Mg alloys is given in Fig. 3.3 and Table 3.3.

The effect of strengthening by grain refinement is only pronounced at small grain sizes, easily visible in Fig. 3.3b. As such small grains cannot be produced by conventional casting, forming processes with a high degree of deformation are necessary. The most common industrial processes to achieve grain refinement are extrusion or rolling. In cases where even finer grain sizes are needed, processes of severe

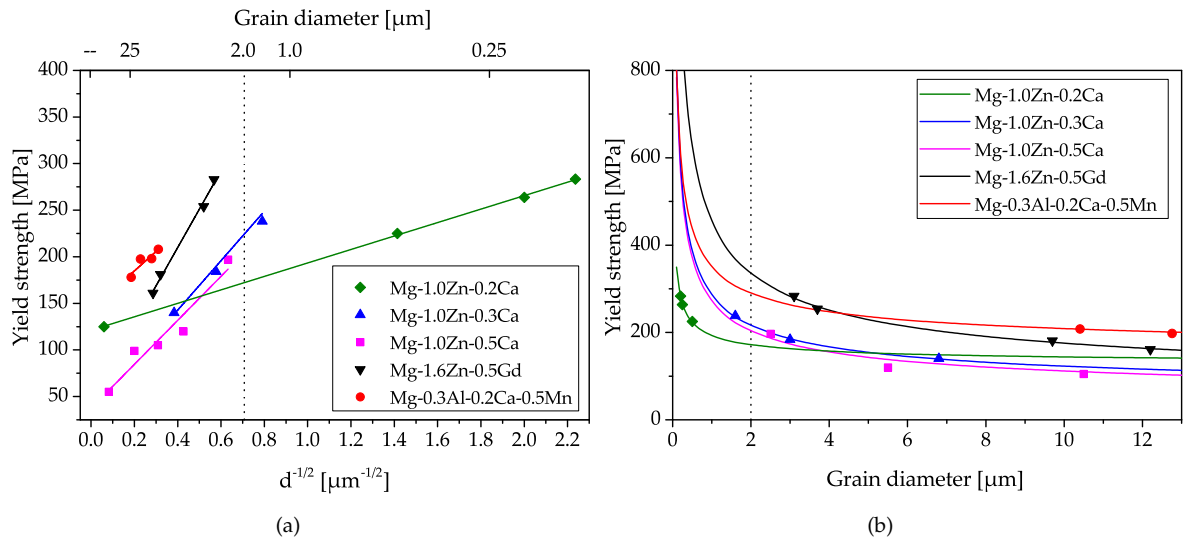


Figure 3.3.: Showing Hall Petch slopes of multiple Mg lean alloys (a), as well as the calculated rise in YS values with decreasing grain size in (b). Experimental data was taken from refs [28; 40–43], further information is given in Table 3.3.

plastic deformation, e.g., equal channel angular pressing (ECAP), high pressure torsion (HPT) or multi axial forging (MAF), might be used [44].

A downside of fine grained materials is the strong grain growth tendency, which poses a major challenge to subsequent processing or use at raised temperatures. To mitigate this effect, the Zener drag provided by precipitating phases (i.e., dispersoids and precipitates) has been used with good success [28].

Precipitation hardening is well known from the use in Al alloys and the main reason for the success of the 2xxx, 6xxx and 7xxx series [45]. While known in Mg alloys as well, the use of precipitation hardening is not that far spread [46] and process chains as are common in Al wrought alloys are few. As shown by Nie [47] precipitation hardening is possible for several Mg alloying systems, but it is important to consider the positioning of the precipitates. The best hardening effects are shown by particles that impede basal slip, as it is the most easily activated slip system of the hexagonal Mg crystal, i.e. the most important for the deformation process at RT. As an example, Al-Ca-rich Guinier-Preston (G.P.) zones in lean Mg-Al-Ca alloys may be mentioned here, which enable a considerable increase in strength [23]. The precipitation of hardening phases can either happen dynamically during processing, where the forming phases are known to delay the dynamic recrystallization [26] and stabilize grain boundaries [48] or can be facilitated with adequate heat treatments, where precipitation can be controlled more easily. Due to the temperatures used, especially during solution heat treatment, an increase of the grain size is often unavoidable, but can be reduced by already existing phases, e.g., dispersoids. Additionally, intermetallic phases (IMP) can play a major role in the corrosion behavior, which is an important aspect in biomedical applications and further described in Section 3.4.2.

While **dispersoids** are neglectable with respect to particle hardening, they can play an important role in processing behavior. These phases, with varying chemical compositions, can either be formed during casting or preferably during subsequent heat treatment/processing steps, where a regulation of particle size and distribution can be achieved by appropriate heat treatment parameters. The dispersoids counteract grain growth due to their Zener pinning pressure [49], which increases with reduced particle size and increasing volume fraction. An example for the pinning effect is given in Fig. 3.4, where two alloys with and without Zr-dispersoids are compared. In Al free Mg alloys Zr is often used as dispersoid forming element, while in Mg-Al alloys the use of Al-Mn intermetallics is appropriate [23]. The Zr additions are also effective as grain refiner during casting, enabling the production of fine grained stock

materials [50].

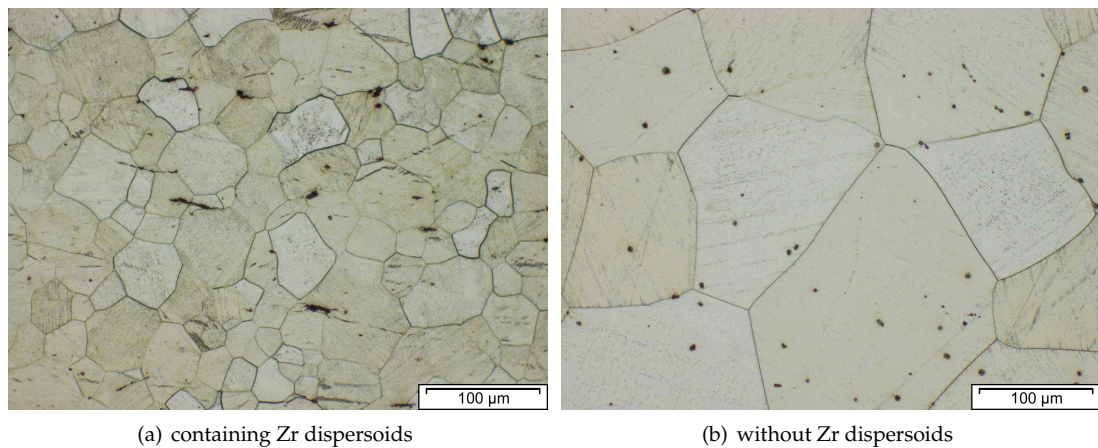


Figure 3.4.: Comparison of the grain size within a forged and solution heat treated low alloyed Mg alloy containing REE. Showing the microstructure (a) with Zr additions (~ 0.4 wt. %) and (b) without Zr. Experiments performed at LKR Light Metals Technologies Ranshofen.

3.4. Mg Alloys with a Low Alloying Content

This section is divided into three parts, analyzing the mostly used alloying systems, namely Mg-Al-Ca (Section 3.4.1) and Mg-Zn-Ca (Section 3.4.2) as well as descriptions on various alloy compositions in Section 3.4.3. An overview of the discussed alloys is compiled in the appendices, where the chemical compositions (App. 3.6.2) and mechanical properties (App. 3.6.3) are listed.

While there are almost unlimited possibilities for variations in the chemical composition of lean alloys, it becomes apparent from examining the published literature that there is a trend towards the use of Mg-Al and Mg-Zn alloys, see Fig. 3.5. This is not surprising, as these systems are the primarily produced and investigated alloying systems for Mg wrought alloys. While (micro-) alloying with REE is common practice for Mg alloys, lean alloys using RE additions are not as common as expected. This might be partly because of the chosen limiting values of ~ 2 wt. % of alloying elements in the investigated materials, which restricts the use of heavy elements accordingly.

Rather surprising is the high number of Ca containing alloys, which can nevertheless be well explained. Ca is increasingly used as a secondary element in both main alloying systems Mg-Al and Mg-Zn, as it can facilitate various interesting properties, such as grain refinement during casting [51], increased oxidation stability [52; 53], potential of IMP phase formation and improved creep resistance [54–56]. The most important feature for wrought alloys might be the promotion of pyramidal slip during deformation [57] and the associated reduction in texture intensity [58–60].

The number of sources and the number of discussed alloys, divided into the sections used in this work, is shown in Fig. 3.5 a. While the number of alloys in Sections 3.4.1 and 3.4.2 have been restricted by using the combination of two major alloying elements, Al-Ca and Zn-Ca respectively, the number of references and alloys is comparable to Section 3.4.3, 'Alloys containing various Elements'. This highlights the focus which is given to these alloying systems throughout the scientific literature. Additionally, it can be noted, that the cited references in Sections 3.4.1 and 3.4.2 are more focused on in depth investigations of potential alloys, when compared to Section 3.4.3, where a general discussion of multiple alloys per publication is more common. This is evident from the smaller number of sources compared to the number of discussed alloys.

Using the overview of the investigated alloys given in Fig. 3.5 b some interesting facts about the composition of Mg alloys in general can be noted. The combination of Mg-Al and REE [61] as well as Zr [62] is avoided in wrought alloys, as Al is known to form high melting IMPs with these elements, which

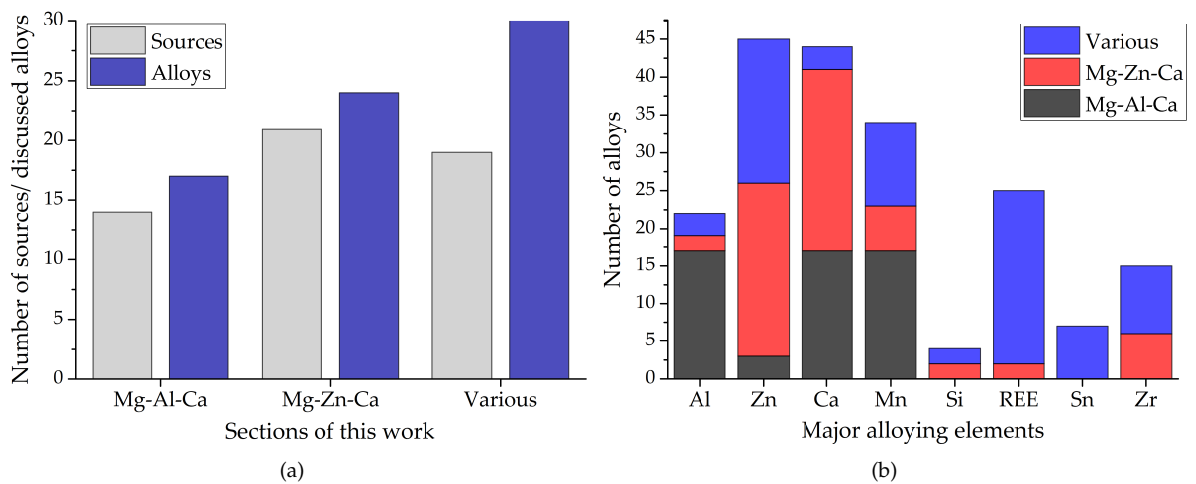


Figure 3.5.: Overview of (a) the number of publications and alloys discussed in this work and (b) the number of alloys separated by major alloying elements found in this review.

cannot be dissolved in subsequent processing steps. The combination of Mg-Zn and REE and/or Zr, on the other hand, is well-established practice and used to increase the overall performance of these alloys [61; 62]. The fact that Ca can be considered as an alternative for REE additions [63; 64] is visible well, as the combination of Ca and REE in the same section is minimal.

3.4.1. Alloys containing Aluminium and Calcium

Wrought alloys of the Mg-Al-Ca (AX) system have been intensively investigated in recent years. These alloys make optimal use of low-cost alloying elements and have shown their ability to achieve strengths [10; 11] or show favorable forming behavior [9; 24]. The optimal combination of these two properties has not yet been found, but alloy developments are steadily advancing towards this goal. Extruded material has been especially well investigated. The processing of such alloys by extrusion is attractive because of the high degree of deformation possible and the almost isotherm forming temperatures at moderate extrusion rates. Nevertheless, the complexity of this process increases markedly at high forming rates and the production of hollow profiles and/or complex cross sections. Therefore, round bars are used as test geometry in most publications investigating extrusion processes [27].

While high strength, up to 450 MPa UTS, is an attractive feature for extruded Mg-Al-Ca-Mn products [11; 65], the achievable ram speed of these alloys was considered insufficient for widespread industrial application. The aim to increase the extrusion speed was the first step towards the development of low alloyed Mg-Al-Ca alloys using complex processing chains. Based on works reporting an increase of extrusion speed with reduced alloying elements [66–69], Nakata et al. [9; 40] presented a heat treatable (T5) Mg-0.3Al-0.2Ca-0.5Mn alloy, which can be extruded with die-exit speeds of up to 60 m min^{-1} , using extrusion temperatures in the range of 350 to 500 °C. In the subsequent work [70], the effect of Mn content (0 to 0.84 wt.%) on the processing behavior, heat treatment and mechanical properties was investigated. Of the tested compositions the Mg-0.3Al-0.3Ca-0.4Mn alloy showed the highest tensile properties, reaching 264 MPa UTS and 220 MPa YS in peak aged state (T6). Further development was aimed at an enhancement of the mechanical strength, which was achieved by slightly increasing the alloying content [71]. As these investigated alloys showed inconsistent age hardening behavior, this strategy was adapted by thermodynamic calculations to achieve maximum age hardening in [22; 23; 72]. This culminated in the development of a Mg-0.6Al-0.3Ca-0.3Mn alloy, reaching a YS of 253 MPa and UTS of 277 MPa at peak hardness (T6), thereby showing a very high ratio of precipitation hardening effect onto alloying content (YS/at.%) [23]. The adaptations done to the alloy composition

and the processing, are subsequently illustrated below with the help of CALPHAD calculations (Fig. 3.6).

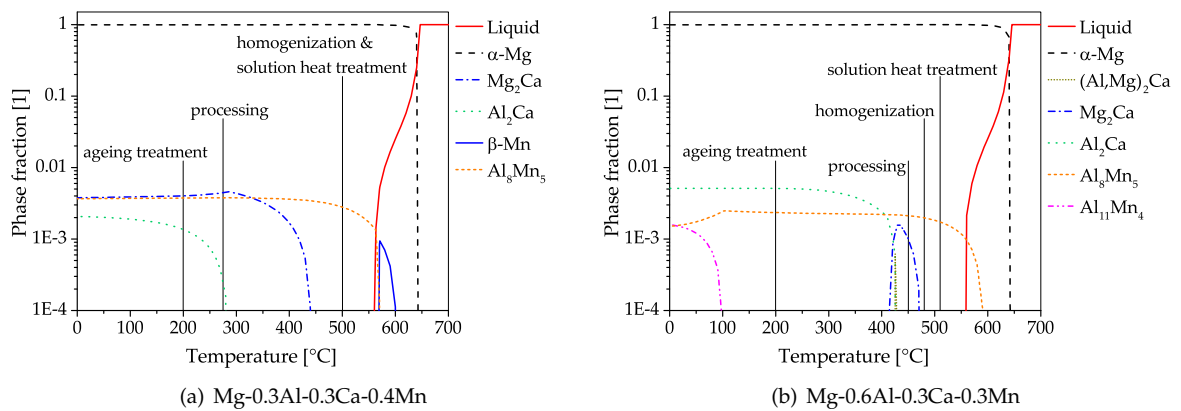


Figure 3.6.: Comparison of CALPHAD calculations of Mg-Al-Ca alloys, including the used processing temperatures. Calculations were done using the alloy compositions given in refs. [23; 71], for further information see App. 3.6.1.2.

When comparing the processing and precipitation behavior of the alloys Mg-0.3Al-0.3Ca-0.4Mn [71] and Mg-0.6Al-0.3Ca-0.3Mn [23], using CALPHAD calculations, only slight overall differences in processing and alloying content are apparent. Both alloys aim to make use of the attractive age hardening possibilities offered in the Mg-Al-Ca system, i.e., the precursor phases of Mg_2Ca (C14) and Al_2Ca (C15) [47]. To achieve peak hardness both alloys are solutionized and age hardened (T6) after extrusion. As the high temperatures used for the solution heat treatment are known to facilitate unwanted grain growth, dispersoids are used as a retardant in both alloys. In this alloying system the utilization of AlMn phases as grain boundary stabilization seems natural, as Mn is an often-used microalloying element, usually applied to increase the corrosion resistance by binding unwanted Fe. When looking at CALPHAD calculations (Fig. 3.6) it can be seen, that these Mn-containing phases already form during the casting process. As these calculations reflect the equilibrium state, the formation can be partially suppressed by appropriate casting processes and adequate cooling speeds. Accordingly, AlMn phases are either formed as coarse primary phases in the casting process itself or precipitate during the subsequent homogenization heat treatment. Because of their high temperature stability, these AlMn dispersoids are present throughout the whole forming and heat treatment process where their pinning effect retards dynamic recrystallization and hampers grain growth.

One obvious difference is the processing temperature which takes place at much lower temperatures in ref. [71]. Nevertheless, precipitation of C15 and C14 phases is possible in both alloys, which might also have a pinning effect on the microstructure, as reported by [26; 48]. In both cases solution heat treatment (at $\sim 500^\circ C$) is used to dissolve existing C14/C15 phases, for the subsequent age hardening. The aging treatment takes place at $200^\circ C$ in both alloys, but the precipitating phases differ. In the Mg-0.3Al-0.3Ca-0.4Mn alloy both C14 and C15 precursor phases are used for hardening, while the Mg-0.6Al-0.3Ca-0.3Mn uses only the Al_2Ca precursor. While the amount of precipitating phases (Σ of C14 and C15) is comparable in both alloys (0.5 to 0.6% molar phase fraction), a distinctive difference in ΔYS is visible after age hardening. The YS of the Mg-0.3Al-0.3Ca-0.4Mn alloy increases by 46 MPa up to 156 MPa [71] while the Mg-0.6Al-0.3Ca-0.3Mn alloy reaches a YS of 253 MPa, which is an increase of 97 MPa [23]. This indicates a higher hardening potential of the Al_2Ca precursor than that of Mg_2Ca in the used T6 process.

Another in-depth investigation on the microstructural development during the processing of a similar alloy, Mg-0.7Al-0.3Ca-0.5Mn, was done recently by Liu et al. [73]. The evolution of second phase particles was analyzed after casting, extrusion, T4 and T6 heat treatments, thereby showing the distinctive changes from phases formed during casting C36, C15 (and Al_8Mn_5) towards C14, C15 (and $\beta-Mn$) after extrusion to the sole hardening phase C15 (and $\beta-Mn$) in T6 state. The highest strength values where

reached in as-extruded state, which also boasts the smallest grain size and the highest amount of hardening phases (in vol. %), the drawback being an elongation of $< 5\%$. The lower amount of precipitating C15 phases in T6 state has been attributed to the formation and growth of β -Mn, which is able to bind large amounts of Al, accordingly reducing the available amount for formation of Al_2Ca phases.

Not only extrusion has been used to shape Mg-Al-Zn lean alloys, also rolled products have been investigated [24; 58; 74; 75]. When analyzing sheet materials, it must be considered that these are mostly used for semi-finished products, which are subsequently further shaped in various sheet-forming processes. Therefore, the aim in sheet production is usually to achieve good formability of the sheets and the possible subsequent hardening processes of the shaped part. The deep-drawing behavior of sheets can be gauged, for example, with the Erichsen test, in which the achievable drawing depth in mm to the first visible crack is measured (I.E.-value). It is well known that the intense texture occurring in Mg alloys is counterproductive for this type of forming, therefore extensive efforts have been made to reduce the texture intensity in Mg sheet materials [4].

As discussed by Sandlöbes et al. [24] the sharp texture and low forming capabilities of Mg sheets is caused by the predominant deformation by basal slip. To produce an alloy with increased activation of the pyramidal slip, a Mg-1.0Al-0.1Ca alloy was chosen based on ab initio simulations. The Ca content can be fully dissolved during homogenization and the forming of Ca containing phases is avoided, producing a UTS of 220 MPa and a tensile elongation of 20% in the investigated sheets.

Chino et al. [58] studied the effect of Ca addition on tensile properties and stretch formability of Mg-Al and Mg-Zn sheets. They report good forming behavior due to texture softening and increased activation of prismatic slip. These findings were validated by Bian et al. [74], using Mg-1.2Al-0.5Ca-0.4Mn and Mg-1.2Al-0.8Zn-0.5Ca-0.4Mn alloys which were investigated for their sheet forming and heat treatment behavior. In ref. [74] it was shown that the I.E.-values of the AXMZ alloy (7.7 mm) were superior to the tested material without Zn (5.9 mm). The heat treatment performance and strength on the other hand were comparable for both types of alloys, reaching a YS of ~ 200 MPa and a UTS of ~ 260 MPa in T6 state. The effects of varying rolling parameters on a similar alloy were analyzed in ref. [75], where low texture intensity and activation of prismatic slip was found especially pronounced in a fine grained homogeneous microstructure (see Fig. 3.7), thereby reaching I.E.-values of 7.0 mm. While the deformation behavior was strongly influenced by the processing parameters, the mechanical properties stayed constant in T4 state.

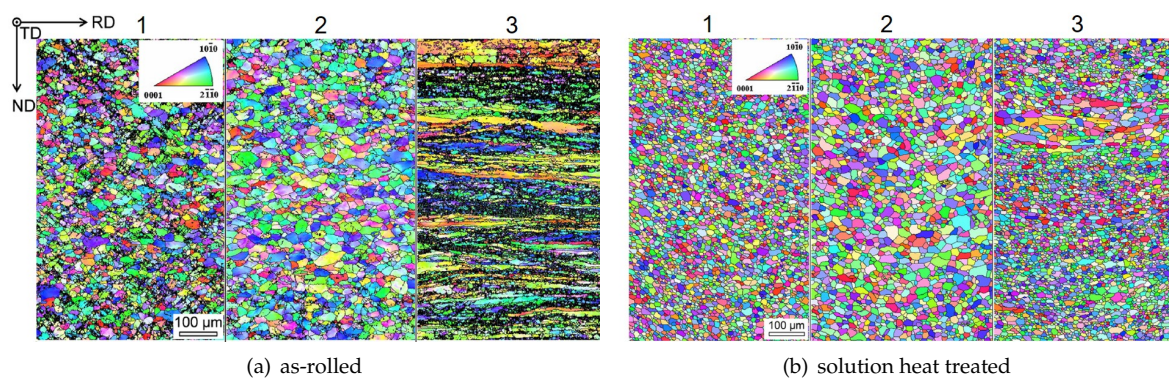


Figure 3.7.: Evolution of microstructure and texture of a Mg-1.2Al-0.3Zn-0.3Ca-0.4Mn alloy, produced by rolling at: (1) 100 °C with reheating, (2) 300 °C with reheating, (3) 300 °C without reheating. Reheating took place at 500 °C for 5 min before each rolling pass, solution heat treatment was done at 450 °C for 1 h [75]. Reproduced with permission of Elsevier.

3.4.2. Alloys containing Zinc and Calcium

The main motivations for the development of Mg-Zn-Ca (ZX) alloys are their good forming behavior, their excellent biocompatibility and their adjustable degradation rate in body fluids, which is an important prerequisite for medical use as implant material. Material strength, on the other hand, only plays a minor role. The good shaping characteristics of Mg-Zn alloys are also the reason for intensive investigation regarding their suitability for structural applications as extruded profiles or rolled sheets [4]. Sheets are often semi-finished products that are to be formed into their final shape in a concluding forming process, i.e. deep drawing, preferable at room temperature. Since the addition of Ca promotes the forming behavior, comparable to the addition of rare earths, dilute Mg-Zn-Ca are investigated in this respect as well.

The investigations of ZX alloys with low alloying content for bio-medical applications are focused on material showing optimal in-vivo degradation. Mg, Zn and Ca are essential trace elements in the human body, and ZX alloys can therefore be used for in-vivo applications without medical incompatibility problems [19].

The interaction of Zn and Ca content was investigated by multiple authors [76–78], analyzing the possible precipitation hardening, grain growth and recrystallization behavior as well as the deformation characteristics. A processing map calculated for an as-cast Mg-1.0Zn-1.0Ca alloy showed two favorable forming domains, featuring dynamic recrystallization, at 280 to 330 °C and 330 to 400 °C with possible forming speeds of 0.0003 to 0.01 s⁻¹ and 0.0003 to 0.1 s⁻¹, respectively [76].

The precipitation hardening of cast and homogenized ZX alloys, with varying Zn content, were analyzed in ref. [77]. There the best hardening results were achieved in a ZX21 alloy, where Zn and Ca containing G.P.- zones formed along the basal plane.

Interesting precipitation hardening results were also found in a hot rolled Mg-0.8Zn-0.2Ca alloy, where marginal plastic strain prior to an annealing treatment at 80 to 200 °C led to an increase of material strength [78]. In contrast, no precipitation strengthening effect could be found in annealed material without prior strain. It was shown that the basal dislocations produced by deformation were pinned by annealing induced formation of G.P.- zones, thereby improving the YS of the samples during repeated tensile testing.

Using such a Mg-0.8Zn-0.2Ca alloy it was shown recently, that the combination of Zn and Ca is necessary for a distinct improvement of room temperature ductility [59; 79]. The material was analyzed after cold rolling and subsequent annealing [20] and hot rolling and annealing [80]. It was found that basal and pyramidal slip was increased at room temperature and the twinning pushed towards higher strains. Subsequent annealing causes solute segregation and precipitation at the grain boundaries, promoting homogeneous grain size distributions by pinning. Nucleation of recrystallized grains starts preferably at tensile twins and shear bands. The combination of the described effects promotes the desired rare earth texture for these alloys.

The texture of a Mg-1.0Zn-0.9Ca alloy was shown to change noticeably during the processing steps in ref. [81]. While the texture from the hot rolled material showed a splitting of basal poles in rolling direction, due to a strong formation of double twins, the subsequent annealing shifted the poles towards the transverse direction. In the analysis of the annealed sheets an I.E.-value of 8.8 mm and a UTS of 234.3 MPa was reached.

Investigations on the effect of Zn on Mg-Ca-Zr alloys showed a large increase of ductility and the potential for age hardening in a Mg-0.2Ca-0.4Zr-0.3Zn sheet [50]. The elongation to fracture was enhanced up to a value of 34 % in TD because failure along the grain boundaries was suppressed. Additionally, this type of alloy can be age hardened, reaching a YS of 220 MPa in T8 state, which accords to an increase of ~70 MPa. This was mostly achieved by the formation of nanoscale plate-like precipitates on the basal plane of the Mg matrix.

An increase in ductility was also found in ref. [82] where annealed sheets from Mg-1.2Zn-0.2Zr with and without Ca additions (0.4 wt. %) were compared. By Ca additions a weak double peak texture was formed and the activation of {10 $\bar{1}$ 2} twinning and pyramidal <c+a> slip was promoted. While the Ca containing sheets showed improved ductility and higher UTS, the mechanical anisotropy increased. Especially the YS varied up to 50 MPa, depending on the testing direction, while the mechanical prop-

erties of the ZK10 alloy were more uniform overall [82].

A complementary study [83] analyzed the influence of Ca (0.4 and 0.8 wt. %) on an extruded and annealed Mg-1.4Zn-0.1MM-0.1Zr alloy. The Ca additions slightly reduced the overall material strength, with the YS being the most affected, decreasing by ~ 30 MPa to 170 MPa. Consequently, the yield anisotropy (YSc/YS) was shifted from 0.75 to 0.85. Solely the alloy modified with 0.8 wt. %Ca showed microstructural changes, i.e., a reduced grain size, a higher degree of recrystallization and a reduction of texture intensity.

Mg-0.6Zn-0.6Ca-0.1Zr sheets, produced by twin-roll casting on an industrial scale, were investigated by Klaumünzer et al. [31] with regard to their forming behavior using Erichsen testing. At RT an I.E.-value of ~ 7 mm was reached, and industrially relevant components could be formed at temperatures of 160 °C. In ref. [32] this ZXK alloy was compared to Mg-1.8Zn-0.1Nd-0.1Ce-0.05La-0.2Y material, which showed comparable I.E.-values at RT. The textures of both sheet materials are similar and show broad basal poles shifted toward the TD. The texture intensity depends on the rolling conditions but is weakened in case of the annealed sheets. In general, the ZEW sheets feature higher strength and increased ductility compared to the ZXK alloy, which on the other hand exhibits reduced planar anisotropy. In the forming investigations (Erichsen testing and deep drawing of cups) the ZEW sheets show better overall performance under all conditions and temperatures tested (up to 200 °C), while the ZXK material failed due to crack initiation at coarse MgCa particles [32].

As described in Section 3.4.1 extrusion is one of the preferred forming methods, which is why lean wrought Mg alloys are also intensively studied in this respect. An investigation of a Mg-1.0 Zn-0.5 Ca alloy illustrates the influence of the processing temperature on the mechanical properties of this material. In the experimental trials the chosen extrusion temperature varied in the range of 310 to 400 °C. A bimodal grain structure of small recrystallized and large deformed grains was formed below 350 °C. This structure shows an increased yield strength but markedly reduced elongation to failure, when compared to samples formed at >350 °C, which exhibit a fully recrystallized microstructure with increasing grain size at increasing extrusion temperatures [42].

In a following investigation the effect of changing the Ca content (0 to 0.5 wt. %) on this alloy was analyzed [60]. The as-cast and subsequently extruded alloys display decreasing grain sizes and texture with raising Ca content. It was shown, that the rising amount of precipitates augments the dynamic recrystallization but the subsequent grain growth is impeded. The resulting texture weakening causes a reduction of YS but a considerable increase of elongation to failure.

The positive effect of Ca-containing precipitations is confirmed in ref. [84], where dilute Mg-Zn-Ca-Mn alloys with increasing Zn content (0.2, 0.5 and 0.7 wt. %) were analyzed regarding their extrusion behavior. While all alloys could be formed with good die-exit speeds of 24 m min^{-1} only the alloy with the lowest Zn content (0.2 wt. %) could be extruded with die-exit speeds of up to 60 m min^{-1} . The uniform elongation for all alloys and extrusion speeds was fairly consistent throughout, reaching $\sim 23\%$. The tensile strength of the alloys on the other hand increased with rising Zn concentration and decreasing forming speed. This was attributed to the increase of solid solution strengthening by the Zn atoms, the lower forming temperature at low extrusion speeds and the resulting reduced grain size. It is assumed that the overall low yield strength (< 110 MPa) of these alloys is due to the texture, which was found favorable for the activation of basal slip systems [84]. The microstructural behavior of the Mg-0.2Zn-0.3Ca-0.1Mn alloy was further analyzed in ref. [85], where the extrusion temperature was varied from 300 to 400 °C. The resulting microstructure changed from a bimodal structure of small recrystallized and larger deformed grains towards a fully recrystallized structure with rising forming temperatures, see Fig. 3.8. All samples benefit from the precipitation of Mg_2Ca and α -Mn phases, which inhibit grain growth. While the material processed at 300 °C shows the best overall mechanical properties, with a YS of 307 MPa and an elongation of 20.6 %, it also exhibits the strongest texture intensity and the strongest yield anisotropy (YS/YSc). The mechanical properties shifted to lower strength and higher elongation to failure for the samples produced with higher extrusion temperatures [85].

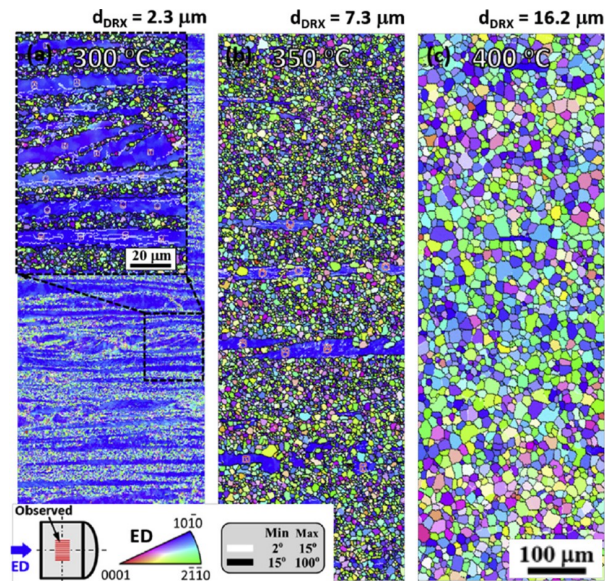


Figure 3.8.: Evolution of microstructure and texture in an as-extruded Mg-0.2Zn-0.3Ca-0.1Mn alloy at rising processing temperatures: (a) 300 °C, (b) 350 °C, (c) 400 °C [85]. Reproduced with permission from Elsevier.

The applicability of lean alloyed ZX alloys for bio-medical applications, i.e. as biodegradable implant material, was the main motivation for the investigations done in refs. [19; 86]. While the used elements Mg, Zn and Ca are essential trace elements and thus harmless for applications in the human body, the dissolution of these materials in-vivo is a complex process. The degradation rate must be well controlled, to avoid damage to the surrounding tissue and bone material by hydrogen production, which is a byproduct of the in-vivo dissolution of Mg. Because of this, the possibilities to customize the mechanical properties by alloying are much reduced and the processing parameters, in addition to the absence of corrosion-promoting impurities, are the main means of adjustment [19].

As the mechanical properties inherently depend on the microstructural features generated during processing, the behavior of IMPs during extrusion is investigated by Hofstetter et al. [28]. There the comparison of a Mg-0.5Zn-0.1Ca-0.1Mn alloy (without IMPs) and Mg-1.0Zn-0.3Ca (with IMPs) illustrates the large influence of the dispersed Mg₂Ca precipitates on grain size (< 2 μm) and tensile properties. Consequently, the Mg-1.0Zn-0.3Ca alloy achieved a YS of 238 MPa and a UTS of 265 MPa with an elongation to fracture of 31 %.

A different approach was used in ref. [41] where SPD was used to improve the mechanical properties of a homogenized Mg-0.8Zn-0.2Ca alloy. By a subsequent use of ECAP and HPT a UTS of up to 283 MPa was reached.

To adjust the biodegradability to an optimum level, in depth studies on corrosion and the corresponding microstructural features were performed.

Cihova et al. [86] state, that the Zn content of ZX alloys has a crucial impact on the corrosion behavior. This is caused by an enhancement of the cathodic activity through Zn re-deposition and the forming of various IMPs, Mg₂Ca or Ca₂Mg₆Zn₃, which is a controlling feature of the degradation behavior of these alloys. The Ca₂Mg₆Zn₃ phases act as cathodes and promote the Mg matrix degradation, while the Mg₂Ca phases dissolve before the matrix, resulting in a slow and homogeneous degradation of the material. The forming of the Mg₂Ca phase is therefore one of the main factors for the reduced corrosion behavior of the tested Mg-1.0Zn-0.3Ca lean alloy, which was shown to be well suitable for in-vivo applications [86].

The alloying and processing scheme used in ref. [86] is depicted in the CALPHAD calculations given in Fig. 3.9. This is an interesting example of how small changes in alloying content can have a distinctive

influence on the material properties (discussed above), as processing is the same for both alloys. The alloy Mg-1.0Zn-0.3Ca allows for the formation of both the $\text{Ca}_2\text{Mg}_6\text{Zn}_3$ and Mg_2Ca phases, while only the $\text{Ca}_2\text{Mg}_6\text{Zn}_3$ phase may precipitate in the Mg-1.5Zn-0.2Ca alloy. The homogenization temperature (up to 450 °C) has been chosen as high as possible, restricted by the Mg-1.5Zn-0.2Ca alloy, which has the lower solidus temperature. IMPs, that could have formed during casting, are fully soluble in both alloys, thereby producing a super saturated solid solution during homogenization heat treatment [86]. To avoid grain growth during extrusion, the alloys are pre-aged, forming Ca-containing precipitates, as described in ref. [28]. The CALPHAD calculations show, that a precipitation of both the $\text{Ca}_2\text{Mg}_6\text{Zn}_3$ and Mg_2Ca phases is possible in the Mg-1.0Zn-0.3Ca alloy during pre-aging. Nevertheless, only the Mg_2Ca phase is present during and after the extrusion process. The Mg-1.5Zn-0.2Ca alloy, on the other hand, retains the ternary phase throughout extrusion. This differing precipitation behavior is, as already discussed above, the controlling feature for the corrosion behavior of these alloys. While, based on the thermodynamic calculations, it may be assumed that dynamic precipitation of the respective IMPs occurs during processing, this has not been discussed in the cited literature [28; 86].

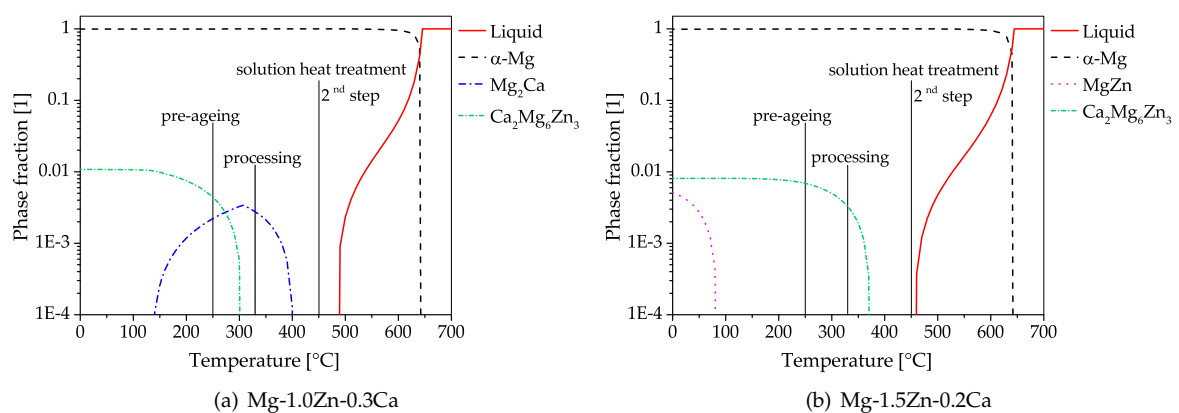


Figure 3.9.: CALPHAD calculations, including the used processing temperatures, of two biodegradable Mg-Zn-Ca alloys. Calculations were done using the alloy compositions given in ref. [86], for further information see App. 3.6.1.2.

3.4.3. Alloys containing various alloying Elements

This section discusses publications using various alloying schemes not specifically mentioned in the previous sections, which have been accordingly restricted to lean alloys containing Al-Ca and Zn-Ca. Therefore, this section contains a broader variation of alloy compositions, i.e. Mg-RE and Mg-Sn alloys.

The **combination of Zn and REE** (sometimes refined by **Zr additions**) is an often-chosen alloying route, known to produce alloys with good forming performances. Some of the works [32; 83] investigating these alloys have already been mentioned in Section 3.4.2.

The influence of micro-alloying with Ge on the corrosion behavior of a cast and extruded lean Mg-Zn alloys in saline solution was investigated by Jiang et al. [87; 88]. As the investigated Mg-0.5Zn-0.2Ge alloy featured Mg_2Ge phases, which are nobler than the surrounding Mg matrix, localized corrosion of the matrix was found in the cast alloy. This behavior changed in the as-extruded material where uniform corrosion was prevalent. In a comparison with a Mg-0.5Zn-0.2Ca alloy the Ge containing material showed superior tensile strength and improved corrosion behavior. This slightly higher corrosion resistance of the Mg-0.5Zn-0.2Ge alloy is due to an increased incorporation of Zn and Ge in the outer layer of the corrosion products film and was less effected by corrosion in short term fatigue tests.

The investigations done by Al-Samman and Li [89] analyzed the effect of different REE additions (Gd, Nd, Ce, La and mischmetal (MM)) on Mg-Zn-Zr alloys, giving insight into the rolling and annealing behavior. All of the RE elements investigated led to a weakening of the rolling texture which was further

reduced by an annealing treatment. This typical behavior for REE containing alloys was confirmed by the tensile properties, showing an overall reduction of mechanical anisotropy and high ductility (up to 32 % true strain). The biggest effect was found in the Gd containing alloy, reflected by the strong texture modification and superior ductility at room temperature, despite exhibiting the coarsest grain structure compared to the other alloys [89].

A Mg-1.6Zn-0.5Gd alloy, analyzed with regard to processing performance [43; 90], microstructural features and recrystallization behavior [91] showed favorable forming surfaces even when produced by high extrusion rates, up to 60 mmin^{-1} die-exit speed. The tensile properties, however, changed considerably with the processing conditions, e.g., the extrusion rate and temperature or pre-deformation. Nevertheless, high values for elongation to failure were measured throughout [90]. It could be shown that the precipitation of $\text{Mg}_3\text{Zn}_3\text{Gd}_2$ particles during the extrusion hinders grain growth, by forming at the grain boundaries and the grain interior [43]. While the texture of the dynamically recrystallized microstructure features $[\bar{2}1\bar{1}0]$ basal fiber components, the typical REE texture mainly develops during the subsequent static recrystallization [91].

The influence of extrusion speed on microstructure and mechanical properties in combination with alloy modifications is an often investigated topic, as it is an essential topic for industrial applications. The effect of Zr additions (0.5 wt. %) on a Mg-1.3Zn-0.1Ce alloy is studied in ref. [92], comparing indirect extrusions with die-exit speeds of 1, 10 and 20 mmin^{-1} . With rising extrusion speed the amount of recrystallized grains increases for both alloys, while the tensile and compressive strengths decrease markedly. Elongations to break, on the other hand, are less dependent on the extrusion rate. The modified Mg-1.3Zn-0.2Ce-0.5Zr alloy, exhibits a smaller grain size and higher strength values throughout all processing speeds. Interestingly, the grain size does not change with the increase of the processing speed to 20 mmin^{-1} but stays constant at $\sim 7 \mu\text{m}$ in this alloy [92].

Complementary investigations were done on ZK alloys, where a Mg-1.0Zn-0.4Zr lean alloy was modified with 0.8 wt. % Ce rich MM [93; 94]. Extrusion trials took place with die-exit speeds of 1, 5 and 10 mmin^{-1} , showing increased grain size, decreasing YS and UTS as well as a reduced overall texture intensity with rising processing speeds. A smaller grain size and higher strength was found in the MM containing alloy.

Mg alloys forming long period stacking order (LPSO) phases show interesting mechanical properties, e.g., high temperature strength. The desired properties of these alloys can be directly correlated to the volume fraction of the LPSO phase, which increases with rising alloying content, as reported in ref. [95]. There, a Mg-0.5Zn-2.2Y alloy was found to reach only 1 % of LPSO volume fraction, showing accordingly reduced properties when compared to the alloys with higher element content. As the possible amount of formed LPSO phase fraction is also controlled by the used Zn/Y ratio, optimization in this regard can lead to increased LPSO phase fractions at comparable overall alloying contents [96]. Nevertheless, it seems questionable if this principle of ordered Mg-Zn-Y(/Gd) phases can show a feasible effect in lean alloys as well.

The influence of precipitation formation and recrystallization is also given special attention for alloys of the **Mg-Mn-RE system**.

In ref. [97] a Mg-1.8Mn alloy was modified with Er and Er/Al additions, homogenized and extruded. The subsequently annealed samples showed increasing elongation to break with rising alloying additions. In case of the Er containing alloys the fraction of recrystallized grains varied between 45 and 100 %. The alloys modified with a combination of Er and Al featured an increasing recrystallized fraction (60 to 80 %) with the amount of alloying elements, also showing a superior elongation to break during tensile testing.

Extensive investigations on an extruded Mg-1.0Mn-1.0Nd alloy were done to analyze the precipitation behavior and the reversed yield asymmetry ($Y_{Sc} > Y_S$), which appears at various temperatures [98]. During annealing at $250 \text{ }^\circ\text{C}$ the precipitating Mg_3Nd -plates orient themselves along the c-axis, causing anisotropic strengthening effects. This causes a preferred deformation via prismatic slip and promoting the yield strength asymmetry at RT. On the contrary the reason for this effect at high temperatures is thought to be caused by the mobility of the pyramidal $\langle c+a \rangle$ dislocations [99].

Investigations on **Mg-Sn lean alloys** indicate good RT forming behavior of extruded sheet material. In a comparison of multiple alloys, both Mg-1.3Sn-0.7Ca and Mg-1.1Sn-0.6Zn-0.5Ca exhibit split basal textures after extrusion [100]. The results of tensile testing in TD indicate a better performance of the Mg-1.1Sn-0.6Zn-0.5Ca alloy. This is attributed to increased activation of prismatic slip, enhanced grain boundary cohesion and improved intergranular strain propagation capacity.

The addition of Y to lean Mg-Sn alloys influences the mechanical properties of as-extruded sheets at RT positively, especially the elongation to break showed marked improvement. Investigations on Mg-0.3Sn-0.7Y [101] and Mg-0.5Sn-0.3Mn-0.3Y [102] alloys attributed this to a decreased grain size, favorable texture and increased activity of non-basal slip when compared to the alloys without Y. Subsequent work confirmed this also for rolled and annealed sheets made from Mg-0.3Sn-0.7Y [103]. Further improvements of the mechanical properties were achieved with a dilute addition of Zn, producing a Mg-0.4Sn-0.6Zn-0.7Y alloy with decreased grain and particle size, increasing the I.E.-value from 6.2 to 7.0 mm [104].

3.5. Concluding Remarks

This review is intended to provide an overview of the works published on Mg alloys with multiple alloying elements, up to a sum of ~2 wt.% and ~1 at.% of additions. The thereby provided excerpt of the current state of research, may serve as an introduction to the various possibilities in the diverse family of Mg lean alloys.

The investigations on these so called low, dilute, HSLA or lean alloys offer a broad variety of properties, processes and applications, ranging from age hardenable alloys with very high processing rates to biomedical applications with controllable in-vivo dissolution.

While most of the works discussed highlight the practical applications and the improvements made by this alloying concept, there are also some drawbacks that need to be addressed. Mechanical properties, that rely on an increased amount of alloying elements, such as high contribution of solid solution hardening, the LPSO effect, or generally those where the focus lies on high strength values, cannot fully be realized with the lean alloying concept. The discussed alloys are often operating in a narrow range or make use of (thermodynamic) features which are strongly dependent on exact chemical compositions. Some may also show a unusually high response to impurities. These characteristics and the sometimes sensitive casting behavior increases the difficulty for stock material production and may impede recyclability.

Regardless of the limitations mentioned above, the 'lean alloy' design concept opens up a wide range of opportunities for the further development of Mg wrought alloys and is strongly orientated towards the suitability for everyday use. The reduction and focus on easily available alloying elements, the full utilization of mechanical properties, i.e., improved ductility or age hardening, increase the viability of these alloys markedly. Therefore, demands of industrial manufacturing, such as high extrusion speed or complex secondary sheet forming operations, can be met easier. The development of these materials is not yet complete, but the successes so far promise an exciting field of work as well as multiple applications in the near future.

The authors hope that this brief introduction to the diverse topic of 'Lean Wrought Magnesium Alloys' can be a stimulus for further development and an aid to the visibility of these interesting alloys.

3.6. Appendix

3.6.1. Additional Information

3.6.1.1. Sources for Literature Research

The literature research for this work was primarily done online, where the following online sources were mainly used: Scopus, Google Scholar, Web of Science and Espacenet.

3.6.1.2. CALPHAD calculations

The figures showing CALPHAD calculations were done with the software Thermo-Calc Version 2021a and the database Thermo-Calc TCMG5. The alloy compositions used are listed in Table 3.1.

3.6.2. Alloy Overview

This section lists the chemical compositions (in wt% and at%) of the investigated Mg alloys. As the discussed works often analyze multiple alloys with varying alloy content, Table 3.1 also includes materials slightly outside the designated range of 1 at.% and 2 wt.%, where thought appropriate and useful for comparison.

Table 3.1.: Chemical composition of alloys discussed in the reviewed works, given in wt. % and (at. %). Alloying content below 0.01 % (100 ppm) is not listed, the RE elements have been combined into a single column for improved readability.

Alloy	Source	Σ Elements	Mg	Al	Zn	Ca	Mn	Si	Σ REE	Sn	Zr
Mg-Al-Ca											
Mg-0.1Al-0.5Ca	[26; 48]	0.60 (0.39)	Bal	0.10 (0.09)		0.50 (0.30)					
Mg-0.3Al-0.2Ca	[26; 48]	0.50 (0.39)	Bal	0.30 (0.27)		0.20 (0.12)					
Mg-0.3Al-0.2Ca-0.5Mn	[9; 40]	0.98 (0.61)	Bal	0.30 (0.27)		0.21 (0.13)	0.47 (0.21)				
Mg-0.3Al-0.3Ca	[70]	0.64 (0.48)	Bal	0.32 (0.29)		0.32 (0.19)					
Mg-0.3Al-0.3Ca-0.2Mn	[70]	0.91 (0.61)	Bal	0.33 (0.30)		0.34 (0.20)	0.24 (0.11)				
Mg-0.3Al-0.3Ca-0.4Mn	[70; 71]	1.09 (0.69)	Bal	0.34 (0.31)		0.32 (0.19)	0.43 (0.19)				
Mg-0.3Al-0.3Ca-0.8Mn	[70]	1.45 (0.84)	Bal	0.30 (0.27)		0.31 (0.19)	0.84 (0.37)				
Mg-0.6Al-0.3Ca-0.3Mn	[23; 72]	1.13 (0.82)	Bal	0.60 (0.54)		0.28 (0.17)	0.25 (0.11)				
Mg-0.6Al-0.5Ca	[10]	1.07 (0.83)	Bal	0.61 (0.55)		0.46 (0.28)					
Mg-0.7Al-0.3Ca-0.5Mn	[73]	1.50 (1.04)	Bal	0.68 (0.62)		0.32 (0.20)	0.50 (0.22)				
Mg-1.0Al-0.1Ca	[24]	1.10 (0.96)	Bal	1.00 (0.90)		0.10 (0.06)					
Mg-1.0Al-1.0Zn-0.1Ca-0.5Mn	[58]	2.60 (1.57)	Bal	1.00 (0.91)	1.00 (0.38)	0.10 (0.06)	0.50 (0.22)				
Mg-1.2Al-0.3Zn-0.3Ca-0.4Mn	[75]	2.20 (1.60)	Bal	1.20 (1.10)	0.30 (0.10)	0.30 (0.20)	0.40 (0.20)				
Mg-1.2Al-0.5Ca-0.4Mn	[74]	2.10 (1.60)	Bal	1.20 (1.10)		0.50 (0.30)	0.40 (0.20)				
Mg-1.2Al-0.8Zn-0.5Ca-0.4Mn	[74]	2.90 (1.90)	Bal	1.20 (1.10)	0.80 (0.30)	0.50 (0.30)	0.40 (0.20)				
Mg-1.3Al-0.3Ca-0.5Mn	[71]	2.10 (1.60)	Bal	1.31 (1.19)		0.33 (0.20)	0.46 (0.21)				
Mg-2.7Al-0.3Ca-0.4Mn	[71]	3.51 (2.88)	Bal	2.73 (2.48)		0.34 (0.20)	0.44 (0.20)				
Mg-Zn-Ca											
Mg-0.2Zn-0.3Ca-0.1Mn	[84; 85]	0.65 (0.32)	Bal		0.21 (0.08)	0.30 (0.18)					
Mg-0.3Zn-0.5Ca	[77]	0.80 (0.40)	Bal		0.30 (0.10)	0.50 (0.30)					0.37 (0.10)
Mg-0.8Ca-0.37Zr	[50]	1.19 (0.60)	Bal			0.82 (0.50)					0.37 (0.10)
Mg-0.8Ca-0.37Zr-0.3Zn	[50]	1.46 (0.70)	Bal		0.27 (0.10)	0.82 (0.50)					
Mg-0.5Zn-0.1Ca-0.1Mn	[28]	0.69 (0.31)	Bal	0.02 (0.02)	0.48 (0.18)	0.14 (0.09)	0.03 (0.01)	0.02 (0.02)			
Mg-0.5Zn-0.2Ca-0.3Mn	[84]	1.04 (0.46)	Bal		0.53 (0.20)	0.24 (0.15)	0.27 (0.12)				
Mg-0.6Zn-0.6Ca-0.1Zr	[31; 32]	1.30 (0.62)	Bal		0.60 (0.22)	0.60 (0.37)					0.10 (0.03)
Mg-0.7Zn-0.4Ca-0.1Mn	[84]	1.14 (0.52)	Bal		0.71 (0.27)	0.36 (0.22)	0.07 (0.03)				
Mg-0.8Zn-0.2Ca	[59]	1.02 (0.43)	Bal		0.80 (0.30)	0.20 (0.12)	0.02 (0.01)				
Mg-0.8Zn-0.2Ca	[20; 78-80]	0.96 (0.40)	Bal		0.80 (0.30)	0.16 (0.10)					
Mg-0.8Zn-0.5Ca	[77]	1.30 (0.60)	Bal		0.80 (0.30)	0.50 (0.30)					
Mg-1.0Zn-0.2Ca	[41; 60]	1.20 (0.49)	Bal		1.00 (0.37)	0.20 (0.12)					
Mg-1.0Zn-0.3Ca	[19]	1.30 (0.56)	Bal		1.00 (0.37)	0.30 (0.18)					
Mg-1.0Zn-0.3Ca	[28]	1.33 (0.59)	Bal	0.02 (0.02)	0.96 (0.36)	0.29 (0.18)	0.03 (0.01)	0.03 (0.03)			
Mg-1.0Zn-0.3Ca	[86]	1.28 (0.56)	Bal		0.96 (0.36)	0.32 (0.20)					
Mg-1.0Zn-0.5Ca	[42; 60]	1.50 (0.68)	Bal		1.00 (0.37)	0.50 (0.31)					
Mg-1.0Zn-0.9Ca	[81]	1.85 (0.91)	Bal		0.95 (0.36)	0.90 (0.55)					0.18 (0.05)
Mg-1.2Zn-0.4Ca-0.2Zr	[82]	1.78 (0.74)	Bal		1.21 (0.45)	0.39 (0.24)					0.10 (0.03)
Mg-1.4Zn-0.1MM-0.1Zr-0.4Ca	[83]	2.00 (0.83)	Bal		1.40 (0.53)	0.40 (0.25)			0.10 (0.02)		0.10 (0.03)
Mg-1.4Zn-0.1MM-0.1Zr-0.8Ca	[83]	2.40 (1.07)	Bal		1.40 (0.53)	0.80 (0.49)			0.10 (0.02)		0.10 (0.03)
Mg-1.5Zn-0.1Ca	[58]	1.60 (0.62)	Bal		1.50 (0.56)	0.10 (0.06)					
Mg-1.5Zn-0.2Ca	[86]	1.72 (0.71)	Bal		1.48 (0.56)	0.24 (0.15)					
Mg-1.6Zn-0.5Ca	[77]	2.10 (0.90)	Bal		1.60 (0.60)	0.50 (0.30)					
Mg-2.6Zn-0.5Ca	[77]	3.10 (1.30)	Bal		2.60 (1.00)	0.50 (0.30)					

Table 3.1 continued from previous page

Alloy	Source	Σ Elements	Mg	Al	Zn	Ca	Mn	Si	Σ REE	Sn	Zr	
Various	Mg-1.0Mn-1.0Nd	[98; 99]	Bal				1.00 (0.45)		1.00 (0.17)			
	Mg-1.8Mn-0.1Er	[97]	Bal				1.80 (0.81)		0.10 (0.01)			
	Mg-1.8Mn-0.1Er-0.1Al	[97]	Bal	0.05 (0.05)			1.80 (0.81)		0.10 (0.01)			
	Mg-1.8Mn-0.4Er	[97]	Bal				1.80 (0.81)		0.40 (0.06)			
	Mg-1.8Mn-0.4Er-0.2Al	[97]	Bal	0.20 (0.18)			1.80 (0.81)		0.40 (0.06)			
	Mg-1.8Mn-0.7Er	[97]	Bal				1.80 (0.81)		0.70 (0.10)			
	Mg-1.8Mn-0.7Er-0.3Al	[97]	Bal	0.34 (0.31)			1.80 (0.81)		0.70 (0.10)			
	Mg-0.3Sn-0.7Y	[101; 103; 104]	1.04 (0.27)						0.71 (0.20)	0.33 (0.07)		
	Mg-0.4Sn-0.7Y-0.6Zn	[104]	1.70 (0.51)		0.64 (0.24)				0.65 (0.18)	0.41 (0.09)		
	Mg-0.5Sn-0.3Mn	[102]	0.82 (0.23)	Bal			0.27 (0.12)			0.55 (0.11)		
	Mg-0.5Sn-0.3Mn-0.3Y	[102]	1.08 (0.31)	Bal			0.27 (0.12)		0.33 (0.09)	0.48 (0.10)		
	Mg-1.1Sn-0.6Zn-0.5Ca	[100]	2.12 (0.73)	Bal		0.47 (0.29)				1.10 (0.23)		
	Mg-1.2Sn-0.5Zn	[100]	1.64 (0.42)	Bal		0.48 (0.18)				1.16 (0.24)		
	Mg-1.3Sn-0.7Ca	[100]	1.97 (0.70)	Bal			0.69 (0.43)			1.28 (0.27)		
	Mg-0.5Zn-0.2Ca	[88]	0.74 (0.34)	Bal		0.47 (0.18)						
	Mg-0.5Zn-0.2Ge	[87; 88]	0.73 (0.27)	Bal		0.49 (0.18)		0.03 (0.01)	0.01 (0.01)			
	Mg-0.5Zn-2.2Y	[95]	2.68 (0.80)	Bal		0.53 (0.20)		0.03 (0.01)	0.01 (0.01)	0.20 (0.07)		
	Mg-0.6Zn-0.3Zr-0.6Nd	[89]	1.46 (0.40)	Bal		0.61 (0.23)				2.15 (0.60)		0.27 (0.07)
	Mg-0.7Zn-0.2Zr-0.7Gd	[89]	1.70 (0.44)	Bal		0.73 (0.27)				0.58 (0.10)		0.24 (0.06)
	Mg-0.7Zn-0.2Zr-0.8Ce	[89]	1.64 (0.45)	Bal		0.68 (0.26)				0.73 (0.11)		0.18 (0.05)
	Mg-0.8Zn-0.3Zr-0.9MM	[89]	2.05 (0.57)	Bal		0.84 (0.32)				0.88 (0.16)		0.33 (0.09)
	Mg-0.9Zn-0.2Zr-0.7La	[89]	1.80 (0.52)	Bal		0.89 (0.34)				0.69 (0.12)		0.22 (0.06)
	Mg-1.0Zn-0.4Zr	[94]	1.40 (0.49)	Bal		1.00 (0.38)				0.80 (0.14)		0.40 (0.11)
	Mg-1.0Zn-0.4Zr-0.8MM	[94]	2.20 (0.63)	Bal		1.00 (0.38)						0.40 (0.11)
	Mg-1.2Zn-0.2Zr	[82]	1.39 (0.51)	Bal		1.22 (0.46)						0.17 (0.05)
	Mg-1.3Zn-0.1Ce	[92]	1.40 (0.51)	Bal		1.30 (0.49)				0.10 (0.02)		
Mg-1.3Zn-0.2Ce-0.5Zr	[92]	2.00 (0.67)	Bal		1.30 (0.49)				0.20 (0.04)			
Mg-1.4Zn-0.1MM-0.1Zr	[83]	1.50 (0.58)	Bal		1.40 (0.53)				0.10 (0.02)			
Mg-1.6Zn-0.5Gd	[43; 90; 91]	2.10 (0.68)	Bal		1.58 (0.60)				0.52 (0.08)			
Mg-1.8Zn-0.1Nd-0.1Ce-0.05La-0.2Y	[32]	2.26 (0.79)	Bal		1.81 (0.68)				0.45 (0.11)			

3.6.3. Mechanical Properties

This section aims to give an overview of mechanical properties of the discussed Mg alloys. For clarification the temper designations used throughout this work are listed in Table 3.2.

Additional information on the Hall Petch parameters depicted in Figure 3.3 is compiled in Table 3.3.

Table 3.4 summarizes the mechanical properties of the selected materials, discussed in App. 3.6.2, at RT. The values are directly taken from the works cited and may include stock material. The respective processing parameters are listed as thorough as feasible.

Table 3.2.: Temper designations used in this work.

Designation	Explanation
F	as-fabricated
O	annealed, recrystallized
T4	solution heat treated and naturally aged [‡]
T5	artificially aged only
T6	solution heat treated and artificially aged
T8	solution heat treated, cold worked and artificially aged

[‡]: As the effect of natural aging in the described Mg alloys is neglectable, solution heat treated material can also be referred to as T4 temper.

Table 3.3.: Overview of the alloys and corresponding constants, Hall Petch slope (k_y) and frictional stress (σ_0) used in Fig. 3.3. The Hall Petch relationship $YS = k_y * d^{-1/2} + \sigma_0$, where d represents the grain diameter, was used for the calculation of the YS depicted in Fig. 3.3 b. The values of the alloys marked with an asterisk (*) have been calculated from the microstructure given in the corresponding source literature.

Alloy	k_y [MPa μm^2]	σ_0 [MPa]	Source
Mg-0.3Al-0.2Ca-0.5Mn	208	143	[40]
Mg-1.0Zn-0.2Ca*	72	121	[41]
Mg-1.0Zn-0.3Ca	241	47	[28]
Mg-1.0Zn-0.5Ca*	236	37	[42]
Mg-1.6Zn-0.5Gd*	411	45	[43]

Table 3.4.: Overview of the mechanical properties (at RT) and processing parameters of the alloys discussed in this work. The following abbreviations are exclusively used in this table: extrusion (extr.), homogenization (hom.), temperature (temp.), material (mat.), solution heat treatment (s.h.t.), water quenched (w.q.), without (w/o), subsequently (subseq.).

Alloy	Temper	YS [MPa]	UTS [MPa]	ϵ_f [%]	YS _c [MPa]	UCS [MPa]	Source	Process Parameters
Mg-0.3Al-0.2Ca-0.5Mn	as-extr.	170		15.5			[9]	cast, hom. at 500 °C for 24 h, w.q., extr. to round bars (indirect, 1:20) at 500 °C with a die-exit speed of 60 mmmin ⁻¹
	T5	207		12.5			[9]	as above, aged at 200 °C for 7 h
	as-extr.	206		29			[40]	cast, extr. to round bars (indirect, 1:20) at 350 °C with a die-exit speed of 60 mmmin ⁻¹
	as-extr.	177					[40]	cast, extr. to round bars (indirect, 1:20) at 500 °C with a die-exit speed of 60 mmmin ⁻¹
Mg-0.3Al-0.3Ca-0.2Mn	as-extr.	136 ± 2	203 ± 2	29 ± 2			[70]	cast, hom. at 450 °C for 1 h, w.q., extr. to round bars (indirect w/o lubricant, 1:20) at 400 °C with a die-exit speed of 60 mmmin ⁻¹
	T6	188 ± 0	247 ± 0	27 ± 0			[70]	as above, s.h.t. (500 °C for 10 min) and w.q., aged at 200 °C
Mg-0.3Al-0.3Ca-0.4Mn	as-extr.	166 ± 1	220 ± 1	24 ± 0			[70]	cast, hom. at 450 °C for 1 h, w.q., extr. to round bars (indirect w/o lubricant, 1:20) at 400 °C with a die-exit speed of 60 mmmin ⁻¹
	T6	220 ± 2	264 ± 0	22 ± 2			[70]	as above, s.h.t. (500 °C for 10 min) and w.q., aged at 200 °C
	T4/s.h.t.	159 ± 3	228 ± 1	29 ± 1	119 ± 5	405 ± 4	[71]	cast, hom. at 500 °C for 1 h, extr. to round bars (indirect, 1:20) at 275 °C with a die-exit speed of 24 mmmin ⁻¹ , s.h.t. (500 °C for 10 min) and w.q.
Mg-0.3Al-0.3Ca-0.8Mn	T5	230 ± 5	262 ± 3	26 ± 1	165 ± 2	434 ± 1	[71]	as above, aged at 200 °C for 8 h
	as-extr.	190 ± 3	229 ± 1	24 ± 3			[70]	cast, hom. at 450 °C for 1 h, w.q., extr. to round bars (indirect w/o lubricant, 1:20) at 400 °C with a die-exit speed of 60 mmmin ⁻¹
Mg-0.6Al-0.3Ca-0.3Mn	T6	199 ± 1	243 ± 0	22 ± 3			[70]	as above, s.h.t. (500 °C for 10 min) and w.q., aged at 200 °C
	as-extr.	165.0 ± 7.8	232.0 ± 2.7	14.0 ± 0.3			[23; 72]	cast, hom. at 480 °C for 6 h, w.q., extr. to round bars (direct, 1:25) at 450 °C with a die-exit speed of 0.75 to 3.75 mmmin ⁻¹
	T5	236.0 ± 2.1	265.0 ± 1.9	7.0 ± 11.0			[23; 72]	as above, aged at 200 °C
Mg-0.6Al-0.5Ca	T4/s.h.t.	156.0 ± 0.1	225.0 ± 5.3	9.0 ± 2.5			[23; 72]	extruded as above, s.h.t. (510 °C for 10 min) and w.q.
	T6	253.0 ± 0.2	277.0 ± 4.2	8.0 ± 2.9			[23; 72]	as above, aged at 200 °C
	as-extr.	182	250	19.4			[10]	cast, hom. at 400 °C for 24 h, extr. (direct, 1:28) at 400 °C with speed of 2 mmms ⁻¹
	as-cast	35.0 ± 1.0	106.0 ± 1.2	5.9 ± 0.1			[73]	cast in steel mold
Mg-0.7Al-0.3Ca-0.5Mn	as-extr.	316.0 ± 6.0	327.0 ± 2.3	4.3 ± 0.5			[73]	cast, hom. at 500 °C for 4 h, extr. (1:12) at 350 °C with ram-speed of 0.1 mmms ⁻¹
	T4	162.0 ± 1.2	247.0 ± 1.9	25.4 ± 0.8			[73]	as above, s.h.t. (500 °C for 10 min)
T6	248.0 ± 1.5	288.0 ± 3.0	21.0 ± 0.4			[73]	as above, aged at 200 °C for 16 h	

Table 3.4 continued from previous page

Alloy	Temper	YS [MPa]	UTS [MPa]	ϵ_f [%]	YSc [MPa]	UCS [MPa]	Source	Process Parameters
Mg-1.0Al-0.1Ca	rolled, O, TD		220	~20			[24]	cast, hot rolled at 430 °C to 50% thickness, annealed at 450 °C for 0.25 h, w.q.
Mg-1.2Al-0.3Zn-0.3Ca-0.4Mn	T4/s.h.t.	~125	~220	~30			[75]	cast, hom. at 300 °C for 4 h followed by 500 °C for 6 h and w.q., rolling at various conditions, s.h.t. at 450 °C for 1 h
Mg-1.2Al-0.5Ca-0.4Mn	T4	145	229	28			[74]	cast, hom. at 300 °C for 4 h followed by 450 °C for 6 h and w.q., rolling at 300 °C (from 10 to 5 mm, 4 passes), subsequent rolling at 100 °C (from 5 to 1 mm, 6 passes, reheated to 450 °C for 5 min, solutionized at 450 °C for 1 h
Mg-1.2Al-0.8Zn-0.5Ca-0.4Mn	T6 T4	196 144	256 242	27 32			[74] [74]	as above, aged at 200 °C for 1 h cast, hom. at 300 °C for 4 h followed by 450 °C for 6 h and w.q., rolling at 300 °C (from 10 to 5 mm, 4 passes), subsequent rolling at 100 °C (from 5 to 1 mm, 6 passes, reheated to 450 °C for 5 min, solutionized at 450 °C for 1 h
Mg-1.3Al-0.3Ca-0.5Mn	T6 T4/s.h.t.	204 187 ± 1	263 267 ± 2	27 18 ± 1	138 ± 3	448 ± 6	[74] [71]	as above, aged at 200 °C for 1 h cast, hom. at 500 °C for 1 h, extr. to round bars (in-direct w/o lubricant, 1:20) at 275 °C with a die-exit speed of 24 mm min ⁻¹ , s.h.t. (500 °C for 10 min) and w.q.
Mg-2.7Al-0.3Ca-0.4Mn	T5 T4/s.h.t.	287 ± 2 188 ± 1	306 ± 1 267 ± 2	20 ± 2 18 ± 1	194 ± 1 121 ± 5	472 ± 3 398 ± 4	[71] [71]	as above, aged at 200 °C for 0.5 h cast, hom. at 500 °C for 1 h, extr. to round bars (in-direct w/o lubricant, 1:20) at 275 °C with a die-exit speed of 24 mm min ⁻¹ , s.h.t. (500 °C for 10 min) and w.q.
	T5	240 ± 2	283 ± 1	18 ± 1	149 ± 1	427 ± 3	[71]	as above, aged at 200 °C for 0.5 h
Mg-Zn-Ca	Mg-0.2Zn-0.3Ca-0.1Mn	36	134	7.3			[85]	cast, cast, hom. at 400 °C for 12 h and 450 °C for 12 h, w.q.
	as-extr.	307		20.6			[85]	as above, extr. to round bars (indirect, 1:20) at 300 °C with a die-exit speed of 1.2 mm min ⁻¹
	as-extr.	164		30			[85]	as above, extr. to round bars (indirect, 1:20) at 350 °C with a die-exit speed of 1.2 mm min ⁻¹
Mg-0.8Ca-0.37Zr	rolled, O, RD	133	196	14			[50]	} cast, hom. at 300 °C for 12 h w.q., rolled at 450 °C from 5 to 1 mm thickness in 4 passes using cold rollers, reheating for 6 min between passes, annealed at 400 °C for 0.5 h
	rolled, O, TD	126	191	9			[50]	
	rolled, O, 45°	130	189	10			[50]	

Table 3.4 continued from previous page

Alloy	Temper	YS [MPa]	UTS [MPa]	ϵ_f [%]	YSc [MPa]	UCS [MPa]	Source	Process Parameters
Mg-0.8Ca-0.37Zr-0.3Zn	rolled, O, RD	134	205	29			[50]	cast, hom. at 300 °C for 12 h w.q., rolled at 450 °C from 5 to 1 mm thickness in 4 passes using cold rollers, reheating for 6 min between passes, annealed at 400 °C for 0.5 h as above, aged in oil at 200 °C for 1 h as above, deformed to 0.015 plastic strain, aged in oil at 200 °C for 1 h
	rolled, O, TD	104	198	34			[50]	
	rolled, O, 45°	110	200	32			[50]	
	rolled, T6	166	220	26			[50]	
Mg-0.6Zn-0.6Ca-0.1Zr	rolled, T8	201	226	20			[50]	
	as-rolled, RD	255 ± 2	276 ± 2	8			[31; 32]	Twin-rolled cast (5.3 mm), rolled at 370 to 400 °C in 7 passes, with intermediate heating for 0.25 h to a thickness of 1.8 mm, cooled at air as above, annealed at 370 °C for 0.5 h
	as-rolled, TD	200 ± 2	265 ± 2	23			[31; 32]	
	as-rolled, 45°	217 ± 3	255 ± 2	19			[31; 32]	
	rolled, O, RD	174 ± 3	239 ± 3	25			[31; 32]	
rolled, O, TD	135 ± 2	226 ± 2	31			[31; 32]		
Mg-0.7Zn-0.4Ca-0.1Mn	rolled, O, 45°	152 ± 3	232 ± 2	27			[31; 32]	
	as-extr.	108	220	37.0			[84]	cast, hom. at 400 °C for 12 h and 450 °C for 12 h, w.q., extr. to round bars (indirect, 1:20) at 300 °C with a die-exit speed of 6 m min ⁻¹
Mg-0.8Zn-0.2Ca	rolled, O, RD	92.5 ± 2.5	182.5 ± 0.5	24 ± 1			[80]	cast, hom. at 400 °C for 24 h, rolled (450 °C) from 5 to 1 mm in 8 passes, annealed at 400 °C for 0.5 h
	rolled, O, TD	61 ± 1	186.5 ± 2.0	30.5 ± 0.5			[80]	
Mg-1.0Zn-0.2Ca	rolled, O, 45°	68.5 ± 0.5	185 ± 2	32 ± 1			[80]	
	as-cast		125	8			[41]	cast, hom. at 430 °C for 22 h and w.q.
	SPD		225	16			[41]	as above, preheated to pressing temp. for 0.3 h, ECAP (120°, 6 mm min ⁻¹) for 2 passes at each temp. 400, 350 and 300 °C
Mg-1.0Zn-0.3Ca	SPD		263.7				[41]	ECAP as above, subseq. HPT (6 GPa) for 0.5 revolutions at RT
	SPD		283.3				[41]	ECAP as above, subseq. HPT (6 GPa) for 1 revolution at RT
	as-extr.	238	265	31	205		[28]	cast, hom. at 350 °C for 12 h and 450 °C for 8 h, cooled with pressurized air, aged at 250 °C for 0.5 h, heated to extr. temp. (300 °C) and held for 0.5 h, indirectly extr. to round bars (1.25) using a ram speed of 0.5 mm s ⁻¹ , cooled with pressurized air
	as-extr.	184	240	32	162		[28]	as above, heated to extr. temp. (325 °C) and held for 0.5 h, indirectly extr. to round bars (1.25) using a ram speed of 0.5 mm s ⁻¹ , cooled with pressurized air
	as-extr.	247	268	20	184		[28]	as above, heated to extr. temp. (325 °C) and held for 0.5 h, directly extr. to round bars (1.25) using a ram speed of 0.5 mm s ⁻¹ , cooled with pressurized air
Mg-1.0Zn-0.3Ca	as-extr.	140	226	25	119		[28]	as above, heated to extr. temp. (400 °C) and held for 0.5 h, directly extr. to round bars (1.25) using a ram speed of 0.5 mm s ⁻¹ , cooled with pressurized air
	as-extr.	240	255	27	205	245	[19]	as above, indirectly extr. to round bars (1.25) at 300 °C using a ram speed of 0.15 mm s ⁻¹

Table 3.4 continued from previous page

Alloy	Temper	YS [MPa]	UTS [MPa]	ϵ_f [%]	YSc [MPa]	UCS [MPa]	Source	Process Parameters
Mg-1.0Zn-0.5Ca	as-cast	55 ± 2	120 ± 5	5.0 ± 0.5			[42]	cast in steel mold
	as-extr.	297 ± 2	300 ± 5	8 ± 1			[42]	cast, hom. at 400 °C for 10 h, extr. (1:16) at 310 °C, using an extr. speed of 4 mm s ⁻¹
	as-extr.	197 ± 3	256 ± 5	17.0 ± 1.5			[42]	as above, extr. (1:16) at 330 °C, using an extr. speed of 4 mm s ⁻¹
	as-extr.	120 ± 3	200 ± 5	40 ± 3			[42]	as above, extr. (1:16) at 350 °C, using an extr. speed of 4 mm s ⁻¹
	as-extr.	105 ± 3	205 ± 5	44 ± 3			[42]	as above, extr. (1:16) at 370 °C, using an extr. speed of 4 mm s ⁻¹
	as-extr.	99 ± 3	201 ± 4	36 ± 2			[42]	as above, extr. (1:16) at 400 °C, using an extr. speed of 4 mm s ⁻¹
Mg-1.0Zn-0.9Ca	as-extr.	105	210	44			[60]	cast, extr. (1:16) at 350 °C, using an extr. speed of 2 mm s ⁻¹
	rolled, T4	154.9	234.3	12.3			[81]	cast, hom. at 440 °C for 1 h and w.q., hot rolled with 5 passes at 300 °C to a overall reduction of 50 %, intermediate reheating between the passes at 300 °C for 0.3 h, annealing at 440 °C for 0.5 h and w.q.
Mg-1.2Zn-0.4Ca-0.2Zr	rolled, O, RD	229.6 ± 2.8	264.0 ± 2.2	24.7 ± 2.4			[82]	cast, hom. at 400 °C for 4 h w.q., machined, rolled at 300 °C (5 passes, with intermediate annealing, total reduction 72%), subseq. annealed at 300 °C for 0.5 h
	rolled, O, 45°	290.8 ± 2.7	247.3 ± 0.2	32.3 ± 1.5			[82]	
Mg-1.4Zn-0.1MM-0.1Zr	rolled, O, TD	171.3 ± 2.2	248.9 ± 2.5	27.5 ± 1.8			[82]	cast, pre-heated at 340 °C, extr. (direct) to round bars at 300 °C, air cooled, annealed at 300 °C for 0.5 h
	extr., O	200 ± 7	250 ± 5	15.3 ± 0.3	150 ± 6	441 ± 3	[83]	
	Mg-1.4Zn-0.1MM-0.1Zr-0.4Ca	171 ± 2	243 ± 1	14.6 ± 0.0	148 ± 1	432 ± 6	[83]	
	Mg-1.4Zn-0.1MM-0.1Zr-0.8Ca	174 ± 1	243 ± 1	15.0 ± 1.1	149 ± 2	410 ± 4	[83]	
Various	extr., O	173	255	7			[97]	cast, hom. at 450 °C for 4 h air-cooled, machined, pre-heated to 450 °C for 1 h, extr. to round bars (1:25) air-cooled, annealed at 390 °C for 1 h
	Mg-1.8Mn-0.4Er	224	276				[97]	
	Mg-1.8Mn-0.7Er	228	275	12.5			[97]	
	Mg-1.8Mn-0.7Er-0.3Al			19			[97]	
	Mg-0.3Sn-0.7Y	99.1 ± 1.0	264.2 ± 2.0	32.7 ± 0.2			[101]	
	as-extr., ED	115.3 ± 0.5	226.8 ± 1.0	25.8 ± 0.3			[101]	
	as-extr., 45°	124.9 ± 1.0	236.7 ± 1.0	24.7 ± 0.2			[101]	
	as-extr., TD	90.9 ± 0.8	191.9 ± 1.3	39.7 ± 0.3			[103; 104]	
	as-extr., ED	115.4 ± 1.1	182.5 ± 1.2	28.3 ± 0.3			[103; 104]	
	as-extr., 45°	119.6 ± 1.2	182.5 ± 1.2	28.3 ± 0.3			[103; 104]	
rolled, T4, RD	110.5 ± 1.3	199.5 ± 0.8	29.7 ± 0.3			[103]	cast, hom. at 400 °C for 12 h, hot rolled with a mat. temp. of 400 °C and roll temp. of 160 °C, mat. reheated for 0.3 h after each pass, rolled to a sheet thickness of 1 mm with reductions of 20 %, subseq. annealed at 400 °C for 1 h and w.q.	
rolled, T4, 45°	109.9 ± 1.4	187.6 ± 0.7	34.7 ± 0.5			[103]		
rolled, T4, TD	133.1 ± 0.9	184.5 ± 1.3	31.2 ± 0.1			[103]		
Mg-0.4Sn-0.7Y-0.6Zn	as-extr., ED	188.4 ± 2.5	251.1 ± 1.4	33.1 ± 0.4			[104]	cast, hom. at 400 °C for 12 h, extr. (1:51) at 400 °C, using a ram speed of 3 mm s ⁻¹ to sheets
	as-extr., 45°	130.3 ± 3.8	221.8 ± 1.9	47.2 ± 0.1			[104]	
	as-extr., TD	124.3 ± 2.0	231.4 ± 1.3	39.1 ± 0.2			[104]	

Table 3.4 continued from previous page

Alloy	Temper	YS [MPa]	UTS [MPa]	ϵ_f [%]	YSc [MPa]	UCS [MPa]	Source	Process Parameters
Mg-0.5Sn-0.3Mn	as-extr., ED	130	239	10.4			[102]	cast, hom. at 400 °C for 10 h air-cooled, machined, extr. to sheets at 400 °C with an extr. speed of 1.2 m min ⁻¹
	as-extr., 45°	137	251	10			[102]	
	as-extr., TD	157	266	8.5			[102]	
Mg-0.5Sn-0.3Mn-0.3Y	as-extr., ED	141	288	30.3			[102]	cast, hom. at 400 °C for 10 h air-cooled, machined, extr. to sheets at 400 °C with an extr. speed of 1.2 m min ⁻¹
	as-extr., 45°	170	286	28.1			[102]	
	as-extr., TD	188	302	28			[102]	
Mg-1.1Sn-0.6Zn-0.5Ca	as-extr., ED	104.2 ± 1.8	311.9 ± 2.4	30.5 ± 1.4			[100]	cast, hom. at 400 °C for 12 h, extr. (1:32) at 400 °C, using a ram speed of 1 mms ⁻¹ to sheets with a thickness of 3 mm
	as-extr., TD	188.9 ± 2.5	295.6 ± 3.4	12.9 ± 0.4			[100]	
	as-extr., ED	129.4 ± 2.4	260.9 ± 2.7	17.6 ± 0.9			[100]	
Mg-1.2Sn-0.5Zn	as-extr., TD	153.1 ± 1.2	262.1 ± 1.9	14.3 ± 0.6			[100]	ram speed of 1 mms ⁻¹ to sheets with a thickness of 3 mm
	as-extr., ED	137.8 ± 3.2	264.8 ± 3.2	17.3 ± 1.1			[100]	
	as-extr., TD	209.3 ± 3.5	293.7 ± 3.2	10.3 ± 0.5			[100]	
Mg-0.5Zn-0.2Ca	as-extr.	119 ± 2	224 ± 1	25 ± 2	93 ± 1	331 ± 3	[88]	cast, hom. at 370 °C for 24 h and quenched in warm water, preheated to 375 °C for 1 h, indirectly extr. (1:25) at 375 °C, using an extr. speed of 2.2 mms ⁻¹ to round bars
	as-extr.	171 ± 2	249 ± 2	10 ± 1	75 ± 1	367 ± 6	[88]	
Mg-0.6Zn-0.3Zr-0.6Nd	rolled, O, RD	111	243	27.58			[89]	cast, hom. at 450 °C for 12 h and w.q., hot rolled at 400 °C from 8 to 2 mm at a reduction of 15 to 20 % per pass, intermediate reheating between the passes at 400 °C for 10 min, subseq. w.q., annealing at 440 °C for 1 h
	rolled, O, 45°	101	234	27.95			[89]	
	rolled, O, TD	84	238	28.61			[89]	
	rolled, O, RD	131	234	16.86			[89]	
	rolled, O, 45°	110	237	22.96			[89]	
	rolled, O, TD	115	222	12.61			[89]	
	rolled, O, RD	88	229	29.33			[89]	
	rolled, O, 45°	78	227	29.93			[89]	
	rolled, O, TD	66	233	32.19			[89]	
	rolled, O, RD	131	233	18.95			[89]	
	rolled, O, 45°	108	243	25.27			[89]	
	rolled, O, TD	99	247	24.86			[89]	
	rolled, O, RD	123	241	22.75			[89]	
	rolled, O, 45°	108	240	24.78			[89]	
	rolled, O, TD	96	243	25.34			[89]	
as-extr.	237	271	24	165	436	[93]	cast, hom. at 350 °C for 15 h, extr. to round bars (indir., 1:30) at 300 °C, using a speed of 1 m min ⁻¹ as above, using a speed of 5 m min ⁻¹	
Mg-1.0Zn-0.4Zr-0.8MM	as-extr.	196	248	19	96	370	[93]	cast, hom. at 350 °C for 15 h, extr. to round bars (indir., 1:30) at 300 °C, using a speed of 1 m min ⁻¹ as above, using a speed of 5 m min ⁻¹
	as-extr.	188	245	21	101	366	[93]	
	as-extr.	296	299	18	184	434	[93]	
Mg-1.0Zn-0.4Zr-0.8MM	as-extr.	221	260	21	156	381	[93]	cast, hom. at 350 °C for 15 h, extr. to round bars (indir., 1:30) at 300 °C, using a speed of 1 m min ⁻¹ as above, using a speed of 5 m min ⁻¹
	as-extr.	201	251	19	142	369	[93]	

Table 3.4 continued from previous page

Alloy	Temper	YS [MPa]	UTS [MPa]	ϵ_f [%]	YSc [MPa]	UCS [MPa]	Source	Process Parameters
Mg-1.2Zn-0.2Zr	rolled, O, RD	211.6 ± 2.3	247.4 ± 2.7	19.8 ± 1.6			[82]	cast, hom. at 400 °C for 4 h w.q., machined, rolled at 300 °C (5 passes, with intermediate annealing, total reduction 72%), subseq. annealed at 300 °C for 0.5 h cast, extr. to round bars (indir., 1:30) at 300 °C, using a speed of 1 m min ⁻¹ as above, using a speed of 10 m min ⁻¹ as above, using a speed of 20 m min ⁻¹ cast, extr. to round bars (indir., 1:30) at 300 °C, using a speed of 1 m min ⁻¹ as above, using a speed of 10 m min ⁻¹ as above, using a speed of 20 m min ⁻¹ cast, hom. at 480 °C for 12 h, indirectly extr. (1:20) at 300 °C with a die-exit speed of 6 m min ⁻¹ to round bars cast, hom. at 480 °C for 12 h, indirectly extr. (1:20) at 400 °C with a die-exit speed of 1.2 m min ⁻¹ to round bars cast, hom. at 480 °C for 12 h, indirectly extr. (1:20) at 350 °C with a die-exit speed of 1.2 m min ⁻¹ to round bars
	rolled, O, 45°	204.3 ± 0.5	242.6 ± 1.6	25.9 ± 1.3			[82]	
	rolled, O, TD	203.1 ± 2.5	243.5 ± 3.4	21.2 ± 0.8			[82]	
Mg-1.3Zn-0.1Ce	as-extr.	206 ± 1	261 ± 3	20.1 ± 0.4	124 ± 2	410 ± 7	[92]	
	as-extr.	176 ± 2	245 ± 2	11.7 ± 2.5	81 ± 1	361 ± 4	[92]	
Mg-1.3Zn-0.2Ce-0.5Zr	as-extr.	156 ± 2	226 ± 2	18.1 ± 1.3	70 ± 1	347 ± 1	[92]	
	as-extr.	305 ± 3	313 ± 3	21.0 ± 4.0	173 ± 1	436 ± 15	[92]	
	as-extr.	204 ± 1	257 ± 1	20.3 ± 0.9	126 ± 4	384 ± 13	[92]	
Mg-1.6Zn-0.5Gd	as-extr.	209 ± 2	259 ± 2	22.6 ± 0.5	124 ± 1	375 ± 3	[92]	
	as-extr.	117	213	30.1			[90]	
	as-extr.	283	295	10	154		[43]	
	as-extr.	161	233	24.7	111		[43]	
	as-extr.	254	284	27.9	190		[43]	
	as-extr.	181	248	34.8	134		[43]	
Mg-1.8Zn-0.1Nd-0.1Ce -0.05La-0.2Y	as-rolled, RD	270 ± 2	288 ± 2	19			[32]	Twin-rolled cast (5.3 mm), rolled at 370 to 400 °C in 7 passes, with intermediate heating for 0.25 h to a thickness of 1.8 mm, cooled at air subseq. cold rolled (2 passes, 0.1 truestrain) as above, annealed at 350 °C for 0.5 h Twin-rolled cast (5.3 mm), rolled at 370 to 400 °C in 7 passes, with intermediate heating for 0.25 h to a thickness of 1.8 mm, cooled at air subseq. cold rolled (2 passes, 0.1 truestrain) as above, annealed at 350 °C for 0.5 h
	as-rolled, TD	190 ± 5	266 ± 2	20			[32]	
	as-rolled, 45°	197 ± 3	250 ± 2	26			[32]	
	rolled, O, RD	181 ± 4	244 ± 4	33			[32]	
	rolled, O, TD	106 ± 3	221 ± 4	35			[32]	
	rolled, O, 45°	118 ± 4	215 ± 3	40			[32]	
	as-rolled, RD	298 ± 2	320 ± 4	16			[32]	
	as-rolled, TD	205 ± 3	286 ± 2	27			[32]	
	as-rolled, 45°	220 ± 3	282 ± 2	33			[32]	
	rolled, O, RD	197 ± 3	257 ± 2	33			[32]	
	rolled, O, TD	121 ± 2	232 ± 3	42			[32]	
	rolled, O, 45°	134 ± 3	231 ± 2	43			[32]	

3.7. References

- [1] B. Mordike, T. Ebert, Magnesium: properties—applications—potential, *Materials Science and Engineering: A* 302 (1) (2001) 37–45. doi:10.1016/S0921-5093(00)01351-4.
- [2] K. U. Kainer, 40 Years of Magnesium Research – Assessment of Contribution to the Progress in Magnesium Technology, in: 79th Annual IMA World Magnesium Conference, Budapest, IMA, 2019.
- [3] M. Esmaily, J. Svensson, S. Fajardo, N. Birbilis, G. Frankel, S. Virtanen, R. Arrabal, S. Thomas, L. Johansson, Fundamentals and advances in magnesium alloy corrosion, *Progress in Materials Science* 89 (2017) 92–193. doi:10.1016/j.pmatsci.2017.04.011.
- [4] J. Nie, K. Shin, Z. Zeng, Microstructure, Deformation, and Property of Wrought Magnesium Alloys, *Metalurgical and Materials Transactions A* 51 (12) (2020) 6045–6109. doi:10.1007/s11661-020-05974-z.
- [5] Y. Yang, X. Xiong, J. Chen, X. Peng, D. Chen, F. Pan, Research advances in magnesium and magnesium alloys worldwide in 2020, *Journal of Magnesium and Alloys* 9 (3) (2021) 705–747. doi:10.1016/j.jma.2021.04.001.
- [6] W. Sillekens, D. Letzig, The MagForge project: European Community research on forging of magnesium alloys, in: K. U. Kainer (Ed.), *Magnesium: Proceedings of the 7th International Conference on Magnesium Alloys and their Applications*, Wiley-VCH, Weinheim, GER, 2007.
- [7] J. Swiostek, J. Bober, C. Blawert, D. Letzig, W. Hintze, K. Kainer, Die forging of commercial and modified magnesium alloys, in: K. U. Kainer (Ed.), *Magnesium: Proceedings of the 7th International Conference on Magnesium Alloys and their Applications*, Wiley-VCH, Weinheim, GER, 2007, pp. 344–351.
- [8] S. Gneiger, Von der Anforderung zur Anwendung - modernes Legierungsdesign für Magnesiumbauteile, 70. BHT - Freiburger Universitätsforum, Germany, Freiberg (2019).
- [9] T. Nakata, T. Mezaki, R. Ajima, C. Xu, K. Oh-Ishi, K. Shimizu, S. Hanaki, T. Sasaki, K. Hono, S. Kamado, High-speed extrusion of heat-treatable Mg–Al–Ca–Mn dilute alloy, *Scripta Materialia* 101 (2015) 28–31. doi:10.1016/j.scriptamat.2015.01.010.
- [10] Z. Jiang, B. Jiang, H. Yang, Q. Yang, J. Dai, F. Pan, Influence of the Al₂Ca phase on microstructure and mechanical properties of Mg–Al–Ca alloys, *Journal of Alloys and Compounds* 647 (2015) 357–363. doi:10.1016/j.jallcom.2015.06.060.
- [11] Z. Li, X. Zhang, M. Zheng, X. Qiao, K. Wu, C. Xu, S. Kamado, Effect of Ca/Al ratio on microstructure and mechanical properties of Mg–Al–Ca–Mn alloys, *Materials Science and Engineering: A* 682 (2017) 423–432. doi:10.1016/j.msea.2016.11.026.
- [12] S. You, Y. Huang, K. U. Kainer, N. Hort, Recent research and developments on wrought magnesium alloys, *Journal of Magnesium and Alloys* 5 (3) (2017) 239–253. doi:10.1016/j.jma.2017.09.001.
- [13] Q. Wang, B. Jiang, D. Chen, Z. Jin, L. Zhao, Q. Yang, G. Huang, F. Pan, Strategies for enhancing the room-temperature stretch formability of magnesium alloy sheets: a review, *Journal of Materials Science* (2021) 1–34doi:10.1007/s10853-021-06067-x.
- [14] A. Schiffl, I. Schiffl, M. Hartmann, S. Brötz, J. Österreicher, W. Kühlein, Analysis of Impact Factors on Crash Performance of High Strength 6082 Alloys Consider Extrudability and Small Modifications of the Profile Geometry, *Materials Today: Proceedings* 10 (2019) 193–200. doi:10.1016/j.matpr.2018.10.396.
- [15] Y. Du, X. Qiao, M. Zheng, K. Wu, S. Xu, Development of high-strength, low-cost wrought Mg–2.5 mass% Zn alloy through micro-alloying with Ca and La, *Materials & Design* 85 (2015) 549–557. doi:10.1016/j.matdes.2015.07.029.
- [16] I. Basu, T. Al-Samman, Hierarchical twinning induced texture weakening in lean magnesium alloys, *Frontiers in Materials* 6 (2019) 187. doi:10.3389/fmats.2019.00187.
- [17] Z. Na, Z. Zhang, D. Jie, J. Li, D. Wenjiang, Selective oxidation behavior of an ignition-proof Mg–Y–Ca–Ce alloy, *Journal of Rare Earths* 31 (10) (2013) 1003–1008. doi:10.1016/S1002-0721(12)60394-9.
- [18] F. Czerwinski, Controlling the ignition and flammability of magnesium for aerospace applications, *Corrosion Science* 86 (2014) 1–16. doi:10.1016/j.corsci.2014.04.047.

- [19] J. Hofstetter, M. Becker, E. Martinelli, A. M. Weinberg, B. Mingler, H. Kilian, S. Pogatscher, P. J. Uggowitzer, J. F. Löffler, High-strength low-alloy (HSLA) Mg–Zn–Ca alloys with excellent biodegradation performance, *JOM* 66 (4) (2014) 566–572. doi:10.1007/s11837-014-0875-5.
- [20] Z. Zeng, Y. Zhu, S. Xu, M. Bian, C. Davies, N. Birbilis, J. Nie, Texture evolution during static recrystallization of cold-rolled magnesium alloys, *Acta Materialia* 105 (2016) 479–494. doi:10.1016/j.actamat.2015.12.045.
- [21] S. Sanyal, S. Kanodia, R. Saha, T. Bandyopadhyay, S. Mandal, Influence of hard plate hot forging temperature on the microstructure, texture and mechanical properties in a lean Mg–Zn–Al alloy, *Journal of Alloys and Compounds* (2019). doi:10.1016/j.jallcom.2019.06.026.
- [22] P. J. Uggowitzer, M. Cihova, D. Horwatitsch, T. Hametner, S. Pogatscher, D. Klaumünzer, J. F. Löffler, Designkonzepte für niedriglegierte hochfeste Magnesiumlegierungen, in: *Proceedings of 9. Ranshofener Leichtmetalltage*, LKR-Verlag, 2016, pp. 109–118.
- [23] M. Cihova, R. Schäublin, L. B. Hauser, S. S. Gerstl, C. Simson, P. Uggowitzer, J. F. Löffler, Rational design of a lean magnesium-based alloy with high age-hardening response, *Acta Materialia* 158 (2018) 214–229. doi:10.1016/j.actamat.2018.07.054.
- [24] S. Sandlöbes, M. Friák, S. Korte-Kerzel, Z. Pei, J. Neugebauer, D. Raabe, A rare-earth free magnesium alloy with improved intrinsic ductility, *Scientific reports* 7 (10458) (2017) 1–8. doi:10.1038/s41598-017-10384-0.
- [25] T. Al-Samman, G. Gottstein, Dynamic recrystallization during high temperature deformation of magnesium, *Materials Science and Engineering: A* 490 (1-2) (2008) 411–420. doi:10.1016/j.msea.2008.02.004.
- [26] J. Su, S. Kaboli, A. S. H. Kabir, I.-H. Jung, S. Yue, Effect of dynamic precipitation and twinning on dynamic recrystallization of micro-alloyed Mg–Al–Ca alloys, *Materials Science and Engineering: A* 587 (2013) 27–35. doi:10.1016/j.msea.2013.08.019.
- [27] Z. Zeng, N. Stanford, C. H. J. Davies, J.-F. Nie, N. Birbilis, Magnesium extrusion alloys: a review of developments and prospects, *International Materials Reviews* 64 (1) (2019) 27–62. doi:10.1080/09506608.2017.1421439.
- [28] J. Hofstetter, S. Rüedi, I. Baumgartner, H. Kilian, B. Mingler, E. Povoden-Karadeniz, S. Pogatscher, P. J. Uggowitzer, J. F. Löffler, Processing and microstructure–property relations of high-strength low-alloy (HSLA) Mg–Zn–Ca alloys, *Acta Materialia* 98 (2015) 423–432. doi:10.1016/j.actamat.2015.07.021.
- [29] G. Zhu, L. Wang, H. Zhou, J. Wang, Y. Shen, P. Tu, H. Zhu, W. Liu, P. Jin, X. Zeng, Improving ductility of a Mg alloy via non-basal $\langle a \rangle$ slip induced by Ca addition, *International Journal of Plasticity* 120 (2019) 164–179. doi:10.1016/j.ijplas.2019.04.020.
- [30] J. Hirth, *Physical Metallurgy* (Fourth Edition). Fourth edition. Chapter 20-Dislocations., Oxford: North-Holland, 1996, ISBN 9780444898753. doi:10.1016/B978-044489875-3/50025-9.
- [31] D. Klaumünzer, J. V. Hernandez, S. Yi, D. Letzig, S.-h. Kim, J. J. Kim, M. H. Seo, K. Ahn, Magnesium process and alloy development for applications in the automotive industry, in: *Magnesium Technology 2019*, Springer, 2019, pp. 15–20. doi:10.1007/978-3-030-05789-3_3.
- [32] J. Victoria-Hernández, S. Yi, D. Klaumünzer, D. Letzig, Comparison of the Mechanical Properties and Forming Behavior of Two Texture-Weakened Mg-Sheet Alloys Produced by Twin Roll Casting, *Frontiers in Materials* 6 (288) (2019) 1–11. doi:10.3389/fmats.2019.00288.
- [33] I. Basu, M. Chen, J. Wheeler, R. Schäublin, J. Löffler, Stacking-fault mediated plasticity and strengthening in lean, rare-earth free magnesium alloys, *Acta Materialia* 116877 (2021) 17. doi:10.1016/j.actamat.2021.116877.
- [34] J. P. Hadorn, K. Hantzsche, S. Yi, J. Bohlen, D. Letzig, J. A. Wollmershauser, S. R. Agnew, Role of solute in the texture modification during hot deformation of Mg-rare earth alloys, *Metallurgical and Materials Transactions A* 43 (4) (2012) 1347–1362. doi:10.1007/s11661-011-0923-5.
- [35] R. Agarwal, D. R. Trinkle, Ab initio magnesium-solute transport database using exact diffusion theory, *Acta Materialia* 150 (2018) 339–350. doi:10.1016/j.actamat.2018.03.025.
- [36] N. P. Papenberg, S. Gneiger, I. Weißensteiner, P. J. Uggowitzer, S. Pogatscher, Mg-Alloys for forging applications—A review, *Materials* 13(4) (985) (2020) 1–61. doi:10.3390/ma13040985.

- [37] W. Yuan, S. Panigrahi, J.-Q. Su, R. Mishra, Influence of grain size and texture on Hall–Petch relationship for a magnesium alloy, *Scripta Materialia* 65 (11) (2011) 994–997. doi:10.1016/j.scriptamat.2011.08.028.
- [38] Y. Wang, H. Choo, Influence of texture on Hall–Petch relationships in an Mg alloy, *Acta Materialia* 81 (2014) 83–97. doi:10.1016/j.actamat.2014.08.023.
- [39] H. Yu, Y. Xin, M. Wang, Q. Liu, Hall-Petch relationship in Mg alloys: a review, *Journal of Materials Science & Technology* 34 (2) (2018) 248–256. doi:10.1016/j.jmst.2017.07.022.
- [40] T. Nakata, T. Mezaki, C. Xu, K. Oh-Ishi, K. Shimizu, S. Hanaki, S. Kamado, Improving tensile properties of dilute Mg-0.27 Al-0.13 Ca-0.21 Mn (at.%) alloy by low temperature high speed extrusion, *Journal of Alloys and Compounds* 648 (2015) 428–437. doi:10.1016/j.jallcom.2015.07.051.
- [41] G. Khudododova, O. Kulyasova, R. Islamgaliev, R. Valiev, Microstructure and mechanical properties of the Mg–Zn–Ca biodegradable alloy after severe plastic deformation, in: *IOP Conference Series: Materials Science and Engineering*, Vol. 672, IOP Publishing, 2019, pp. 1–4. doi:10.1088/1757-899X/672/1/012030.
- [42] B. Zhang, L. Geng, L. Huang, X. Zhang, C. Dong, Enhanced mechanical properties in fine-grained Mg–1.0 Zn–0.5 Ca alloys prepared by extrusion at different temperatures, *Scripta Materialia* 63 (10) (2010) 1024–1027. doi:10.1016/j.scriptamat.2010.07.038.
- [43] M. Jiang, C. Xu, T. Nakata, H. Yan, R. Chen, S. Kamado, Enhancing strength and ductility of Mg-Zn-Gd alloy via slow-speed extrusion combined with pre-forging, *Journal of Alloys and Compounds* 694 (2017) 1214–1223. doi:10.1016/j.jallcom.2016.10.109.
- [44] S. Razavi, D. Foley, I. Karaman, K. Hartwig, O. Duygulu, L. Kecskes, S. Mathaudhu, V. Hammond, Effect of grain size on prismatic slip in Mg–3Al–1Zn alloy, *Scripta Materialia* 67 (5) (2012) 439–442. doi:10.1016/j.scriptamat.2012.05.017.
- [45] I. Polmear, *Aluminium Alloys—A Century of Age Hardening*, in: A. M. J.F. Nie, B. Muddle (Eds.), *Materials forum*, Vol. 28, 2004, pp. 1–14.
- [46] K. Hono, C. Mendis, T. Sasaki, K. Oh-Ishi, Towards the development of heat-treatable high-strength wrought Mg alloys, *Scripta Materialia* 63 (7) (2010) 710–715. doi:10.1016/j.scriptamat.2010.01.038.
- [47] J.-F. Nie, Precipitation and hardening in magnesium alloys, *Metallurgical and Materials Transactions A* 43 (11) (2012) 3891–3939. doi:10.1007/s11661-012-1217-2.
- [48] J. Su, S. Kaboli, A. S. H. Kabir, P. Vo, I.-H. Jung, S. Yue, Precipitation behaviour of micro-alloyed Mg-Al-Ca alloys during heat treatment and hot compression, in: *Magnesium Technology 2012*, Springer, 2012, pp. 317–322. doi:10.1007/978-3-319-48203-3_58.
- [49] P. Manohar, M. Ferry, T. Chandra, Five decades of the Zener equation, *ISIJ international* 38 (9) (1998) 913–924. doi:10.2355/isijinternational.38.913.
- [50] M. Z. Bian, Z. R. Zeng, S. W. Xu, S. M. Zhu, Y. M. Zhu, C. H. J. Davies, N. Birbilis, J. F. Nie, Improving formability of Mg–Ca–Zr sheet alloy by microalloying of Zn, *Advanced Engineering Materials* 18 (10) (2016) 1763–1769. doi:10.1002/adem.201600293.
- [51] Y. Zuo, X. Fu, D. Mou, Q. Zhu, L. Li, J. Cui, Study on the role of Ca in the grain refinement of Mg–Ca binary alloys, *Materials Research Innovations* 19 (sup1) (2015) S1–94. doi:10.1179/1432891715Z.0000000001376.
- [52] F. Jianfeng, C. Zhiyuan, Y. Weidong, F. Shuang, X. Bingshe, Effect of yttrium, calcium and zirconium on ignition-proof principle and mechanical properties of magnesium alloys, *Journal of Rare Earths* 30 (1) (2012) 74–78. doi:10.1016/S1002-0721(10)60642-4.
- [53] F. Jianfeng, Y. Changlin, X. Bingshe, Effect of Ca and Y additions on oxidation behavior of magnesium alloys at high temperatures, *Journal of Rare Earths* 30 (5) (2012) 497–502. doi:10.1016/S1002-0721(12)60079-9.
- [54] O. Mihriban, E. B. Pekguleryuz, Creep resistant magnesium diecasting alloys based on alkaline earth elements, *Mater Trans JIM* 42 (7) (2001) 1258–1293. doi:10.2320/matertrans.42.1258.
- [55] A. A. Luo, B. R. Powell, M. P. Balogh, Creep and microstructure of magnesium-aluminum-calcium based alloys, *Metallurgical and Materials Transactions A* 33 (3) (2002) 567–574. doi:10.1007/s11661-002-0118-1.

- [56] A. A. Luo, Recent magnesium alloy development for elevated temperature applications, *International materials reviews* 49 (1) (2004) 13–30. doi:10.1179/095066004225010497.
- [57] Z. Pei, J. Yin, The relation between two ductility mechanisms for Mg alloys revealed by high-throughput simulations, *Materials & Design* 186 (108286) (2020) 1–6. doi:10.1016/j.matdes.2019.108286.
- [58] Y. Chino, T. Ueda, Y. Otomatsu, K. Sassa, X. Huang, K. Suzuki, M. Mabuchi, Effects of Ca on tensile properties and stretch formability at room temperature in Mg-Zn and Mg-Al alloys, *Materials Transactions* 52 (7) (2011) 1477–1482. doi:10.2320/matertrans.M2011048.
- [59] D. Guan, X. Liu, J. Gao, L. Ma, B. P. Wynne, W. M. Rainforth, Exploring the mechanism of “Rare Earth” texture evolution in a lean Mg-Zn-Ca alloy, *Scientific reports* 9 (7152) (2019) 1–11. doi:10.1038/s41598-019-43415-z.
- [60] B. Zhang, Y. Wang, L. Geng, C. Lu, Effects of calcium on texture and mechanical properties of hot-extruded Mg-Zn-Ca alloys, *Materials Science and Engineering: A* 539 (2012) 56–60. doi:10.1016/j.msea.2012.01.030.
- [61] M. M. Avedesian, H. Baker, et al., *ASM specialty handbook: magnesium and magnesium alloys*, ASM International, Materials Park, OH, USA, 1999, ISBN 978-0-87170-657-7.
- [62] E. F. Emley, *Principles of magnesium technology*, Pergamon Press, Oxford, UK, 1966, ISBN 9780080106731.
- [63] L. Rokhlin, T. Dobatkina, N. Nikitina, I. Tarytina, Calcium-alloyed magnesium alloys, *Metal Science and Heat Treatment* 51 (3–4) (2009) 164–169. doi:10.1007/s11041-009-9127-7.
- [64] K. P. Rao, Y. V. R. K. Prasad, C. Dharmendra, K. Suresh, N. Hort, H. Dieringa, Review on Hot Working Behavior and Strength of Calcium-Containing Magnesium Alloys, *Advanced Engineering Materials* 20 (1701102) (2018) 1–19. doi:10.1002/adem.201701102.
- [65] S. Xu, K. Oh-Ishi, S. Kamado, F. Uchida, T. Homma, K. Hono, High-strength extruded Mg-Al-Ca-Mn alloy, *Scripta Materialia* 65 (3) (2011) 269–272. doi:10.1016/j.scriptamat.2011.04.026.
- [66] T. Murai, S.-I. Matsuoka, S. Miyamoto, Y. Oki, S. Nagao, H. Sano, Effects of zinc and manganese contents on extrudability of Mg-Al-Zn alloys, *Journal of Japan Institute of Light Metals* 53 (1) (2003) 27–31. doi:10.2464/jilm.54.472.
- [67] C. Davies, M. Barnett, Expanding the extrusion limits of wrought magnesium alloys, *JOM* 56 (5) (2004) 22–24. doi:10.1007/s11837-004-0121-7.
- [68] T. Murai, Extrusion of magnesium alloys, *Journal of Japan Institute of Light Metals* 54 (11) (2004) 472–477. doi:10.2464/jilm.53.27.
- [69] D. L. Atwell, M. R. Barnett, Extrusion limits of magnesium alloys, *Metallurgical and Materials Transactions A* 38A (12) (2007) 3032–3041. doi:10.1007/s11661-007-9323-2.
- [70] T. Nakata, C. Xu, Y. Matsumoto, K. Shimizu, T. Sasaki, K. Hono, S. Kamado, Optimization of Mn content for high strengths in high-speed extruded Mg-0.3Al-0.3Ca (wt%) dilute alloy, *Materials Science and Engineering: A* 673 (2016) 443–449. doi:10.1016/j.msea.2016.07.098.
- [71] T. Nakata, C. Xu, R. Ajima, K. Shimizu, S. Hanaki, T. Sasaki, L. Ma, K. Hono, S. Kamado, Strong and ductile age-hardening Mg-Al-Ca-Mn alloy that can be extruded as fast as aluminum alloys, *Acta Materialia* 130 (2017) 261–270. doi:10.1016/j.actamat.2017.03.046.
- [72] M. Cihova, R. Schäublin, S. Gerstl, L. Hauser, C. Simson, N. Papenberg, S. Gneiger, C. M. Schlögl, P. J. Uggowitzer, J. F. Löffler, Mikrostruktur-Eigenschafts-Korrelationen in aushärtbaren mageren Mg-Legierungen, in: *Proceedings of 10. Ranshofener Leichtmetalltage*, LKR-Verlag, 2018, pp. 51–61.
- [73] X. Liu, X. Qiao, Z. Li, M. Zheng, High strength and excellent ductility of dilute Mg-0.68 Al-0.32 Ca-0.50 Mn (wt%) extrusion alloy obtained by T6 treatment, *Materials Characterization* 162 (110197) (2020) 1–9. doi:10.1016/j.matchar.2020.110197.
- [74] M. Bian, T. Sasaki, B. Suh, T. Nakata, S. Kamado, K. Hono, A heat-treatable Mg-Al-Ca-Mn-Zn sheet alloy with good room temperature formability, *Scripta Materialia* 138 (2017) 151–155. doi:10.1016/j.scriptamat.2017.05.034.

- [75] M. Bian, T. Sasaki, T. Nakata, S. Kamado, K. Hono, Effects of rolling conditions on the microstructure and mechanical properties in a Mg–Al–Ca–Mn–Zn alloy sheet, *Materials Science and Engineering: A* 730 (2018) 147–154. doi:[10.1016/j.msea.2018.05.065](https://doi.org/10.1016/j.msea.2018.05.065).
- [76] K. P. Rao, K. Suresh, Y. V. R. K. Prasad, C. Dharmendra, N. Hort, H. Dieringa, High Temperature Strength and Hot Working Technology for As-Cast Mg–1Zn–1Ca (ZX11) Alloy, *Metals* 7 (405) (2017) 1–16. doi:[10.3390/met7100405](https://doi.org/10.3390/met7100405).
- [77] K. Oh-Ishi, R. Watanabe, C. Mendis, K. Hono, Age-hardening response of Mg–0.3 at.% Ca alloys with different Zn contents, *Materials Science and Engineering: A* 526 (1-2) (2009) 177–184. doi:[10.1016/j.msea.2009.07.027](https://doi.org/10.1016/j.msea.2009.07.027).
- [78] Z. Zeng, Y. Zhu, M. Bian, S. Xu, C. Davies, N. Birbilis, J. Nie, Annealing strengthening in a dilute Mg–Zn–Ca sheet alloy, *Scripta Materialia* 107 (2015) 127–130. doi:[10.1016/j.scriptamat.2015.06.002](https://doi.org/10.1016/j.scriptamat.2015.06.002).
- [79] Z. Zeng, M. Bian, S. Xu, C. Davies, N. Birbilis, J. Nie, Texture evolution during cold rolling of dilute Mg alloys, *Scripta Materialia* 108 (2015) 6–10. doi:[10.1016/j.scriptamat.2015.06.009](https://doi.org/10.1016/j.scriptamat.2015.06.009).
- [80] Z. Zeng, M. Bian, S. Xu, C. Davies, N. Birbilis, J. Nie, Effects of dilute additions of Zn and Ca on ductility of magnesium alloy sheet, *Materials Science and Engineering: A* 674 (2016) 459–471. doi:[10.1016/j.msea.2016.07.049](https://doi.org/10.1016/j.msea.2016.07.049).
- [81] D.-W. Kim, B.-C. Suh, M.-S. Shim, J. Bae, D. H. Kim, N. J. Kim, Texture evolution in Mg–Zn–Ca alloy sheets, *Metallurgical and Materials Transactions A* 44 (7) (2013) 2950–2961. doi:[10.1007/s11661-013-1674-2](https://doi.org/10.1007/s11661-013-1674-2).
- [82] N. Xia, C. Wang, Y. Gao, Z.-M. Hua, C.-Y. Ma, C.-F. Du, H. Zhang, H.-M. Zhang, M.-X. Li, M. Zha, H.-Y. Wang, Enhanced ductility of Mg–1Zn–0.2 Zr alloy with dilute Ca addition achieved by activation of non-basal slip and twinning, *Materials Science and Engineering: A* 813 (141128) (2021) 1–8. doi:[10.1016/j.msea.2021.141128](https://doi.org/10.1016/j.msea.2021.141128).
- [83] S. Kamrani, C. Fleck, Effects of calcium and rare-earth elements on the microstructure and tension–compression yield asymmetry of ZEK100 alloy, *Materials Science and Engineering: A* 618 (2014) 238–243. doi:[10.1016/j.msea.2014.09.023](https://doi.org/10.1016/j.msea.2014.09.023).
- [84] M. Jiang, C. Xu, T. Nakata, H. Yan, R. Chen, S. Kamado, High-speed extrusion of dilute Mg–Zn–Ca–Mn alloys and its effect on microstructure, texture and mechanical properties, *Materials Science and Engineering: A* 678 (2016) 329–338. doi:[10.1016/j.msea.2016.10.007](https://doi.org/10.1016/j.msea.2016.10.007).
- [85] M. Jiang, C. Xu, T. Nakata, H. Yan, R. Chen, S. Kamado, Development of dilute Mg–Zn–Ca–Mn alloy with high performance via extrusion, *Journal of Alloys and Compounds* 668 (2016) 13–21. doi:[10.1016/j.jallcom.2016.01.195](https://doi.org/10.1016/j.jallcom.2016.01.195).
- [86] M. Cihova, E. Martinelli, P. Schmutz, A. Myrissa, R. Schäublin, A. M. Weinberg, P. Uggowitzer, J. F. Löffler, The role of zinc in the biocorrosion behavior of resorbable Mg–Zn–Ca alloys, *Acta biomaterialia* 100 (2019) 398–414. doi:[10.1016/j.actbio.2019.09.021](https://doi.org/10.1016/j.actbio.2019.09.021).
- [87] P. Jiang, C. Blawert, R. Hou, N. Scharnagl, J. Bohlen, M. L. Zheludkevich, Microstructural influence on corrosion behavior of MgZnGe alloy in NaCl solution, *Journal of Alloys and Compounds* 783 (2019) 179–192. doi:[10.1016/j.jallcom.2018.12.296](https://doi.org/10.1016/j.jallcom.2018.12.296).
- [88] P. Jiang, C. Blawert, R. Hou, J. Bohlen, N. Konchakova, M. L. Zheludkevich, A comprehensive comparison of the corrosion performance, fatigue behavior and mechanical properties of micro-alloyed MgZnCa and MgZnGe alloys, *Materials & Design* 185 (2020) 108285. doi:[10.1016/j.matdes.2019.108285](https://doi.org/10.1016/j.matdes.2019.108285).
- [89] T. Al-Samman, X. Li, Sheet texture modification in magnesium-based alloys by selective rare earth alloying, *Materials Science and Engineering: A* 528 (10-11) (2011) 3809–3822. doi:[10.1016/j.msea.2011.01.080](https://doi.org/10.1016/j.msea.2011.01.080).
- [90] M. Jiang, C. Xu, T. Nakata, H. Yan, R. Chen, S. Kamado, Rare earth texture and improved ductility in a Mg–Zn–Gd alloy after high-speed extrusion, *Materials Science and Engineering: A* 667 (2016) 233–239. doi:[10.1016/j.msea.2016.04.093](https://doi.org/10.1016/j.msea.2016.04.093).
- [91] M. Jiang, C. Xu, H. Yan, S. Lu, T. Nakata, C. Lao, R. Chen, S. Kamado, E. Han, Correlation between dynamic recrystallization and formation of rare earth texture in a Mg–Zn–Gd magnesium alloy during extrusion, *Scientific reports* 8 (16800) (2018) 1–11. doi:[10.1038/s41598-018-35170-4](https://doi.org/10.1038/s41598-018-35170-4).

- [92] P. Dobroň, F. Chmelík, K. Parfenenko, D. Letzig, J. Bohlen, On the Effect of the Extrusion Speed on Microstructure and Plastic Deformation of ZE10 and ZEK100 Magnesium Alloys-an Acoustic Emission Study., *Acta Physica Polonica*, A. 122 (3) (2012) 593–596. doi:10.12693/APhysPolA.122.593.
- [93] E. Meza-García, Influence of alloying elements on the microstructure and mechanical properties of extruded Mg-Zn based alloys, Ph.D. thesis, Technischen Universität, Berlin, Germany (2010).
- [94] E. Meza-García, J. Bohlen, S. Yi, D. Letzig, V. Kräusel, D. Landgrebe, K. Kainer, Influence of alloying elements and extrusion process parameter on the recrystallization process of Mg-Zn alloys, *Materials Today: Proceedings* 2 (2015) 19–25. doi:10.1016/j.matpr.2015.05.004.
- [95] R. Matsumoto, M. Otsu, M. Yamasaki, T. Mayama, H. Utsunomiya, Y. Kawamura, Application of mixture rule to finite element analysis for forging of cast Mg-Zn-Y alloys with long period stacking ordered structure, *Materials Science and Engineering: A* 548 (2012) 75–82. doi:10.1016/j.msea.2012.03.088.
- [96] E. Zhang, W. He, H. Du, K. Yang, Microstructure, mechanical properties and corrosion properties of Mg-Zn-Y alloys with low Zn content, *Materials Science and Engineering: A* 488 (1-2) (2008) 102–111. doi:10.1016/j.msea.2007.10.056.
- [97] J. Zhang, F. Yuan, M. Liu, F. Pan, Microstructure and mechanical properties of Mg-1.8% Mn alloy modified by single Er and composite Er/Al microalloying, *Materials Science and Engineering: A* 576 (2013) 185–191. doi:10.1016/j.msea.2013.03.086.
- [98] P. Hidalgo-Manrique, J. Robson, M. Pérez-Prado, Precipitation strengthening and reversed yield stress asymmetry in Mg alloys containing rare-earth elements: A quantitative study, *Acta Materialia* 124 (2017) 456–467. doi:10.1016/j.actamat.2016.11.019.
- [99] P. Hidalgo-Manrique, V. Herrera-Solaz, J. Segurado, J. Llorca, F. Gálvez, O. A. Ruano, S. Yi, M. T. Pérez-Prado, Origin of the reversed yield asymmetry in Mg-rare earth alloys at high temperature, *Acta Materialia* 92 (2015) 265–277. doi:10.1016/j.actamat.2015.03.053.
- [100] Y. Chai, B. Jiang, J. Song, B. Liu, G. Huang, D. Zhang, F. Pan, Effects of Zn and Ca addition on microstructure and mechanical properties of as-extruded Mg-1.0 Sn alloy sheet, *Materials Science and Engineering: A* 746 (2019) 82–93. doi:10.1016/j.msea.2019.01.028.
- [101] Q. Wang, Y. Shen, B. Jiang, A. Tang, J. Song, Z. Jiang, T. Yang, G. Huang, F. Pan, A micro-alloyed Mg-Sn-Y alloy with high ductility at room temperature, *Materials Science and Engineering: A* 735 (2018) 131–144. doi:10.1016/j.msea.2018.08.035.
- [102] X. Qian, Y. Zeng, B. Jiang, Q. Yang, Y. Wan, G. Quan, F. Pan, Grain refinement mechanism and improved mechanical properties in Mg-Sn alloy with trace Y addition, *Journal of Alloys and Compounds* 820 (153122) (2020) 1–12. doi:10.1016/j.jallcom.2019.153122.
- [103] Q. Wang, Y. Shen, B. Jiang, A. Tang, Y. Chai, J. Song, T. Yang, G. Huang, F. Pan, A good balance between ductility and stretch formability of dilute Mg-Sn-Y sheet at room temperature, *Materials Science and Engineering: A* 736 (2018) 404–416. doi:10.1016/j.msea.2018.09.011.
- [104] Q. Wang, B. Jiang, A. Tang, C. He, D. Zhang, J. Song, T. Yang, G. Huang, F. Pan, Formation of the elliptical texture and its effect on the mechanical properties and stretch formability of dilute Mg-Sn-Y sheet by Zn addition, *Materials Science and Engineering: A* 746 (2019) 259–275. doi:10.1016/j.msea.2019.01.040.

4. Forging of AXMZ1000 Alloy on Industrial Scale

The development process from material investigation up to industrial sized forging trials is shown in the following section. Cast and homogenized AXMZ1000 material is analyzed regarding its forming behavior and compiled into a processing map. The predicted forming window is verified by laboratory sized trials and a complex part geometry is subsequently forged on industrial scale.

The following section has been published in the shape of a scientific paper.

Forging of an age-hardenable Mg–Al–Ca–Mn–Zn alloy on industrial scale

Published in: SN Applied Sciences, (2023)5:14; [doi:10.1007/s42452-022-05240-4](https://doi.org/10.1007/s42452-022-05240-4)
Received: 10 August 2022; Accepted: 28 November 2022

Authors: Nikolaus Papenberg, Thomas Hatzenbichler, Florian Grabner, Peter J. Uggowitzer, Stefan Pogatscher

Author contribution: Conceptualization: Nikolaus Papenberg, Peter J. Uggowitzer; Methodology: Florian Grabner; Formal analysis and investigation: Nikolaus Papenberg; Writing - original draft preparation: Nikolaus Papenberg; Writing - review and editing: Nikolaus Papenberg, Thomas Hatzenbichler, Florian Grabner, Peter J. Uggowitzer, Stefan Pogatscher; Funding acquisition: Stefan Pogatscher; Resources: Thomas Hatzenbichler; Supervision: Peter J. Uggowitzer, Stefan Pogatscher

Keywords: magnesium wrought alloy, Mg-Al-Ca-Mn-Zn alloy, closed die forging, material characterization, processing map

Abstract: Weight reduction plays an important role in transportation industries, directly impacting on fuel consumption and vehicle range. The use of multi-material mixes is common practice, allowing for an optimum application of specific material properties. Light metals, primarily aluminum alloys, are used in both, cast and wrought state, to good effect. On the other hand, magnesium alloys, which are still lighter by one third, are used in castings exclusively. While scientific research and development on Mg wrought alloys is progressing steadily, industrial implementation is still scarce. As a result, safety relevant and structural applications made from Mg wrought products are nearly nonexistent. To increase acceptance and facilitate industrial application for this interesting class of materials we investigated the forging process of an original-sized automotive control arm. To ease industrial access, the used age hardenable Mg-Al-Ca-Zn-Mn lean alloy, can be processed similarly to Al alloys, e.g. 6xxx series. This work describes the development sequence, starting with the analysis of the forming window, followed by laboratory forging trials and industrial sized part production, providing information on forming characteristics as well as possible difficulties.

Funding: We gratefully acknowledge the financial support of this work within the scope of the AMALFI project. AMALFI is a COMET Project within the COMET–Competence Centers for Excellent Technologies Program and funded by BMK, BMDW, and the federal state of Upper Austria. The COMET Program is managed by the FFG (grant number 872641).

Published as an open access article distributed under the terms and conditions of the Creative Commons Attribution (CC BY) license (<https://creativecommons.org/licenses/by/4.0/>). The only changes made are related to layout and internal document accessibility.

4.1. Introduction

Given the ever-increasing pressure on the transportation industries to improve vehicle fuel efficiency and range, lightweighting is a topic of high interest. As light metals, especially Al alloys, are increasingly used in mid to high class cars [1], the industry has started to look for further optimization potential in terms of structural light metals. Mg alloys can provide a good combination of low weight and high specific properties for such structural applications. This has already been recognized for consumer electronics and various non-structural applications, where castings are in common use [2]. Nevertheless, the use of Mg wrought alloys, which can provide increased mechanical properties when compared to castings, is still lacking. This is mainly based on the large disparity in the production effort of castings versus wrought products made from Mg alloys. While the casting of complex geometries is appealing because of the good melt flow behavior of Mg [3], the deformation of Mg alloys is often considered problematic. This judgment is mainly based on the fact that forming has to be done at elevated temperatures, as well as on the lack of know-how resulting from the missing industrial utilization of Mg wrought products [4; 5].

To counteract this, scientific investigations concerning the production of sheets, extrusion and forgings made from Mg alloys are steadily increasing [6]. Nevertheless, the upscaling from laboratory trials to industrial production poses a multitude of challenges, which must be overcome.

To ease access of new materials for industrial applications, changes in standard production routines, such as processing and material handling, should be kept to a minimum. Therefore, a Mg alloy, which follows the same processing route as age-hardenable Al alloys (e.g. 6xxx series) has been chosen for industrial production trials by forging. Forgings allow for a broad variation of processing parameters by the interaction of material and die temperatures, forming speed and part complexity, thereby markedly increasing the process flexibility. Additionally, the processing of Mg alloys takes place at similar or slightly lower material temperatures when compared to Al forgings, further reducing complexity for industrial trials [7–9].

Age-hardenable Mg alloys, which have a similar processing sequence as Al alloys, consisting of casting, homogenization, forming operation, solution heat treatment and artificial ageing, have been well discussed in literature [10]. The resulting alloys are often characterized by a low amount of alloying elements to reduce solute drag and increase the available temperature window for solution heat treatment procedures. Also, there is a visible trend towards Ca containing alloys, allowing for a broad range of useable alloying elements. The used Mg-Al-Ca-Mn-Zn alloy (AXMZ1000) has a well-balanced elemental spectrum: Mn improves the corrosion behavior and is able to form dispersoids in combination with Al (e.g. Al_8Mn_5), stabilizing the grain structure at high temperatures [11]. The combination of Al and Ca provides the main hardening phase (Al_2Ca) [12] and Ca additionally improves the oxidation resistance of the alloy [13]. Zn and Ca additions have been proven to reduce the texture intensity and therefore increase the ductility of Mg-alloys, which is an important effect for wrought alloys [14].

In this work, we illustrate the sequence of material analysis, laboratory trials and industrial scaled production of Mg forged parts, using an age-hardenable Mg-Al-Ca-Mn-Zn alloy with low overall alloying content.

4.2. Material and Methods

Laboratory forging trials, heat treatments and analysis steps were done at Light Metals Technologies Ranshofen (LKR), industrial forging trials took place at Krenhof.

4.2.1. Material Design

The used Mg-0.75Al-0.4Ca-0.3Mn-0.25Zn alloy (AXMZ1000), given in weight percent (wt. %), follows the trend of other age hardenable Mg alloys and has a low overall alloying content of 1.7 wt. %. This

allows for a homogenization and solution heat treatment window in the range of approximately 480 to 530 °C, as Ca-containing phases can be dissolved adequately. This is of course not the case for the Mn containing phases, which are precipitated during homogenization at the latest and cannot be dissolved at the used processing temperatures. The artificial ageing is designed to make full use of the available Ca and Al in the Mg matrix, as hardening is enabled by precipitation of Al_2Ca precursor phases. The formation of the occurring phases is depicted in the thermodynamic equilibrium calculations, computed using Pandat™ software package, MatCalc database mc mg v1.006, given in Figure 4.1

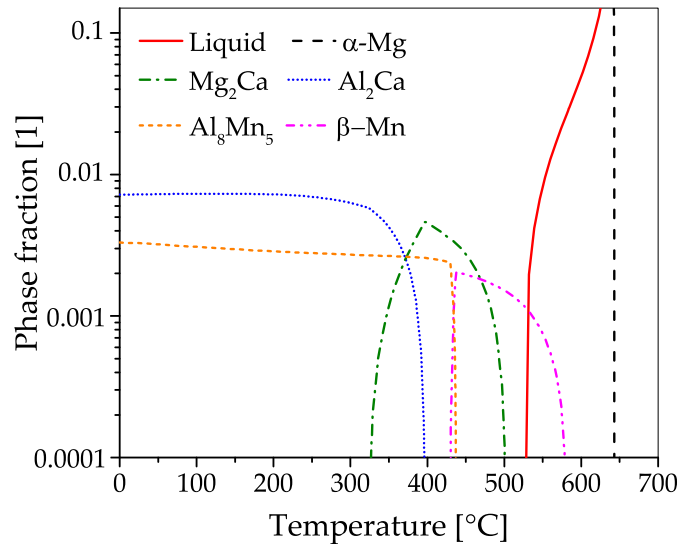


Figure 4.1.: Thermodynamic equilibrium calculations for the alloy AXMZ1000. Showing equilibrium phase fractions of α -Mg and the liquid as well as the intermetallic phases Al_2Ca , Mg_2Ca , Al_8Mn_5 and β -Mn as a function of temperature.

4.2.2. Processing

Industrial produced ingots of AXMZ1000 alloy were remelted and cast into rectangular plates (570×45×300 mm) at LKR, using low pressure die casting. Forging stock with a size of 12×25×95 mm (rectangular) and \varnothing 38×541 mm (round bar) was machined for the laboratory and the industrial trials, respectively. A three-step homogenization heat-treatment was done at material temperatures of 300 °C/3 h, 350 °C/2 h and 480 °C/4 h, and subsequently cooled at air. Laboratory sized piston rods were produced in a two-step isotherm forging process, which took place on a 160 t hydraulic forming press (DZP 160, Walter Neff Maschinenbau GmbH, Karlsruhe, Germany) with a ram speed of 10 mm s^{-1} . Forging was done at temperatures of 250, 300, 350, 400, 450 and 500 °C, the finished parts were cooled at air. An in-depth description of a comparable forging process, including a time-temperature diagram (at 350 °C isothermal forming temperature) can be found in Ref. [15].

Forgings in the shape of an automotive control arm were produced in the industrial forging trials, using a three-step forming process, on a hydraulic press (LASCO Umformtechnik GmbH, Coburg, Germany) with a maximum press force of 1600 tonnes at Krenhof. A graphite-water lubricant, applied by spray gun, was used in all forging operations. Forged parts from both forming trials are depicted in Figure 4.2. The produced parts were solution heat treated (490 °C/20 min./water quenched) and artificially aged to peak hardness, i.e. T6-temper (200 °C/1 h). All heat treatments were done at air using a laboratory sized forced convection chamber furnace (N120/85HA, Nabertherm GmbH, Lilienthal, Germany) at LKR.

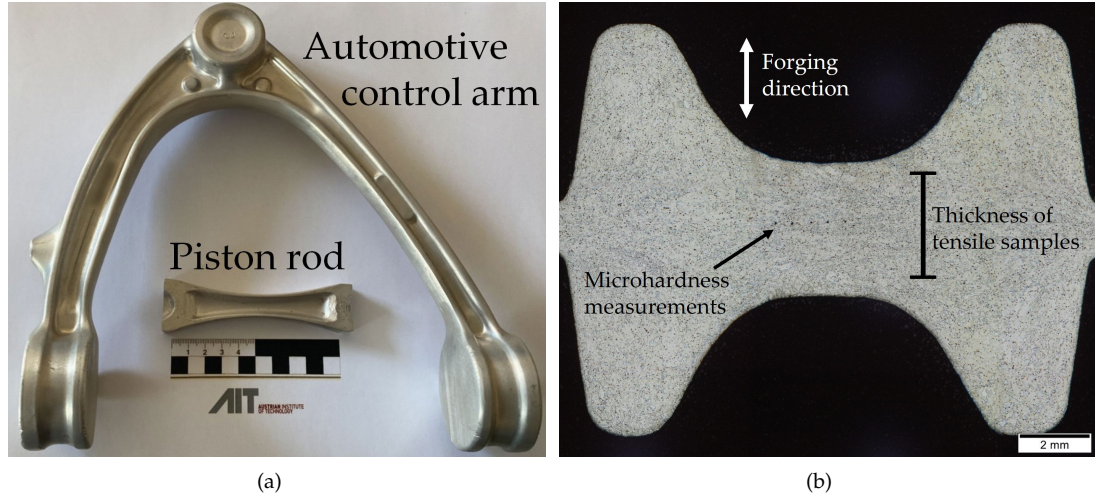


Figure 4.2.: Showing (a) Mg parts produced in laboratory (piston rod) and industrial sized forging (automotive control arm), (b) cross section of a piston rod (in T6-temper) and measurement positions.

4.2.3. Characterization

The processing behavior was characterized by microhardness measurements (LM700 AT, LECO Corporation, St. Joseph, MI, USA) and isothermal compression tests (Gleeble 3800-GTC, Dynamic Systems Inc., Poestenkill, NY, USA) in the range of 250 to 500 °C (step size of 50 °C) using cylindrical samples ($\varnothing 10 \times 12$ mm). The resulting flow curves were used to calculate a processing map as described in Section 4.2.4. The microstructure of the forged parts was analyzed by optical light microscopy (BX60, Olympus, Tokyo, Japan) and the grain size measured using line-intersecting method (ISO ASTM E112-13). Tensile testing was performed at room temperature (Z100, ZwickRoell GmbH & Co. KG, Ulm, Germany) acc. to EN ISO 6892-1, using flat specimens ($E 3 \times 8 \times 25$ mm) acc. to DIN 50125. The samples were taken from the center plane of the forgings, as indicated in Figure 4.2b.

4.2.4. Processing Map

Processing maps are valuable tools to determine feasible process windows for forming operations. To create these maps, stress-strain curves at various strain rates and temperatures are used. The concept is based on the power dissipation rate (η) discussed in [16] and is derived from the strain rate sensitivity exponent (m), see Equations (1) and (2). At a fixed strain (φ), m is derived for various temperatures (T) and strain rates ($\dot{\varphi}$), reformulated as $\eta(T, \dot{\varphi})$ and depicted as a contour plot, see Figure 4.3.

$$\eta = \frac{2m}{m+1}, \eta \leq 1 \quad (4.1)$$

$$m = \left. \frac{\partial \ln \sigma}{\partial \ln \dot{\varphi}} \right|_{\varphi} \quad (4.2)$$

As η describes the dissipation of kinetic energy during the forming process in heat and plastic deformation, a high power dissipation correlates to high deformation capabilities, which is desired for forming operations [17]. Thereby, a processing map allows for a good interpretation of favorable forming regions and expected process instabilities which must be avoided when designing forming processes. These instabilities were interpreted using the failure criterion $2m < \eta$, introduced by Murty and Rao [18].

4.3. Results

4.3.1. Processing Window

To obtain reliable indications of the possible forming parameters, isothermal compression tests were carried out over a broad range of temperatures and forming speeds, ranging from 250 to 500 °C and 0.001 to 10 s⁻¹. The samples tested at 250 °C showed shearing damage at low speeds while samples at 500 °C and a forming speed of 10 s⁻¹ broke by grain boundary failure. Otherwise, the alloy showed adequate results throughout, indicating good forming behavior in the temperature range of ~300 to 450 °C at the speeds used.

The resulting flow curves (not temperature compensated) were compiled into a processing map for easier interpretation and evaluation. This processing map, depicted in Figure 4.3, shows two instability domains (shaded areas) and a wide range of possible forming parameters. The best forming behavior is calculated at 450 °C using a forming speed of 1 s⁻¹. The data is depicted at a strain of 0.8 [-1] showing a relevant degree of deformation, as it corresponds to the local degree of deformation in the sample center of the parts produced in laboratory trials. As the compression tests and therefore the resulting processing map do not consider hydrostatic stresses, which are applied in closed die forging operations, the results can be considered as a worst-case scenario.

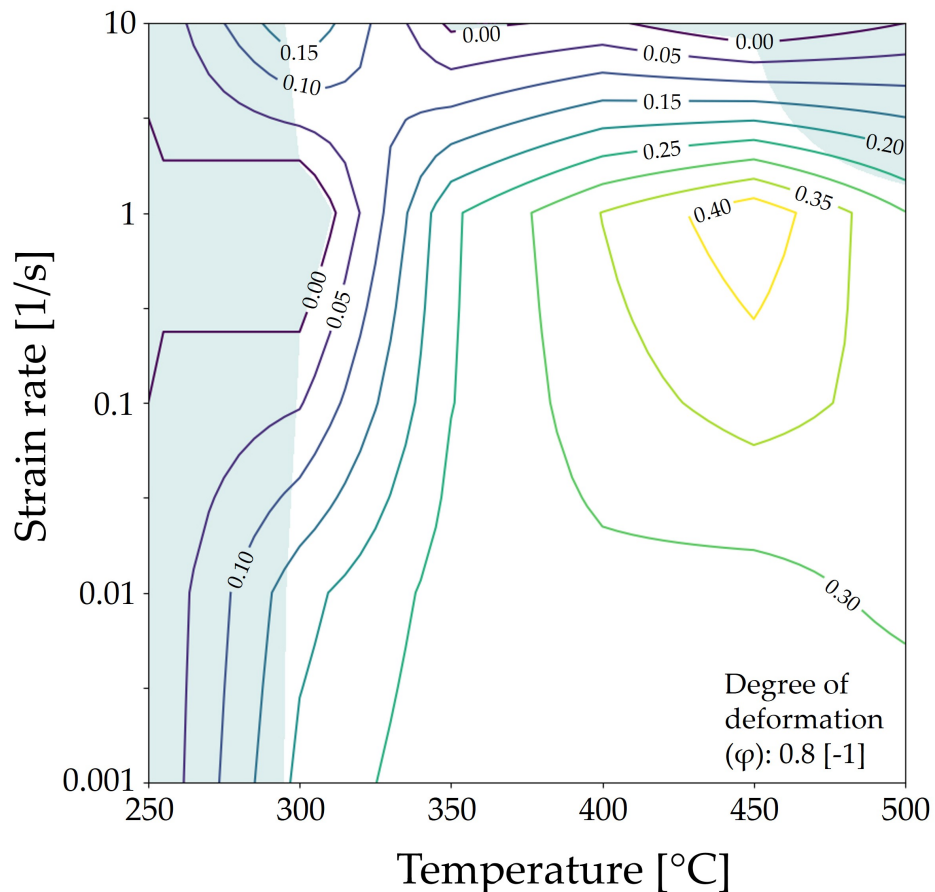


Figure 4.3.: Processing Map of AXMZ1000 alloy in the range of 250 to 500 °C and 0.001 to 10 s⁻¹, at a strain of 0.8 [-1]. Contour lines show the power dissipation rate, shaded areas indicate instability domains.

4.3.2. Laboratory Forging Trials

The findings of the processing map were evaluated in laboratory forging trials, producing piston rods in an isothermal forging process in two forming steps. To match industrial forming conditions the deformation speed of the laboratory trials was set to a ram speed of 10 mm s^{-1} , this also corresponds well to the maximum speed investigated in the compression tests.

The forged parts verified the results of the processing map. While an optically sound piston rod was produced at 250°C , the part formed at 500°C fractured during the first forging step (see Fig. 4.4a). The reason for this was massive grain boundary failure in combination with insufficient lubrication of the forging die, caused by the evaporation of the used graphite-water lubricant on the hot die surface. Nevertheless, the parts formed at 250°C have to be considered faulty, as shear fracture was detected in metallographic analysis (Fig. 4.4b). Therefore, the results of the preliminary compression tests and the calculated processing map were fully confirmed.

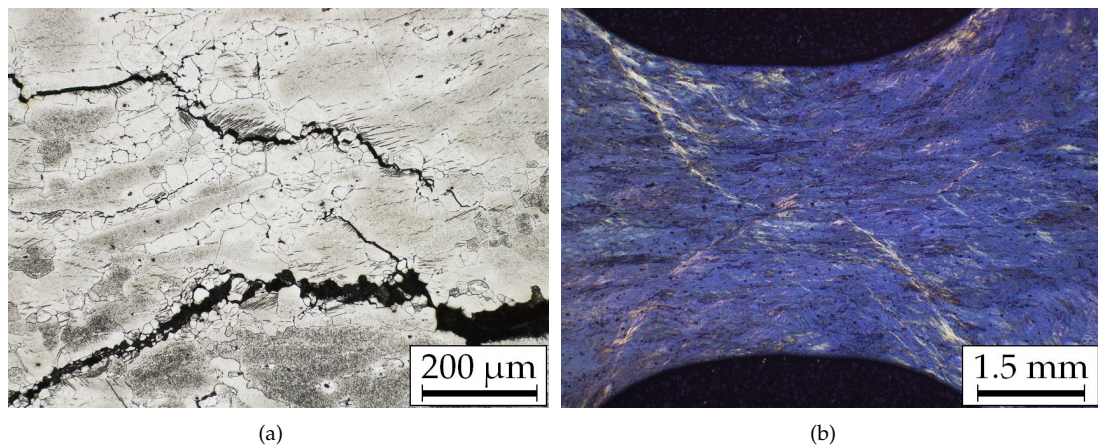


Figure 4.4.: OM images of laboratory forged piston rods (a) grain boundary fracture at high forging temperature of 500°C , (b) shear band damage during the forging at 250°C .

The trial sequence for the piston rods was completed with T6 heat treatment, and the parts were evaluated by microhardness test (HV0.1) and optical microscopy (OM). The microhardness measurements, shown in Figure 4.5, provide an overview of the combined effect of forging and heat treatment parameters on the material properties. In the as-forged state the material hardness drops significantly with increased forging temperature. This behavior has a negligible effect on the material hardness in T6 state, which constantly remains on a high level. The largest effect of the age hardening treatment on the measured microhardness can be seen when comparing a solution heat treated (SHT) sample with the peak aged material, there an increase of $\sim 25 \text{ HV0.1}$ is achieved.

In view of the experience gained in laboratory forging, the subsequent industrial forging trials were performed in a temperature regime of 300 to 450°C , followed by T6 heat treatment of the formed parts.

4.3.3. Industrial Forging Trials

The industrial forged part (automotive control arm) was produced with a die used for Al forgings, at the same ram speed used in the regular production process. As Al forgings are usually not produced in isothermal forging, the permitted temperatures for this die were restricted to a maximum of $\sim 200^\circ\text{C}$. To counterbalance this low die temperature, the stock material was pre-heated to 450°C before forming. The forging operation was done in three-steps, bending – pre-forging – final forging, without intermediate reheating. Finished parts were cooled at air and subsequently heat treated to peak hardness (T6).

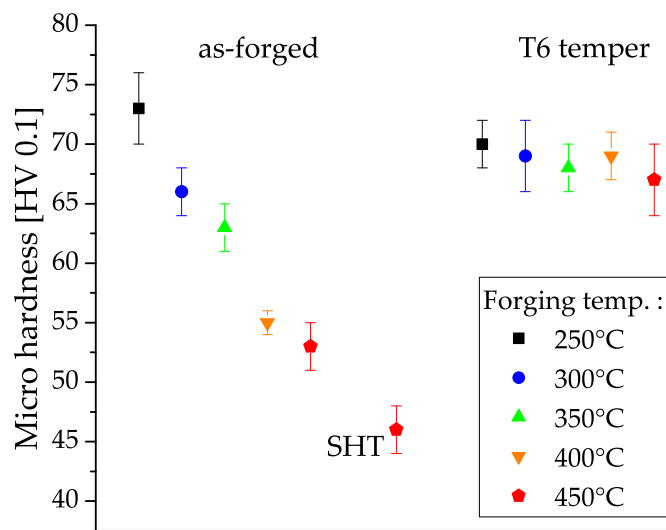


Figure 4.5.: Results from microhardness testing (HV0.1) of laboratory forged piston rods, showing as-forged, solution heat treated and peak aged material, including standard deviation.

4.3.4. Microstructure

The microstructural investigations of the laboratory forgings show a coherent picture throughout. In case of the as-forged material the amount of dynamically recrystallized (DRX) grains steadily increases with rising forging temperature. While the samples formed at 250 °C show shearing damage in the part center, twinning is visible throughout the microstructure of the 300 °C samples. In the parts formed at 350 and 400 °C dynamic recrystallization increases, progressing along twin and grain boundaries. This results in a mostly recrystallized microstructure at 450 °C forging temperature (Figure 4.6).

After T6 heat treatment of the laboratory forged piston rods, the microstructure of all samples is fully recrystallized (RX). Nevertheless, the differing forming temperatures can still be seen in the microstructure, as the grains coarsen with higher process temperatures. The grain size in the sample center thereby increases by over 60 %, rising from 16 to 26 μm in diameter, see Figure 4.6 and Table 4.1.

The microstructure of the industrially forged automotive control arm is shown in Figure 4.7. The as-forged microstructure is permeated by twins and shows a low degree of DRX, mostly comparable to the piston rods forged at 300 °C. The T6 heat-treated material on the other hand shows a fully RX microstructure with a fine grain size, 11 μm in diameter.

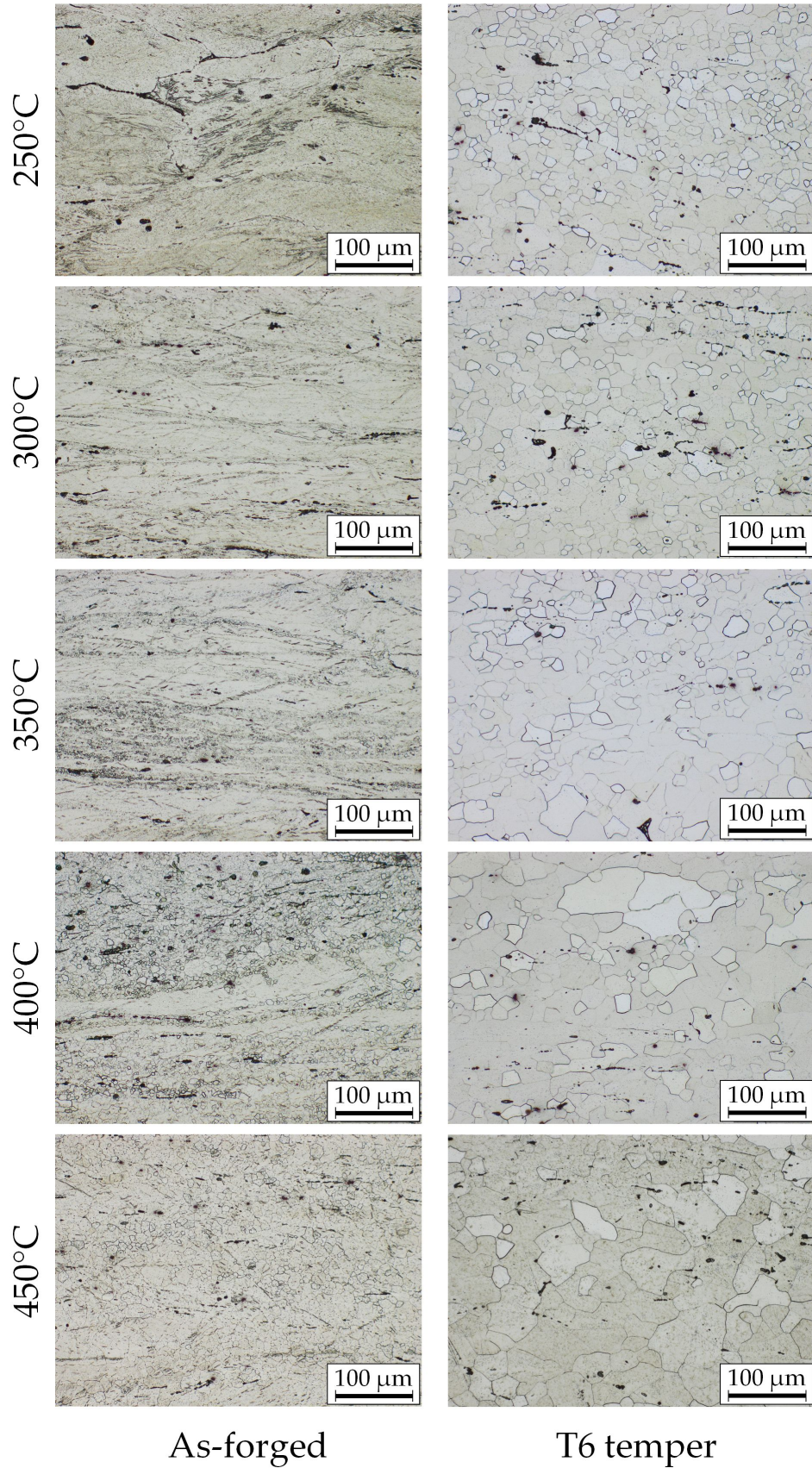


Figure 4.6.: OM images showing the microstructure of laboratory forged piston rods (part center) isothermally produced at 250 to 450°C. The images show as-forged as well as peak aged material (T6-temper).

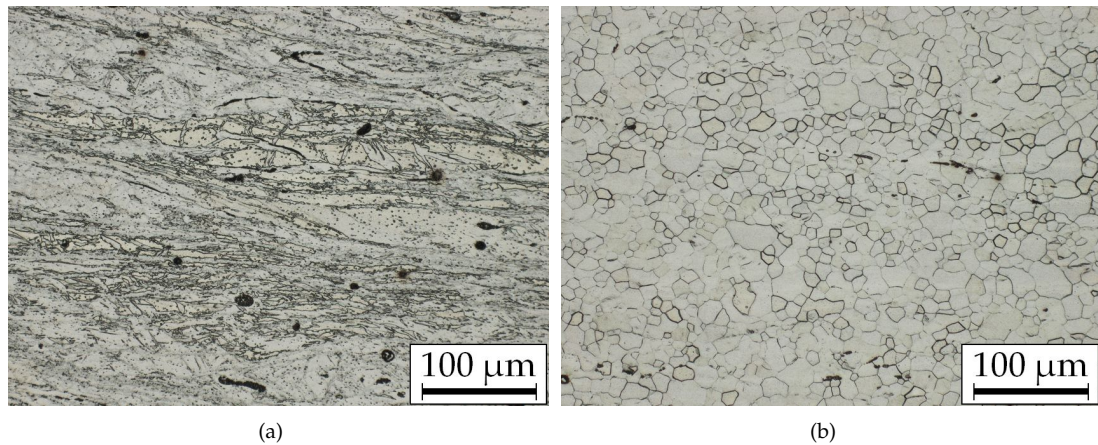


Figure 4.7.: Microstructure (OM images) of industrially forged automotive control arm in (a) as-forged state and (b) T6 temper.

4.3.5. Tensile Properties

Tensile testing was done at room temperature for both, the isothermally forged piston rods and the industrially forged parts. The laboratory forgings show fluctuating mechanical properties with changing forming temperature. The highest tensile strengths were achieved at 400 °C. The industrially forged part in T6 temper shows the best overall properties, reaching an ultimate tensile strength (UTS) of ~260 MPa and a uniform elongation (ϵ_u) of > 7%, while the yield strength (YS) amounts to ~170 MPa. An overview of the mechanical properties and measured grain size of the peak aged parts is given in Table 4.1, representative stress-strain curves from tensile testing are depicted in Figure 4.8.

Table 4.1.: Microstructural and mechanical properties of AXMZ1000 forged parts in peak aged state (T6), including standard deviation.

	Forging temp. [°C]	YS [MPa]	UTS [MPa]	Uniform elongation [%]	Micro hardness [HV0.1]	Grain diameter [μm]
Laboratory forgings	250	160±7	226±14	2.2±1	70±2	16±2
	300	151±2	235±1	3.3±0	69±3	17±3
	350	170±3	229±2	1.7±0	68±2	18±2
	400	185±2	247±5	2.0±1	69±2	25±6
	450	139±1	230±8	1.6±0	67±3	26±5
Industrial forging		168±2	258±7	7.2±1	69±3	11±1

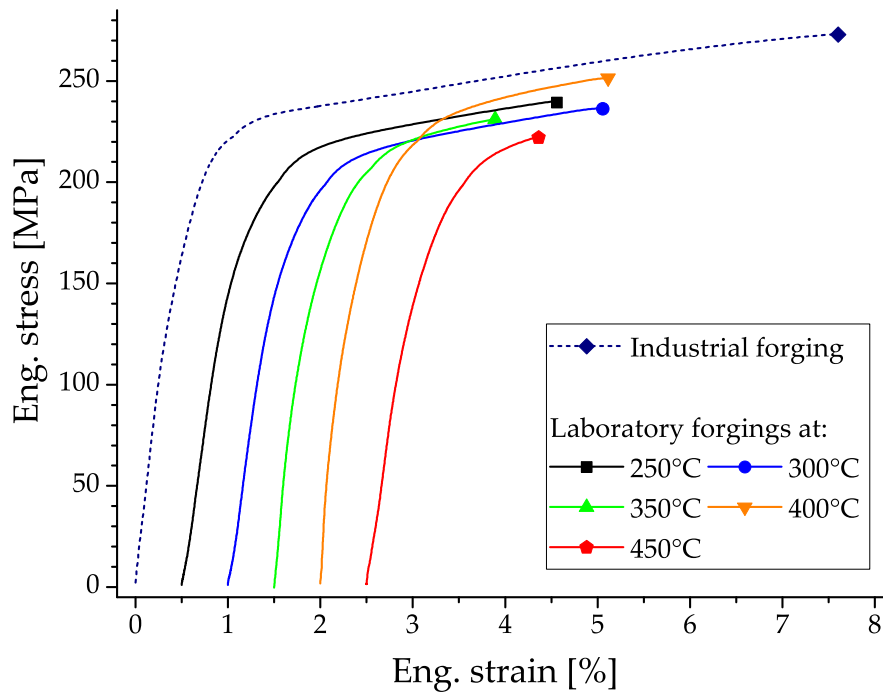


Figure 4.8.: Representative measurements from tensile testing of forged parts in T6 temper. For an improved overview the stress-strain curves are shifted by 0.5 % eng. strain and fracture is marked by symbols.

4.4. Discussion

4.4.1. Processing Window and Laboratory Forging Trials

The preliminary investigations using **compression testing and the calculation of the processing map** indicate a good forming behavior in a broad processing window of 300 to 450 °C. This temperature range as well as the calculated power dissipation rate corresponds to literature available for Ca containing Mg alloys [19]. It is well known that the forming behavior and ductility in Mg alloys is strongly temperature dependent. This is caused by the large differences in critical resolved shear stress (CRSS) necessary for the activation of various slip systems. As these differences diminish with rising material temperature, the amount of available slip systems increases, allowing for easier slip deformation and correspondingly enhanced ductility. At room temperature deformation processes are restricted to basal slip and twinning processes. Only at temperatures above 225 °C additional slip systems gradually become available [20]. This is the cause for the low deformation capabilities shown by the processing map at temperatures below 300 °C, regardless of the used forming speed, see Figure 4.3. A slight improvement in forming behavior can be seen at a strain rate of 10 s^{-1} . At this strain rate the sample temperature might be increased by the dissipated deformation energy [4], thereby enhancing the forming behavior. The same effect can be seen on the samples tested at 500 °C, while forming at low speeds is possible without problems, the material temperature increases at higher forming speeds, causing sample failure. As the solidus temperature of this alloy is at $\sim 530 \text{ °C}$, see Figure 4.1, and an increase in sample temperature of $>10 \text{ °C}$ is likely, material failure is not surprising.

The best forming behavior, i.e. a η of 0.4, has been calculated at 450 °C and a strain rate of $\sim 1 \text{ s}^{-1}$. As the processing map has been created with material data from cylindrical compression testing, the results can be considered as a lower limit. It is well known that material forming behavior can be improved by an increase in hydrostatic stresses during forming processes, such as closed die forging

operations [4; 21]. Therefore, it can be assumed that the reduced formability caused by an increase in forging speed can be offset by the enhanced material ductility, provided by the hydrostatic stresses in closed die forging. Nevertheless, attention must be paid to processing at high forging temperatures, as an increase in material temperature must be expected which can cause material failure, as shown in the processing map at 500 °C and 10 s⁻¹.

The **isothermal laboratory forging trials** showed a good correlation to the results from compression testing and the processing map. The forging window in the range of 300 to 450 °C was confirmed using a ram speed of 10 mm s⁻¹, producing well-formed piston rods without surface damage or internal forging defects.

To appraise the results of the processing map fully, also the limiting temperatures of 250 and 500 °C were investigated. While the piston rod forged at 250 °C was fully formed, shearing damage was found in the part center. This shows the positive effects of the applied hydrostatic stresses when compared to the compression samples, which fractured completely at lower strains. The isothermal forging at 500 °C failed after the first forging step, as the part ruptured in the center plane. This was most likely caused by the high processing temperature, which (i) facilitated grain boundary fracture and (ii) decreased lubrication effect on the surface of the forging die. Fracture along the grain boundaries, as shown in Figure 4.4a, is not surprising as Mg-Ca alloys are known to have reduced grain boundary strength, caused by Ca segregation [22; 23]. Furthermore, the high forging temperatures, additionally increased by deformation heat, might cause incipient melting at locations with enrichment of alloying elements, e.g. grain boundaries.

4.4.2. Industrial Forging Trials

In case of Mg forming operations, the industry is often concerned with the conceived flammability of Mg alloys [5]. While Mg melts, chips and powders have to be handled with particular care, forming operations can be done with standard equipment. As Mg has a high heat transfer coefficient, industrial sized parts are usually able to dissipate heat from hot spots immediately; oxidation events are mainly found in areas where the heat transfer is reduced, e.g. edges and tips. Nevertheless, care has to be taken in case of high temperatures (e.g. homogenization) and machining [4].

To further alleviate industrial concerns, the used AXMZ1000 alloy has been shown to be stable at solution heat treatment conditions for 12 hours and allows temperature peaks up to the liquidus temperature for short periods in heat treatment trials performed at the LKR. Nevertheless, in case of Al processing industries, it should be mentioned, that a direct contact of Al and Mg parts during heat treatments must be avoided, as formation of Mg₁₇Al₁₂ phase in contact areas might occur. Mg₁₇Al₁₂ is a low melting eutectic phase (437 °C) [24], which can cause oxidation events in otherwise stable parts.

The **industrial forging process** setup was identical to the Al forgings of the automotive control arm: the same hydraulic press, forging die, lubrication and comparable forming speeds were used. The forging stock was formed without intermediate heat treatments, which are avoided in industrial settings whenever possible. Material flow behavior as well as die filling was adequate and no sticking was observed in the three-step forging process, resulting in well-formed parts.

While the Mg forged parts were identical to Al forgings at a first glance, differences in the flash areas were visible. The forging flash of the control arm showed cracks, skewers, as well as sharp fractured edges. Small material flakes repeatedly broke away from the flash during forging operation. These fractures on the forging flash can be explained by two main factors: the high speeds at which the flash is formed, see [4; 25], and the reduction of temperature in this region, caused by small cross-sections and large surface areas. While this behavior poses a stark contrast to typical Al forgings, there was no detrimental effect on the forming process or part quality.

Further analysis of the forged Mg parts showed surface cracks, only visible after cleaning procedure (nitric acid 6%) to remove the lubrication residue. These cracks were found on all forged parts, distributed over the whole surface, accumulating in areas of low part thickness and high exposure to the forging die, see Figure 4.9. Additionally, shear band damage, comparable to Figure 4.4b, was

sporadically found in these areas as well. It may therefore be assumed, that the low die temperatures are responsible for these impairments. This is not wholly unexpected as the deformation behavior of Mg is markedly reduced below 250 °C, fully relying on basal slip and twinning [26].

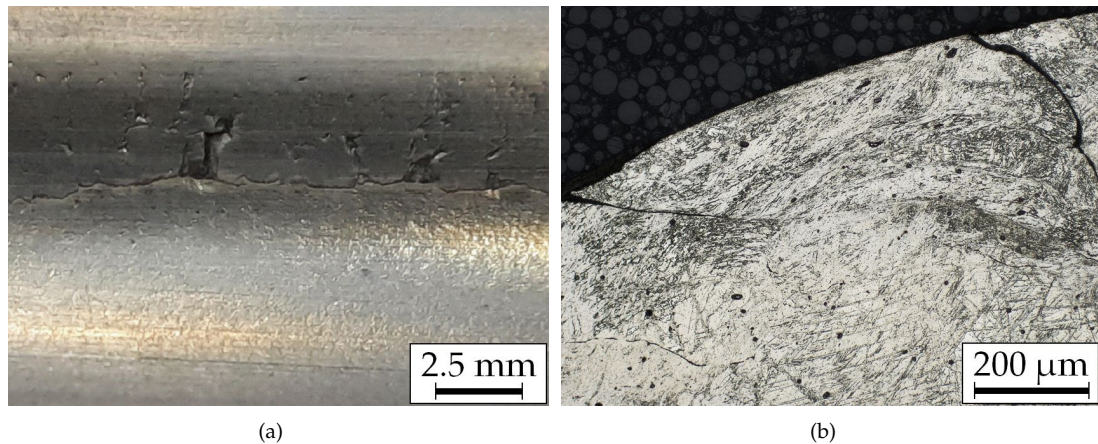


Figure 4.9.: Images of the automotive control arm showing (a) cracks on part surface (b) OM image of crack propagation in the part interior.

While the heat transfer of Al and Mg is comparable, the heat capacity of Mg is lower than Al. Therefore, the heat transferred from the part into the forging die has a larger effect on the temperature of the Mg part. This would confirm the effect of the low die temperature: material temperature reduction occurs in areas of low part thickness and high exposure to the (colder) forging die, where cracks were mostly found. Additional confirmation can be found in the laboratory forgings, as such surface damage did not occur in the isothermally produced piston rods. The die temperature during laboratory forgings was 250 °C minimum, while the temperature in the industrial forging die was still lower at ~150 °C.

Deburring of Al parts is usually done using a deburring die, which removes the flash material and trims the part to the desired size. This takes place at room temperature for ease of handling and to avoid sticking / smearing of the material during removal. This process cannot be identically replicated with Mg parts, as the flash areas tend to fracture brittle in case of room temperature removal, which might cause the fracture to extend into the part itself. Additionally, the part size may differ from the Al parts as the used forging temperatures and the heat expansion coefficient are different. The forged Mg parts were therefore deburred using a band saw, which is an adequate alternative in case of small lot sizes.

Heat treatment (T6-temper) was done with the same parameters as applied to the laboratory forgings. There is a distinct difference in part thickness within the forged control arm, as well as in comparison to the piston rods. To investigate effects caused by this difference in cross-section, comparative temperature measurements were done during solution heat treatment, as it is the most critical heat treatment step in this regard (high temperature, short treatment times). Only a difference of ~1 min was measured between the thickest and thinnest part of the automotive control arm in reaching the solution heat treatment temperature. Obviously, the good heat conduction of Mg makes this problem mostly irrelevant for the used part sizes. A major difference between the T6 heat treatment of Mg and Al parts is the missing effect of natural ageing in case of the Mg forgings [27; 28], which simplifies the sequential arrangement of the heat treatments accordingly.

4.4.3. Microstructure and Mechanical Properties

The **microstructure** of all laboratory forged parts, in as-forged state, is directly dependent on the forming temperature: with rising temperature the amount of DRX-grains increases, while the number of deformed grains from casting is reduced, compare Figure 4.6. This behavior is confirmed by microhardness measurements, given in Figure 4.5. The hardness is reduced with increasing forming temperature, as the microstructure increasingly recrystallizes and defect hardening is diminished [7].

The as-forged microstructure of the industrially produced parts cannot directly be correlated to a forging temperature, as it is created by the combination of different material and die temperatures. Here, mostly deformed grains and twinning structures are visible. Such a structure is strongly dependent on the degree of deformation, which facilitates either fracture at twin boundaries or DRX, depending on the forming temperature [29].

Of higher interest is the microstructure of the parts in T6-state, where a fully recrystallized grain structure can be found, see Figure 4.6. The DRX grains are enlarged during the heat treatment while the deformed remnants of the cast microstructure are replaced by new statically recrystallized grains. This recrystallization process is dependent on the applied heat treatment temperatures (here 490 °C), as well as on the deformation present in the microstructure. The deformation provides both, starting points and stored energy for the static recrystallization [30]. Thereby explaining the dependence of the resulting grain size on the microstructure created during the forging process. Accordingly, the smallest grain size is achieved by the industrially forged part, which has a high amount of deformed grains but only a small proportion of DRX in the as-forged microstructure, see Figure 4.7. This results from low forming temperature and high degree of deformation, up to a local degree of deformation of ~5.

Tensile properties in peak aged state vary for all forged parts due to the differing forming temperatures, e.g. the YS ranges between 140 and 185 MPa. The lowest value was measured for the parts isothermally forged at 450 °C. These forgings show the highest fraction of dynamically RX grains during the forging process as well as the largest grain size. Mg alloys benefit strongly from small grain sizes, as they have high Hall-Petch constants, i.e. k_y of 250 MPa $\mu\text{m}^{-1/2}$ [11]. Nevertheless, large strength improvements by grain boundary hardening primarily take place at grain diameters below ~5 μm , therefore only differences of smaller 25 MPa YS can be expected in the produced parts.

While the main hardening effect in the discussed samples clearly stems from precipitation hardening, as visible in Figure 4.5, also the forming texture can play an important part. The strong basal texture developed in Mg wrought alloys is often reported to have noticeable impact on the mechanical behavior [14], thereby playing an important role on both the achievable YS and ductility. The YS can be improved by high basal intensities if the applicable Schmid factors are reduced. On the other hand, a low texture intensity can be associated with an improved ductility, by allowing for a more heterogeneous distribution of slip directions. Especially parts produced by directional processes, i.e. rolling and extrusion, are known for their sharp textures, which are less pronounced in forgings. Additionally, the overall texture of the discussed forged parts is markedly reduced by the heat treatment processes, as discussed in [15]. However, a noticeable impact on material properties must also be assumed here. This is affirmed by a comparison with the stable microhardness values in T6 temper, which are less affected by differences in the texture when compared to tensile measurements.

The industrial forgings show low grain sizes and a higher degree of deformation when compared to the laboratory forgings, this is reflected in their good YS, but especially in the high ϵ_u reached (>7%). The superior UTS (~260 MPa) of these samples is most likely linked to the ductility, which is the highest value achieved in this investigation. The elongation of the forged parts is mainly controlled by element enrichment and phases at the grain boundaries, which may cause premature fracture. Nevertheless, when comparing the tensile properties of the industrially sized Mg part to the performance of the Al part produced in the standard process, adequate specific properties are reached. The Al forgings reach minimum YS and UTS values of 300 and 340 MPa, respectively. Accordingly, the specific strength values of the Al and Mg parts deviate by ~15 %, showing possible improvements by weight parity design. Note, that an increase of the elongation, YS and UTS of the AXMZ1000 parts seems achievable by using extruded forging stock [15].

4.5. Conclusion

The necessary production steps of Mg forged parts were analyzed in this work. Thereby, we investigated the (i) material selection, (ii) determination of suitable process parameters (by means of compression test), (iii) laboratory and (iiii) industrial scaled forging trials including heat treatment procedures. The lessons learned can be summarized as follows:

- The use of isothermal compression testing and the subsequent calculation of a processing map for the used AXMZ1000 alloy reveal a forming window in the range of 300 to 450 °C, at strain rates of 0.001 to 10 s⁻¹.
- Laboratory forging trials verify the results from compression testing and enable the achievement of reproducible component qualities with stable hardness values (HV0.1) after T6 heat treatment, regardless of the used forming temperature.
- Automotive control arms were successfully produced in industrial forging trials. Favorably, with the lean Mg alloy used, large variations in material and mould temperatures are possible.
- The die temperature has proven to be a limiting factor for the production of Mg forgings, which can lead to surface cracks if it is chosen too low.

It can be concluded that the step from Al industrial forgings to the production of Mg parts made from AXMZ1000 alloy is straightforward. Existing forging and heat treatment equipment can be used without problems, solely the die temperatures have to be raised accordingly.

Nevertheless, special care must be taken to avoid material mix-ups, as Al processing conditions are unsuitable for Mg parts and can cause oxidation events. This must be kept in mind also for the following production steps, such as cleaning and machining.

4.6. References

- [1] F. Czerwinski, Current Trends in Automotive Lightweighting Strategies and Materials, *Materials* 14 (6631) (2021) 1–27. doi:10.3390/ma14216631.
- [2] K. U. Kainer, 40 Years of Magnesium Research – Assessment of Contribution to the Progress in Magnesium Technology, in: 79th Annual IMA World Magnesium Conference, Budapest, International Magnesium Association, 2019.
- [3] A. A. Luo, Magnesium casting technology for structural applications, *Journal of Magnesium and Alloys* 1 (1) (2013) 2–22. doi:10.1016/j.jma.2013.02.002.
- [4] N. P. Papenberg, S. Gneiger, I. Weißensteiner, P. J. Uggowitzer, S. Pogatscher, Mg-Alloys for forging applications—A review, *Materials* 13(4) (985) (2020) 1–61. doi:10.3390/ma13040985.
- [5] F. D’Errico, M. Tauber, M. Just, Magnesium Alloys for Sustainable Weight-Saving Approach: A Brief Market Overview, New Trends, and Perspectives, in: S. Sunkari (Ed.), *Current Trends in Magnesium (Mg) Research*, IntechOpen, 2022. doi:10.5772/intechopen.102777.
- [6] Z. Zeng, N. Stanford, C. H. J. Davies, J.-F. Nie, N. Birbilis, Magnesium extrusion alloys: a review of developments and prospects, *International Materials Reviews* 64 (1) (2019) 27–62. doi:10.1080/09506608.2017.1421439.
- [7] E. F. Emley, *Principles of magnesium technology*, Pergamon Press, Oxford, UK, 1966, ISBN 9780080106731.
- [8] Y. Birol, O. Ilgaz, S. Akdi, E. Unuvar, Comparison of cast and extruded stock for the forging of AA6082 alloy suspension parts, in: *Advanced Materials Research*, Vol. 939, Trans Tech Publ, 2014, pp. 299–304. doi:10.4028/www.scientific.net/AMR.939.

- [9] G. Drossel, S. Friedrich, C. Kammer, W. Lehnert, W. Thate, M. Ullman, H.-W. Wenglorz, et al., *Aluminium Taschenbuch 2: Umformung, Gießen, Oberflächenbehandlung, Recycling*, Beuth Verlag, 2018, ISBN 978-3-410-26104-9.
- [10] N. P. Papenberg, S. Gneiger, P. J. Uggowitzer, S. Pogatscher, Lean Wrought Magnesium Alloys, *Materials* 14 (4282) (2021) 1–30. doi:10.3390/ma14154282.
- [11] M. Cihova, R. Schäublin, L. B. Hauser, S. S. Gerstl, C. Simson, P. Uggowitzer, J. F. Löffler, Rational design of a lean magnesium-based alloy with high age-hardening response, *Acta Materialia* 158 (2018) 214–229. doi:10.1016/j.actamat.2018.07.054.
- [12] J.-F. Nie, Precipitation and hardening in magnesium alloys, *Metallurgical and Materials Transactions A* 43 (11) (2012) 3891–3939. doi:10.1007/s11661-012-1217-2.
- [13] B.-H. Choi, B.-S. You, W.-W. Park, Y.-B. Huang, I.-M. Park, Effect of Ca addition on the oxidation resistance of AZ91 magnesium alloys at elevated temperatures, *Metals and Materials International* 9 (4) (2003) 395–398. doi:10.1007/BF03027194.
- [14] I. Basu, M. Chen, J. Wheeler, R. Schäublin, J. Löffler, Stacking-fault mediated plasticity and strengthening in lean, rare-earth free magnesium alloys, *Acta Materialia* 211 (116877) (2021) 1–17. doi:10.1016/j.actamat.2021.116877.
- [15] N. P. Papenberg, A. Arnoldt, B. Trink, P. J. Uggowitzer, S. Pogatscher, Closed die forging of a Mg–Al–Ca–Mn–Zn lean alloy, *Materials Science and Engineering: A* 857 (144079) (2022) 1–13. doi:10.1016/j.msea.2022.144079.
- [16] K. Rao, Y. Prasad, K. Sivaram, Deformation processing map for control of microstructure in Al-4Mg alloy, *Materials Letters* 10 (1-2) (1990) 66–70. doi:10.1016/0167-577X(90)90016-F.
- [17] G. Zhou, H. Ding, F. Cao, B. Zhang, A comparative study of various flow instability criteria in processing map of superalloy GH4742, *Journal of Materials Science & Technology* 30 (3) (2014) 217–222. doi:10.1016/j.jmst.2013.07.008.
- [18] S. N. Murty, B. N. Rao, On the development of instability criteria during hotworking with reference to IN 718, *Materials Science and Engineering: A* 254 (1-2) (1998) 76–82. doi:10.1016/S0921-5093(98)00764-3.
- [19] K. P. Rao, Y. V. R. K. Prasad, C. Dharmendra, K. Suresh, N. Hort, H. Dieringa, Review on Hot Working Behavior and Strength of Calcium-Containing Magnesium Alloys, *Advanced Engineering Materials* 20 (1701102) (2018) 1–19. doi:10.1002/adem.201701102.
- [20] K. Suresh, K. Rao, Y. Prasad, N. Hort, K. Kainer, Study of hot forging behavior of as-cast Mg–3Al–1Zn–2Ca alloy towards optimization of its hot workability, *Materials & Design* 57 (2014) 697–704. doi:10.1016/j.matdes.2014.01.032.
- [21] P. Skubisz, J. Sińczak, Precision forging of thin-walled parts of AZ31 magnesium alloy, *Archives of Metallurgy and Materials* 52 (2) (2007) 329–336.
- [22] T. Trang, J. Zhang, J. Kim, A. Zargaran, J. Hwang, B.-C. Suh, N. Kim, Designing a magnesium alloy with high strength and high formability, *Nature communications* 9 (2522) (2018) 1–6. doi:10.1038/s41467-018-04981-4.
- [23] R. Pei, Y. Zou, D. Wei, T. Al-Samman, Grain boundary co-segregation in magnesium alloys with multiple substitutional elements, *Acta Materialia* 208 (116749) (2021) 1–11. doi:10.1016/j.actamat.2021.116749.
- [24] P. Liang, H.-L. Su, P. Donnadieu, M. G. Harmelin, A. Quivy, P. Ochin, G. Effenberg, H. J. Seifert, H. L. Lukas, F. Aldinger, Experimental investigation and thermodynamic calculation of the central part of the Mg–Al phase diagram, *International Journal of Materials Research* 89 (8) (1998) 536–540.
- [25] A. Sabroff, F. Boulger, H. Henning, J. Spretnak, *A Manual on Fundamentals of Forging Practice*, Tech. rep. (1964).
- [26] C. Bettles, M. Barnett, *Advances in wrought magnesium alloys: fundamentals of processing, properties and applications*, Elsevier, Woodhead Publishing, Cambridge, UK, 2012. doi:10.1016/B978-1-84569-968-0.50017-X.

- [27] L. Sturkey, J. Clark, Mechanism of age-hardening in magnesium-zinc alloys, *Journal of the Institute of Metals* 88 (177-181) (1959).
- [28] G. Mima, Y. Tanaka, The aging characteristics of magnesium-4wt% zinc alloy, *Transactions of the Japan Institute of Metals* 12 (2) (1971) 71–75. doi:10.2320/matertrans1960.12.71.
- [29] T. Al-Samman, G. Gottstein, Dynamic recrystallization during high temperature deformation of magnesium, *Materials Science and Engineering: A* 490 (1-2) (2008) 411–420. doi:10.1016/j.msea.2008.02.004.
- [30] Z. Li, T. Sasaki, M. Bian, T. Nakata, Y. Yoshida, N. Kawabe, S. Kamado, K. Hono, Role of Zn on the room temperature formability and strength in Mg–Al–Ca–Mn sheet alloys, *Journal of Alloys and Compounds* 847 (156347) (2020) 1–11. doi:10.1016/j.jallcom.2020.156347.

5. Characterization of Isothermal Forged AXMZ1000 Alloy

To provide further information on the behavior and potential of the used AXZM1000 alloy, laboratory forged material, using isotherm forming conditions at 350 °C, is investigated in detail. The influence of cast and homogenized forging stock is compared with extruded stock material in terms of forming behavior, microstructural and mechanical properties of the forged parts. The forgings are analyzed regarding their grain size and texture development as well as tensile and fatigue properties.

The following section has been published in the shape of a scientific paper.

Closed die forging of a Mg-Al-Ca-Mn-Zn lean alloy

Published in: Materials Science & Engineering A, 2022, 857, 144079, doi:10.1016/j.msea.2022.144079
Received 3 June 2022; Accepted 21 September 2022

Authors: Nikolaus P. Papenberg, Aurel Arnoldt, Bernhard Trink, Peter J. Uggowitzer and Stefan Pogatscher

Author contribution: Nikolaus P. Papenberg: Conceptualization, Investigation, Data curation, Writing – original draft, Writing – review and editing. Aurel Arnoldt: Investigation, Data curation, Writing – original draft. Bernhard Trink: Investigation, Writing – original draft. Peter J. Uggowitzer: Conceptualization of this study, Thermodynamic calculations, Writing – review and editing. Stefan Pogatscher: Conceptualization, Writing – review and editing, Supervision, Project administration.

Keywords: wrought magnesium alloy; Mg-Al-Ca alloy; processing; die forging; artificial aging

Abstract: The intensifying search for light weighting possibilities in transportation have repeatedly brought attention on wrought Mg alloys. While various alloys have been investigated a trend in development towards heat treatable Mg alloys with low alloying content has been noticeable. Investigations on wrought alloys are done predominantly by extrusion or rolling, but not by forging. As forgings are an indispensable part in structural components used today, it is important to gain an in depth understanding of the interaction between material, forming process and heat treatments of forged parts. In this study, the forging process of a piston rod using an age-hardenable lean Mg alloy AXMZ1000 is investigated on a semi-industrial scale, comparing two different stock materials: cast and homogenized versus extruded forging material. The microstructural evolution and mechanical properties during the production process are analyzed and assessed. Comparable microstructures are obtained with both starting materials. The mechanical properties achieved are slightly better with extruded feedstock than with the cast counterpart, but are at a satisfactory level comparable to extruded or rolled components made of similar alloys.

Funding: The authors would like to thankfully acknowledge the work done by the technical staff at the LKR Ranshofen as well as the support by their colleagues and partners of the scientific community. We gratefully acknowledge the financial support of this work within the scope of the AMALFI project. AMALFI is a COMET Project within the COMET–Competence Centers for Excellent Technologies Program and funded by BMK, BMDW, and the federal state of Upper Austria. The COMET Program is managed by the FFG (grant number 872641).

This work was published as an open access article distributed under a Creative Commons license (<https://creativecommons.org/licenses/by-nc-nd/4.0/>). The only changes made are related to layout and internal document accessibility.

5.1. Introduction

Lightweighting is a topic of steadily increasing importance for the transportation industries, aiming to reduce emissions and increase vehicle range [1; 2]. Nowadays, multi-material mixes consisting of high strength steels, fiber reinforced polymers as well as light-weight nonferrous materials, in particular Al alloys, have become common practice [3; 4]. As the search for materials with increased lightweighting potential intensifies, interest in the application of Mg alloys increases as well. A range of applications for Mg castings, i.e. die castings, can be found in today's transportation industry [5], where the combination of low material mass and complex shaped part geometry are well received. These components are predominantly used for nonstructural applications in the vehicle interior as mechanical properties can be insufficient for parts with higher operational demands [6; 7].

A change towards Mg parts with improved properties might be achieved with the use of wrought products, which typically show increased material homogeneity and mechanical properties when compared to castings [8]. While this can further increase the lightweighting potential of Mg alloys, the use of wrought products has yet to be realized in large-scale industrial settings. Investigations in this regard have mostly studied the potential of sheet products [9] and extruded profiles [10]. In comparison, studies on Mg forgings are less common, notwithstanding the fact that forgings contain large untapped potential for industrial use [11].

While forging behavior of various Mg alloys has been analyzed and discussed, the impact of different types of stock material, which can be used for Mg forgings (e.g. castings, rolled plates, extruded profiles), are rarely compared. If such investigations take place, they are mostly limited to simple testings, e.g. upsetting tests, and focus solely on the deformation behavior during the forging process. This is unsatisfactory, as it has been shown, that not only the the forming behavior is influenced by the stock material but also the resulting mechanical properties can differ markedly [12].

In general, most studies analyze well-known Mg alloys such as the AZ-series, which are predominantly used in as-produced (F-temper) or annealed states (O-temper) and have low age-hardening potential [13]. This poses a stark contrast to state-of-the-art Al alloys, which predominantly realize their potential in age-hardened state (i.e. T6-temper) [14]. The scientific community has recognized this discrepancy and multiple studies have recently been conducted on the use of age hardenable Mg alloys, e.g. [15–17]. In these studies, a shift towards lean alloys, i.e. materials with reduced content of alloying elements, became evident. This development can be explained by two main factors: improved workability during forming and full utilization of the hardening potential of the alloying elements used [18]. Again, the focus of these investigations has been mainly on material production by extrusion or rolling, while forgings have not yet been adequately investigated.

To gain insight into the complex process of age hardenable Mg forgings, this work examines and compares the microstructure and mechanical properties of peak aged Mg forgings made from both, cast and extruded forging stock. The Mg-Al-Ca-Mn-Zn alloy used was specifically designed for good age hardening potential and aims to enable Mg forgings produced in a process setup comparable to state-of-the-art Al alloys.

5.2. Design Considerations

The material used in this work is an age-hardenable Mg-0.75Al-0.4Ca-0.3Mn-0.25Zn (wt.%) alloy (AXMZ1000) with a low overall alloying content of 1.7 wt.% (1.15 at.%), see Table 5.1. The design of this alloy is based on the works of Cihova et al. [16], and Bian et al. [17; 19; 20]. Being strongly influenced by the concept of age-hardenable Al alloys it follows the conventional production steps of homogenization, deformation and final heat treatment, see Figure 5.1.

Featuring a well balanced composition of alloying elements, the alloy should provide the high age-hardening response and low grain growth tendency required for the processing scheme addressed. The elements used are common in many Mg alloys and each provides various benefits for material perfor-

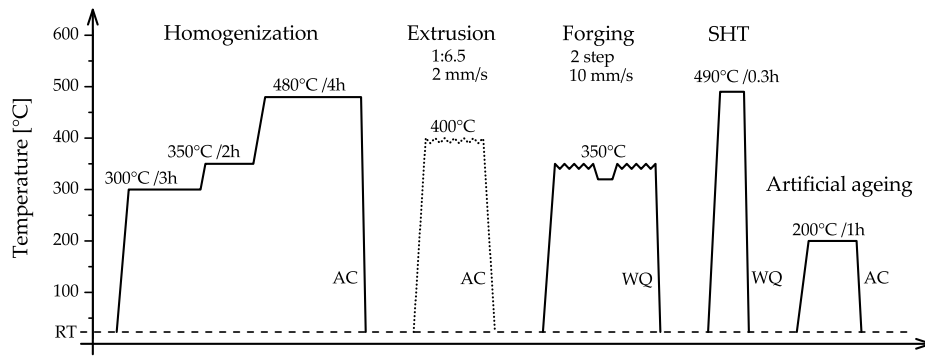


Figure 5.1.: Processing scheme used in this work. The heat treatment times refer to material temperature. Subsequent to the various processing steps, the material was either cooled at air (AC) or quenched in water (WQ). The extrusion process, which is the only difference between the two processing routes, is depicted by a dotted line.

Table 5.1.: Alloy composition of the chosen AXMZ1000 alloy, given in weight (wt. %) and atomic percent (at. %).

	Mg	Al	Ca	Mn	Zn	Σ
wt. %	Bal	0.75	0.40	0.30	0.25	1.70
at. %	Bal	0.68	0.24	0.13	0.09	1.15

mance. Mn is known to improve the corrosion behavior by binding unwanted Fe from the melt [21] and can stabilize the microstructure by the formation of AlMn-dispersoids [16]. The hardening response of this alloy is provided by the combination of Al and Ca, i.e. the precursor phases of Al_2Ca [13]. The use of Ca also provides enhanced oxidation stability [22] and is known to reduce texture formation during processing [23; 24]. The combination of Ca and Zn increases this effect of texture control and can enhance material ductility by providing easier slip system activation [25; 26].

To illustrate phase evolution during processing, a thermodynamic simulation (Pandat™ software package, MatCalc database mc mg v1.006) of the different phases in equilibrium state is shown in Figure 5.2.

The formation of primary β -Mn phases in the melt should be avoided as much as possible by applying fast solidification. Primary β -Mn tends to form blocky shapes, which are detrimental for ductility and cannot be dissolved during subsequent homogenization heat treatment. In addition, the Mn bound in this primary phase is not available for the formation of Al_8Mn_5 dispersoids during homogenization heat treatment, which are a prerequisite for suppressing grain growth during subsequent processing steps [16].

The homogenization heat treatment was performed in three successive temperature steps (300, 350 and 480 °C), to (i) allow homogeneous and uniformly distributed precipitation of Al_8Mn_5 dispersoids [27] and (ii) ensure that low melting phases, solidified in disequilibrium, completely dissolve before reaching the maximum heat treatment temperature. At this final homogenization temperature the intermetallics should be mostly dissolved, except for the Mn containing phases.

The subsequent forming steps (extrusion and forging) took place between 350 and 400 °C. In this temperature range Al_2Ca and Mg_2Ca precipitates may form, but will dissolve during the final solution annealing treatment. Therefore, the deformation steps are not explicitly labeled in Figure 5.2 and will not be discussed further with respect to phase formation.

Solution annealing at 490 °C followed by water quenching (SHT, T4-temper) was used to dissolve the Ca containing phases which might have formed during the preceding processing steps, i.e. deformation as well as heating and cooling times. Thereby, a maximum amount of Al and Ca is provided in the Mg matrix prior to the aging treatment. The solution heat treatment also results in recrystallization of the

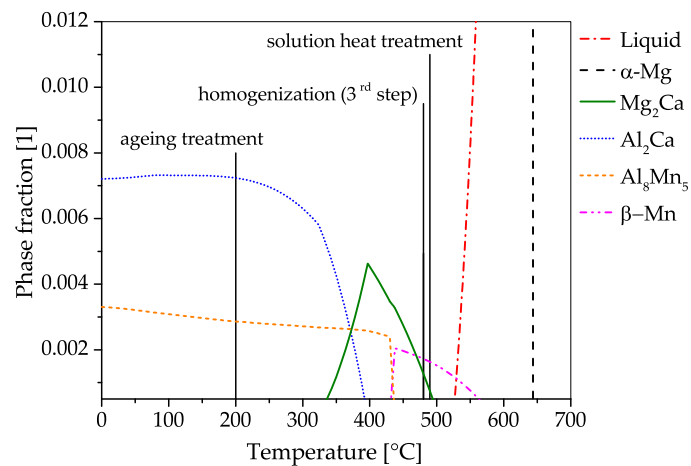


Figure 5.2.: Thermodynamic equilibrium calculations for AXMZ1000. Shown are the equilibrium phase fractions of the intermetallic phases β -Mn, Al_8Mn_5 , Al_2Ca , Mg_2Ca , α -Mg and the liquid as a function of temperature.

deformed, lattice defect-rich microstructure. As natural aging is neglectable in this alloy, material in SHT state and T4-temper can be considered as equal.

To achieve final strength, the material needs to be artificially aged, which is done in the temperature range of Al_2Ca formation, i.e. at 200 °C. The supersaturated Al and Ca atoms present in the Mg matrix precipitate in the form of G.P.-zones [16], providing an increase in strength, while maintaining an acceptable level of ductility.

5.3. Methods

As forging stock of this alloy is not commercially available, the stock material was produced at LKR Ranshofen by remelting industrially cast ingots (1 t batch size). The purchased Mg-0.75Al-0.4Ca-0.3Mn-0.25Zn alloy was remelted and cast into round billets ($\varnothing 75 \times 275$ mm, for extrusion) and rectangular plates ($570 \times 45 \times 300$ mm, for as-cast forging stock) using low-pressure die casting. The cast material was homogenized in a three-step heat treatment and the round billets (machined to $\varnothing 50$ mm) were subsequently extruded to rectangular profiles with a cross section of 12×25 mm, corresponding to an extrusion ratio of 6.5. The profiles were produced on an 1.5 MN extrusion press (NEHP 1500.01, Müller Engineering, Todtenweis, Germany) at 400 °C using a ram speed of 2 mm s^{-1} , i.e. a production speed of $\sim 7.5 \text{ mm min}^{-1}$. To produce piston rods on laboratory scale rectangular forging stock, with a size of $12 \times 25 \times 180$ mm, was cut from the cast plates and extruded profiles. Isothermal two-step forging was done using a hydraulic 160 t forming press (DZP 160, Walter Neff Maschinenbau GmbH, Karlsruhe, Germany) at a speed of 10 mm s^{-1} . The electrically heated die was kept at a constant temperature of 350 °C, while the stock material was heated to processing temperature in a forced convection chamber furnace (N120/85HA, Nabertherm GmbH, Lilienthal, Germany). Pre-forming and final forging, up to a local deformation strain of $\varphi \sim 1$ (in the part center), took place without intermediate heat treatment. The forged parts were solution heat treated (SHT, T4-temper) and artificially aged to achieve approximately peak hardness (T6-temper).

The processing steps for both, the cast & forged (CF) as well as the extruded & forged (EF) material are schematically shown in Figure 5.1.

Tensile testing was done at room temperature (RT) according to DIN50125 for all depicted processing steps, using flat specimen ($E 3 \times 8 \times 30$ mm) on a Z100 testing machine (ZwickRoell GmbH & Co. KG, Ulm, Germany); 3-5 samples were tested each.

High cycle (HCF) and long life (LLF) fatigue behavior of both processing routes in T6 temper were measured according to DIN 50100:2016, using a RUMUL Testronic 100 kN resonance testing machine, with a 20 kN loading cell (Russenberger Prüfmaschinenbau AG, Neuhausen am Rheinfall, Switzerland). As flat specimens were used, the HCF and LLF behavior was measured with a load ratio (R_L) of 0, meaning the load minimum is kept constant at 0 MPa and solely tensile loads are applied. The LLF measurements were done according to the staircase method while the pearl string method was used for HCF testing. Further information on the fatigue testing parameters is given in the Supplementary (Section 5.7.3) and in refs. [28; 29].

Samples for both tensile and fatigue testing were taken from the center of the forged piston rods. The testing direction was therefore parallel to extrusion direction and normal to the forging direction of the produced parts. A forged part and the testing geometries as well as the forming directions are depicted in Figure 5.3.

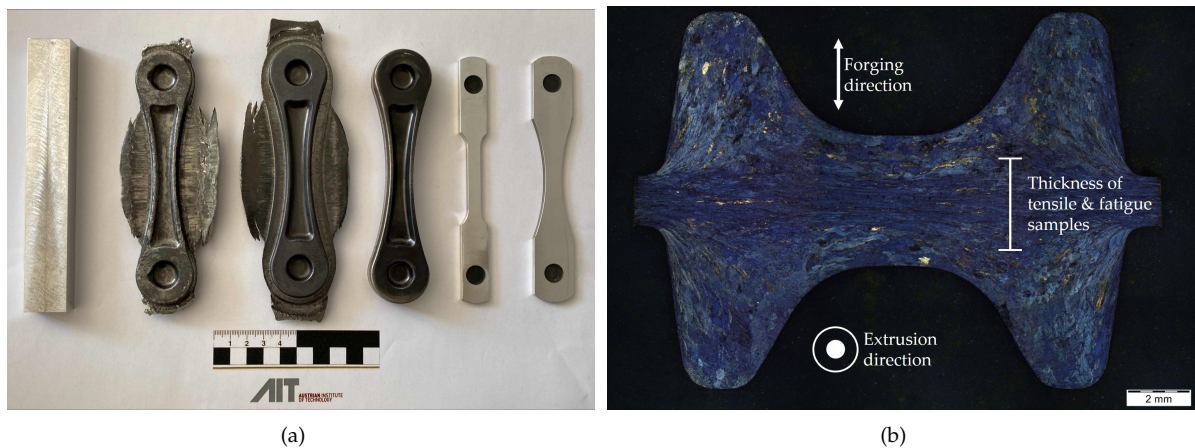


Figure 5.3.: (a) Showing (from left to right) forging stock, pre-forged piston rod, part after final forging, deburred piston rod as well as samples for tensile testing and fatigue measurements, (b) OM image of a piston rod cross-section.

Microstructural investigations were carried out using optical microscopy (OM) and scanning electron microscopy (SEM). The samples for OM images were prepared by polishing and etching (as described in ref. [30]) and subsequently investigated using BX60 (Olympus, Tokyo, Japan) and VHX-7000 (Keyence, Mechelen, Belgium) optical microscopes. For SEM as well as electron backscatter diffraction (EBSD) analysis a Mira 3 (TESCAN, Brno, Czech Republic) was used, including an EDAX Hikari Plus EBSD camera, with EDAX OIM Analysis 8 software (EDAX Inc., Mahwah, NJ, USA). The scans for EBSD analysis were done at the sample center of the extruded profile and the forged parts. The scan position therefore also correlates to the center of the samples used for mechanical testing. The parameters of the EBSD scans were adapted with regards to the sample microstructure: a higher resolution was required for the as-forged samples, reaching a step size of $0.3 \mu\text{m}$ on a scan area of $130 \times 100 \mu\text{m}$. The extruded as well as all heat treated samples were analyzed using a step size of $2.0 \mu\text{m}$ and an area of $1000 \times 775 \mu\text{m}$. For texture analysis an orientation distribution function (ODF) was calculated by a harmonic series expansion (order $l=16$, smoothing 5°). The differences in grain orientation spread (GOS) were used to separate recrystallized and non-recrystallized grains according to [31].

The size and distribution of AlMn dispersoids were measured using SEM in back-scattered electron (BSE) mode, making use of the good particle-matrix contrast based on the respective atomic mass. To ensure sufficient statistical sample size, three pictures with a cumulative area of $321 \mu\text{m}^2$ were analyzed for each sample, an micrograph each is shown in Figure 5.10. Particles in the range of 10 to 80 nm diameter (d_{AlMn}) are included in the measurements, the three dimensional volume fraction (f_{AlMn}) and number density (N_{AlMn}) of the particles were calculated based on the approach of Österreicher et al. [32]. Accordingly, the maximum depth of detection (z_{Info}) is corrected by a material and particle size dependent function, in this case $-0.0038 d_{AlMn}^2 + 1.6863 d_{AlMn}$ [30].

5.4. Results

To achieve an in-depth understanding of the material behavior throughout the forming process, all production steps (from stock material to final heat treatments) have been investigated. Results of processing as well as the microstructure and the mechanical properties are presented as follows.

5.4.1. Processing Characteristics

The isothermal forging of the piston rods at 350 °C was successful for both stock materials used, with no noticeable difference in part quality. While the parts were fully formed, the forging flash showed cracking in the outer areas. Here, the difference in stock material is well visible. While the EF-F samples exhibited small fractures and skewers, cracking of the cast material (CF-F) was more pronounced and larger, sharp-edged skewers appeared on the flanges, see Figure 5.4a. Additionally, the open surface area of the CF-F flange had a rough pattern, while the parts made from extruded stock showed a smooth surface, indicating an effect caused by the differences in stock material grain size.

The forming process itself took place within ~1 min, including 30 s material transition time from the furnace to the forging die and another 30 s for both forging steps. While the temperature of the furnace and the forging die was kept constant at 350 °C, the material temperature varied between 330 and 360 °C. These temperature changes during the forming operation were caused by the transition from the furnace to the die and the deformation applied in the forging steps. Subsequent to the second forging step the piston rods were immediately water quenched to room temperature. The time-temperature curve of the described isothermal forging process is shown in Figure 5.4b.

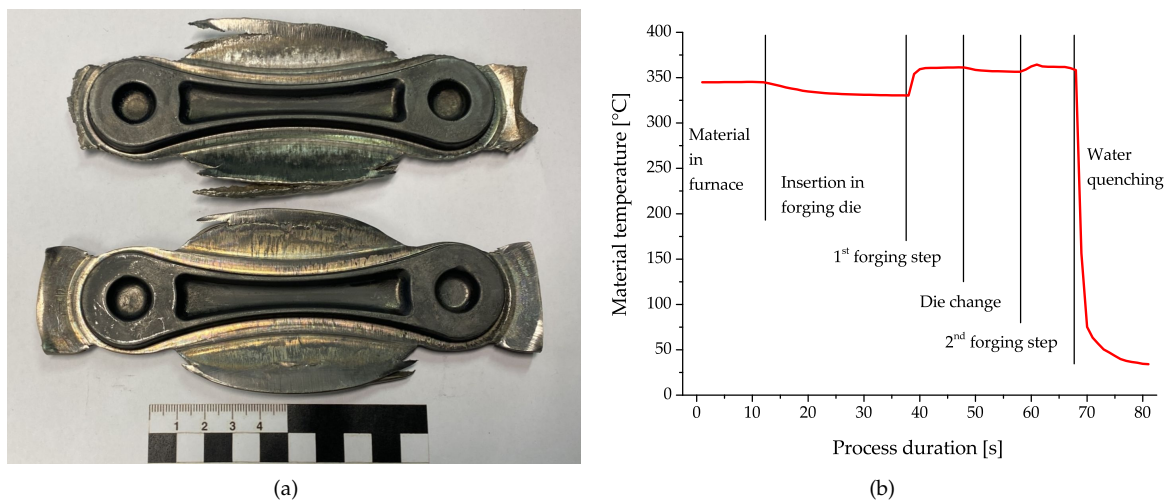


Figure 5.4.: (a) As-forged parts made from cast (upper) and extruded stock material (bottom); (b) Material temperature during the forging process.

5.4.2. Microstructure

5.4.2.1. Optical Microscopy

While the microstructure of the cast forging stock exhibits a typical coarse-grained cast structure, the as-extruded stock material shows a structure of large deformed non-recrystallized (nRX) grains and fine dynamically recrystallized (DRX) grains, as illustrated in Figure 5.5. The swirl-like grain shape of the deformed areas is caused by the extrusion process and is visible when the microstructure is viewed in extrusion direction.

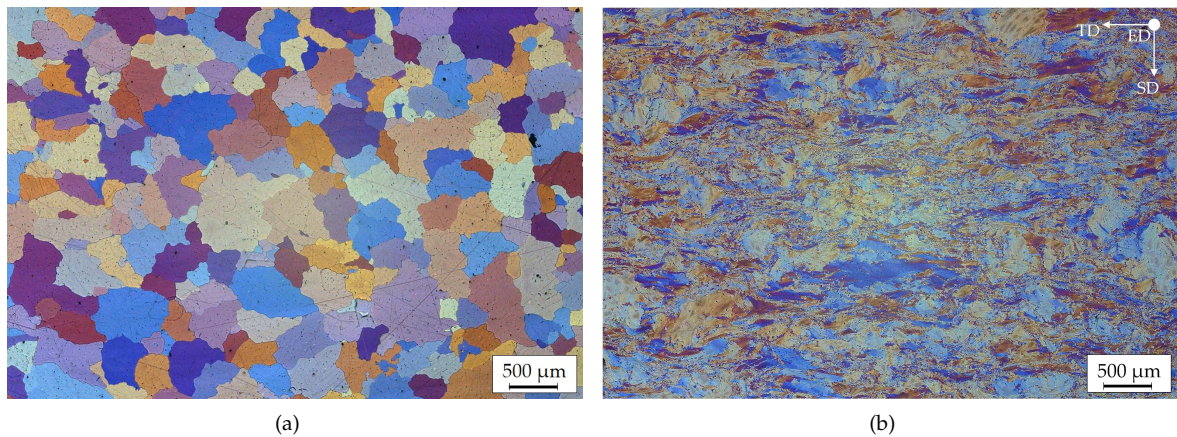


Figure 5.5.: Microstructure (OM-image) of the stock material: (a) cast & homogenized forging stock, (b) extruded forging stock.

The as-forged parts produced from the cast material (CF-F) display a grain evolution corresponding to the local degree of deformation: in the center of the sample the grain structure shows a combination of very small DRX grains and deformed grains, which are elongated normally to the forming direction, see Figure 5.6. Since a lower degree of deformation is applied to the sample rim, the grains originating from casting can still be seen. These grains are permeated by primary and secondary twins, but no DRX grains are apparent. In comparison, the forged part made from the extruded forging stock (EF-F) shows a high amount of DRX grains. The level of DRX grains already existing in the as-extruded stock is increased by the temperature and deformation applied in the forging process. This can be seen in the center of the forged part as well as in the peripheral rim areas. In the contact areas of part and die the grains are fully recrystallized and enlarged, see Figure 5.6d. This is typically caused by the higher degree of deformation and/or temperatures during deformation. Twinning in the deformed grains is visible as well, but the amount is drastically reduced when compared to the part made from cast forging stock.

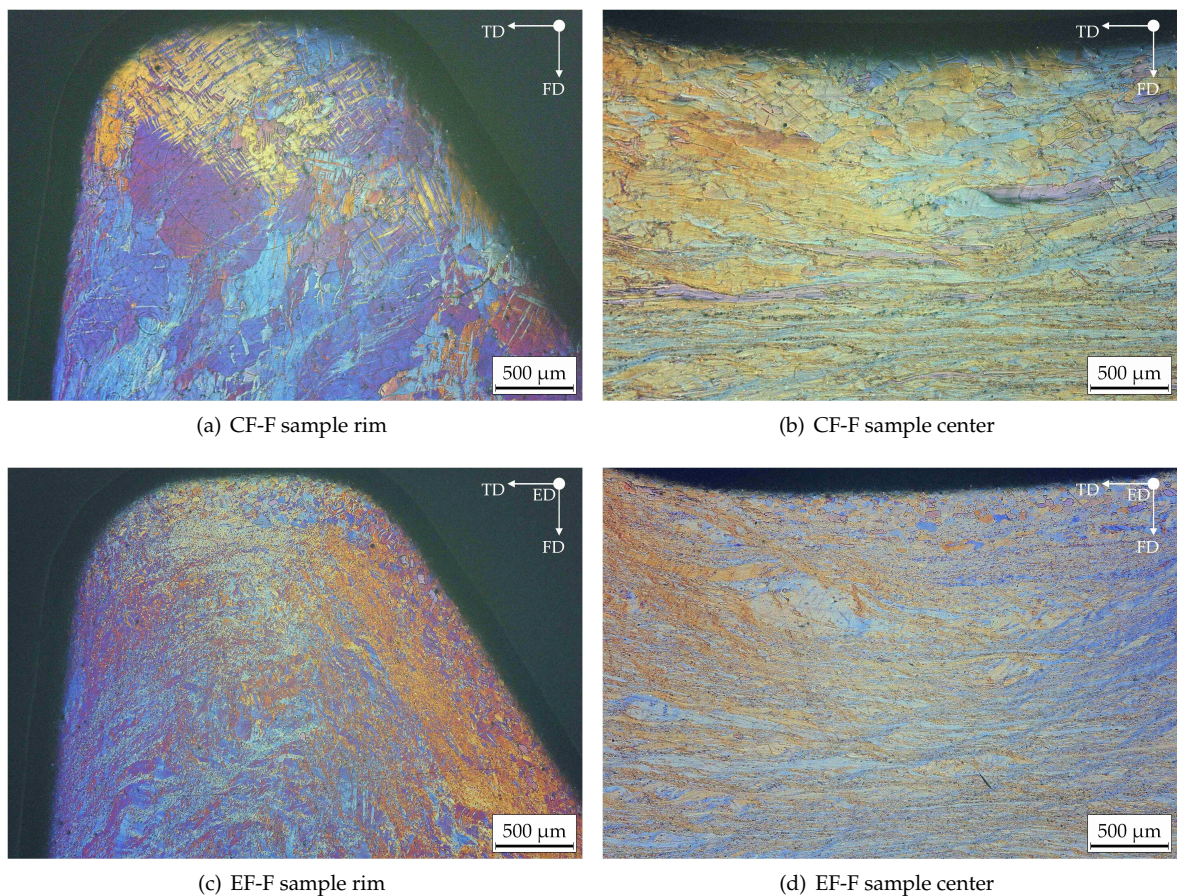


Figure 5.6.: Microstructure (OM-image) of the as-forged piston rods, made from: (a), (b) cast & homogenized forging stock (CF-F), (c), (d) extruded forging stock (EF-F).

The microstructures of forged components after artificial aging (T6-temper) are shown in Figure 5.7. As there is no difference in grain structure between the samples after solution heat treatment (T4) and T6 temper, only the samples in T6-temper are shown. All samples are fully recrystallized and exhibit a surprisingly homogeneous grain size, consisting of slightly enlarged DRX grains and newly statically recrystallized grains. The overall grain size of the CF-T6 samples is slightly larger when compared to the EF-T6 material. This is mostly visible in areas of lower forging deformation, i.e. the sample rim. These rim regions are quite interesting in that they show homogeneous decomposition of the deformed grains into newly RX grains, providing a large reduction of grain size during the solution heat treatment. This is especially well visible in the CF-F material, where large nDRX grains are predominant in the rim region before T6 heat treatment.

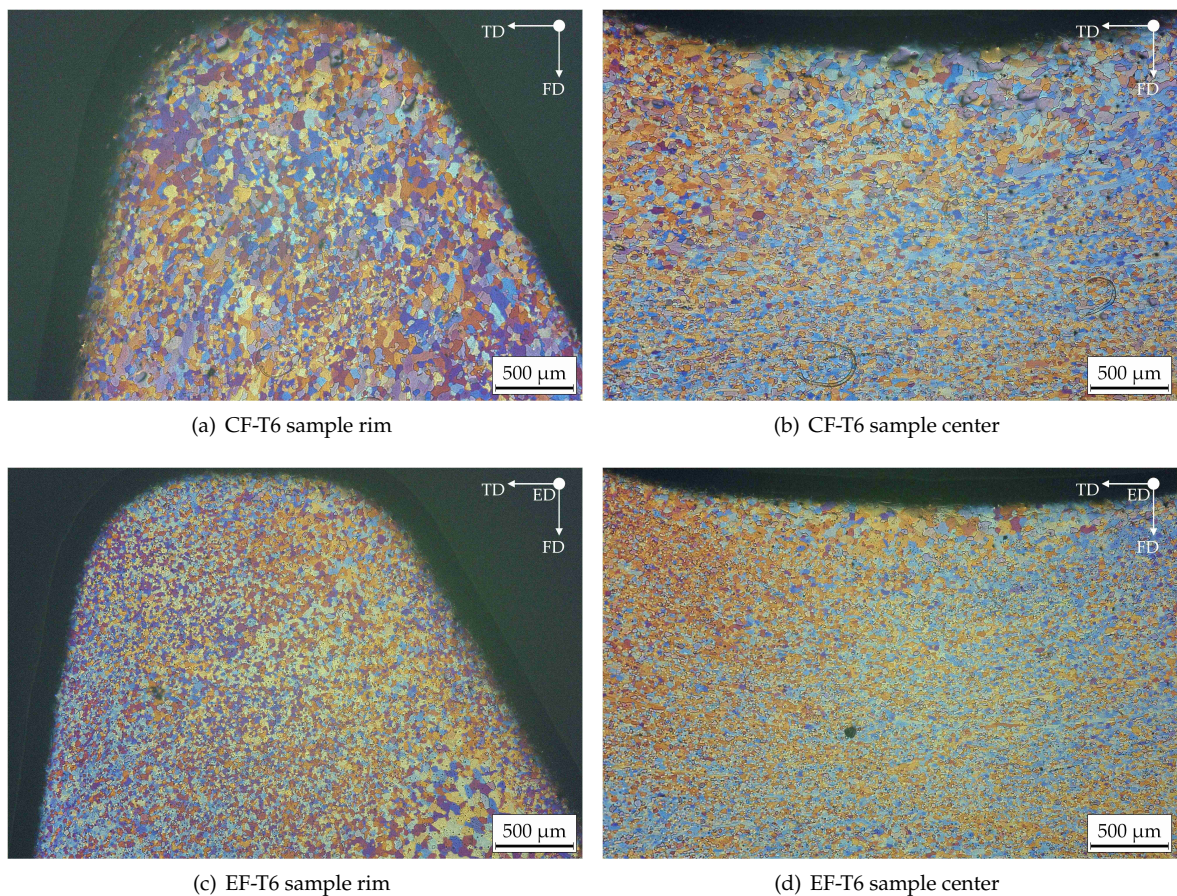


Figure 5.7.: Microstructure (OM-image) of the piston rods in T6-temper, made from: (a), (b) cast & homogenized forging stock, (c), (d) extruded forging stock.

5.4.2.2. EBSD Measurements

To evaluate material texture evolution during the forging process, EBSD analysis was done using parts in as-forged condition (EF-F and CF-F) as well as the peak aged forgings (EF-T6 and CF-T6). In order to provide a good correlation of the measured texture to the results from mechanical testing, the center areas of the profile and forgings were investigated. For all materials the measurements were done in extrusion direction (ED) and rotated accordingly. To investigate possible asymmetric grain growth behavior during recrystallization the peak aged samples were additionally analyzed in forging direction (FD). For discussion of the measured texture, orientation density functions (ODF) were calculated from the discrete datapoints and plotted in pole figures (PF) as depicted in Figure 5.8. While the texture of the cast stock can be assumed to be random [33; 34], the extruded material shows a typical extrusion texture, further discussed in Section 5.7.1 of the Supplementary.

The EBSD measurements have also been used to gain an overview of the grain sizes and the respective degree of recrystallization, as listed in Table 5.2 and Figure 5.9, confirming the grain structures described in Section 5.4.2.1. While the as-extruded, EF and CF materials show a partly RX microstructure, the T6 heat treated parts are fully recrystallized. The evolution of the RX grain size is clearly visible as well; while DRX is responsible for the formation of small grains during the forming operations, a distinct grain growth accompanies the RX grains during static recrystallization in solution heat treatment. The grain size analysis in ED of both heat treated materials show a comparable grain size, the analysis in FD on the other hand displays significant differences. The CF-T6 sample shows enlarged grains and a higher variation in grain size diameter (15 μm vs. 21 μm). In contrast, a symmetric

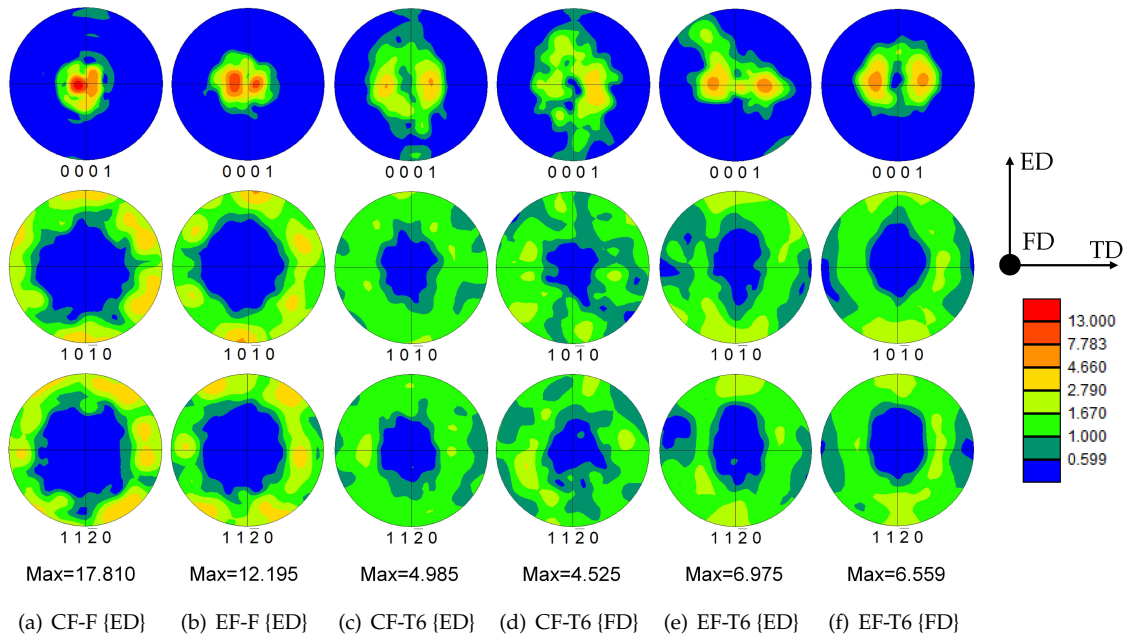


Figure 5.8.: Pole figures (PF) of the as-forged (a), (b) and the peak aged parts (c) to (f) produced from both, cast as well as extruded stock materials. The original scan direction is indicated in parentheses, the data has been subsequently rotated into the given directions for all samples.

grain size distribution for both directions was measured in case of the EF-T6 material (15 μm and 14 μm).

Table 5.2.: Recrystallized grain diameter (including standard deviation) and area fraction calculated from EBSD measurements.

Sample		RX grain diam. [μm]	RX area [%]
as-extr.	ED	7 ± 3	64
CF-F	ED	2 ± 1	44
CF-T6	ED	15 ± 7	95
	FD	21 ± 11	96
EF-F	ED	2 ± 1	60
EF-T6	ED	15 ± 6	91
	FD	14 ± 6	94

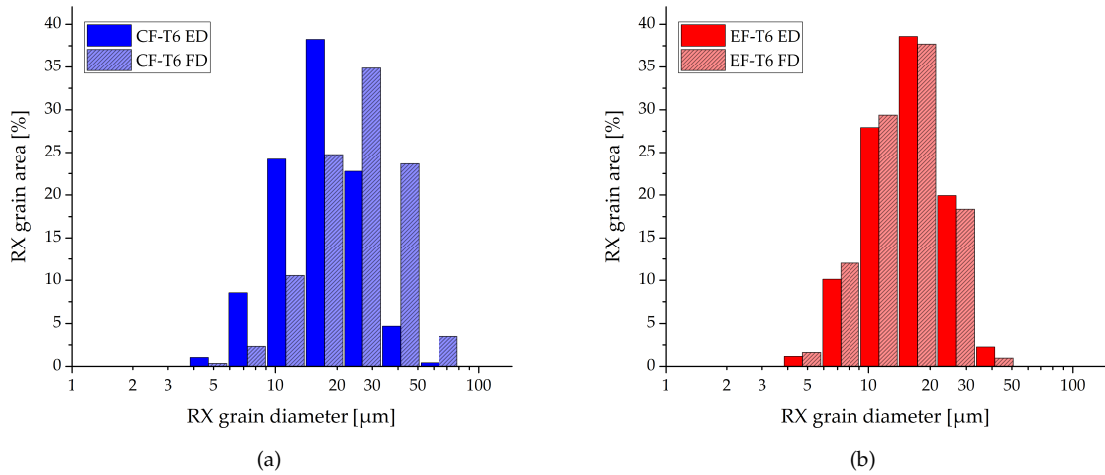


Figure 5.9.: Grain size distribution of RX grains measured with EBSD analysis in ED and FD directions for (a) CF-T6 and (b) EF-T6 samples.

5.4.2.3. AlMn Dispersoid Measurements

The analysis of AlMn dispersoid size and distribution in the peak aged samples indicate a smaller size and a higher volume fraction of particles within the EF-T6 material. This combination leads to the large difference in dispersoid number density measured, i.e. 44 vs. 111 μm^{-3} . Additionally, the CF-T6 material shows a larger spread of particle size as well as a heterogeneous distribution of dispersoids, e.g. banded structures along grain boundaries, well visible in Figure 5.10. An additional overview of the measured dispersoid distribution by particle size is given in Figure 5.18 of the Supplementary.

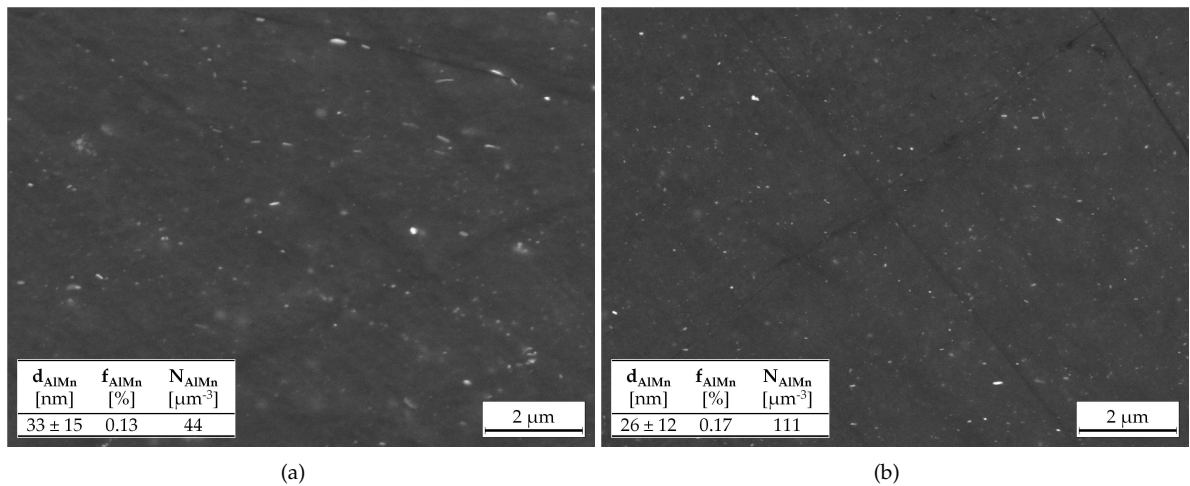


Figure 5.10.: SEM/BSE images of intermetallic particles in the Mg matrix, showing (a) CF-T6 material and (b) EF-T6 material. Calculated values of AlMn dispersoid distribution show particle diameter with standard deviation (d_{AlMn}), volume fraction (f_{AlMn}) and number density (N_{AlMn}).

5.4.3. Tensile Properties

5.4.3.1. Tensile Testing

Tensile testing has been done throughout the processing chain, assisting the analysis of the material evolution during the production process. A representative stress-strain curve from each processing step is depicted in Figure 5.11, while an overview of the averaged values is given in Table 5.3.

While the tensile properties change readily in the different processing steps, the stress strain curves show that the forgings made from extruded stock material achieve higher strength and better elongation throughout the whole process. Nevertheless, when comparing the as-forged with the heat treated material, it can be seen that the artificial aging treatment increases the YS by ~70 MPa regardless of the used forging stock.

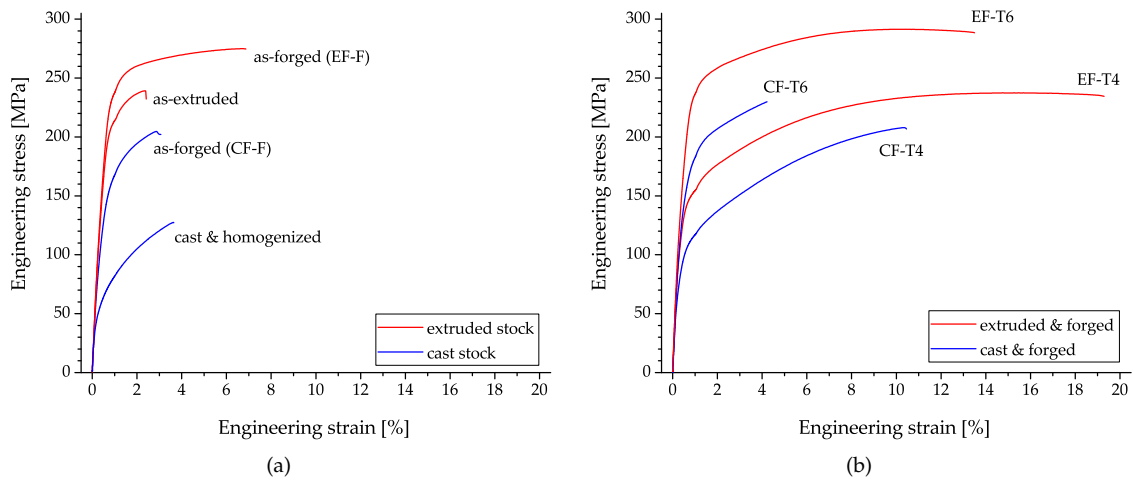


Figure 5.11.: Showing representative tensile testing curves of (a) the stock material (cast & homogenized, as-extruded) and the as-forged parts; (b) depicts the stress-strain curves of the heat treated parts (T4 and T6 temper).

Table 5.3.: Results of tensile measurements showing yield strength (YS), ultimate tensile strength (UTS) and uniform elongation (ϵ_u) including standard deviation.

	YS [MPa]	UTS [MPa]	ϵ_u [%]
cast	52 ± 2	99 ± 23	2.0 ± 1.0
CF-F	126 ± 2	193 ± 17	1.9 ± 0.9
CF-T4	90 ± 1	208 ± 1	9.3 ± 0.5
CF-T6	159 ± 13	235 ± 6	2.9 ± 0.9
as-extruded	172 ± 10	225 ± 10	1.5 ± 0.3
EF-F	210 ± 1	269 ± 5	3.7 ± 1.8
EF-T4	129 ± 1	237 ± 1	14.5 ± 0.2
EF-T6	201 ± 4	290 ± 2	9.6 ± 0.7

5.4.3.2. Fractography

In the following the results concerning the fracture behavior of the tensile samples are presented in detail. For this purpose tensile samples, tested until fracture, were analyzed using OM and SEM.

As the microstructure of both forged & T6 heat treated materials consist of predominantly RX grains, the crack propagation occurs mainly via intergranular fracture. Figure 5.12 illustrates this behavior for both forging conditions. OM and SEM pictures of the fracture surface for the CF-T6 and the EF-T6 material both confirm this behavior, besides fracture along twin boundaries is occurring as well. Bright particles visible in the SEM images of both samples are AlMn containing phases, which can also include Fe and Si impurities. The extruded & forged material (EF-T6) features a slightly raised amount of twins throughout the sample volume, which are most likely a result of the higher elongation achieved in tensile testing.

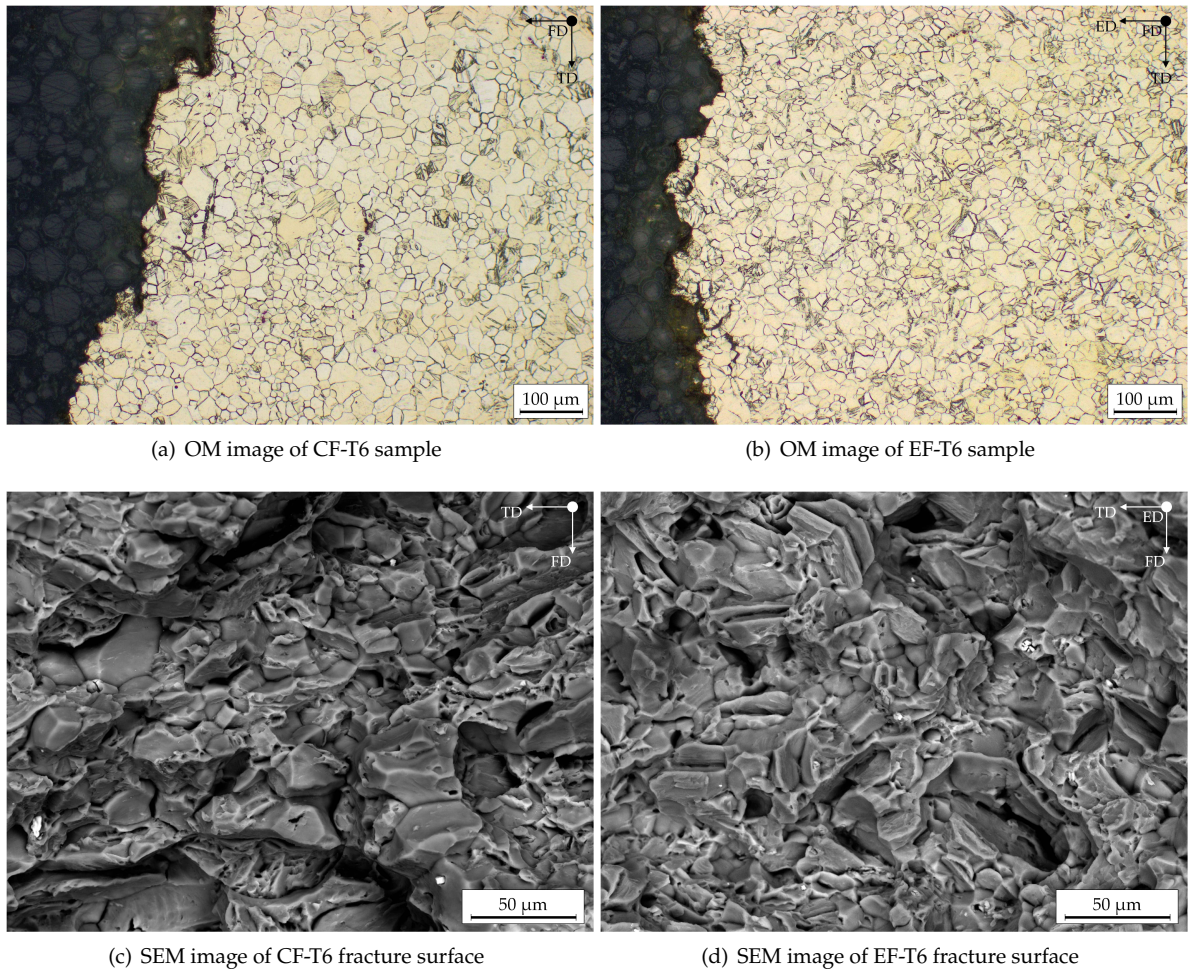


Figure 5.12.: Showing the comparable fracture behavior in tensile samples from different forging stock CF-T6 in (a),(c) and EF-T6 in (b), (d). The sample loading direction is perpendicular to the fracture surface in all shown images, i.e. horizontal in case of the OM images.

5.4.4. Fatigue Measurements

The results of the fatigue measurements of both peak aged materials, EF-T6 and CF-T6, are illustrated in Figure 5.13. The S/N curves show distinct differences in applicable stress levels for the two used stock materials. While the differences are reduced with increasing load levels, the EF-T6 samples consistently show a better performance. This is especially apparent for higher cycles to failure, i.e. the LLF measurements. The reached 10^7 LLF strength of the CF-T6 material was found to be L_{aL} : 43 MPa (L_{maxL} : 86 MPa) while the EF-T6 samples reached L_{aL} : 67 MPa (L_{maxL} : 134 MPa).

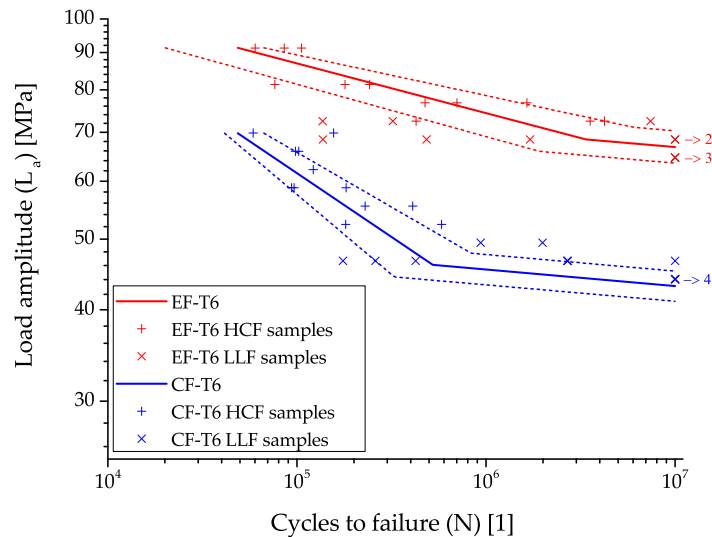


Figure 5.13.: Results of fatigue testing for the CF-T6 and the EF-T6 samples. Dotted lines represent the upper (PA 10 %) and lower (PA 90 %) limit. The numbers indicate the amount of runout samples.

5.5. Discussion

In the following the microstructural and mechanical properties of the investigated material are discussed and compared with literature. Special attention is paid on the difference in YS of the peak aged parts, which is correlated to the respective microstructure of the investigated samples.

5.5.1. Microstructure

The material in the as-extruded and as-forged states (EF-F and CF-F) shows a mixed structure of DRX and nDRX grains, ranging between ~45 to 60 % DRX area. Such a bi-modal grain structure can often be found in as-extruded Mg alloys [35; 36]. The size and volume fraction of the DRXed grains are mainly dependent on the processing temperature and can vary accordingly [37]. The large, deformed, nDRX grains also show twinning, which is known to provide starting points for RX grain formation [38]. The solution heat treated samples on the other hand are confirmed to be fully recrystallized (>90 % area fraction). The static recrystallization which uses deformation defects, e.g. twin boundaries, as starting points and takes place during solution heat treatment, decomposes and reforms the majority of the large, deformed grains [16]. The occurrence of static recrystallization indicates that sufficient lattice defects remain in the nDRX grains to allow primary recrystallization. A similar observation was made by Hofstetter et al. in extrusion of ZX alloys [39]. Due to the relatively low stacking fault energy and the absence of independent slip systems, dynamic recovery during hot forming obviously plays a minor role [40].

When analyzing the grain size, a distinctive difference between the DRX and nDRX grains in the as-forged samples can be seen; the non-recrystallized, deformed grains are larger, when compared to the newly recrystallized grains. It is well visible that the DRX grains are also smaller than the statically recrystallized grains created during solid solution treatment. This is expected, as the solution heat treatment takes place at higher temperatures when compared to the forging process. Nevertheless, the measured grain sizes prove that the use of extruded stock of this alloy in forgings does not cause excessive grain growth, as known from Al forgings (i.e. using extruded AA6082 stock material [41]). On the contrary, the grains in the heat treated EF-T6 samples show a slightly smaller grain size than the CF-T6 samples. The difference in grain size can predominantly be seen when investigating the material in FD, compare Figure 5.9. This indicates an asymmetric grain shape of the CF-T6 material, with elongated grains normal to FD. When comparing the results to the measurements from extruded and peak aged profiles shown by ref. [16], a slightly smaller grain size is prevalent in the material discussed here. This is most likely caused by the differing processing temperatures, which are lower in the present work by 50 °C in extrusion and 100 °C in case of forgings. The good stability of the microstructure during the forming and SHT processes, which is provided by the AlMn dispersoids, is affirmed nevertheless.

The textures of the as-forged samples are well comparable, both show the maximum intensity along the FD and a six-fold symmetry in $\{10\bar{1}0\}$ and $\{11\bar{2}0\}$ pole figures. In case of compression samples, which can provide a comparable deformation behavior to simple forgings [11], this distinctive symmetry is attributed to pyramidal I and II slip [42], which can be activated at temperatures above 300 °C in Mg alloys [43]. Interestingly, the texture intensity of the EF-F part is lower than that of the CF-F sample. This may be explained by the splitting of the poles along the FD in the EF-F measurement and the fact, that the forging direction is orientated perpendicular to the extrusion direction, thereby allowing a reduction of material anisotropy stemming from the extrusion process [44]. The area fraction of recrystallized grains can also be well correlated to the overall texture intensity measured. Higher texture intensities can be found in the samples with a lower amount of recrystallized grains. The CF-F sample, which has the highest texture intensity, shows the highest amount of deformed, nDRX grains. This relationship between the degree of recrystallization and the texture intensity is well known and has been described for extruded alloys [35].

In the samples of the heat treated material, which exhibits a fully recrystallized grain structure, the splitting of the poles along $\{0001\}$ can be seen for both, the EF-T6 and the CF-T6 parts. This type of texture development during solution heat treatment has been reported for Mg-Al-Ca alloys and has been found to be amplified by the addition of Zn [17; 19]. The heat treated material also shows a distinct reduction in texture intensity, correlating well with the general broadening of the texture during heat treatment and the increased amount of RX grains. Furthermore, it should be emphasized that the maximum texture intensity for the EF variant with >6.5 m.r.u. is notably higher than that of the CF variant (<5.0 m.r.u.), showing a difference of ~ 2 m.r.u. when comparing the same original measurement direction.

5.5.2. Tensile Properties

An overview of the results from tensile testing is shown in Figure 5.14. The samples using the extruded stock material show better values, i.e. higher strength and larger elongations, throughout.

The differences of deformed and heat treated samples can be easily recognized in the elongation as well as the spread of the measurements. The low ductility of the as-extruded and as-forged materials (CF-F and EF-F) can be attributed to the varying amount of deformed grains and the resulting fracture behavior of such bi-modal grain structure. Examples of extruded stock, showing such a behavior, can be found in Section 5.7.1 of the Supplementary. The peak aged samples, on the other hand, predominantly fail by intergranular fracture, which has been documented for various Mg alloys [45–47], and is known to be promoted by segregation of Ca atoms at grain boundaries [48]. While the segregation of Ca into to grain boundary regions reduces grain boundary mobility [49], thereby suppressing grain growth and facilitating texture weakening, the resulting lattice mismatch decreases grain boundary cohesion, promoting intergranular fracture [50; 51]. In terms of elongation of the heat treated parts, the performance varies considerably, depending on temper and forging stock. The heat treated samples

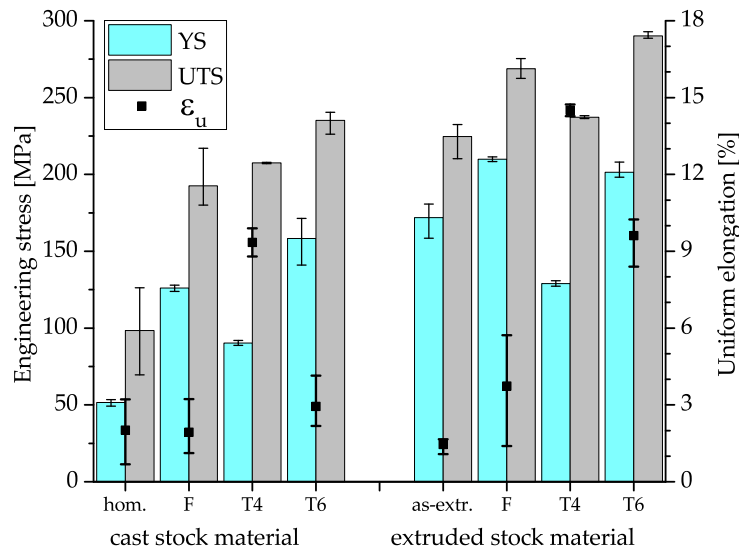


Figure 5.14.: Overview of tensile properties throughout the processing steps; showing yield strength (YS), ultimate tensile strength (UTS) and uniform elongation (ϵ_u). Standard deviation is displayed by error bars.

reach the highest ductility in T4 state, as this Mg alloy shows no natural aging response and processing temperatures were too low to produce a fully recrystallized microstructure. Such a behavior has been repeatedly shown for comparable alloys and processing schemes [16; 52]. In case of the peak hardened samples the elongation is reduced but of course higher strengths are achieved in exchange.

Of higher interest are the differences between the extruded and cast stock materials, where the cast stock shows lower elongations throughout. The lower ductility of the cast material is most likely caused by the larger spread in grain size, exhibiting grains reaching over $50\ \mu\text{m}$ in diameter, see Figure 5.9a. Such detrimental effects of the grain size have been discussed in ref [16] for a comparable alloying and processing scheme. Additionally, samples made from the cast stock repeatedly show remnants of the casting process, influencing the elongation markedly. As the CF-T6 samples are fully recrystallized, intergranular fracture would be expected, but casting defects may facilitate premature fracture of the samples. These defects seem to be dispersed during the extrusion process, with the effect of higher ductility and reduced spread of the measured values in EF-T6 material [52].

In case of the measured tensile strength, both types of forgings show expected behavior: the strength increases during deformation and decreases after solution heat treatment, the peak strength is reached in T6-temper – after artificial aging. When comparing forged parts produced with different stock materials, the differences vary in the individual processing steps but the parts produced with the extruded forging stock show higher values throughout. The microstructure of the parts differ in various ways, such as grain size, but primarily the variation in the degree of recrystallization must be taken into account, which in turn influences the texture intensity. Additionally, there is the possibility of different precipitation formation in the preceding processing steps, which is difficult to evaluate. Therefore, a detailed analysis of the individual contributions throughout all processing steps is not undertaken here. This is considered justifiable, since the technically relevant state is only reached after the solution heat treatment.

In the following, we discuss the relevant strengthening mechanisms in the peak aged samples and subsequently analyze their individual contributions to the YS. Special attention is paid on the differences in strength, caused by the different stock materials, which amounts to ~40 MPa between the CF-T6 and EF-T6 parts.

A 'bake hardening' effect taking place in the extruded stock material, as described in refs. [19; 53], can be excluded. But also the factor of age hardening has to be excluded in this regard, showing a comparable increase in YS (~70 MPa) in both forged and heat treated parts, regardless of the used forging stock. As this increase of strength by precipitation hardening can be seen in both processing routes, it may be assumed that material behavior during solution heat treatment (SHT/T4) and artificial aging, i.e. the amount of dissolved and subsequently precipitated phases, is identical.

Microstructural differences between the forged parts can be found in the presence of AlMn dispersoids. A higher number and slightly lower size of dispersoids was measured in the EF-T6 material, see Section 5.4.2.3. The YS generated by the AlMn dispersoids was assessed based on the considerations in ref. [16], resulting in 12 and 17 MPa for the CF-T6 and EF-T6 material, respectively. Therefore, the difference between the EF-T6 and CF-T6 specimen only amounts to ~5 MPa.

A comparison of grain size and degree of recrystallization shows small differences for the CF-T6 and EF-T6 parts. Both materials are fully recrystallized and have an avg. grain diameter of ~14 to 21 μm . Interestingly, differences in the grain size distribution are only apparent when analyzing the parts in FD, showing an increase of more than 6.5 μm in the avg. grain diameter for the CF-T6 material. Additionally, the CF-T6 samples show a higher grain size spread in all measured directions, indicating an increased amount of overly enlarged grains, possibly influencing the tensile properties. Calculating the grain boundary hardening for both materials results in a difference of ~12 MPa; an Hall-Petch constant of k_y of 250 MPa $\mu\text{m}^{-1/2}$, as applicable for grains of this size [16] has been used.

The texture of Mg wrought products, i.e. sheets and extrusions, is known to play an important role in material behavior, these effects are less well known for forgings. Obviously, the EF-T6 material exhibits a higher texture intensity by > 30 % when compared to the CF-T6 samples. A basal texture is present in all samples, which is the prevailing texture found in wrought Mg alloys. As the slip systems are aligned unfavorably for basal slip when deforming in ED, resulting in a low Schmidt factor, the YS is consequently increased. As the EF-T6 material shows a higher texture intensity, the result is an increase of the strength measured along ED [54].

It can be concluded that the differences in grain size, in combination with the variations in texture and dispersoid distribution, is the most likely cause for the differences in measured YS.

5.5.3. Fatigue Properties

The tested materials show a clear difference in fatigue strength, with the EF-T6 material reaching higher values. This is not surprising, as tensile values of these parts are also superior to the CF-T6 samples. While a direct comparison with the existing literature is difficult, depending on closely matching testing parameters, i.e. R_L and fatigue regime, general conclusions can still be drawn. Similar results have been found in [12], comparing cast, extruded, CF-F and EF-F parts, showing an increase of fatigue properties with increasing amount of processing steps. The improvement in the HCF regime is attributed to the increased elongation found in the EF-F specimen.

To gain further insight on the fracture behavior during fatigue testing, a notched sample was used to introduce a fatigue crack which was stopped before the sample could fracture fully. As the fracture behavior was found to be similar in both types of tested materials, only the EF-T6 material is discussed exemplarily. As can be seen in Figure 5.15a, grains in the direct vicinity of the crack are heavily twinned, while the surrounding microstructure is mostly unchanged. This crack propagation behavior is confirmed by SEM investigations of the fracture surface: distinctive twinning structures dominate the surface of the fatigue fracture. While this type of fracture poses a stark contrast to the material behavior during tensile testing, it is not uncommon for Mg alloys. Samples with large grains and, likely more important, in a heat treated state show a tendency for such a type of fracture [55]. While testing with a R_L :-1 seems to promote twinning, fracture along the twin boundaries can be found as well, when solely applying tensile loads [56].

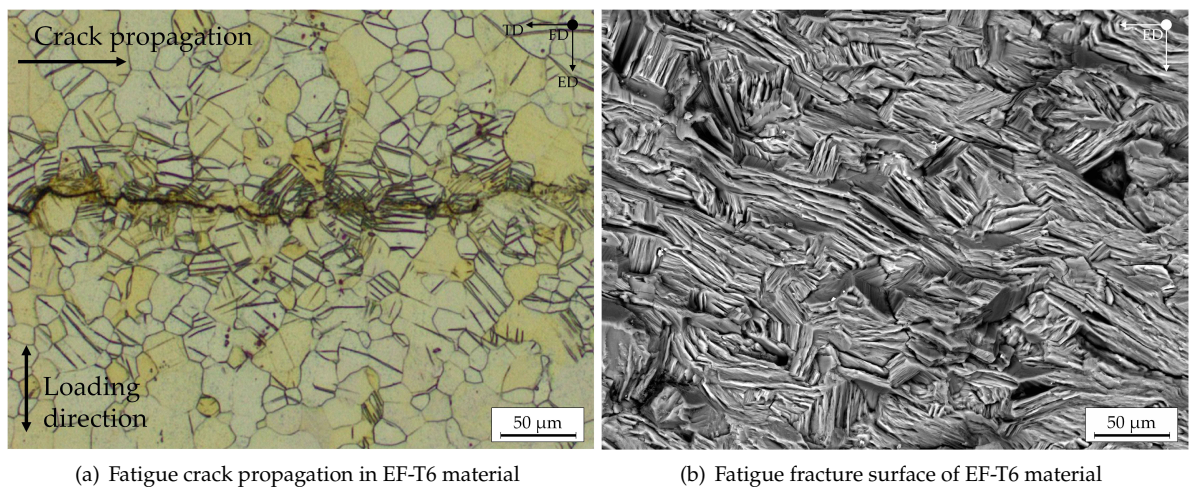


Figure 5.15.: Fracture behavior in fatigue testing (a) OM image of crack propagation in a notched sample (b) of fracture surface of a tested sample (SEM image).

5.6. Conclusions

In this work, the mechanical properties during the processing of age hardenable Mg forgings were investigated for different stock materials, concluding that:

1. Isothermal forging at 350 °C is adequate to produce well formed parts from both stock materials, i.e. from cast as well as from extruded lean alloy AXMZ1000.
2. Piston rods made from both stock materials exhibit comparable microstructures in as-forged state as well as after the heat treatment procedures (solution heat treatment and artificial aging).
3. Artificial aging of the used AXMZ1000 alloy provides an adequate increase in YS (~70 MPa) regardless of the forging stock used.
4. The extruded and forged samples show an increased overall mechanical performance when compared to the cast and forged material. This is affirmed by tensile testing as well as in fatigue measurements.
5. The achieved mechanical properties, i.e. a yield strength of 200 MPa and elongation of ~10 %, are well comparable to similar alloys produced by extrusion or rolling [18].

5.7. Supplementary Materials

5.7.1. Extruded Stock Material

The as-extruded material shows a typical basal extrusion texture, with the $(10\bar{1}0)$ planes oriented in extrusion direction, shown in Figure 5.16a. However, the maximum intensity as well as the symmetry around the ED are less pronounced, when compared to typical extrusion textures discussed in scientific literature. This difference is most likely caused by the shape of the extruded profile; while most published works use round profiles for analysis, the profile produced in this work has a square cross-section.

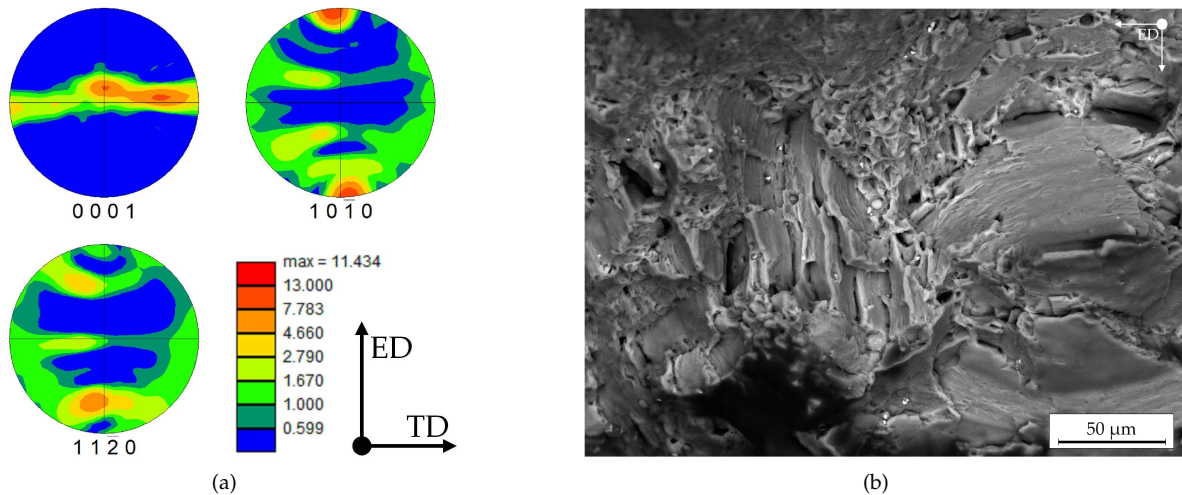


Figure 5.16.: SEM analysis of the as-extruded stock material, showing (a) pole figure from EBSD measurement and (b) fracture surfaces taken from tensile sample.

The fracture behavior of the as-extruded stock material shows a combination of grain boundary fracture in areas of DRX grains (Figure 5.17a) and cleavage fracture in areas of deformed nDRX grains (Figure 5.17b). As variations in the grain structure of the samples in the as-extruded state are common, the fracture surface varies accordingly, influencing the tensile properties, i.e. elongation. Additionally, cleavage fractures within the samples can be seen in both OM images, while not causing the sample to fail, it clearly confirms the tendency of fracture along the twin boundaries in the nDRX grains. This behavior is confirmed by the fracture surface shown in Figure 5.16b. It consists of grain boundary fracture of the fine DRX grains and large areas of smooth fracture surface in the area of the deformed, nDRX grains. When compared to the samples in T6 state, the differences in RX grain size can be clearly seen on the fracture surface.

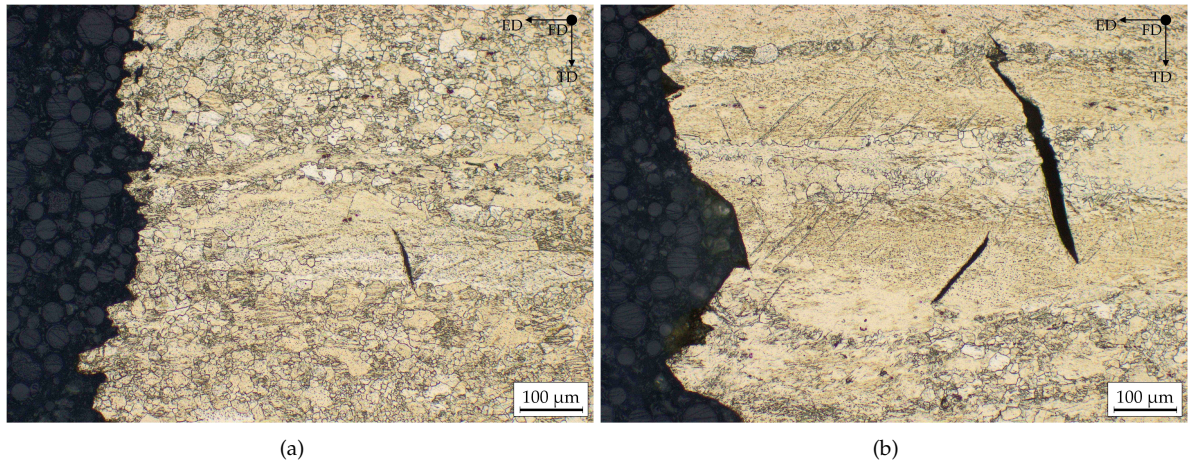


Figure 5.17.: OM image of fractured tensile samples of the as-extruded material, horizontal loading direction. Showing (a) grain boundary fracture along DRXed grains, (b) cleavage fracture at nDRXed grains.

5.7.2. Dispersoid measurement

The measurement of the AlMn dispersoids showed differences in both size and numbers, as shown in Section 5.4.2.3. The measured dispersoid size is correlated to the respective number and area fraction in Figure 5.18. It is apparent, that the EF-T6 material has a higher overall number of dispersoids, at the same time the size of the measured particles is smaller than in the CF-T6 samples, indicating a preferable distribution of phases throughout the Mg matrix.

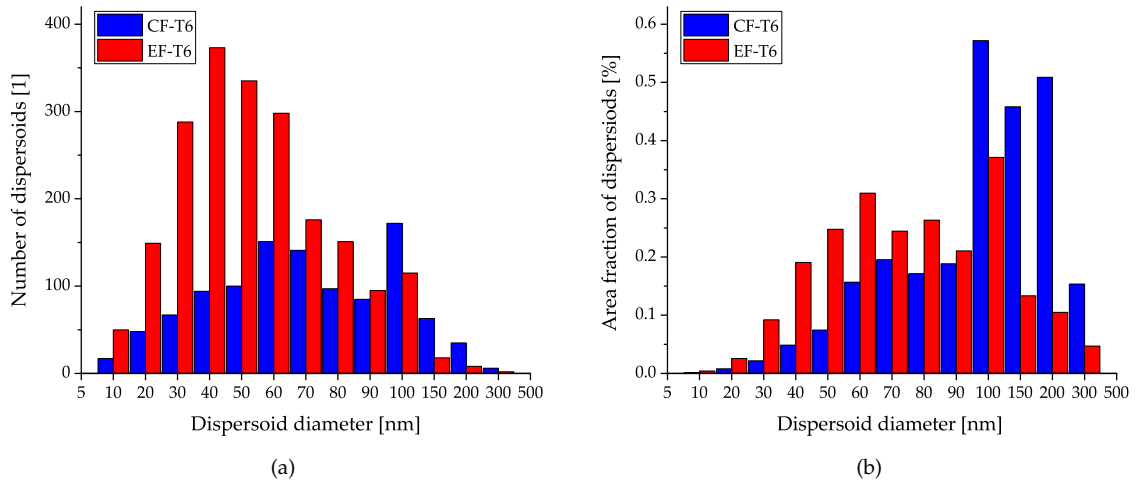


Figure 5.18.: Showing AlMn dispersoid size vs. (a) number of particles and (b) area distribution for the EF-T6 and CF-T6 samples.

5.7.3. Fatigue Measurements

Samples for fatigue measurements were machined in accordance with DIN EN 6072:2011 (sample Type 1), the tested cross-section was 3×10 mm. Fatigue testing was done according to DIN 50100:2016, with sinusoidal load application using a loading ratio (R_L) of 0 up to an ultimate number of cycles (N_G) of 10^7 . The testing frequency was in the range of 75 to 80 Hz, the failure criteria defined as ± 2 Hz. The measurements were done at room temperature ($22 \pm 1.5^\circ\text{C}$). For the HCF testing a $N_{50\%1}/N_{50\%2}$ ratio of 3.7 and 25.1 was calculated for the CF-T6 and EF-T6 material, respectively. It has to be mentioned, that the interval of cycles to failure in the HCF measurement of the CF-T6 specimen is small ($N_{50\%1}/N_{50\%2} = 3.7$) and might therefore be inaccurate. The HCF measurement of the EF-T6 material on the other hand was well within the limits defined by the standard. As the S-N curve of Mg is defined as Type II, i.e. decreasing beyond the knee point [28], a k_2 value of 45 [29] has been applied. An overview of the tested samples is given in Figure 5.19 and Table 5.4.

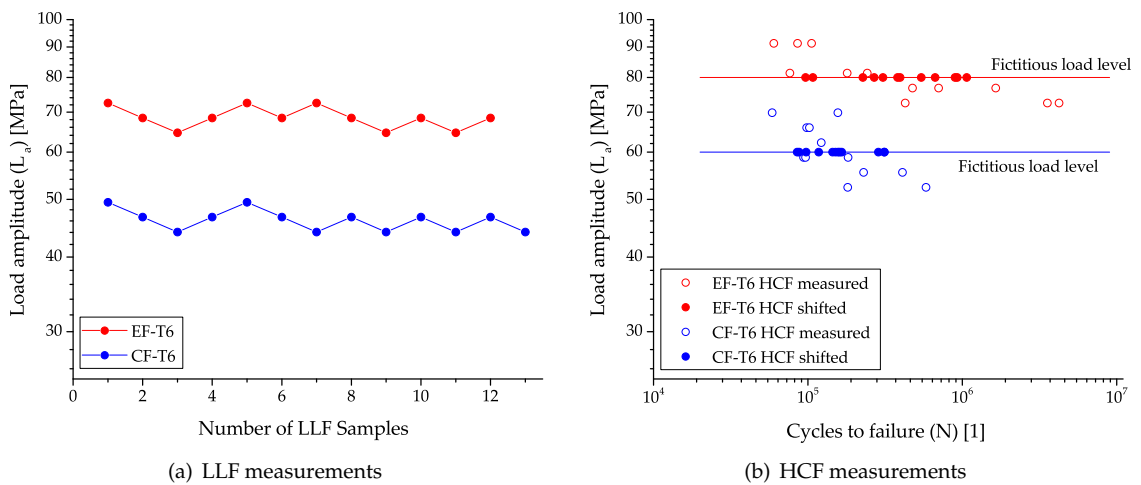


Figure 5.19.: Samples tested for fatigue analysis (a) LLF trials (last value given is fictitious) according to staircase method, (b) HCF measurements and shift on a fictitious load level using pearl string method.

Table 5.4.: Overview of the tested samples for fatigue analysis according to DIN 50100:2016.

Samples	extr. & forged T6 temper			cast & forged T6 temper		
	Cycles to failure [1]	Load amplitude [MPa]	Load max. [MPa]	Cycles to failure [1]	Load amplitude [MPa]	Load max. [MPa]
LLF	7417415	73	145	937354	49	99
	1708480	68	137	423866	47	93
	10000000	65	129	10000000	44	88
	10000000	68	137	10000000	47	93
	321181	73	145	1991012	49	99
	10000000	68	137	2706666	47	93
	136900	73	145	10000000	44	88
	137067	68	137	2687232	47	93
	10000000	65	129	10000000	44	88
	485377	68	137	175220	47	93
	10000000	65	129	10000000	44	88
				259840	47	93
	HCF	426274	73	145	181996	59
4235747		73	145	229667	55	111
60096		91	183	581844	52	105
105507		91	183	98164	66	132
179469		81	163	58683	70	140
242131		81	163	156306	70	140
701374		77	154	102102	66	132
476125		77	154	122114	62	124
1643727		77	154	93681	59	118
3557746		73	145	96588	59	118
76373		81	163	409303	55	111
85680		91	183	181155	52	105

5.8. References

- [1] I. Polmear, D. StJohn, J.-F. Nie, M. Qian, *Light Alloys: Metallurgy of the Light Metals*, 5th Edition, Elsevier, Butterworth-Heinemann, Oxford, UK, 2017. doi:10.1016/B978-0-08-099431-4.00009-9.
- [2] F. Czerwinski, Current Trends in Automotive Lightweighting Strategies and Materials, *Materials* 14 (6631) (2021) 1–27. doi:10.3390/ma14216631.
- [3] J. Benedyk, Aluminum alloys for lightweight automotive structures, in: *Materials, design and manufacturing for lightweight vehicles*, Elsevier, 2010, pp. 79–113. doi:10.1533/9781845697822.1.79.
- [4] DuckerFrontier, Aluminium Content in European Passenger Cars, Tech. rep. (2019).
- [5] M. Tauber, H. Fischer, M. Just, H. Fackler, Magnesium Parts in Serial Production: A Virtual Demonstrator, IMA Webinar (2020).
- [6] T. Abbott, M. Easton, Properties of magnesium die castings for structural applications, in: *Materials Forum*, Vol. 25, 2001, pp. 181–201.
- [7] A. A. Luo, Magnesium casting technology for structural applications, *Journal of Magnesium and Alloys* 1 (1) (2013) 2–22. doi:10.1016/j.jma.2013.02.002.
- [8] R. Nunes, J. Adams, et al., *ASM-Handbook Volume 2: Nonferrous Alloys and Special-Purpose Materials*, ASM International, Materials Park, OH, USA, 1992. doi:10.31399/asm.hb.v02.a0001075.
- [9] D. Klaumünzer, J. V. Hernandez, S. Yi, D. Letzig, S.-h. Kim, J. J. Kim, M. H. Seo, K. Ahn, Magnesium process and alloy development for applications in the automotive industry, in: *Magnesium Technology 2019*, Springer, 2019, pp. 15–20. doi:10.1007/978-3-030-05789-3_3.
- [10] Z. Zeng, N. Stanford, C. H. J. Davies, J.-F. Nie, N. Birbilis, Magnesium extrusion alloys: a review of developments and prospects, *International Materials Reviews* 64 (1) (2019) 27–62. doi:10.1080/09506608.2017.1421439.
- [11] N. P. Papenberg, S. Gneiger, I. Weißensteiner, P. J. Uggowitzer, S. Pogatscher, Mg-Alloys for forging applications—A review, *Materials* 13(4) (985) (2020) 1–61. doi:10.3390/ma13040985.
- [12] A. Gryguc, S. Behraves, S. Shaha, H. Jahed, M. Wells, B. Williams, X. Su, Low-Cycle Fatigue Characterization and Texture Induced Ratcheting Behaviour of Forged AZ80 Mg Alloys, *International Journal of Fatigue* 116 (2018) 429–438. doi:10.1016/j.ijfatigue.2018.06.028.
- [13] J.-F. Nie, Precipitation and hardening in magnesium alloys, *Metallurgical and Materials Transactions A* 43 (11) (2012) 3891–3939. doi:10.1007/s11661-012-1217-2.
- [14] Aluminium Alloys Market Outlook (2022-2032), Tech. rep., <https://www.factmr.com/report/aluminium-alloys-market/toc> (2022).
- [15] T. Nakata, C. Xu, R. Ajima, K. Shimizu, S. Hanaki, T. Sasaki, L. Ma, K. Hono, S. Kamado, Strong and ductile age-hardening Mg-Al-Ca-Mn alloy that can be extruded as fast as aluminum alloys, *Acta Materialia* 130 (2017) 261–270. doi:10.1016/j.actamat.2017.03.046.
- [16] M. Cihova, R. Schäublin, L. B. Hauser, S. S. Gerstl, C. Simson, P. Uggowitzer, J. F. Löffler, Rational design of a lean magnesium-based alloy with high age-hardening response, *Acta Materialia* 158 (2018) 214–229. doi:10.1016/j.actamat.2018.07.054.
- [17] M. Bian, T. Sasaki, B. Suh, T. Nakata, S. Kamado, K. Hono, A heat-treatable Mg-Al-Ca-Mn-Zn sheet alloy with good room temperature formability, *Scripta Materialia* 138 (2017) 151–155. doi:10.1016/j.scriptamat.2017.05.034.
- [18] N. P. Papenberg, S. Gneiger, P. J. Uggowitzer, S. Pogatscher, Lean Wrought Magnesium Alloys, *Materials* 14 (15) (2021) 4282. doi:10.3390/ma14154282.
- [19] M. Bian, T. Sasaki, T. Nakata, Y. Yoshida, N. Kawabe, S. Kamado, K. Hono, Bake-hardenable Mg-Al-Zn-Mn-Ca sheet alloy processed by twin-roll casting, *Acta Materialia* 158 (2018) 278–288. doi:10.1016/j.actamat.2018.07.057.

- [20] M. Bian, T. Sasaki, T. Nakata, S. Kamado, K. Hono, Effects of rolling conditions on the microstructure and mechanical properties in a Mg–Al–Ca–Mn–Zn alloy sheet, *Materials Science and Engineering: A* 730 (2018) 147–154. doi:10.1016/j.msea.2018.05.065.
- [21] M. Esmaily, J. Svensson, S. Fajardo, N. Birbilis, G. Frankel, S. Virtanen, R. Arrabal, S. Thomas, L. Johansson, Fundamentals and advances in magnesium alloy corrosion, *Progress in Materials Science* 89 (2017) 92–193. doi:10.1016/j.pmatsci.2017.04.011.
- [22] F. Czerwinski, Controlling the ignition and flammability of magnesium for aerospace applications, *Corrosion Science* 86 (2014) 1–16. doi:10.1016/j.corsci.2014.04.047.
- [23] G. Zhu, L. Wang, H. Zhou, J. Wang, Y. Shen, P. Tu, H. Zhu, W. Liu, P. Jin, X. Zeng, Improving ductility of a Mg alloy via non-basal slip induced by Ca addition, *International Journal of Plasticity* 120 (2019) 164–179. doi:10.1016/j.ijplas.2019.04.020.
- [24] J. Victoria-Hernández, S. Yi, D. Klaumünzer, D. Letzig, Comparison of the Mechanical Properties and Forming Behavior of Two Texture-Weakened Mg-Sheet Alloys Produced by Twin Roll Casting, *Frontiers in Materials* 6 (288) (2019) 1–11. doi:10.3389/fmats.2019.00288.
- [25] Y. Chino, T. Ueda, Y. Otomatsu, K. Sassa, X. Huang, K. Suzuki, M. Mabuchi, Effects of Ca on tensile properties and stretch formability at room temperature in Mg–Zn and Mg–Al alloys, *Materials Transactions* 52 (7) (2011) 1477–1482. doi:10.2320/matertrans.M2011048.
- [26] I. Basu, M. Chen, J. Wheeler, R. Schäublin, J. Löffler, Stacking-fault mediated plasticity and strengthening in lean, rare-earth free magnesium alloys, *Acta Materialia* 116877 (2021) 17. doi:10.1016/j.actamat.2021.116877.
- [27] J. Robson, D. Henry, B. Davis, Particle effects on recrystallization in magnesium–manganese alloys: particle pinning, *Materials Science and Engineering: A* 528 (12) (2011) 4239–4247. doi:10.1016/j.msea.2011.02.030.
- [28] R. Masendorf, C. Müller, Execution and evaluation of cyclic tests at constant load amplitudes–DIN 50100: 2016, *Materials Testing* 60 (10) (2018) 961–968. doi:10.3139/120.111238.
- [29] C. M. Sonsino, Course of SN-curves especially in the high-cycle fatigue regime with regard to component design and safety, *International Journal of Fatigue* 29 (12) (2007) 2246–2258. doi:10.1016/j.ijfatigue.2006.11.015.
- [30] B. Trink, Mikrostrukturelle Charakterisierung einer Mg–Al–Ca–Mn–Legierung bei der Herstellung von Schmiedeteilen, Master's thesis, Montanuniversität Leoben (2020).
- [31] A. Cross, D. Prior, M. Stipp, S. Kidder, The recrystallized grain size piezometer for quartz: An EBSD-based calibration, *Geophysical Research Letters* 44 (13) (2017) 6667–6674. doi:10.1002/2017GL073836.
- [32] J. A. Österreicher, F. Grabner, A. Schiffl, S. Schwarz, G. R. Bourret, Information depth in backscattered electron microscopy of nanoparticles within a solid matrix, *Materials Characterization* 138 (2018) 145–153. doi:10.1016/j.matchar.2018.01.049.
- [33] A. Zi, H.-G. Brokmeier, H. Palkowski, Texture and mechanical properties of strip cast and hot rolled magnesium AZ31, *International Journal of Materials Research* 102 (2) (2011) 168–172. doi:10.3139/146.110463.
- [34] H. Asgari, J. Szpunar, A. Odeshi, Texture evolution and dynamic mechanical behavior of cast AZ magnesium alloys under high strain rate compressive loading, *Materials & Design* 61 (2014) 26–34. doi:10.1016/j.matdes.2014.04.049.
- [35] S. Xu, K. Oh-Ishi, S. Kamado, F. Uchida, T. Homma, K. Hono, High-strength extruded Mg–Al–Ca–Mn alloy, *Scripta Materialia* 65 (3) (2011) 269–272. doi:10.1016/j.scriptamat.2011.04.026.
- [36] S. Gneiger, N. P. Papenberg, A. R. Arnoldt, C. M. Schlögl, M. Fehlbier, Investigations of High-Strength Mg–Al–Ca–Mn Alloys with a Broad Range of Ca+ Al Contents, *Materials* 14 (5439) (2021) 1–15. doi:10.3390/ma14185439.
- [37] M. Jiang, C. Xu, T. Nakata, H. Yan, R. Chen, S. Kamado, High-speed extrusion of dilute Mg–Zn–Ca–Mn alloys and its effect on microstructure, texture and mechanical properties, *Materials Science and Engineering: A* 678 (2016) 329–338. doi:10.1016/j.msea.2016.10.007.

- [38] T. Al-Samman, G. Gottstein, Dynamic recrystallization during high temperature deformation of magnesium, *Materials Science and Engineering: A* 490 (1-2) (2008) 411–420. doi:10.1016/j.msea.2008.02.004.
- [39] J. Hofstetter, S. Rüedi, I. Baumgartner, H. Kilian, B. Mingler, E. Povoden-Karadeniz, S. Pogatscher, P. J. Uggowitzer, J. F. Löffler, Processing and microstructure–property relations of high-strength low-alloy (HSLA) Mg–Zn–Ca alloys, *Acta Materialia* 98 (2015) 423–432. doi:10.1016/j.actamat.2015.07.021.
- [40] Y.-b. He, Q.-l. Pan, C. Qin, Z.-y. Zhang, X.-y. Liu, W.-b. Li, Modeling of strain hardening and dynamic recrystallization of ZK60 magnesium alloy during hot deformation, *Transactions of Nonferrous Metals Society of China* 22 (2) (2012) 246–254. doi:10.1016/S1003-6326(11)61167-9.
- [41] Y. Birol, E. Gokcil, M. A. Guvenc, S. Akdi, Processing of high strength EN AW 6082 forgings without a solution heat treatment, *Materials Science and Engineering: A* 674 (2016) 25–32. doi:10.1016/j.msea.2016.07.062.
- [42] M. Zecevic, I. J. Beyerlein, M. Knezevic, Activity of pyramidal I and II $\langle c+a \rangle$ slip in Mg alloys as revealed by texture development, *Journal of the Mechanics and Physics of Solids* 111 (2018) 290–307. doi:10.1016/j.jmps.2017.11.004.
- [43] A. Chapuis, J. H. Driver, Temperature dependency of slip and twinning in plane strain compressed magnesium single crystals, *Acta Materialia* 59 (5) (2011) 1986–1994. doi:10.1016/j.actamat.2010.11.064.
- [44] A. Sabroff, F. Boulger, H. Henning, J. Spretnak, *A Manual on Fundamentals of Forging Practice*, Tech. rep. (1964).
- [45] Y. Ortega, T. Leguey, R. Pareja, Tensile fracture behavior of aging hardened Mg–1Ca and Mg–1Ca–1Zn alloys, *Materials Letters* 62 (23) (2008) 3893–3895. doi:10.1016/j.matlet.2008.05.021.
- [46] B. Kondori, A. Benzerga, On the notch ductility of a magnesium-rare earth alloy, *Materials Science and Engineering: A* 647 (2015) 74–83. doi:10.1016/j.msea.2015.08.077.
- [47] X. Shang, H. Zhang, L. Wang, G. Zhu, Z. Cui, M. Fu, X. Zeng, The effect of stress state and strain partition mode on the damage behavior of a Mg–Ca alloy, *International Journal of Plasticity* 144 (103040) (2021). doi:10.1016/j.ijplas.2021.103040.
- [48] T. Trang, J. Zhang, J. Kim, A. Zargarani, J. Hwang, B.-C. Suh, N. Kim, Designing a magnesium alloy with high strength and high formability, *Nature communications* 9 (2522) (2018) 1–6. doi:10.1038/s41467-018-04981-4.
- [49] Z. Zeng, Y. Zhu, S. Xu, M. Bian, C. Davies, N. Birbilis, J. Nie, Texture evolution during static recrystallization of cold-rolled magnesium alloys, *Acta Materialia* 105 (2016) 479–494. doi:10.1016/j.actamat.2015.12.045.
- [50] H. Somekawa, T. Inoue, K. Tsuzaki, Effect of solute atoms on fracture toughness in dilute magnesium alloys, *Philosophical Magazine* 93 (36) (2013) 4582–4592. doi:10.1080/14786435.2013.838008.
- [51] S. Nandy, S.-P. Tsai, L. Stephenson, D. Raabe, S. Zaeferrer, The role of Ca, Al and Zn on room temperature ductility and grain boundary cohesion of magnesium, *Journal of Magnesium and Alloys* 9 (5) (2021) 1521–1536. doi:10.1016/j.jma.2021.03.005.
- [52] X. Liu, X. Qiao, Z. Li, M. Zheng, High strength and excellent ductility of dilute Mg-0.68 Al-0.32 Ca-0.50 Mn (wt%) extrusion alloy obtained by T6 treatment, *Materials Characterization* 162 (2020) 110197. doi:10.1016/j.matchar.2020.110197.
- [53] Y.-J. Li, Y. Fang, C. Wang, Z.-M. Hua, Y. Gao, M. Zha, H.-Y. Wang, Enhanced strength-ductility synergy achieved through twin boundary pinning in a bake-hardened Mg–2Zn–0.5 Ca alloy, *Materials Science and Engineering: A* 831 (142239) (2021) 1–9. doi:10.1016/j.msea.2021.142239.
- [54] Z. Li, X. Qiao, C. Xu, S. Kamado, M. Zheng, A. Luo, Ultrahigh strength Mg–Al–Ca–Mn extrusion alloys with various aluminum contents, *Journal of Alloys and Compounds* 792 (2019) 130–141. doi:10.1016/j.jallcom.2019.03.319.
- [55] B. Wang, D. Xu, S. Wang, E. Han, Fatigue crack initiation of magnesium alloys under elastic stress amplitudes: A review, *Frontiers of Mechanical Engineering* 14 (1) (2019) 113–127. doi:10.1007/s11465-018-0482-1.
- [56] D. Yu, D. Zhang, Q. Dai, W. Lan, J. Peng, J. Xu, F. Qi, F. Pan, Effect of stress ratio on high cycle fatigue properties in Mg–6Zn–1Mn alloy, *Materials Science and Engineering: A* 711 (2018) 624–632. doi:10.1016/j.msea.2017.10.082.

6. Summary & Outlook

This work investigated the forming behavior and microstructural development of a lean age-hardenable Mg-Al-Ca-Zn-Mn alloy (AXMZ1000) in detail, focusing on the forging process and its processing parameters.

The applications, forming parameters and mechanical properties of Mg forgings have been investigated via literature study. The forging process is highly flexible and has the potential to produce Mg parts over a large range of temperatures and forming parameters. In terms of used material compositions large differences are possible, ranging from well-known alloys, i.e. AZ91, ZK60, to REE containing alloys. Nevertheless, most of the parts described in literature are used in the as-formed state, a stark contrast to Al-forgings which are often used in T6-temper.

While literature has shown a large variety of possible Mg forging alloys, the alloying system investigated in this work, an age-hardenable Mg alloy with a low overall amount of alloying elements, has not yet been investigated regarding its forging performance. It has been found, that these so-called lean alloys can have a multitude of possible designs and aims, being specifically created to take full advantage of the contained alloying elements to increase mechanical properties or adjust corrosion behavior. Especially in case of age-hardenable Mg alloys a trend towards the lean-alloy design scheme is visible. This is caused by the need of solution heat treatment windows, while avoiding primary phases from casting, as well as the aim to improve deformation behavior by reduced solid drag.

The chosen Mg-Al-Ca-Zn-Mn alloy was designed with good forming behavior, increased processing window and high age-hardening capabilities in mind. Each alloying element is used to its fullest, e.g. to provide precipitates for the hardening process (Al, Ca) or dispersoids for microstructure stabilization (Al, Mn). High processing speeds are possible, i.e. by extrusion, thereby allowing for an easy production of extruded forging stock.

The forming process of the AXMZ1000 alloy was investigated over a broad range of temperatures, a processing map was calculated and mechanical properties measured. Differing forging stock, i.e. cast and extruded, was processed in laboratory-scale as well as industrial scale forgings, thereby showing that isothermal and non-isothermal forging is possible in the range of 300 to 450 °C material temperature. When die or material temperatures are chosen too low surface damages or part failures by shearing may occur, fracture by grain boundary failure on the other hand was found at temperatures of ~500 °C. The investigations showed that forgings made from cast stock were able to reach the specific tensile strength of conventional Al forging alloys. The forgings made from AXMZ1000 extruded stock showed superior performance regarding their tensile and fatigue properties when compared to the cast and forged parts. Additionally, due to its reduced grain size, the extruded stock showed better forming behavior throughout the investigations.

The used AXMZ1000 alloy showed good age hardening behavior and adequate process stability during forming and heat treatments. On the other hand, this alloy poses some challenges in the casting process, as the low overall amount of alloying elements impedes reproducibility and aggravates the effect of chemical fluctuations during alloy preparation.

The present work showed that the production of Mg forgings, even on industrial scale, is possible with manageable effort, if inherent material limitations are kept in mind. The use of adequate material and die temperatures is especially important to achieve proper part quality.

It can be concluded, that even though a multitude of alloys, applications and process variations for Mg forgings can be found in scientific literature, industrial applications in Europe are still sparse. While the benefits of Mg in terms of weight reduction and good specific properties are well known, the large-scale use of Mg wrought parts is hampered by technical, bureaucratic and economic reservations.

A. Appendix

A.1. Abbreviations & Symbols

The following abbreviations and symbols are used in this work:

Abbreviations		Symbols	
AC	air cooled	ϕ	volume fraction
BSE	back-scattered electron	ϵ_f	elongation to failure
CRSS	critical resolved shear stress	ϵ_p, ϵ_u	elongation at peak
DRX	dynamic recrystallization	ϵ_{other}	undefined elongation
DSC	differential scanning calorimetry		
EBSD	electron backscatter diffraction	at. %	atomic percent
ECAP	equal channel angular pressing	wt. %	weight percent
ED	extrusion direction		
EDS	energy dispersive X-ray spectroscopy	d	grain diameter
FAA	Federal Aviation Administration	k_y	Hall Petch slope
FD	forging direction	σ_0	frictional stress
FEM	finite element method		
G.P.-zone	Guinier-Preston zone	d_{AlMn}	diameter of AlMn dispersoids
GOS	grain orientation spread	f_{AlMn}	volume fraction of AlMn disp.
HAADF	high-angle annular dark field	N_{AlMn}	number density of AlMn disp.
HCF	high cycle fatigue	Z_{Info}	max. depth of detection
HPT	high pressure torsion		
HSLA	High Strength Low Alloyed	L_{aL}	LLF strength (amplitude)
I.E.-value	Ericksen Index	L_{maxL}	LLF strength (max.)
IMA	International Magnesium Association	N_G	max. number of cycles (10^7)
IMP	intermetallic particle/phase	R_L	load ratio
LCF	low cycle fatigue		
LLF	long life fatigue	η	power dissipation rate
LPDC	low pressure die casting	m	strain rate sensitivity exponent
LPSO	long period stacking order	φ	strain
MAF	multi axial forging	$\dot{\varphi}$	strain rate
MM	mischmetal	σ	stress
nRX	non-recrystallized		
ODF	orientation distribution function		
OM	optical microscope		
PF	pole figure		
RE, REE	rare earth elements		
RT	room temperature		
RX	recrystallized		
SEM	scanning electron microscope		
SHT	solution heat treatment		
SPD	severe plastic deformation		
STEM	scanning transmissions electron microscope		
TEM	transmission electron microscope		
UCS	ultimate compressive strength		
UTS	ultimate tensile strength		
WQ	water quenched		
XRD	X-ray diffraction		
YS	tensile yield strength		
YSc	compressive yield strength		
ZH	Zener-Hollomon parameter		

A.2. Unpublished Results

Forging of Cast Round Billets

Casting of stock material has been discussed in Section 1.5.2, showing that two different shapes of castings had to be produced. This resulted in slightly different microstructures, visible in e.g. the size and distribution of the Mn containing phases after homogenization heat treatment.

While the forging process of the stock material produced from the plate shaped castings was discussed in detail, the material from the round billets was solely presented as extruded forging stock. In the following, results from forging trials using cast and homogenized material from round billets is summarized.

The approach used for the forging trials of the cast round billets was the same as described for the cast material in Section 5.3. The cast round billets were homogenized in a three step process and isothermal forged at 350 °C, the forged piston rods were subsequently heat treated to reach peak hardness.

Analysis of the piston rods in T6 temper showed, that the microstructure consists of fully recrystallized grains in both the sample center as well as the sample rim, see Figure A.1. The mechanical properties were investigated using tensile testing, resulting in a YS of 149 ± 1 MPa, UTS of 223 ± 14 MPa and ϵ_u of 4.0 ± 1.4 %. Thereby showing no substantial differences to the CF-T6 samples, made from cast and homogenized plates, discussed in Chapter 5.

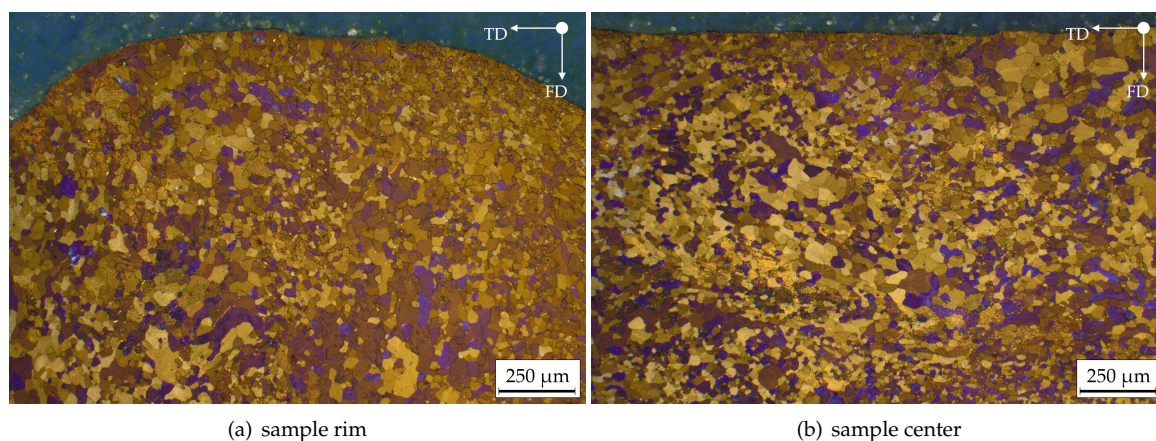


Figure A.1.: Microstructure (OM-image) of piston rods in T6-temper, forging stock made from cast & homogenized round billets.